Flexible Polyhedra

Exploring finite mechanisms of triangulated polyhedra

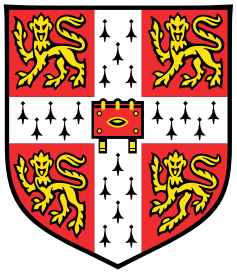

Jingjiao Li

Department of Engineering
University of Cambridge

This dissertation is submitted for the degree of
Doctor of Philosophy

Murray Edwards College

January 2018

This dissertation is dedicated to my grandmother.

Declaration

I hereby declare that except where specific reference is made to the work of others, the contents of this dissertation are original and have not been submitted in whole or in part for consideration for any other degree or qualification in this, or any other university. I further state that no substantial part of my dissertation has already been submitted, or, is being concurrently submitted for any such degree, diploma or other qualification at the University of Cambridge or any other University of similar institution except as declared in the Preface and specified in the text.

This dissertation is my own work and contains nothing which is the outcome of work done in collaboration with others, except as specified in the text and Acknowledgements. This dissertation does not exceed the prescribed word limit for the relevant Degree Committee. It contains fewer than 65,000 words including appendices, bibliography, footnotes, tables and equations and has fewer than 150 figures.

Jingjiao Li
January 2018

Acknowledgements

I would like to acknowledge my supervisor, Prof Simon Guest, for his guidance, encouragement, advice and provisional manner of supervisions. I wish to express my gratitude to my academic advisor, Allan McRobie, for his interest in the topic and inspiring questions.

I am grateful for all the training and opportunities for both PhD development and personal development that Cambridge University provided.

Abstract

In a quest to design novel deployable structures, flexible polyhedra provide interesting insights. This work follows the discovery of flexible polyhedra and aims to make flexible polyhedra more useful.

The dissertation describes how flexible polyhedra can be made. The flexible polyhedra first considered in this dissertation have a rotational degree of freedom. The range of this rotational movement is measured and maximised in this work by numerical maximisation. All polyhedra are established computationally: an iterative solution method is used to find vertex coordinates; several clash detecting methods are described to define whether each rotational position of a flexible polyhedron is physically possible; then a range of motion is defined between occurrences of clashes at the two ends; finally, an optimisation tool is used to maximise the range of motion.

By using these tools, the range of motion of two types of simplest flexible polyhedra are maximised. The first type is a series of flexible polyhedra generalised from the Steffen flexible polyhedron. The range of motion of this type is improved to double that of Steffen's original, from 27° to 59°. Another type of flexible polyhedron is expanded from a model provided by Tachi. Based on the understanding of Steffen's flexible polyhedron, optimisation parameters are carefully given. This new type has achieved a wider range of motion, so now the range of motion of flexible polyhedron is tripled to 80°.

After enlarging the range of motion of the degree of freedom in the 1-dof systems, the dissertation found multiple degrees of freedom in one polyhedron. The multiple mechanisms can be even repetitive, so that an n-dof polyhedron is found. A polyhedron of two degrees of freedom is first presented. Then, a unit cell for any number of mechanisms is found. As a repetitive structure, a 3-dof polyhedron is presented. Finally, this work presents the possibility of configuring a flexible polyhedral torus and a closed polyhedral surface that is able to flex without the need to stop.

Table of contents

List of figures

List of tables

Chapter 1

Introduction

1.1 Overall aim of the dissertation

This dissertation is primarily concerned with flexible polyhedra, a special form of polyhedra that are not rigid. The dissertation concentrates on understanding the techniques that can be used to form flexible polyhedra. Further, methods are explored to maximise the possible motions of flexible polyhedra, and new flexible polyhedra are described. Although the results presented are all essentially geometric, it is hoped that this might provide inspiration for novel morphing or deployable structures. For instance, the 'crinkle' introduced later might provide a useful way to hinge a component along a line without actually requiring any material on the line.

Polyhedra have long been considered to be rigid structures — indeed, the pioneering mathematician Euler conjectured in 1766 that all such structures are rigid. A polyhedron is considered to be a sealed envelope composed of panels, formed of rigid planar polygons, which share edges. The edges and vertices are connected in such a way that adjacent panels are able to freely rotate about their common edges. In the 1970s, Connelly found a counterexample to the rigidity conjecture — a flexible polyhedron! This dissertation takes this counterexample as a starting point, with the aim of understanding how it was developed, how the techniques used can be generalised, and how they might have engineering applications. As an introduction, this chapter describes how to make a flexible polyhedron and demonstrates its key components.

1.2 A broad overview of flexible polyhedra

The way Connelly composed the world's first flexible polyhedron [8, 10, 11] is demonstrated in Figure 1.1. This figure shows a closed polyhedral surface. It is able to bend so that some of its polygons can rotate about their edges. This is enabled by an important replacement. Figure 1.1a first shows a non-flexible, closed polyhedron, which has two edges clashing against each other internally. A true polyhedron does not contain a clash, and so it is named a *near-polyhedron*. This near-polyhedron is carefully chosen as described by Connelly [11] so that the clash between edges is the only matter preventing flexibility. Figure 1.1b shows one of the clashing edges being removed, along with the two panels it belongs to. These two panels are triangulated, therefore, the cut-out figure consists of two triangles sharing an edge. This is defined as a *dihedral*. After this dihedral is cut out of the closed near-polyhedron, it is replaced by a crinkled surface as shown in Figure 1.1c. This crinkled surface is not merely any creased surface: it is a clever component called a *crinkle*. This section will focus on introducing this special idea of replacement. After the replacement by the crinkle, the polyhedron becomes complete, closed and able to rotate as shown in Figure 1.1d. (Note the subfigures are shown clockwise to line up the replaced and replacing components.)

The replacement of a dihedral by a crinkle is illustrated in Figure 1.2. This inserted crinkle is not any crinkled surface: it is able to bend to match the kinematics of the original dihedral, while maintaining the edge length of the replaced dihedral. As shown in Figure 1.2, the dihedral (represented in pink) is originally part of a surface that is able to rotate about a *hinge*. This surface that is two panels containing a hinge is called a *dihedal surface*. After replacement, the crinkle (in green) is still able to rotate about the same hinge as the original dihedral surface.

A proper description of how to construct a crinkle will be introduced in Section 2.4. Here a simple example is given in Figure 1.3. First, an equilateral quadrilateral (a polygon with four edges of equal lengths, called a diamond for simplicity) is cut out of a piece of paper. Then, another two diamonds (coloured in purple), of the same edge length as the cut-off diamond (in blue), are prepared to be glued onto the cut-off diamond by edges. As Figure 1.3a shows, all pieces are folded in half to create a hinge line in the middle to allow rotation before the assembly of a crinkle. As Figure 1.3b shows, when the three diamond shapes are glued together by the edges, one diamond in purple stands at the front, and the other diamond in purple goes to the back. Both diamonds in purple have to bend about their hinges in order to be glued onto the middle diamond in blue: the front diamond in purple bends backward and the back diamond in purple bends forward. This assembly is a crinkle. In Figure 1.3c, the assembled crinkle is then glued to the original paper where the middle diamond in blue was cut off initially. The crinkle has four free edges from the other two

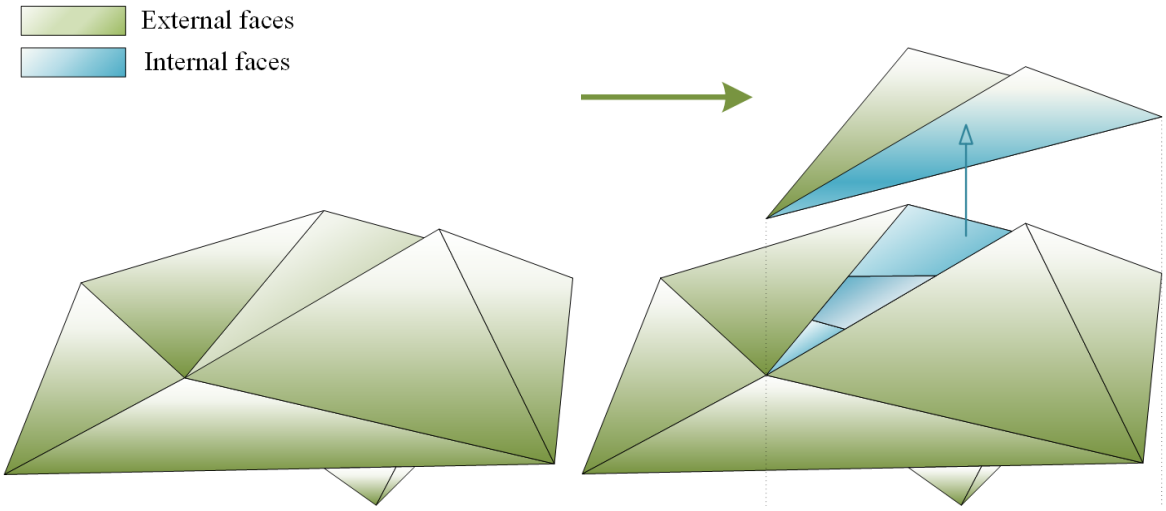

(a) Initial: Connelly's flexible polyhedron starts as a specially chosen 'near-polyhedron' [11] where two pairs of edges intersect, and the resultant clash is the only reason the polyhedron is not flexible.

(b) Step 1: One of the internally clashing dihedrals is taken out of the closed surface.

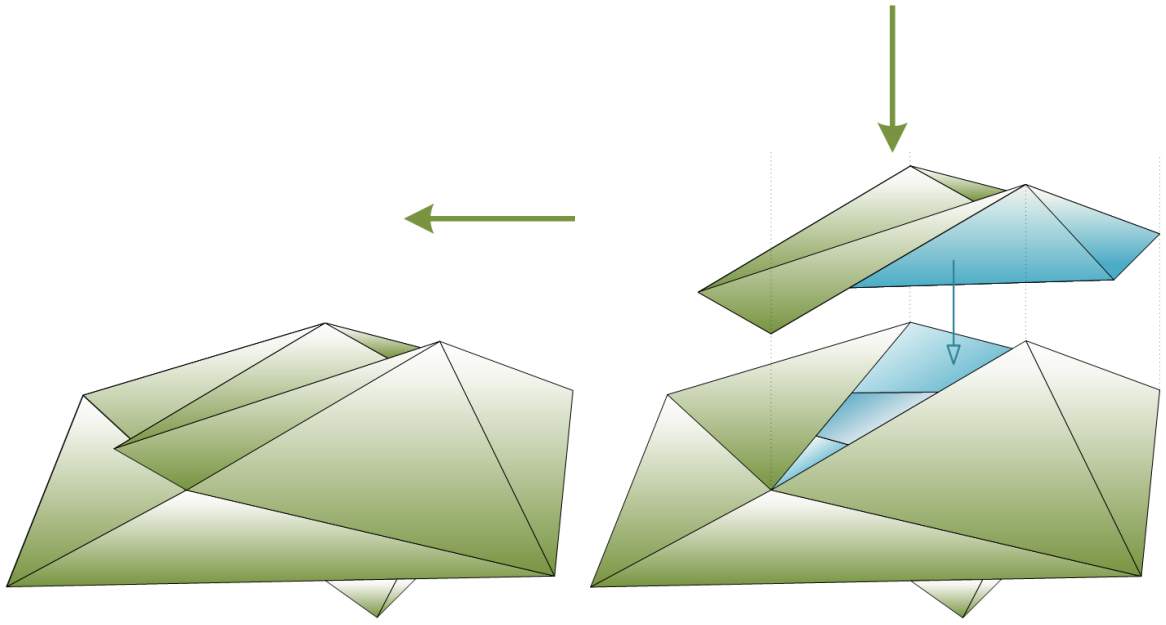

(d) Outcome: The very first flexible polyhedron, described by Connelly in [10]

(c) Step 2: The dihedral is replaced by a crinkle to avoid clashing against an edge beneath internally.

Fig. 1.1 The process of making a flexible polyhedron described by Connelly [8, 10, 11]. A near-polyhedron that clashes against itself is carefully chosen to have a dihedral replaced by a crinkle in order to avoid the clash and allow rotation before other clashes. Pictures re-drawn from Connelly's original drawing [11].

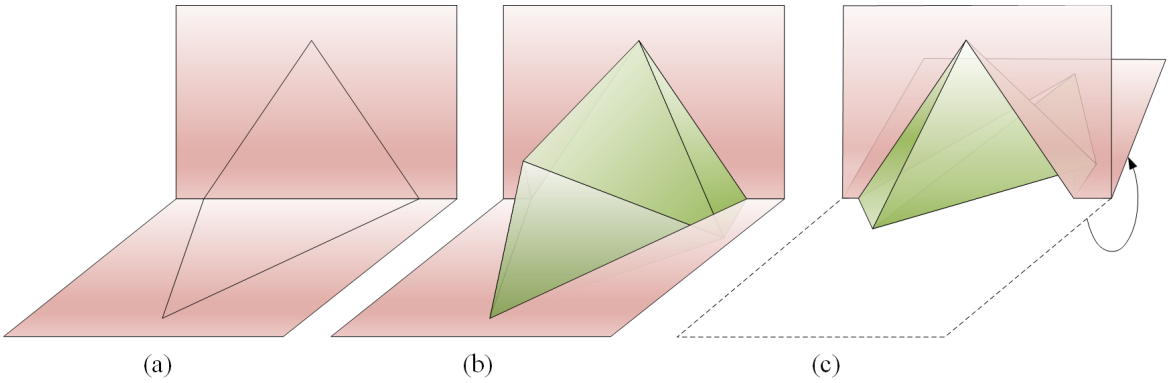

Fig. 1.2 Insertion of a crinkle into a dihedral surface. The crinkle is kinematically compatible with the dihedral surface. (a) A dihedral (coloured pink) is composed of two triangles sharing an edge and is part of a creased surface. (b) A crinkle (coloured green) replaces the dihedral and is able to rotate about the same hinge. The crinkle maintains the length of the original hinge as it moves. (c) When the surface rotates backwards, the inserted crinkle is able to bend along with the dihedral surface. The length of the replaced hinge stays the same during the whole rotation.

edges of the diamonds in purple; they are hence glued to the edges of the cut in the paper. Then, a crinkle inserted into a dihedral surface is complete. The whole resultant creased surface, including all components in blue and purple, is able to rotate about all hinges created previously. Therefore, as the original piece of paper (the dihedral surface) bends about its hinge, the crinkle is also able to bend about this hinge.

The crinkle created in Figure 1.3 is doubly flat-foldable. Its doubly flat-folding process is shown in Figure 1.4. In the first row, the crinkle unfolds from a flat, folded up position. In the second row, the crinkle opens up to the middle position. In the third row, the hinges in the middle diamond and in the original dihedral surface both changes direction from being valleys to hills in the current perspective. In the last row, the crinkle folds up backwards into another flat position. These two flat positions are different: the first (numbered as 1) and the last (numbered as 12) pictures have the crinkle folded up in different positions.

Connelly used a crinkle to create the world's first flexible polyhedron. Soon after, Steffen found a simple version as shown in Figure 1.5a. This is the simplest known flexible polyhedron [11]. It has only nine vertices, one more than a cube. The flexibility of this polyhedron is also enabled by replacement of dihedrals by crinkles. The near-polyhedron before this replacement is shown both in Figure 1.5a next to the polyhedron from the same view point and in Figure 1.5b from a different view point for a clearer observation of the hinge. The near-polyhedron is a tetrahedron sharing an edge with a triangle flap. It is able to rotate about the sharing edge as a *hinge*. Like Connelly's near-polyhedron, this

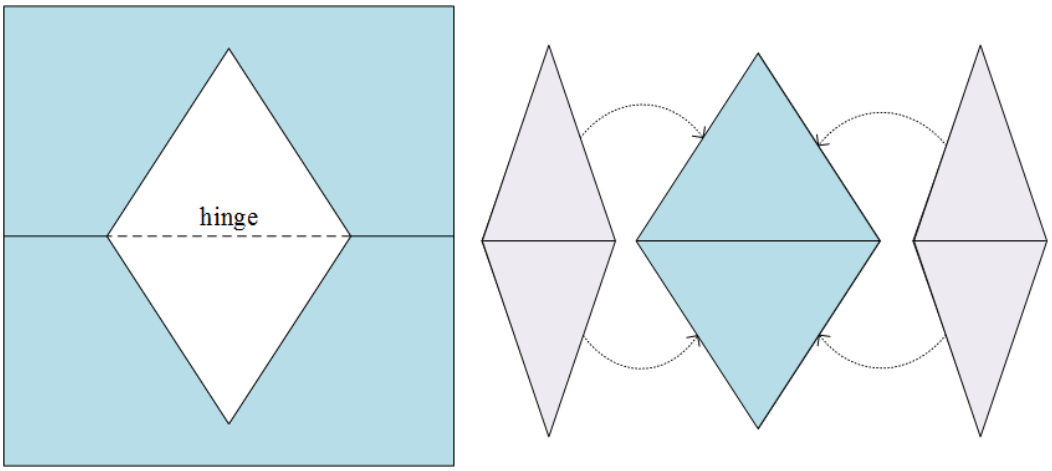

(a) Cut an equilateral quadrilateral (diamond) out of a piece of paper. Then produce another two diamonds (in purple) of the same edge lengths as the cut-out diamond, to be glued onto the cut-out diamond later. Fold all components to form a hinge for assembly later.

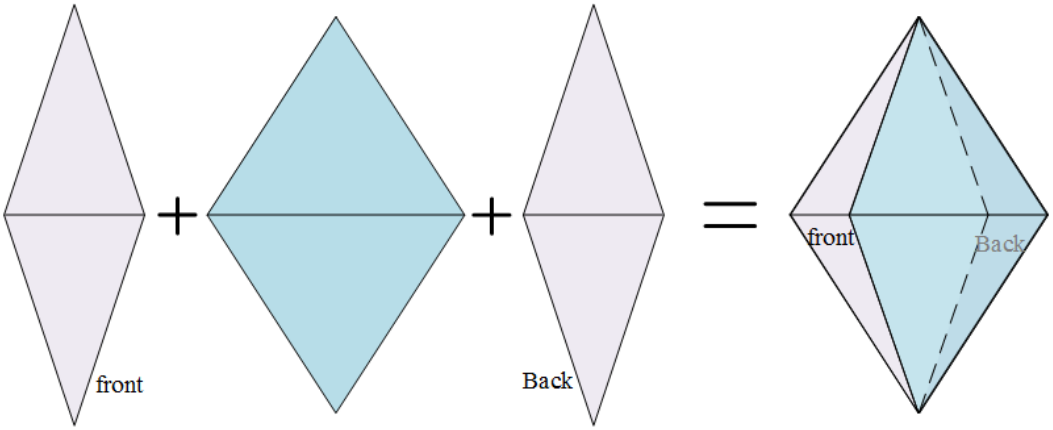

(b) Glue the edges of the three diamonds: one diamond in purple comes to the front, the other diamond in purple is rendered to the back, so that a crinkled shape is produced.

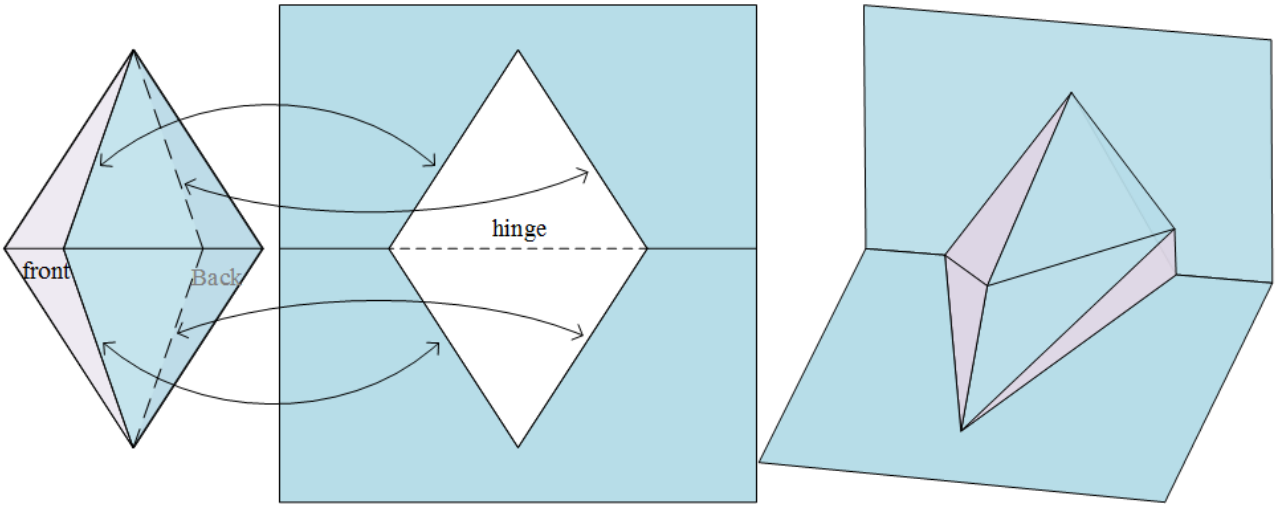

(c) Glue this crinkle to the original paper by four free edges. A crinkle is now inserted in a piece of paper and is able to rotate as the paper does about the previously made hinge.

Fig. 1.3 The process of making a crinkle. The length of the dashed hinge is invariant as the crinkle moves, because this crinkle forms part of a Type I Bricard flexible octahedron — all three types of this terminology will be introduced in Section 2.3.

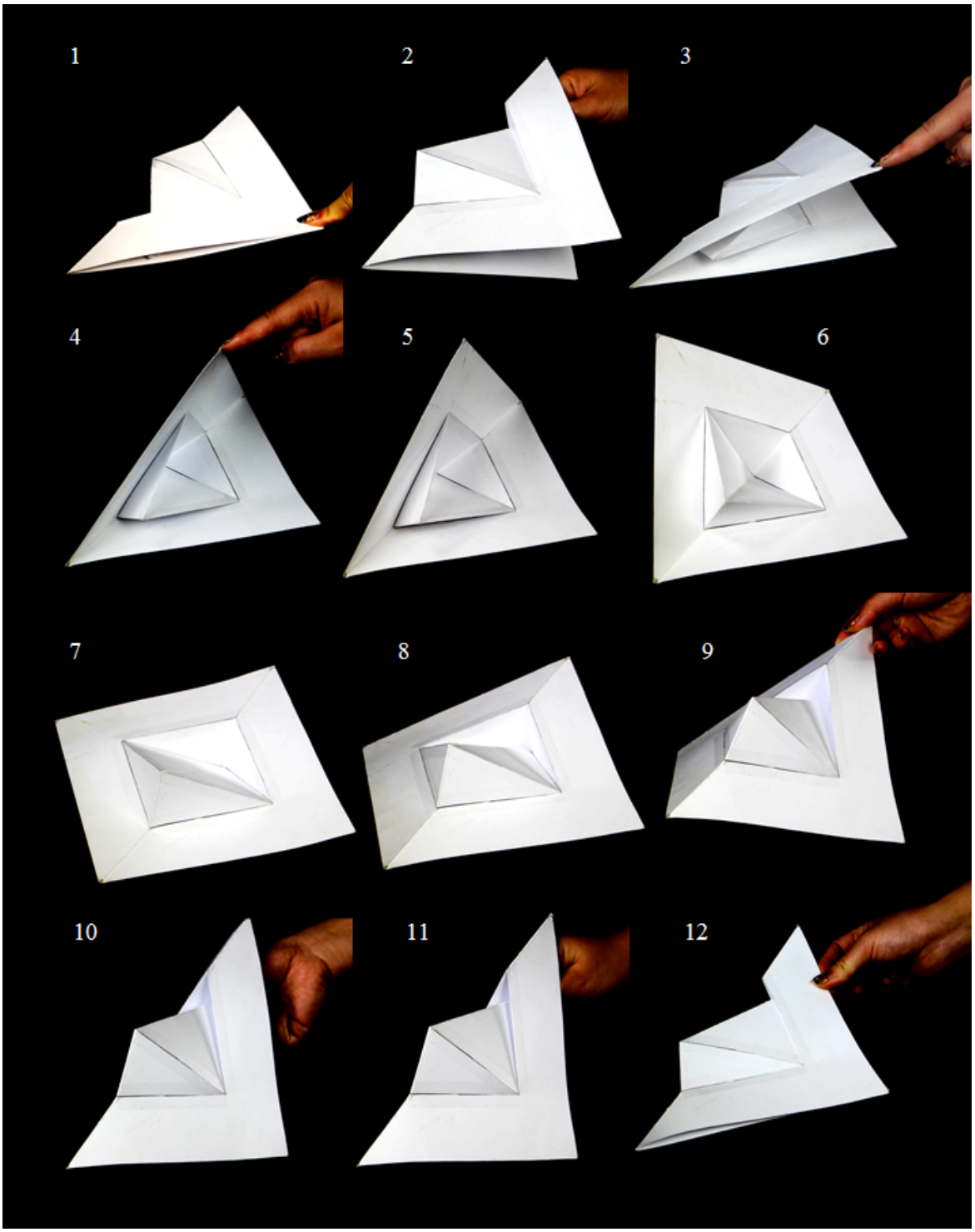

Fig. 1.4 The doubly flat-folding process of a crinkle. During this process, the replaced hinge retains the same length. This is a plane-symmetric, doubly flat-foldable Type I crinkle, which will be described formally in detail in the next chapter.

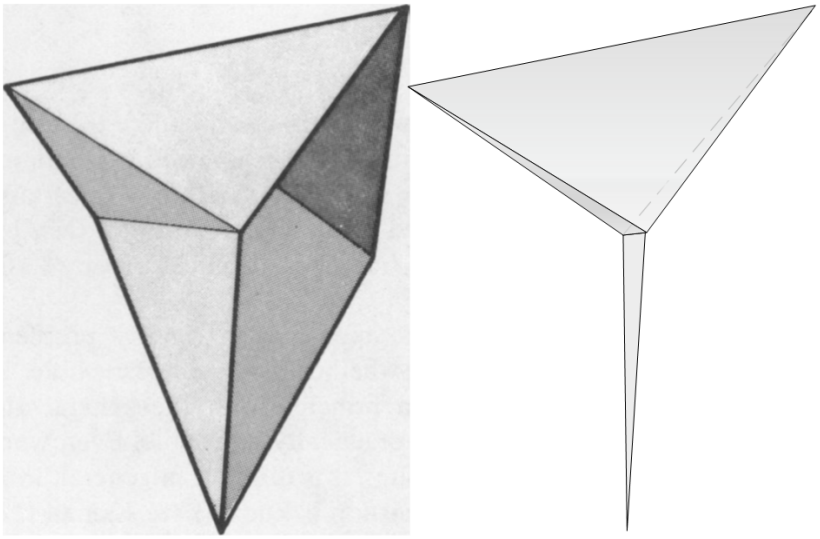

(a) The Steffen flexible polyhedron drawn by Connelly [11] and its near-polyhedron. The near-polyhedron is composed of a tetrahedron and a triangle linked by a sharing edge.

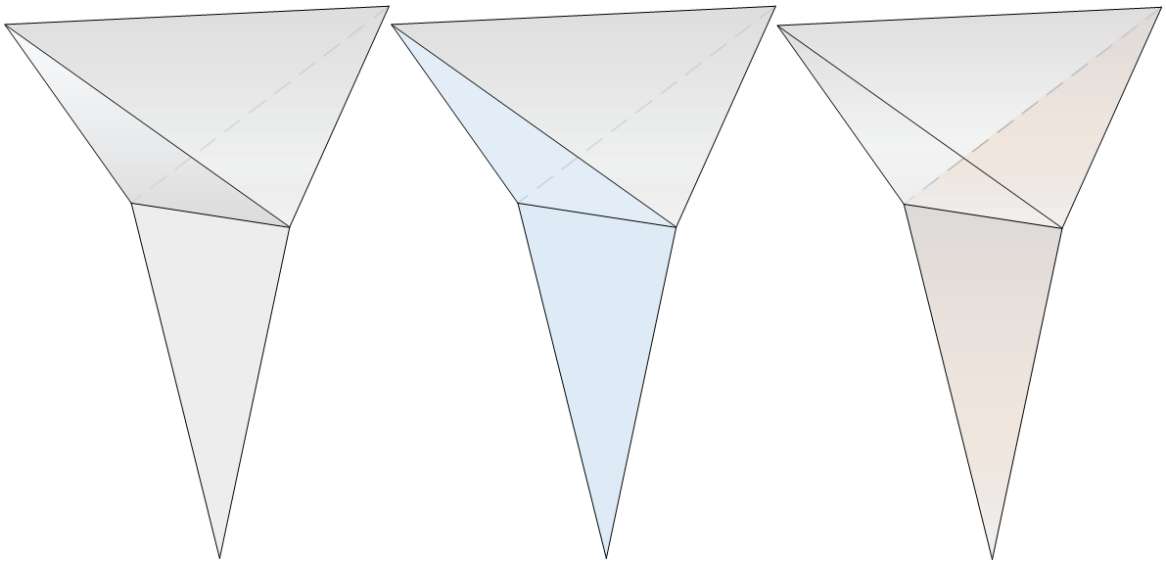

(b) The near-polyhedron for the Steffen flexible polyhedron from a different view point to show the hinge. The dihedral coloured in blue on the left is to be replaced by a crinkle; the dihedral coloured in orange on the right is to be replaced by another identical crinkle.

Fig. 1.5 The Steffen flexible polyhedron and its near-polyhedron

near-polyhedron has clashes. Its triangular flap can be regarded as double layers, linked only along two edges but not the hinge. Then this near-polyhedron is a closed surface with some faces touching each other. To avoid the touch, the touching faces are replaced by crinkles. The near-polyhedron has two dihedrals to be replaced: in Figure 1.5b they are coloured in blue on the left and in orange on the right. These two dihedrals share both the hinge and the triangle flap. When these two dihedrals are replaced, the crinkles are placed carefully to avoid each other. Figure 1.6 shows such replacement and the resultant Steffen flexible polyhedron. The polyhedron is able to bend about hinge 3-4.

In 2011, an origami researcher, Tachi, configured another flexible polyhedron that is also very simple[1]. It has only one more vertex than Steffen's. It also involves the replacements by crinkles. The only difference is that its near-polyhedron is composed of two tetrahedra as shown in Figure 1.7. Therefore, this flexible polyhedron is here called the *two-tetrahedron flexible polyhedron*. The two tetrahedra in the near-polyhedron share an edge. The sharing edge is the hinge that the polyhedron bends about. The dihedral coloured in blue on the left is again to be replaced by a crinkle as Figure 1.8 shows; the dihedral in orange on the right is to be replaced by another crinkle. The result replaces the sharing hinge, shown as a dashed line in Figure 1.8.

Both the Steffen flexible polyhedron and the two-tetrahedron flexible polyhedron are simple and have considerable range of movement. They have only one and two vertices more than a cube respectively. They are both triangulated. Triangulated polyhedra can have their polygonal faces (triangular panels) removed but still retain the same kinematic property. Therefore, studying triangulated polyhedra might help understanding the rigidity of truss structures. This dissertation is interested in understanding these two flexible polyhedra and tries to improve their range of rotation. Further, different flexible polyhedra may easily be produced from the same components — different near-polyhedra and crinkles.

1.3 Structure of the dissertation

The discovery of flexible polyhedron and previous improvements are explained in Chapter 2. To improve the flexibility of polyhedron, this dissertation uses a set of numerical tools. These tools are described in Chapter 3 using as examples the Steffen and Tachi flexible polyhedra. This chapter describes how to establish a computational model and measure the range of movement of a flexible polyhedron; then an optimisation method is used to maximise the range of movement. Chapter 4 describes the Steffen flexible polyhedron in detail and maximises its range of movement. A multi-objective optimisation was conducted

[1] Personal communication

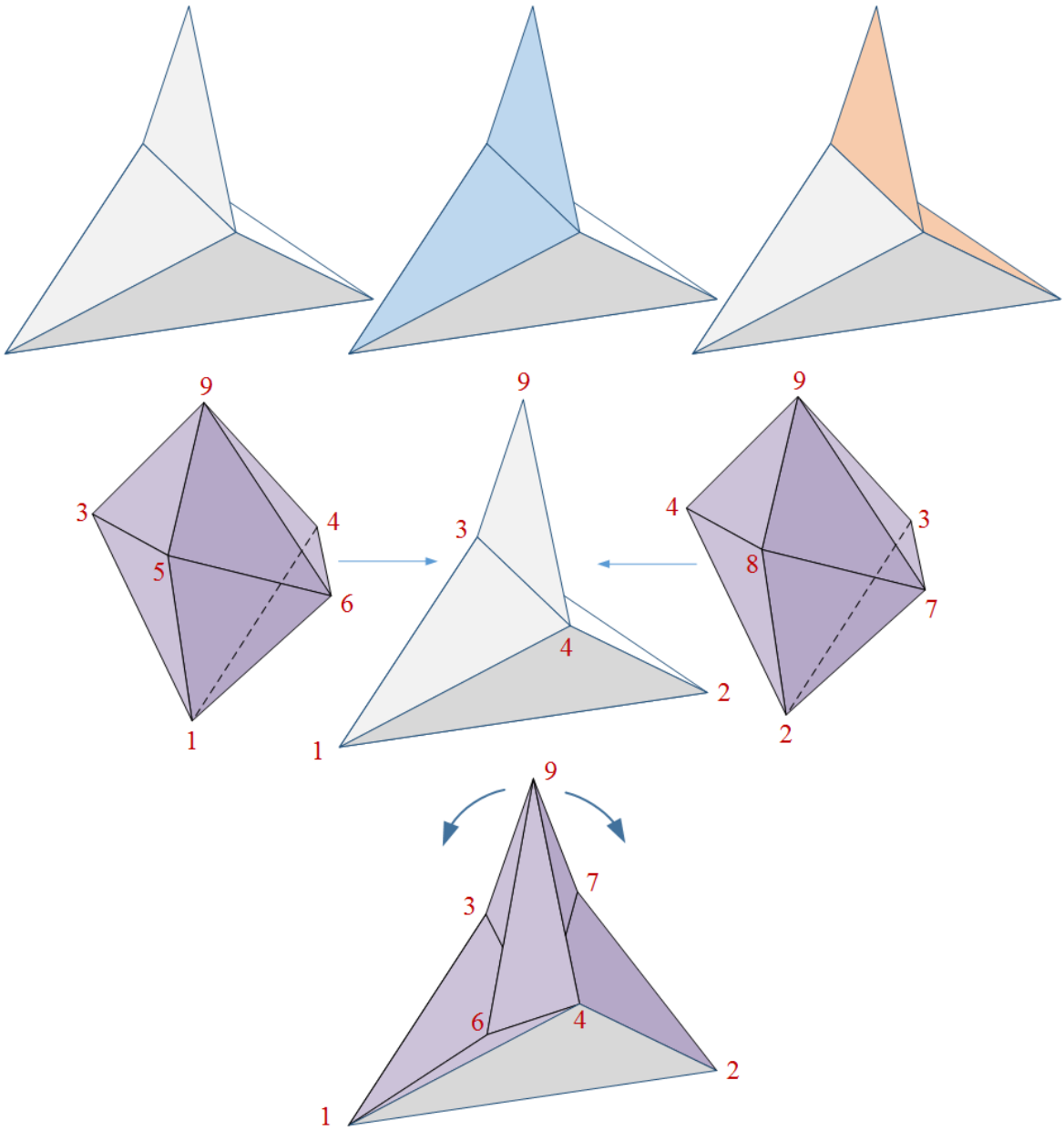

Fig. 1.6 Replacement of dihedrals by crinkles of the Steffen flexible polyhedron. The two identical crinkles (represented in purple) replacing two dihedrals (coloured in blue and orange respectively). When the dihedral 1-3-9-4 is replaced by the left crinkle, and dihedral 2-3-9-4 is replaced by the crinkle on the right, the near-polyhedron only has two triangle faces left: △1-2-3 at the back and △1-2-4 at the front. The hinge 3-4 is removed by replacement with these two crinkles. The resultant polyhedron is able to rotate about the same hinge 3-4 as the near-polyhedron. The length of hinge 3-4 does not change during the motion.

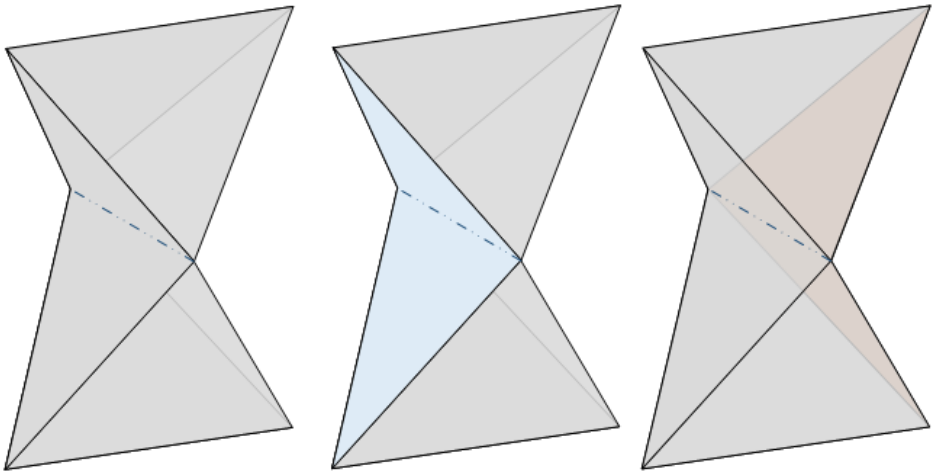

Fig. 1.7 Near-polyhedron of the flexible polyhedron created by Tachi. It is composed of two tetrahedra. These two tetrahedra are linked by one sharing edge as a hinge. The dihedral on the left (coloured in blue containing the hinge) is to be replaced by a crinkle; the dihedral on the right (coloured in orange bending about the same hinge) is to be replaced by a crinkle too.

to both improve the range of movement and regulate the shape. Chapter 5 presents the two-tetrahedron flexible polyhedron extended from Tachi's discovery: the composition of this type of polyhedron is explained in more detail; a parameter scheme is given from previous understanding of the Steffen flexible polyhedron; the polyhedron is also optimised to find the maximal range of motion with controlled regularity. Chapter 6 presents new discoveries of multiple degrees of freedom in a single polyhedron: the range of motion of a two-dof polyhedron is presented; a unit cell of a repetitive flexible polyhedron is presented. This unit cell is able to form any number of degrees of freedom, hence an n-dof flexible polyhedron is produced. This might enable a flexible polyhedral torus that is able to flex without the need to stop. Chapter 7 concludes on improvements and discoveries the dissertation has made, and expects potential work that can be done in the future. The relationship among the chapters is presented in Figure 1.9.

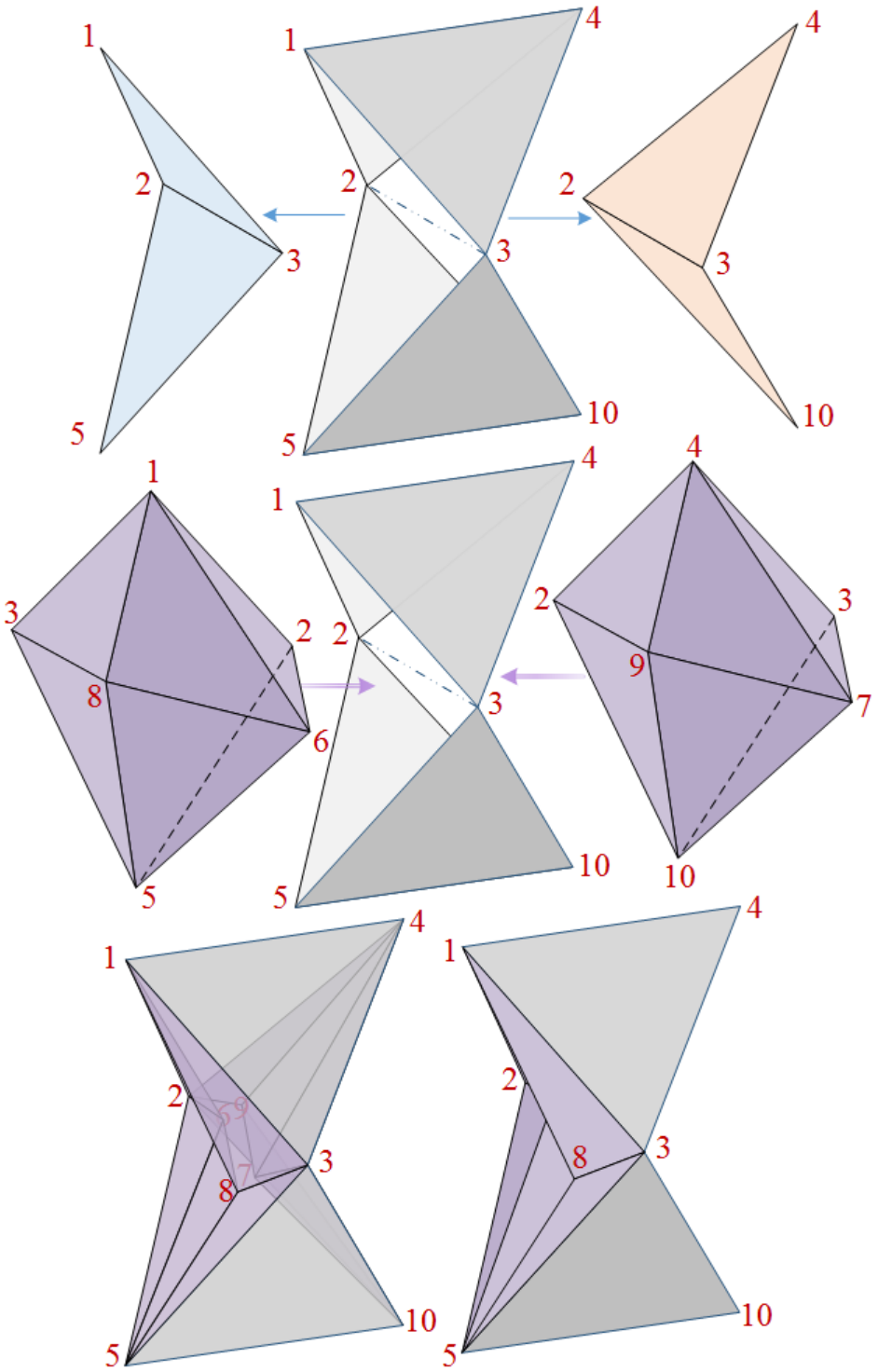

Fig. 1.8 Replacement of dihedrals by crinkles in the two-tetrahedron flexible polyhedron. The dihedrals to be replaced are taken out of the near-polyhedron. Two crinkles represented in purple are inserted. The dihedral represented in blue is replaced by the crinkle coloured in purple on the left; this crinkle flexes about the same line 2-3. The dihedral in orange is replaced by another crinkle in purple on the right. The resultant polyhedron is still able to flex about line 2-3. From the semi-opaque image, a gap between edge 6-8 and edge 7-9 can be observed.

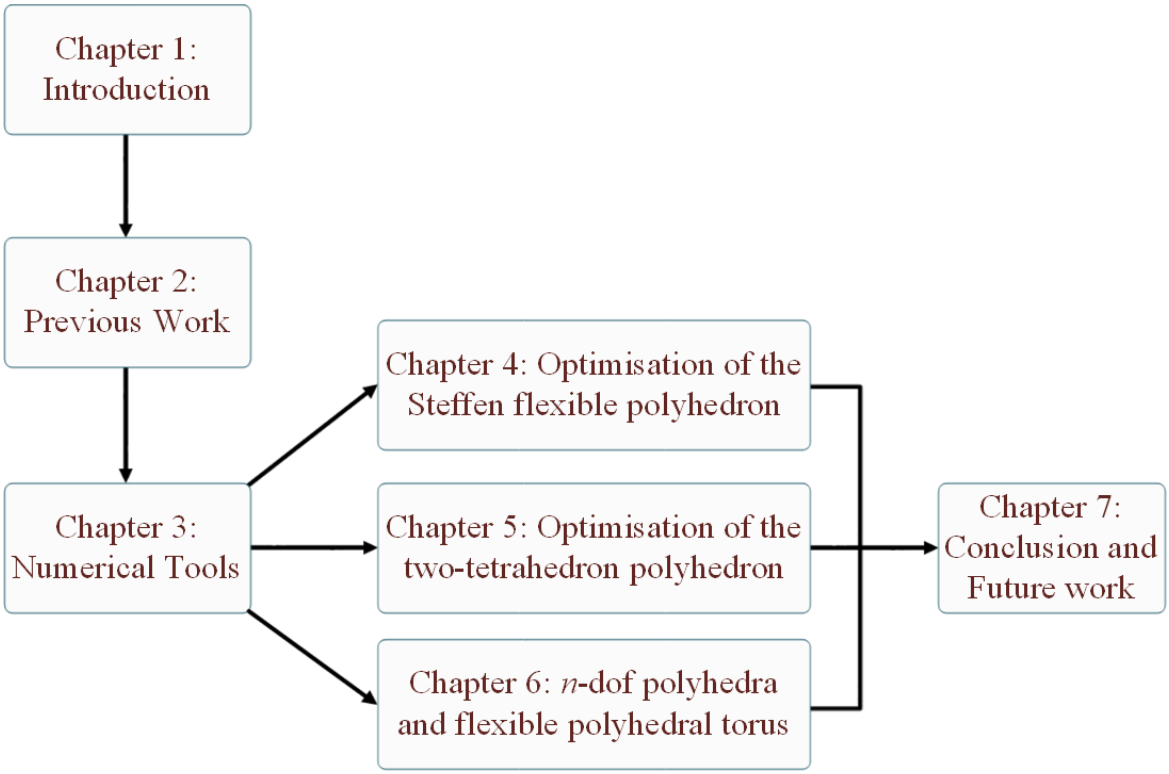

Fig. 1.9 Structure of the dissertation. Chapters 4, 5 and 6 use the numerical tools described in Chapter 3 to improve the range of movement the one-dof simplest flexible polyhedra or to find multiple-dof flexible polyhedra.

Chapter 2

Previous work

This chapter describes the discovery of flexible polyhedra in detail. It will first introduce the mathematical idea of polyhedron more formally from a geometric point of view; it will then introduce the mathematical term — flexibility — from an engineering view point (Section 2.1). Based on these concepts, it will tell the story of human understanding of the rigidity or flexibility of polyhedra in mathematics (Section 2.2). Then, an important octahedron — Bricard flexible octahedron — will be described in detail (Section 2.3). Following on, a derivative of Bricard flexible octahedron — a crinkle — will be introduced (Section 2.4). Finally, two types of simple flexible polyhedra enabled by the replacement with crinkles will be introduced (Section 2.5).

2.1 What is a flexible polyhedron?

A polyhedron here is defined as a closed surface, isomorphic[1] to a sphere, embedded in 3-dimensional space, composed of rigid polygonal faces whose edges are linked freely by hinges. These polygons share common edges; the edges are connected in such a way that the polygonal faces have potential to move in relation to one another and bend freely about the edges like a door rotates about its hinge. The facets of the polygons are stiff, so the polygons are unable to deform. The overall closed polygonal surface is then usually found to be rigid.

A polyhedron being able to $flex$ or being $flexible$ means the overall closed polyhedron is able to distort so that its polygons relatively rotate about their edges without any distortion of the polygonal faces. This property is called $flexibility$ in mathematics as opposed to *rigidity*. In engineering, this would be considered as 'finite mechanisms'. In other words, a flexible polyhedron possesses kinematic degrees of freedom apart from the six free-body motions.

[1] If a polyhedron is isomorphic to a sphere, then such a structure has the same topology as a closed sphere but consists of flat polygons.

In both the Steffen flexible polyhedron and the two-tetrahedron flexible polyhedron described in Chapter 1, the underlying motion is a relative rotation of two parts of the polyhedron. The range of this rotation is called the *range of motion* in this dissertation. To measure the range of this rotational movement, this dissertation fixes part of the polyhedron to constrain free-body motions and calculates the positive and negative rotational angles before clashes occur. The difference between the two limiting values of rotation is the range of motion.

2.2 History of flexible polyhedra

Polyhedra have been long regarded as rigid. Two centuries and a half ago, Leonhard Euler [13] concluded in his memoirs on geometry, "Unde quatenus superficies sphaerica est integra, nullam mutationem admittit". In English this sentence can be understood as, "To the extent that a spherical surface is integral, no motion is allowed." Connelly [11] translated this conclusion of Euler's as, "A closed spacial figure allows no changes, as long as it is not ripped apart." This is a conclusion on the rigidity of closed surfaces. Since polyhedra are closed spherical surfaces, Connelly said that Euler "apparently thought" polyhedra are rigid.

It turns out that most polyhedra are indeed rigid. Gluck [15] proved this two centuries after Euler, "Almost all simply connected closed surfaces are infinitesimally rigid, hence rigid." [11] This is saying that polyhedra are *generically* rigid. Any random polyhedra that one can think of (as shown in Figure 2.1) are, with probability 1, going to be rigid. Although the polygons are simply connected by hinges that allow free rotations, none of these hinges is actually able to rotate. A very common and simple example (although not generic) is a cube, shown in Figure 2.2a.

Euler's conjecture in 1766 [13] is "one of the oldest unsolved problems in geometry" [15]. Neither a proof nor a counterexample was found until half a century later in 1813 Cauchy proved that convex polyhedra are all rigid [5, 7, 11], which formed the foundation of rigidity theorems. A convex polyhedron has all vertices extending outwards, as opposed to a concave polyhedron, which has at least one vertex hollowed inwards. In Cauchy's proof, a strictly convex polyhedron with rigid edges and flexible joints has neither infinitesimal flexibility nor continuous finite mechanisms, as the convex polyhedra in Figure 2.1a and Figure 2.2a are. However, whether all concave polyhedra are also rigid or not was still unknown; hence, it was still not known whether all polyhedra are rigid. Euler's conjecture remained unproven.

Another half a century later, in 1864 Maxwell [19] found a counting method to determine the rigidity of frames. Whether it is convex or concave, by counting the number of joints and the number of bars, a simple equation can define a frame as rigid or flexible. This

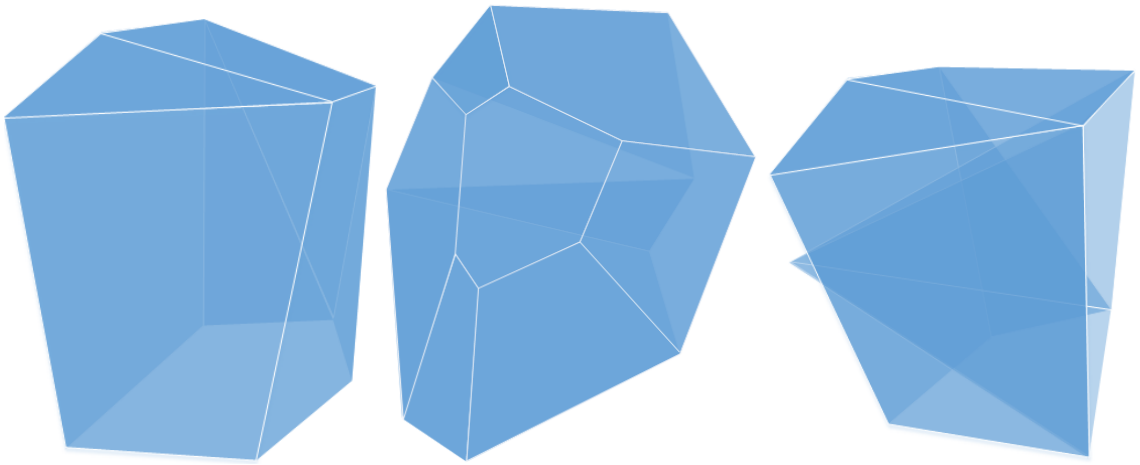

(a) A convex polyhedron (b) A concave polyhedron (c) A concave, self-intersected polyhedron

Fig. 2.1 Generic examples of rigid polyhedra (composed of stiff polygons)

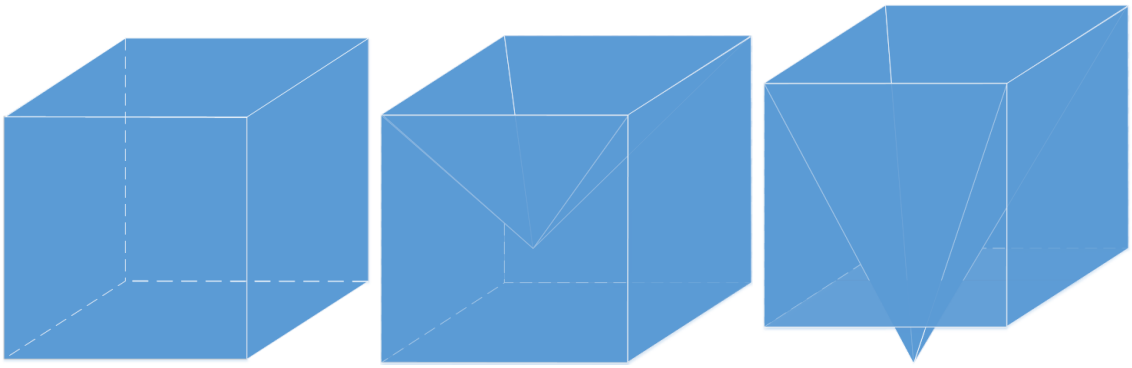

(a) A cube is a convex polyhedron (b) A concave polyhedron (c) A concave polyhedron that intersects itself

Fig. 2.2 Particular examples of rigid polyhedra, to demonstrate that a concave and self-intersected polyhedron is likely to be rigid. (a) A cube is a common, simple, rigid polyhedron, although not generic. Extended from this simple example, a concave polyhedron (b) and a self-intersecting polyhedron (c) are shown, which are both rigid.

rule is the well known Maxwell's rule in structural engineering for identifying the rigidity of truss structures. A triangulated polyhedron has the same *kinematic determinacy* or *indeterminacy* [21] as its frame. This is because a triangular frame is as rigid as a triangular face, so whether a triangulated structure has rigid faces or not, it does not change the rigidity or flexibility. Therefore, Maxwell's equation can be used to determine whether triangulated polyhedra are rigid. However, Maxwell's rule fails to predict the flexibility of triangulated polyhedra discussed in this dissertation, which will be shown in detail in Chapter 3. Specifically, Chapter 3 will demonstrate how Maxwell's rule predicts them as rigid whereas modified Maxwell's equations [21] allow that these structures each have a mechanism.

Three decades after Maxwell, the discovery of Bricard flexible octahedra exemplifies one way in which Maxwell's rule may fail to predict the flexibility of triangulated polyhedra. In 1897, a French engineer and mathematician, Raoul Bricard [3], found three types of flexible octahedra. The special ways to construct them ensure that they each have one redundant constraint in the system. That redundancy, according to modified Maxwell's equations, allows one degree of freedom. They are completely closed surfaces, yet they are able to rotate about some edges for even 360°, as Figure 1.4 showed earlier. However, this does not disprove Euler's conjecture, because these flexible octahedra are self-intersected, so they are not embedded in 3-dimensional space but 4-dimensional space.

However a century later, in 1976 Connelly derived "crinkles" from Bricard flexible octahedra. With the use of a crinkle, he created the first flexible polyhedron embedded in 3-dimensional space [10]. This counterexample finally proved Euler's conjecture untrue. Soon afterwards, in 1978 Steffen found the simplest known triangulated flexible polyhedron. In 2011 Tachi found the second simplest known triangulated flexible polyhedron. This dissertation finds that Tachi's polyhedron has more potential to increase the range of motion and also to form the near-polyhedra of new flexible polyhedra which have more than one degree of freedom. These are the only flexible polyhedra known to the author, whose motion is all due to the use of crinkles.

Another half a century after Connelly, this dissertation aims to make a flexible polyhedron a commonly existing object and to enable engineers to take advantage of its mathematical properties, such as constant volume, which will be introduced in the following section. This dissertation improves the range of rotation of existing flexible polyhedra from 27° to 80° and shows that any degrees of freedom are possible in one polyhedron.

2.3 Bricard flexible octahedra

This section provides a detailed description of the compositions of all three types of Bricard flexible octahedra, and shows their self-intersection, symmetry, redundancy and mechanism. Based on the properties of these Bricard flexible octahedra, corresponding crinkles will be introduced in detail in the next section.

A Bricard flexible octahedron is a concave octahedron that is self-intersected. Previously, it is discussed in Figure 2.1 and Figure 2.2 that any polyhedron, whether concave or self-intersected, is highly likely to be rigid. A simple example of a rigid, although not generic, polyhedron is a cube. With solid faces, as shown in Figure 2.2a, it is rigid. When it becomes a concave polyhedron as shown in Figure 2.2b, it is still rigid, no matter it self-intersects (Figure 2.2c) or not. Furthermore, in Figure 2.3 octahedra are presented to show the difference between any octahedron and a Bricard octahedron. Figure 2.3a shows a regular octahedron. It is a convex polyhedron and is rigid. When one vertex is pushed into the octahedron as shown in Figure 2.3b, so that it becomes a concave octahedron, it is still rigid. If the vertex is pushed not just into the octahedron but also through some of the faces as Figure 2.3c shows, it becomes a self-intersected octahedron. This still does not enable the flexibility. However, a Bricard octahedron is both concave and self-intersected. This section shows what gives the flexibility to a Bricard octahedron and makes it different from the concave, intersected octahedron in Figure 2.3c.

Bricard flexible octahedra are the world's first polyhedra that have a finite mechanism, although they are not embedded in 3 dimensional space due to intersections. They are

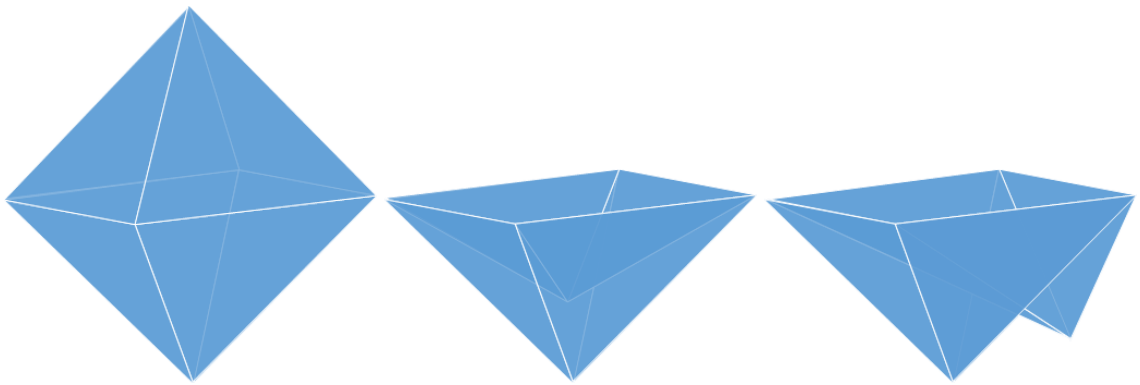

(a) A regular octahedron, convex (b) A concave octahedron (c) A self-intersected octahedron

Fig. 2.3 Examples of rigid octahedra. A regular octahedron is a rigid convex polyhedron; generically a concave octahedron is also rigid; even if the concave octahedron becomes self-intersected, it is still rigid. However, a Bricard octahedron is concave and self-intersected, but is flexible.

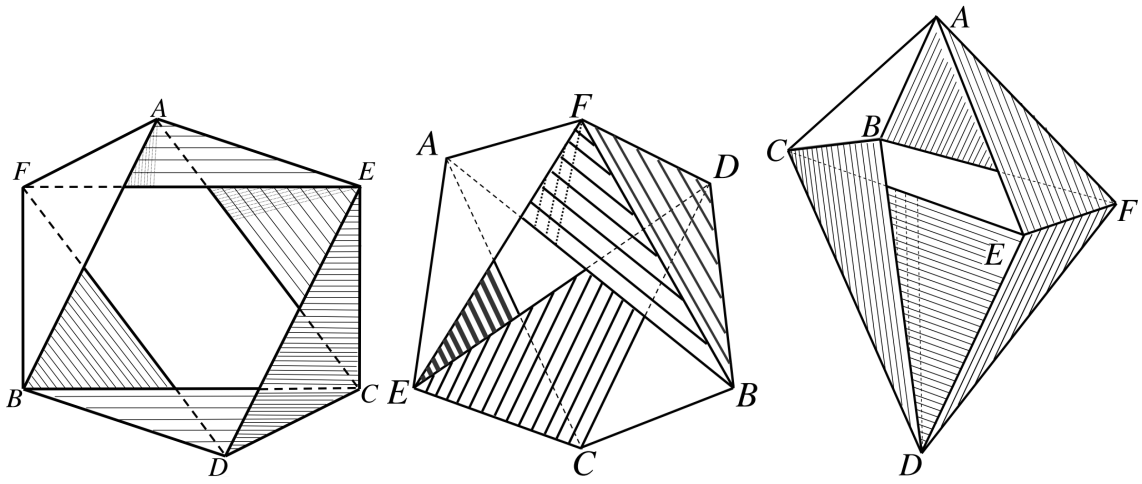

(a) A Type I Bricard flexible octahedron. Faces $\triangle ABC$ and $\triangle DEF$ are not shown.

(b) A Type II Bricard flexible octahedron. Faces $\triangle ABC$ and $\triangle DEF$ are removed.

(c) A Type III Bricard flexible octahedron. Faces $\triangle ACE$ and $\triangle BDF$ are omitted.

Fig. 2.4 Three types of Bricard flexible octahedra, each with two intersecting faces removed. Figures are taken from Bricard's original work [3]. There are eight triangles in an octahedron; Bricard shows six triangles only in each drawing to avoid showing intersections.

triangulated, composed of eight triangles. The drawings of them by Bricard are presented in Figure 2.4. In Bricard's drawing, two faces are removed in order to draw them without showing intersections. Since each edge connects two faces, the Bricard octahedron is a closed spacial figure. Because of the self-intersection, there is a positive volume and a negative volume in each Bricard octahedron, which are of the same amount no matter how the octahedron flexes [2]. Therefore, the overall volume of a Bricard flexible octahedron is constantly zero.

Not only is the volume of Bricard flexible octahedra constant, the volume of all polyhedra, rigid or flexible, has been shown to be invariant. There is the well known Bellows Conjecture [12] [26] (now Theorem), "It was observed that the volume enclosed by the surfaces stays constant during the deformation, and this leads to the following general conjecture: 'The generalized volume of a flexible polyhedron in $\mathbf{R}^n$ stays constant during a continuous flex.' " The Bellows Conjecture states, "Every orientable closed polyhedron (even with self-intersections) flexes with conservation of volume." [1]. This is proven by Sabitov [22] in 1995 for $\mathbf{R}^3$. Then afterwards, "Subsequent research has been based on his ideas."[26] The volume of all three types of Bricard octahedra is proven to be constant and equal to zero in 2011 [2], "We prove that the Dehn invariants of any Bricard octahedron remain constant during the flex and that the Strong Bellows Conjecture holds true for the Steffen

flexible polyhedron." Polyhedra also have many other constant properties in mathematics. The property of constant volume has great engineering potential in, for example, space exploration or under ocean work. For a closed structure containing gas or liquid, polyhedron guarantees no pressure change on inside and outside the faces of the structure while flexing.

Bricard flexible octahedra should be rigid according to Maxwell's rule, whereas modified Maxwell's rule allows that they can be flexible. Here modified Maxwell's rule is used to show what provides the flexibility.

It might be helpful to be reminded of Maxwell's rule [19] and modified Maxwell's rule [4] [21]. Maxwell's rule states that in a 2D or 3D frame system, if the number of dimensions d, the number joints j, the number of bars b and the number of external constraints k satisfy this equation $b-dj+k=0$, then this frame should be rigid, having no mechanisms. This is true for generic frames. For special cases, modified Maxwell's rule has a more general application. It considers the number of states of self-stress s, i.e. redundancies, and the number of mechanisms m, and includes them into the equation $b-dj+k=s-m$. As a result, even when Maxwell's rule suggests a system as rigid, $b-dj+k=0$, modified Maxwell's rule suggests that it must have the same number of redundancies and mechanisms, $s-m=0$.

A triangulated octahedron without triangular faces is a triangulated frame with 12 bars. There are six joints, A, B, C, D, E and F in each octahedron in Figure 2.4, and 12 bars, AF, DC, AB, DE, DB, AE, DF, AC, BF, CE, FE, BC. In three dimensions $d=3$, six joints $j=6$, between 12 bars $b=12$, with six free-body motion constraints $k=6$, give that Maxwell's equation is satisfied, $b-dj+k=12-3\times 6+6=0$, hence this frame is supposed to be rigid. However, this structure obviously has a large movement by observation, which was shown in Figures 1.2–1.4 and will be shown with physical models in subsections. According to modified Maxwell's rule, $b-dj+k=s-m=1-1=0$, the structure has to have one redundancy to allow this degree of freedom. These redundancy and degree of freedom are unforeseen by Maxwell's rule. The following subsections show what gives this redundancy to each type of Bricard octahedron and what the motion of the degree of freedom look like.

2.3.1 Type I: Line-symmetric

The first type of Bricard flexible octahedron has a line of symmetry according to Bricard's description [3]. This line of symmetry is presented by a C_2 axis in Figure 2.5a, through the midpoints of AD, BE and CF and perpendicular to them. Note that the notation for n-fold rotational symmetry is C_n and that a C_n operation rotates everything for $\frac{360^\circ}{n}$. This C_2 axis of rotation for 180° renders the 6 vertices, 12 edges and 8 faces in pairs. For example, in Figure 2.5a, vertex A rotated 180° about C_2 becomes vertex D; edge AF similarly becomes

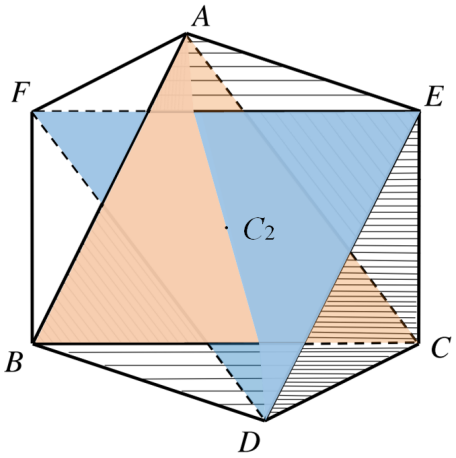

(a) A Type I octahedron drawn by Bricard [3], as shown in Figure 2.4a, with the label of a C_2 axis added. The originally omitted intersecting faces, $\triangle ABC$ and $\triangle DEF$, in Bricard's drawing are re-drawn in coloured panels in order to demonstrate the intersections.

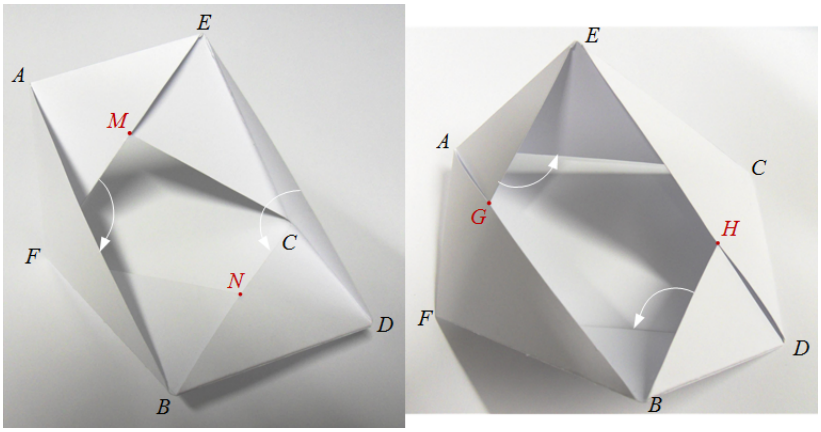

(b) Cardboard model of the Type I Bricard octahedron in (a), showing the movement with the two end positions of this physical model. $\triangle ABC$ and $\triangle DEF$ are removed as in Bricard's original drawing in order to show the movement without intersections. The end position shown on the left is caused by two symmetric clashes at M and N. M is a clash between $\triangle AEF$ and $\triangle AEC$. The overlap of these two faces is $\triangle AEM$. According to the line symmetry, $\triangle DBC$ and $\triangle DBF$ clash at N. The overlap is $\triangle DBN$. From the position in the picture on the left to the position in the picture on the right, when the polyhedron flexes away from these two clashes M and N, it flexes continuously until the flex is stopped by the other pair of symmetric clashes, G and H. The white arrow on the left between $\triangle AFE$ and $\triangle AFB$ in the left picture indicates that these two triangles come together to a clash G in the right picture. The white arrow in the left picture on the right between $\triangle ECD$ and $\triangle BCD$ indicates that these two triangles come together to a clash H in the picture on the right. The white arrow in the right picture on the top indicates that $\triangle AEF$ and $\triangle AEC$ come together to a clash M in the picture on the left. The white arrow in the right picture at the bottom indicates that $\triangle FDB$ and $\triangle BDC$ come together to a clash N.

Fig. 2.5 A Type I Bricard flexible octahedron, line-symmetrical as constructed by Bricard [3], with $\triangle ABC$ intersects with $\triangle AEF$ and $\triangle DEF$, and $\triangle DEF$ also intersects with $\triangle BCD$.

edge DC; and $\triangle ABC$ becomes $\triangle DEF$. The same applies to the other lines and triangles as Equations (2.1) and (2.2) show respectively. There are then six pairs of lines and four pairs of triangles. Each pair of lines has equal length; and each pair of triangles is congruent.

$$AF = DC, \quad AB = DE, \quad DB = AE, \quad DF = AC, \quad BF = CE, \quad FE = BC \tag{2.1}$$

$$\triangle ABC \cong \triangle DEF, \quad \triangle AEF \cong \triangle DBC, \quad \triangle AFB \cong \triangle DCE, \quad \triangle FBD \cong \triangle CEA \tag{2.2}$$

This is a self-intersected octahedron. Its self-intersections are between two pairs of triangles: $\triangle AEF$ and $\triangle DBC$ and $\triangle ABC$ and $\triangle DEF$, observable in Figure 2.5a. $\triangle ABC$ intersects with $\triangle AFE$ and $\triangle FED$, and $\triangle DEF$ intersects with $\triangle ABC$ and $\triangle BCD$. Only six faces are shown in Bricard's original drawing, $\triangle AEF$, $\triangle DBC$, $\triangle AFB$, $\triangle DCE$, $\triangle FBD$ and $\triangle CEA$. To demonstrate the intersections, Figure 2.5a coloured the two faces omitted by Bricard. In the cardboard model in Figure 2.5b, these two faces are removed to avoid intersections of physical faces.

There is one redundancy in this octahedron. Any five pairs of equal edges will guarantee the equal distances of the sixth pair of edges. This is because any five equations in (2.1) will define the congruence of two pairs of triangles, which defines the symmetrical position of the six vertices. This symmetry guarantees equal lengths of all pairs of edges. Therefore, any one of the 12 edges is considered redundant. That is to say, when any edge of this Bricard octahedron is removed, the distance between the two vertices of this edge will still be invariant. This is guaranteed by the other five equations in (2.1). As discussed above, the satisfaction of Maxwell's equation, $b - Dj + k = 12 - 3 \times 6 + 6 = 0$ and the redundancy by symmetry require a mechanism for the balance of modified Maxwell's rule, $b - Dj + k = s - m = 0$. This unexpected mechanism is therefore produced.

To show the movement of this mechanism, a cardboard model of Bricard's Type I octahedron in Figure 2.5a is displayed in Figure 2.5b. It has the same omitted two faces as Bricard's choice and the omission makes it possible for this physical model to exist in 3-dimensional space. The two invisible triangles still have their frames invariable in shape, as their edges are shared with the edges of the other six physical faces. Figure 2.5b shows two end positions of the flexing: on the left, at one end, edge AC clashes with edge EF at M, and edge BC clashes with edge DF at N; on the right, at the other end, edge AB clashes with edge EF at G, and edge BC clashes with edge DE at H.

2.3.2 Type II: Plane-symmetric

A Bricard Type II flexible octahedron has a plane of symmetry as described by Bricard [3]. This plane contains line FC in Figure 2.6a and is perpendicular to AD and EB. According

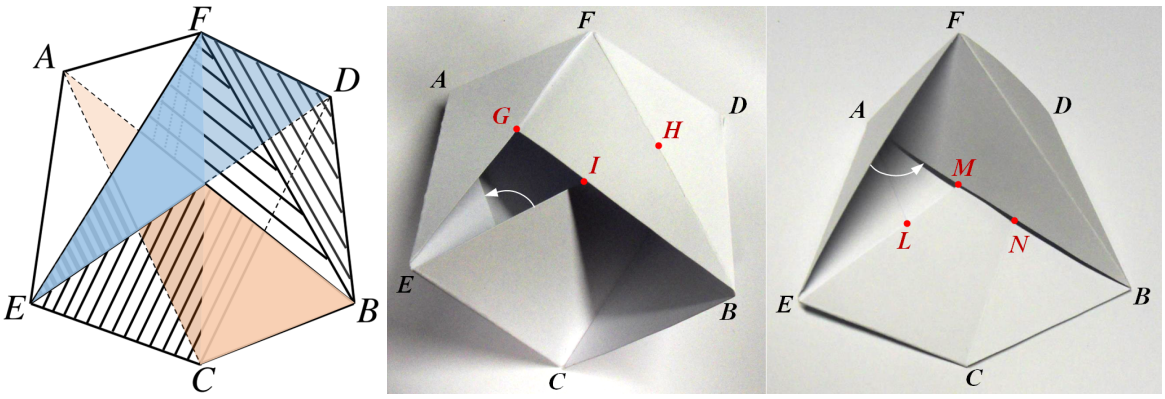

(a) A Type II octahedron drawn by Bricard [3], having a plane of symmetry through C and F, perpendicular to the page.

(b) Cardboard model of the Type II Bricard octahedron in (a), demonstrating the movement by showing the two end positions of the physical model. On the left, when $\triangle AEF$ clashes with $\triangle ABF$, $\triangle DBF$ also clashes against $\triangle DEF$; on the right, $\triangle AEC$ clashes with $\triangle DEC$, and $\triangle DBC$ with $\triangle ABC$.

Fig. 2.6 A Type II Bricard flexible octahedron, plane-symmetrical as constructed by Bricard [3], $\triangle ABC$ intersects with $\triangle DEC$, and $\triangle DEF$ intersects with $\triangle ABF$

to this plane of symmetry, there are six pairs of equal edges and four pairs of congruent triangles, as Equations 2.3 and 2.4 show.

$$AF = DF, \quad AE = DB, \quad EC = BC, \quad AC = DC, \quad FE = FB, \quad AB = DE \tag{2.3}$$

$$\triangle AFE \cong \triangle DFB, \quad \triangle AEC \cong \triangle DBC, \quad \triangle AFB \cong \triangle DFE, \quad \triangle ABC \cong \triangle DEC \tag{2.4}$$

As Equations (2.4) show that the eight symmetrical faces in pairs are $\triangle AFE$ and $\triangle DFB$, $\triangle AEC$ and $\triangle DBC$, $\triangle AFB$ and $\triangle DFE$, and $\triangle ABC$ and $\triangle DEC$ in Figure 2.6. The four intersecting faces are: $\triangle ABC$ with $\triangle DEC$, and $\triangle DEF$ with $\triangle ABF$. To avoid intersection, one triangle from each pair need to be removed. Bricard chose to remove $\triangle ABC$ and $\triangle DEF$ in his figure; the six faces remained are $\triangle AFE$, $\triangle DFB$, $\triangle AEC$, $\triangle DBC$, $\triangle AFB$ and $\triangle DEC$. In Figure 2.6a, the two removed triangles are coloured to show what the intersections are like; in the physical model in Figure 2.6b, the two triangles are removed to allow the model to flex in 3D.

There is one redundant edge in this octahedron. If any one edge is removed, the distance between the two vertices of the removed edge will be invariant. This is because any five pairs of equal edges will guarantee the equal length of the sixth pair of edges. This is due to the fact that any five pairs of equal edges define the symmetrical position of all six vertices. (For example, when the first five equations in Equations (2.3) are satisfied, the congruence of $\triangle AFE$ and $\triangle DFB$ and of $\triangle AEC$ and $\triangle DBC$ is ensured. Then, the plane symmetrical

arrangement of F, C, A, D, E and B is defined.) This symmetry guarantees equal lengths of all pairs of edges. Therefore, any one of the 12 edges is considered redundant. As for Type I Bricard octahedron, the satisfaction of Maxwell's equation, $b-Dj+k=12-3\times 6+6=0$ and the redundancy suggest that according to modified Maxwell's rule, $b-Dj+k=s-m=0$, there must be a mechanism for the balance. The unexpected mechanism of this octahedron is as a result explained.

To demonstrate the motion of this mechanism, a cardboard model of Bricard's drawing is shown by its side. Two end positions of this physical model are shown in respectively in the two pictures to illustrate the flexing movement. The omission of $\triangle ABC$ and $\triangle DEF$ makes it possible for this physical model to exist. These two invisible faces are, as for Type I, invariable in shape, because their edges are the edges of the other triangles: one edge of each existing triangle. In Figure 2.6b, on the left, one end is shown with edge AB clashing against edge EF at G and against edge DE at I; symmetrically, edge DE also clashes with edge BF at H. On the right, at the other end position, edge AB clashes with edge DE at M and with edge CD at N, and by symmetry edge DE also clashes with edge AC at L.

2.3.3 Type III: Doubly flat-foldable

A Type III Bricard flexible octahedron is a flat-foldable octahedron according to Bricard's description [3]. Alexandrov [2] described a way of constructing such an octahedron from three concentric circles in a flat position. As Figure 2.7a shows, first draw a circle of any radius, K_C, and then a tangential quadrilateral of this circle, $A_1B_1A_2B_2$. Secondly, draw another circle of a random radius, K_A, to be concentric with K_C. Then, also draw a tangential quadrilateral of K_A by using the vertices B_1 and B_2, so that the tangential quadrilateral of K_A is $B_1C_1B_2C_2$. Lastly, link A_1C_1, C_1A_2, A_2C_2 and C_2A_1. Now, treat $A_1C_1A_2C_2$ as a self-intersected quadrilateral in 2 dimensions. It has an incircle, K_B, which is again concentric to K_A and K_C, and is tangential to A_1C_2 and C_1A_2 and the extension lines of A_1C_1 and A_2C_2. The six vertices A_1, A_2, B_1, B_2, C_1 and C_2, and the 12 edges of the three quadrilaterals, along with the 8 faces $\triangle A_iB_jC_k$ for any choices of i, j, k, $\in \{1, 2\}$, form a Type III Bricard flexible octahedron.

A Type III Bricard octahedron is doubly flat-foldable. Flexing from the flat position in Figure 2.7a, the octahedron can come to another flat position. The process of flexing from this flat position to the other is shown in Figure 2.7b with a cardboard model. This cardboard model in Figure 2.7b is at the flat position in Figure 2.7a, at a middle position, and at another flat position from top to bottom. In the bottom flat position, the three quadrilaterals, $A_1C_1A_2C_2$, $A_1B_1A_2B_2$ and $B_1C_1B_2C_2$, have another three concentric incircles.

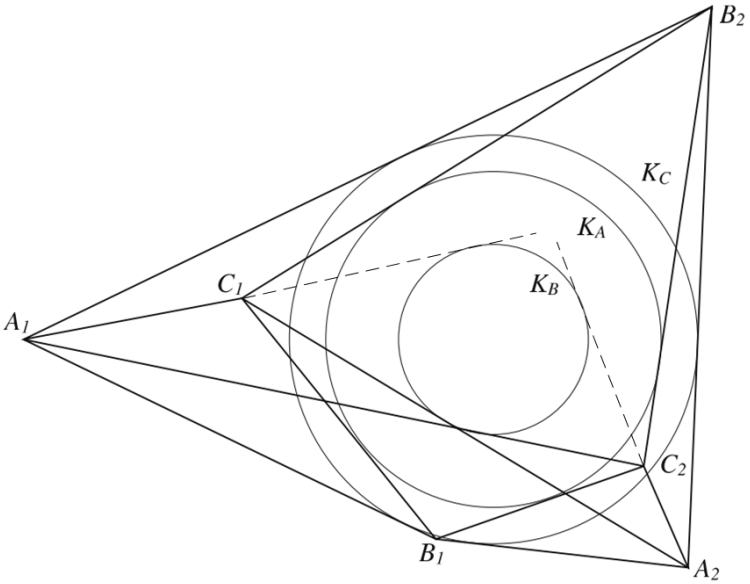

(a) Construction of a Type III Bricard octahedron from a flat position: draw three concentric circles K_A, K_B and K_C, and draw tangents from two points B_1 and B_2 to obtain A_1, A_2, C_1, and C_2. Figure taken from [2].

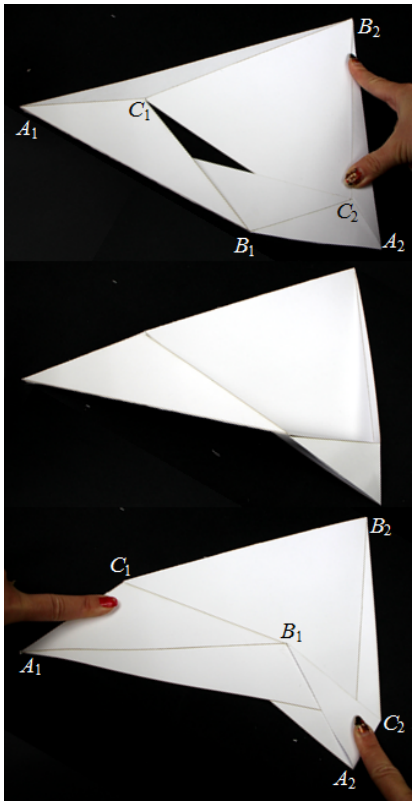

(b) The Type III octahedron constructed in (a), flexing from the flat position in (a) to the other, with $\triangle B_2A_1C_2$ and $\triangle C_1A_2B_1$ removed to avoid intersections.

Fig. 2.7 A Type III Bricard flexible octahedron, constructed from a flat position described by Alexandrov [2]

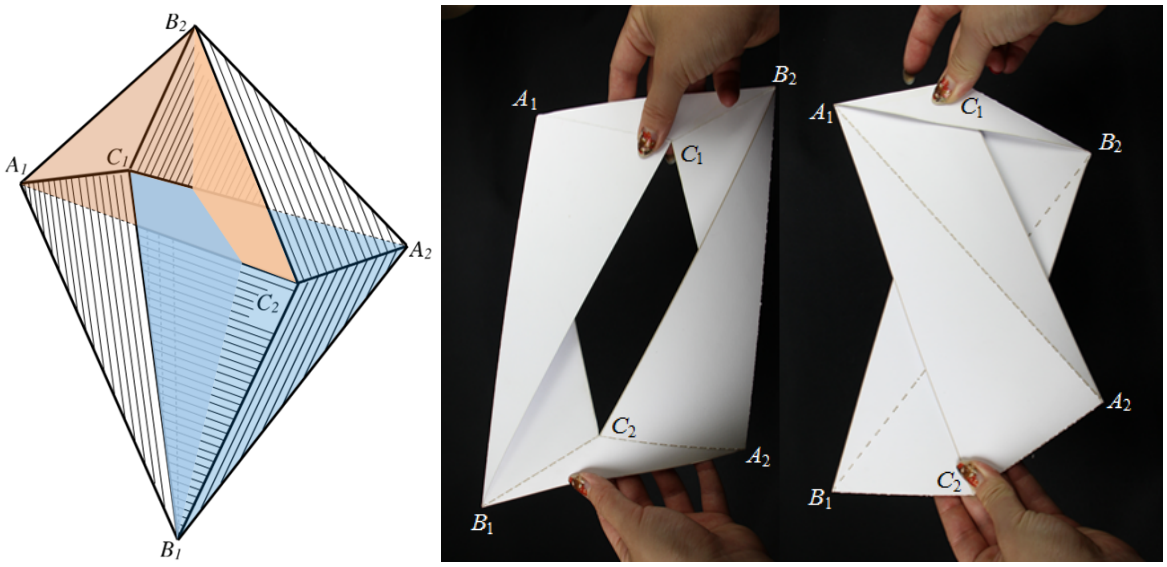

(a) A Type III octahedron drawn by Bricard. The originally removed faces $\triangle B_2A_1C_2$ and $\triangle C_1A_2B_1$ are coloured here to show the intersections. Vertices are re-notated from original drawing.

(b) Two flat positions of a doubly flat-foldable Type III Bricard octahedron, the folding pattern of which is downloadable from *http://www.cutoutfoldup.com/920-bricard-s-flexible-octahedron.php*. The same two triangles are removed as in (a) and Figure 2.7b, $\triangle B_2A_1C_2$ and $\triangle C_1A_2B_1$, in order show the physical model in 3D space.

Fig. 2.8 Two Type III Bricard flexible octahedra, one draw by Bricard, and the other available online.

In this model, two physical faces are removed to avoid self-intersections. These two faces are the same choices as Bricard's in his original drawing, shown in Figure 2.4c. However, in Figure 2.8a these two faces are coloured in order to demonstrate the self-intersections. When the octahedron in Figure 2.8a flexes from one flat position to another, C_1 moves from the right hand side of A_1 to its left by going out of the paper, and A_2 moves from the right hand side of C_2 to its left side by going into the paper.

As a Type III Bricard octahedron flexes from one flat position to another, all the faces rotate about their edges for 180°. This is observable in both Figure 2.7b and Figure 2.8b. In Figure 2.8b is another physical example, whose folding pattern is downloadable on *http://www.cutoutfoldup.com/920-bricard-s-flexible-octahedron.php*. The removed faces of this Type III octahedron is the same as in Figure 2.8a and Figure 2.7b.

2.4 Crinkled surfaces

The word 'crinkle' was first used by Connelly in 1977 [9] to describe a special surface. As its name suggests, this surface must have hills and valleys to provide a crinkled shape. The term

crinkle in flexible polyhedron is more than a simply crinkled surface. This section introduces what defines a crinkle and the flexible polyhedra enabled by crinkles.

2.4.1 What is a crinkle?

A crinkle is a derivative of a Bricard flexible octahedron. In the three types of Bricard flexible octahedra, it was mentioned that two faces of the four intersecting triangles need to be removed in order to show the octahedron in 3D space. In the previous section, two non-adjacent faces were chosen to allow the remainder to be a ring of triangles. Here if two adjacent faces are removed, the sharing edge is also removed along with the two triangles. The remainder is a crinkled surface of six triangles, as Figure 2.9 shows.

Vertices in Figure 2.9 are re-labelled from Bricard's drawings in Figure 2.4 in order to have a uniformed notation to discuss the composition of crinkles. A crinkle has a vertex that can be described as a "north pole", A, and a "south pole", D. This is similar to the regular octahedron in Figure 2.3a who obviously has a "top" vertex and a "bottom" vertex. Moreover, the regular octahedron also has a quadrilateral "belt" in the middle like an "equator". In fact, every octahedron can be considered to have a "north pole" vertex, a "south pole" vertex and a quadrilateral "equator". Each Bricard octahedron in Figure 2.9 has an equator of the quadrilateral $BCEF$. In the derived crinkles in Figure 2.9, the quadrilateral $BCEF$ lacks the

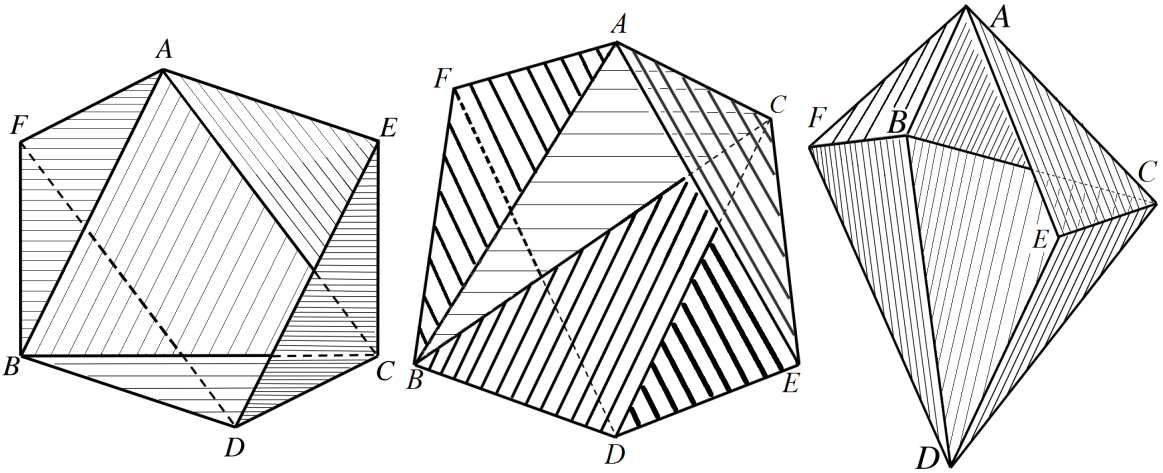

(a) A Type I crinkle (b) A Type II crinkle (c) A Type III crinkle

Fig. 2.9 Three types of crinkles derived from Bricard flexible octahedra, each with two adjacent triangles removed, $\triangle AFE$ and $\triangle FED$, along with the edge FE, instead of the two triangles described in Figure 2.4. The remained surface is crinkled: vertex B sticks outwards and vertex C goes into the paper. Figures modified from Bricard's work [3].

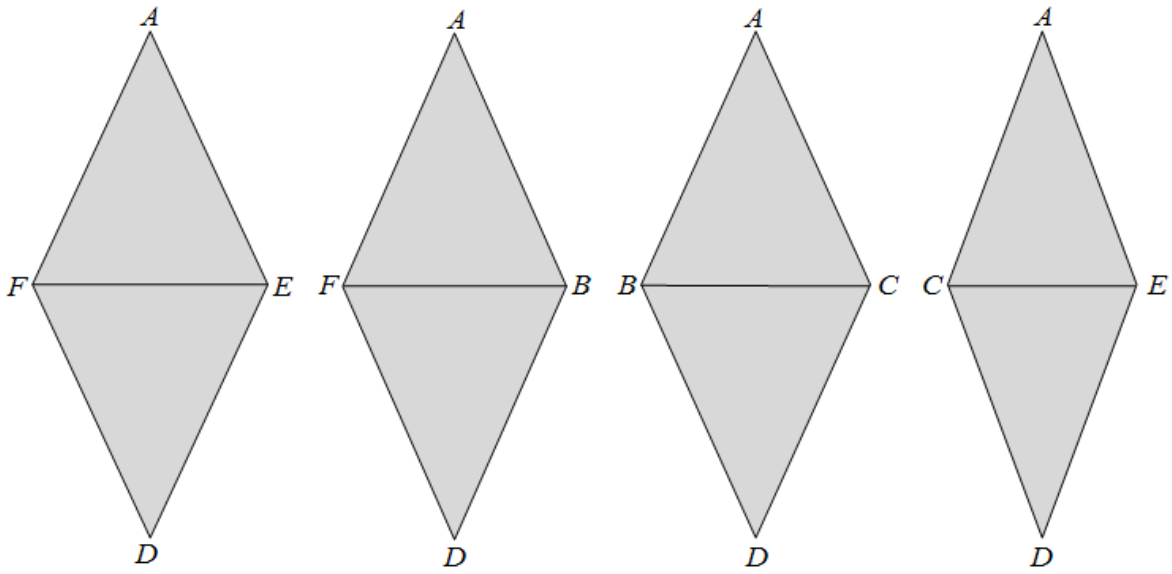

Fig. 2.10 The four dihedrals that compose an octahedron in Figure 2.9. In the crinkles in Figure 2.9, dihedral $AFDE$ is removed and dihedrals $AFDB$, $ABDC$ and $AEDC$ remain. The "north pole" is A; the "south pole" is D; the quadrilateral "equator" is $FBCE$.

edge FE. This is because when the adjacent $\triangle AFE$ and $\triangle FED$ are removed, one piece of the equator is removed, FE. The removed surface containing two triangles sharing a hinge is called a *dihedral* in this dissertation. A Bricard octahedron can be considered as being composed of four dihedrals where the hinges of the dihedrals form the equator. The four dihedrals are shown in Figure 2.10: dihedral $AFDE$ is removed in Figure 2.9; the remaining three dihedrals are $AFDB$, $ABDC$, and $AEDC$. A crinkle is given such a name, because of its "ridge" and "valley" that give a shape of a crinkled surface: in Figure 2.9 vertex B goes out of the page, while vertex C sticks inwards. Because crinkles are derivatives from Bricard octahedra, here the notation used for Bricard octahedra is applied to crinkles: they are similarly defined as a Type I crinkle, a Type II crinkle and a Type III crinkle.

To explain the relationship among the omitted dihedral, the crinkle, and the original Bricard octahedron, the process of producing a Type I crinkle by rotating a dihedral about any chosen line of symmetry, a C_2 axis, is shown in Figure 2.11. The dihedral before rotation is coloured in purple in (a – b), and the rotated dihedral in (c – e) and resultant crinkle in (f) are in orange. The final crinkle in (f) can replace the first purple dihedral in (a) in a surface. The crinkle in (f) also contains the rotated dihedral in (c – e). This crinkle has the same underlying mechanism as the dihedral $ABA'C$ (purple) shown in (a). It is still able to rotate about the virtual hinge BC.The distance between vertices B and C is invariant and is equal to $B'C'$. Here the notation of vertices A, B, C, A', B' and C' is used as opposed to the notation

used previously in this section in order to demonstrate the C_2 operation (180° rotation due to the line of symmetry) clearly. The line-symmetrical pairs of vertices are A and A', B and B', and C and C'.

A Type I octahedron is always line-symmetric, but can sometimes be plane-symmetric too. When it is plane-symmetric, it becomes doubly flat-foldable at the same time. However, its plane-symmetry and doubly flat-foldability is different from those of Type II and Type III. The Type I Bricard octahedron is plane-symmetric when edge BF and edge EC are parallel with the C_2 axis. As a result, its plane of symmetry contains vertices B, F, E and C; whereas a Type II octahedron contains vertices A and D. Overall, they are different planes of symmetry. A Type III octahedron rotates about each of the 12 edges for 180° from one flat position to another. This is observable in Figure 2.12. However, a Type I octahedron rotates about two central edges BC and FE for 360°, about two side edges BF and EC for 0° between two flat positions, and about eight edges for 180°. This can be observed in Figure 1.4 by the underlying octahedron of a Type I crinkle.

The Type III Bricard octahedron in Figure 2.7 and the Type III Bricard octahedron in Figure 2.8b are shown in the same folding sequence in Figure 2.12. The Type III Bricard octahedron in Figure 2.7 is constructed with the instructions described by Alexandrov [2] from a flat position; the Type III Bricard octahedron in Figure 2.8b is from an online sauce where cut-and-fold paper model can be downloaded. They both have the same two faces removed and the remainder is a ring of six triangles. They are shown in the middle two columns respectively in Figure 2.12. Additionally, another cardboard model of each of them with two adjacent faces removed instead is shown in the column by their side. The adjacent faces are chosen to be the same here: they are the dihedral $B_2C_1B_1A_2$ in Figure 2.7 and Figure 2.8. In each column, they are flexing from one same flat position to the other same flat position. They all rotate about each of the 12 edges for 180° during the whole process.

2.4.2 Replacement with crinkles

The replacement of a dihedral by a crinkle is demonstrated in this subsection because later flexible polyhedra are enabled with this kind of replacement.

A Type I crinkle can replace a dihedral in a dihedral surface. A *dihedral surface* is composed of two half-planes linked by a line as a hinge, as the dihedral surface K in Figure 2.13 and K and F in Figure 2.14. In Figure 2.13 the dihedral $AFDE$ in the dihedral surface K is replaced by its corresponding Type I crinkle from the same Bricard octahedron. Dihedral $AFDE$ is part of the dihedral surface K, containing part of the hinge line of K. It flexes about hinge FE as does K. Because dihedral $AFDE$ and the replacing crinkle are from the same octahedron, and the octahedron is able to flex about edge FE, when $AFDE$ is cut

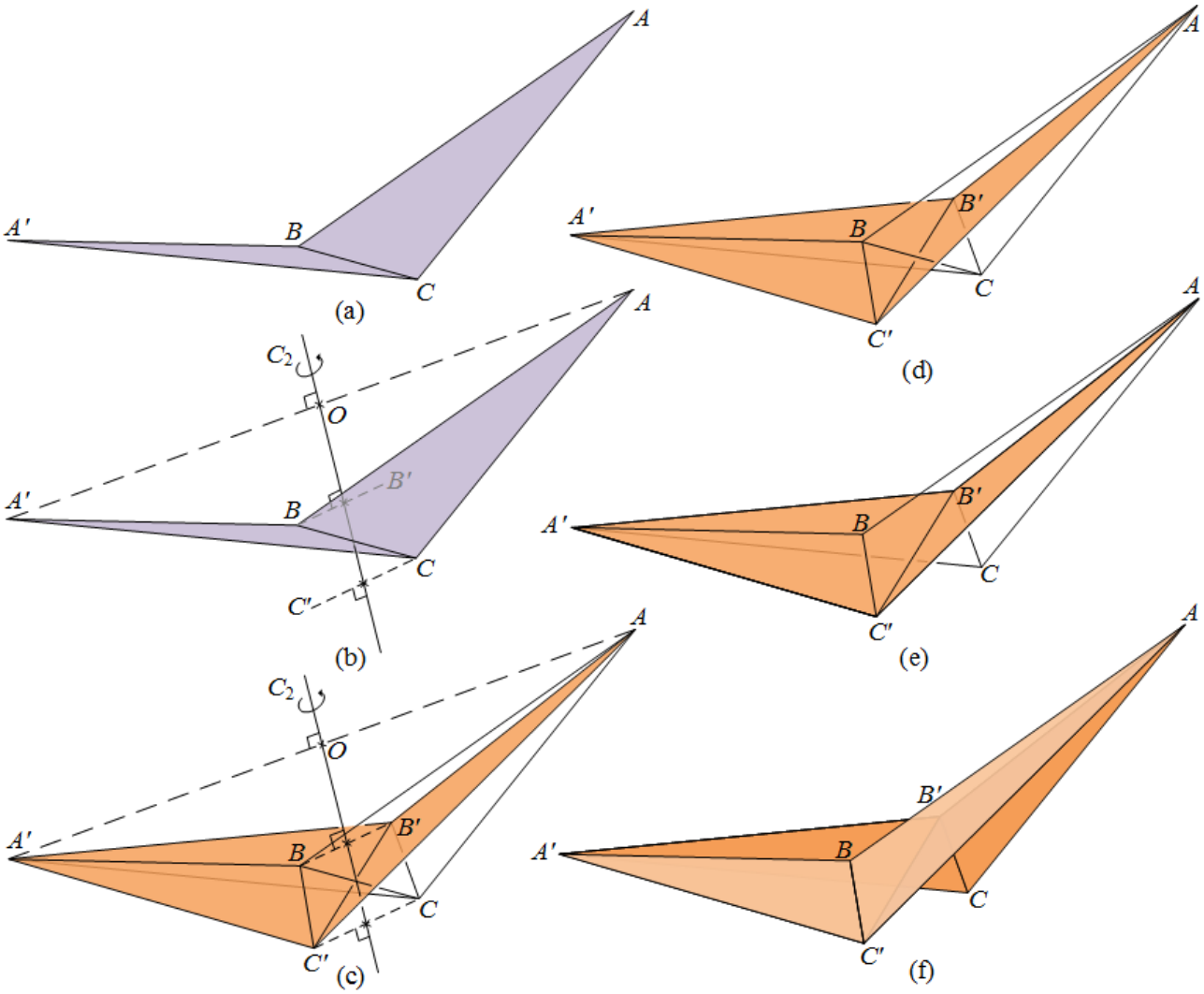

Fig. 2.11 Formation of a Type I crinkle by a line C_2 symmetry operation of a dihedral. (a) A dihedral: two triangular faces joined along a common edge BC, viewed from below. (b) A randomly chosen C_2 axis that is any perpendicular bisector of the line AA', in general not intersecting edge BC. The C_2 symmetry operation generates two additional vertices B' and C'. (c) Edges AB', AC', $A'B'$, $A'C'$, BC', $B'C$ and $B'C'$ are added to form the framework of a Type I Bricard octahedron where every pair of vertices are joined, except for the construction lines of symmetry AA', BB' and CC'. The original dihedral $ABA'C$ (purple) is rotated into dihedral $A'B'AC'$ (orange). (d) The framework of octahedron without the construction lines, containing the rotated dihedral $A'B'AC'$ (orange). (e) The hinge of the original dihedral BC is deleted. (f) The resultant Type I crinkle, where 6 faces are restored: the rotated dihedral $A'B'AC'$ and two side dihedrals $AB'A'C$ and $ABA'C'$. All figures (a – f) have the same underlying mechanism.

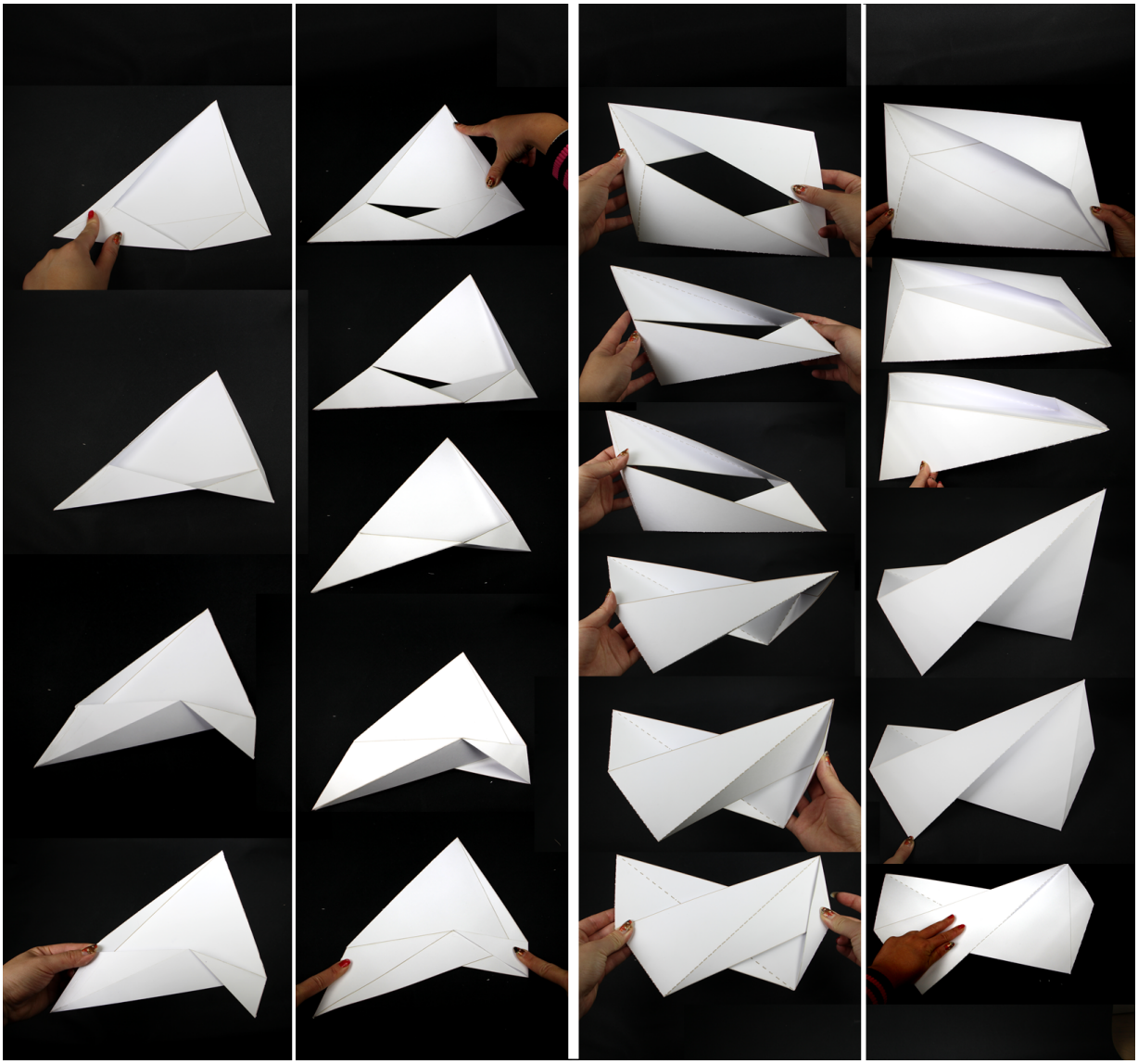

Fig. 2.12 Physical examples of two pairs of corresponding Type III crinkles and rings. In the first column is the crinkle constructed from Figure 2.7a; in the second column is the Bricard ring from the same pattern. The third column shows the Bricard ring online shown in Figure 2.8b; the last column shows its corresponding crinkle. For comparison, the underlying Bricard octahedra of all these four models are flexed from one equivalent flat position to the other equivalent flat position. Therefore, the eight panels of all these Type III Bricard octahedra are at the same positions during the this same process of folding.

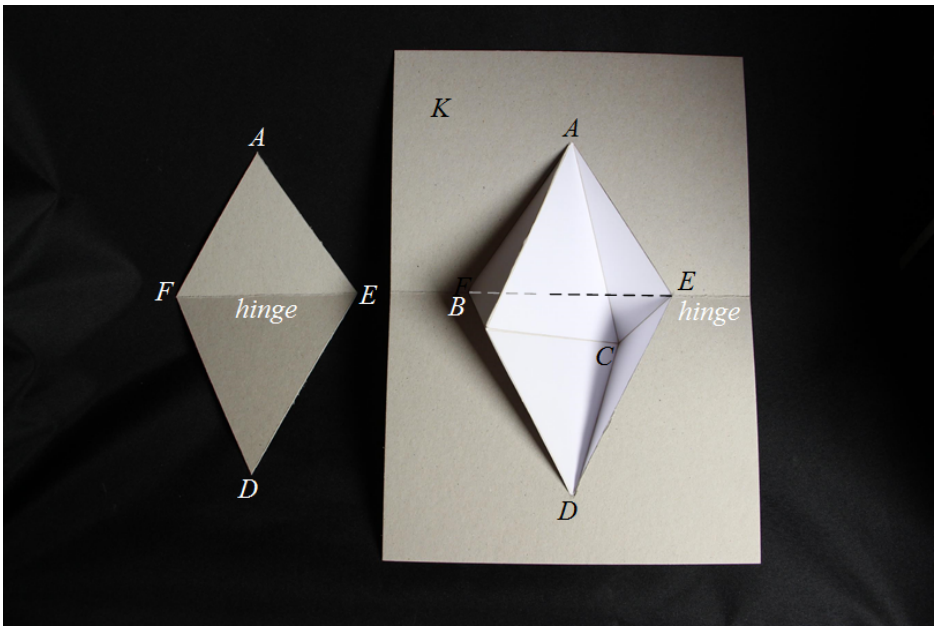

Fig. 2.13 Replacement of a dihedral $AFDE$ in a dihedral surface K with a Type I crinkle. The dihedral surface K is composed of two half-planes and the hinge line FE. The replaced dihedral $AFDE$ is part of the dihedral surface K; it is composed of two triangles $\triangle AFE$ and $\triangle FED$, sharing the hinge FE. The replacing crinkle bends about the same hinge, so the resultant surface bends about the original edge too, although FE becomes invisible, indicated in a dashed line. FE stays invariant during the flex. Vertex B sticks out of the page and vertex C goes behind the hinge FE. Hence, the dashed line FE is in front of $\triangle ACE$; it goes through $\triangle ABC$ and is hidden behind $\triangle ABF$.

out of K and the crinkle is inserted in, the crinkle and K together are able to flex around the same hinge, FE. Therefore, replacement with a crinkle does not change the kinematics of the dihedral surface K.

The replacement does not alter the length of the original hinge either, due to the redundancy of Bricard octahedra. The distance between vertices F and E is guaranteed to be invariant and equal to BC due to the equality of the other five pairs of edges of this crinkle, $AF = DC$, $AB = DE$, $DB = AE$, $DF = AC$, $BF = CE$. When hinge FE is replaced in Figure 2.13, it becomes invisible as the crinkle and K flex around it. This virtual hinge FE is behind vertex B and in front of vertex C, because B sticks out and C goes in in the photo. Note that a crinkle should have one vertex sticking out and the other vertex sticking in for the crinkled shape, and that this crinkled shape is due to the fact that a Bricard octahedron self-intersects and hence has a positive and a negative volume. If two vertices are on the same side, for example, B and C both pop out or into the page, then when the surface flexes, $\triangle AFE$ and $\triangle FED$ will deform, because the length of bar FE will definitely change. This is because

the original octahedron in this case is a convex octahedron. A convex polyhedra is strictly rigid. When one dihedral is removed, along with one edge of the octahedron, the flex of the remaining surface do not preserve the length of the removed edge. Only in a Bricard octahedron is any one of the edges redundant, hence the length preserved.

A replacement with a crinkle does not change the volume in front of and behind the dihedral surface. This is because a Bricard octahedron has zero volume: the positive and the negative volumes are equal, so that on one side of any dihedral in a Bricard octahedron, there is a positive volume and the other side a negative volume. Therefore, a crinkle provides a positive and a negative volume of the same amount. If this dihedral surface is part of a sphere, then the replacement with a crinkle does not alter the volume of the sphere.

The only feature a crinkle does possibly change is the range of motion of the dihedral surface. A dihedral is able to flex by 360° before a clash occurs, but crinkle may have earlier clashes. A Type I crinkle is not doubly flat-foldable as a Type III crinkle; even a Type III crinkle is only able to flex about each edge for 180°; only a Type I or Type II crinkle can possibly flex about two edges for 360°. Therefore, the range of motion of a Type I or Type II crinkle is no greater than 360°; and that of a Type III crinkle is always 180°. Overall, crinkles limit the range of rotation to no greater than 360°. For example, in Figure 2.13, as vertex A moves out of the page and rotate around FE, before it reaches vertex D, a clash will occur between $\triangle FBD$ and $\triangle BCD$; as it rotates backwards, symmetrically $\triangle CED$ will clash with $\triangle BCD$. Therefore, $\triangle AFE$ and $\triangle FED$ can never touch: the range of rotation of the dihedral surface is reduced from 360° due to clashes within the crinkle itself. When it is earlier than other clashes in the polyhedron, the range of motion is limited by self-clashes in crinkles.

2.4.3 The first flexible polyhedron

Replacing a dihedral with a crinkle can avoid clashes against another object. Connelly first demonstrated this idea as shown in Figure 2.14. A dihedral surface K can clash against another dihedral surface F at point X. However, if K has a crinkle $Np_1p_2p_3p_4S$ to replace dihedral Np_1Sp_3 in the way shown in Figure 2.13, then the clash at point X is avoided as shown in Figure 2.14 on the right. Connelly found a near-polyhedron that has two dihedral surfaces clashing like K and F. This near-polyhedron is carefully chosen so that if this clash is avoided then this polyhedron will be able to flex. Then, he used a crinkle to replace a dihedral in one of K and F: the process of this replacement was shown previously in Figure 1.1, where the taken out dihedral is part of dihedral surface K, who clashes against F beneath. The inserted crinkle avoids the clash at X. This allowed a flexible polyhedron in 3-space to be found – the original drawing of the resultant polyhedron is shown in Figure 2.15a.

Then, the first physical metal model was made: in Figure 2.15b, this polyhedron does not have the whole dihedral in the middle replaced as in Figure 2.15a but only a smaller dihedral in it, so the big dihedral can be considered as K. Through the 'windows', the other dihedral surface beneath can be observed, which can be considered as F in Figure 2.14. How the inserted crinkle avoids the clash X between K and F can be seen through the windows as well. This concave polyhedron finally shows as a first physical example that a concave polyhedron can be flexible. The movement of this model can be watched in a video online, following the link in [9], which is also searchable on YouTube with "flexible polyhedron".

The range of motion of Connelly's polyhedra is highly limited. This is caused by the restriction of clashes. There are two types of clashes that can possible occur. The first type is caused within a crinkle itself. As described above, although the kinematic property of a dihedral surface is not changed by the replacement with a crinkle, the range of the flex is reduced from 360° because of the physical clashes in the crinkle itself. Another type of clash is between K and F after a certain amount of movement. This can be observed in the online video of the metal model in Figure 2.15b.

Because a crinkle does not change the amount of space on either side of the dihedral surface, the use of a crinkle does not affect the volume of a polyhedron. Therefore, the calculation of the volume of a flexible polyhedron only needs to consider the original near-polyhedron before crinkle replacement. This allows the calculation to be easier and more straightforward. Note that all polyhedra have constant volume, so during the flex, the volume of flexible polyhedra stays the same as the volume of its near-polyhedron. All the known flexible polyhedra embedded in 3-dimensional space are devised with the replacement of crinkles, which changes neither the kinematics nor the hinge length nor the volume of the

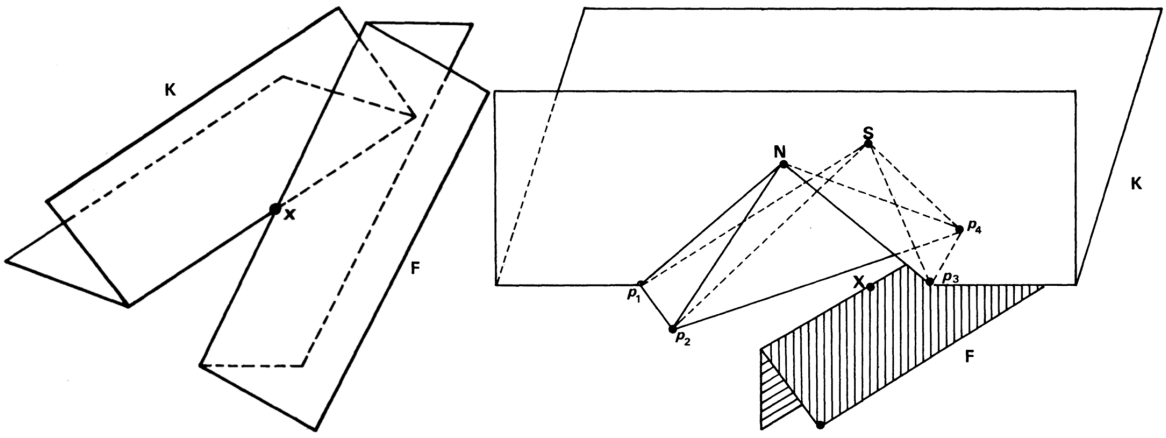

Fig. 2.14 The clash between two dihedral surfaces and the replacement of a dihedral with a crinkle to avoid the clash between the two dihedral surfaces. Figures taken from Connelly's work [9].

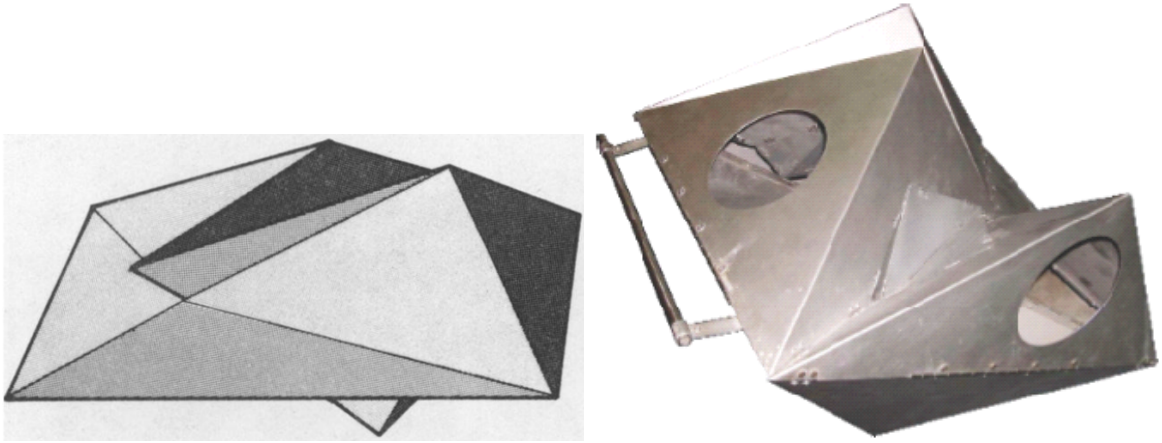

(a) A triangulated Connelly flexible polyhedron with the replacement by a Type I crinkle, the very first flexible polyhedron, constructed by Connelly in 1979 [11]. Connelly's original drawing of Figure 1.1d

(b) A metal model of a Connelly flexible polyhedron with the replacement with a Type II crinkle. This is the world's first physical model of a flexible polyhedron and is stored in IHES library.

Fig. 2.15 Two examples of Connelly flexible polyhedra, original pictures from Connelly's work

original shape. In the next section, the volume of the near-polyhedron of each triangulated flexible polyhedron will be shown, which is the constant volume of the flexible polyhedron.

2.5 Triangulated flexible polyhedra

Soon after Connelly's counterexample for the existence of flexible polyhedron, Klaus Steffen found a very simple version of Connelly's polyhedra in 1978 [23], shown in Figure 2.16. This polyhedron is composed of triangles only, so it is a triangulated polyhedron. Connelly commented it as the simplest known flexible polyhedron [11]. After Steffen, another simple, triangulated example was found by Tachi[2], shown in Figure 2.16. These two flexible polyhedra have only 9 and 10 vertices respectively. This dissertation is interested in maximising their range of motion. Triangulated polyhedra have the same kinematic mechanisms as their frames, when all rigid polygonal faces are removed. Therefore, the finite mechanisms of triangulated polyhedra can be applied to truss structures. As a result, studying triangulated flexible polyhedra may help design truss structures. This section introduces the Steffen's flexible polyhedron and Tachi's flexible polyhedron to show their configurations and triangulated shapes.

[2]Personal communication

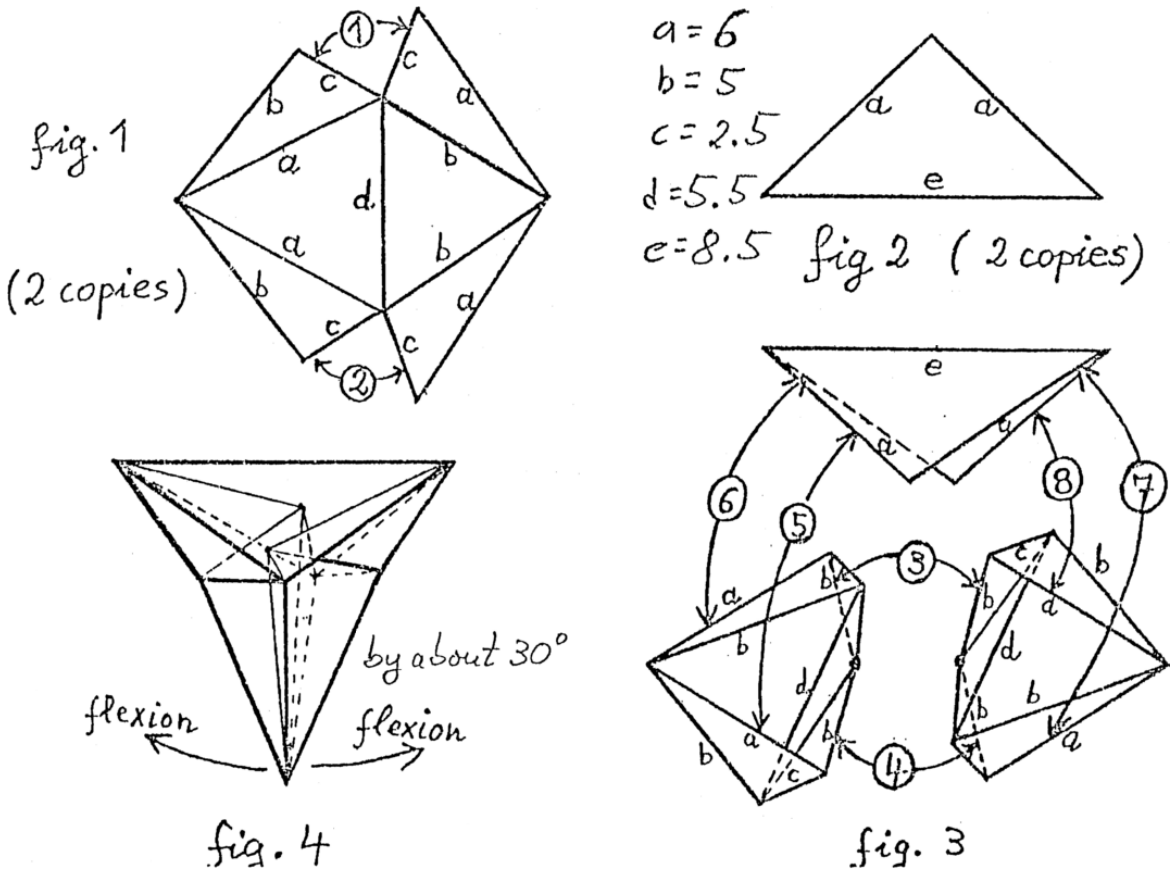

Fig. 2.16 The flexible polyhedron found by Steffen in his letter to I.H.E.S [23] (unpublished work). Steffen showed all the components of this polyhedron in the first two figures, the assembly in fig.3, and the result in fig.4. In fig.1 the pattern of a crinkle in a plane is shown; the two crinkles are identical. His fig.2 showed two identical triangles. In the first three figures, dimensions of the edges are given. The values of dimensions written next to fig.2 and the value of the range of motion written in fig.4 are extracted from Steffen's original text. The values of length parameters are given as a good choice to allow 27° range of motion.

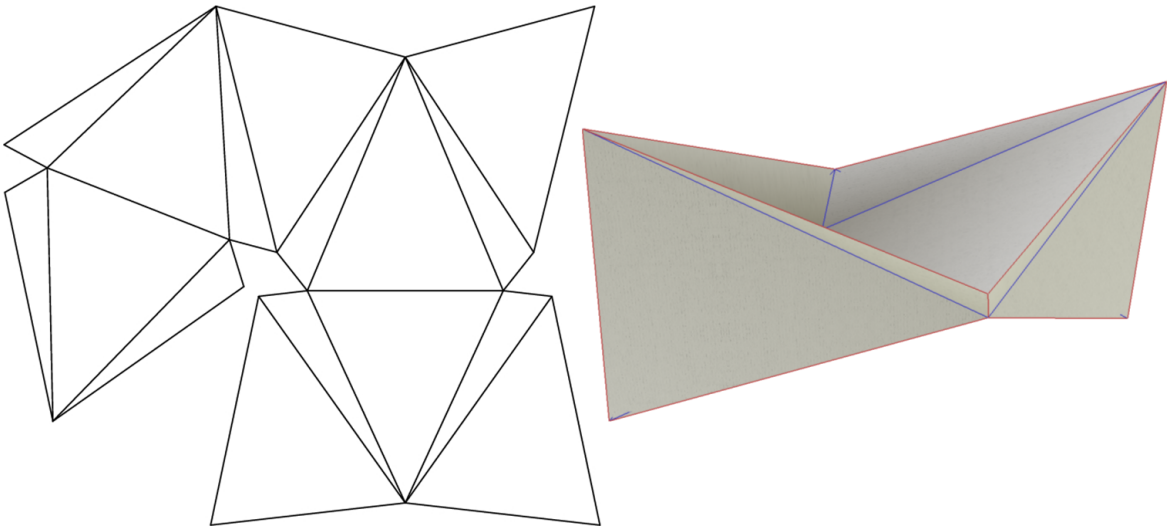

Fig. 2.17 The folding pattern and a constructed model of the flexible polyhedron found by Tachi. Images provided by Tachi through personal contact.

2.5.1 The Steffen flexible polyhedron

The composition of Steffen's flexible polyhedron is described by Connelly [10] with parameters and connecting edges indicated clearly, as shown in Figure 2.18a, and also by Alexandrov, as shown in Figure 2.18b, when proving the constant volume of this polyhedron [2].

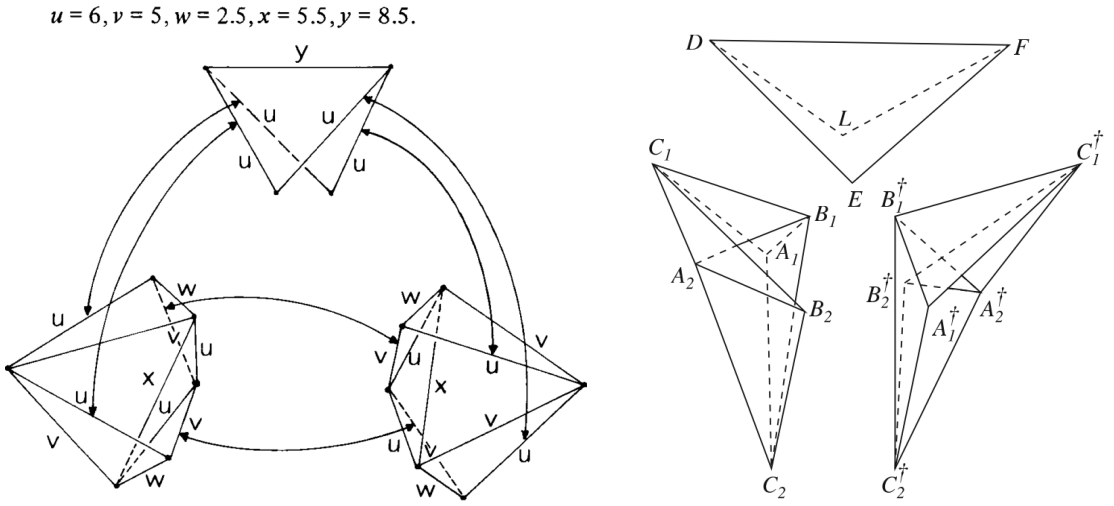

(a) Connelly re-described Steffen's flexible polyhedron [10] from Steffen's letter.

(b) Alexandrov described the composition of the Steffen flexible polyhedron [2]. He pointed out that two Type I Bricard octahedra are used.

Fig. 2.18 Re-descriptions of the assembly of the Steffen flexible polyhedron

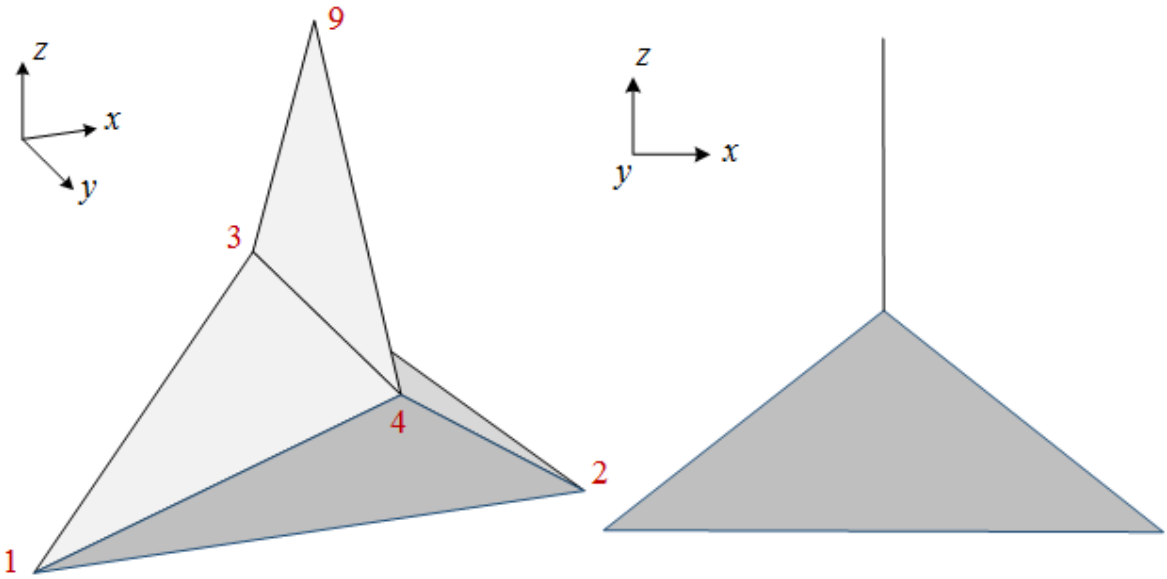

Fig. 2.19 The near-polyhedron of the Steffen flexible polyhedron. It is a triangulated surface and is able to bend about hinge 3-4, but it is not yet a polyhedron. A tetrahedron and a double-layer flap are attached by an edge. The two faces of the double flap coincide; the hinge 3-4 is regarded as a double edge linked at the ends only. Thus, the near-polyhedron has 5 vertices, 6 faces and 9 edges, considering the double flap with the double hinge. This figure is from [17].

The Steffen flexible polyhedron has only nine vertices, only one more vertex than a cube. The near-polyhedron of the Steffen flexible polyhedron is shown in Figure 2.19. It has five vertices, and is composed of a tetrahedron linked to a triangle flap. The other four vertices are added in by the introduction of crinkles. As the near-polyhedron is triangulated and the crinkles from Bricard octahedra are triangulated as well, the whole assembled polyhedron is triangulated.

As mentioned above, dihedrals need to be replaced by crinkles in order to allow a polyhedron to be flexible. Steffen's flexible polyhedron with parameters defined by Steffen is a symmetrical polyhedron: it has two identical dihedrals to be replaced by two identical crinkles. The unnecessity of this symmetry will be discussed in Chapter 4. The near-polyhedron in Figure 2.19 is able to flex around hinge 3-4 but is not a polyhedron. If we consider the triangle 3-4-9 as a double flap, then the dihedral 1-3-9-4 is to be replaced by the crinkle on the left in Figure 2.20, which adds vertices 5 and 6 into the system; and the dihedral 2-3-9-4 is to be replaced by the crinkle on the right, which adds vertices 7 and 8 in. These two replacements remove the the double edge 3-4, but the distance between vertices 3 and 4 is guaranteed to be invariable and is the same as edge 5-6 and edge 7-8. This is because Steffen chose to use a pair of Type I crinkles, so that the line symmetry of both

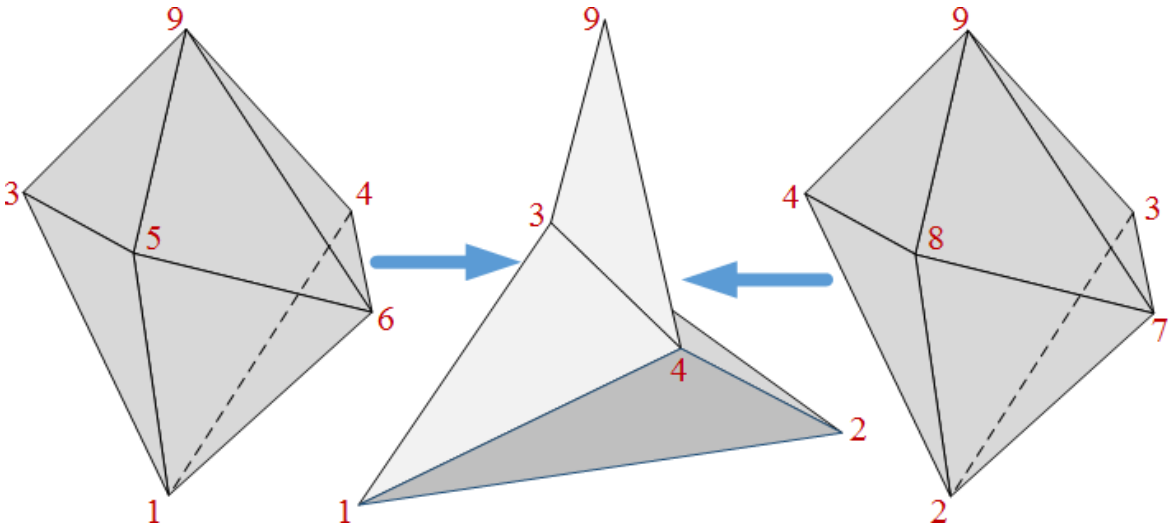

Fig. 2.20 Insertion of crinkles into the 'near-polyhedron'. Two faces of the double flap 3-4-9 are replaced; one face on each side of the tetrahedron 1-3-4 and 2-3-4 is replaced. Each crinkle replaces one face of the double flap 3-4-9 and one face on one side of the tetrahedron 1-3-4 or 2-3-4, along with one of the double hinges in between 3-4. Because the insertion does not alter the volume behind the replaced dihedrals, the volume of the resultant flexible polyhedron is the volume of tetrahedron 1-2-3-4.

crinkles guarantees $l_{56} = l_{34} = l_{78}$. The replacement of the double flap 3-4-9 and the hinge 3-4 let the "near-polyhedron" become a closed polyhedron with a continuous volume, shown in Figure 2.21. Because crinkles do not change the kinematics of the replaced dihedrals, this polyhedron is able to flex around the same hinge 3-4, which does not physically exist anymore.

Since the replacement with crinkles do not alter the volume of the original surface, the insertion of crinkles in the Steffen near-polyhedron does not change the volume of the polyhedron. Therefore, the volume of the overall complete Steffen flexible polyhedron is equal to the volume of its near-polyhedron, in this case, is the volume of the tetrahedron 1-2-3-4. During the flex of the Steffen flexible polyhedron, its volumes stays constant and equal to $V_{1-2-3-4}$.

As mentioned in Connelly's polyhedra, although the replacement of crinkles can avoid clashes between two dihedral surfaces, clashes can still occur after a certain distance of flex, so that the polyhedron has a highly limited range of motion. The dimensions of the polyhedral edges are varied in order to let the clashes occur as late as possible. During this process, it is found that the Type I crinkles need not be as symmetrical as Steffen defined, and the "near-polyhedron" need not be symmetrical at all, so that more freedom is allowed to produce a better range of motion. A generalised set of parameters are shown in Figure 2.22;

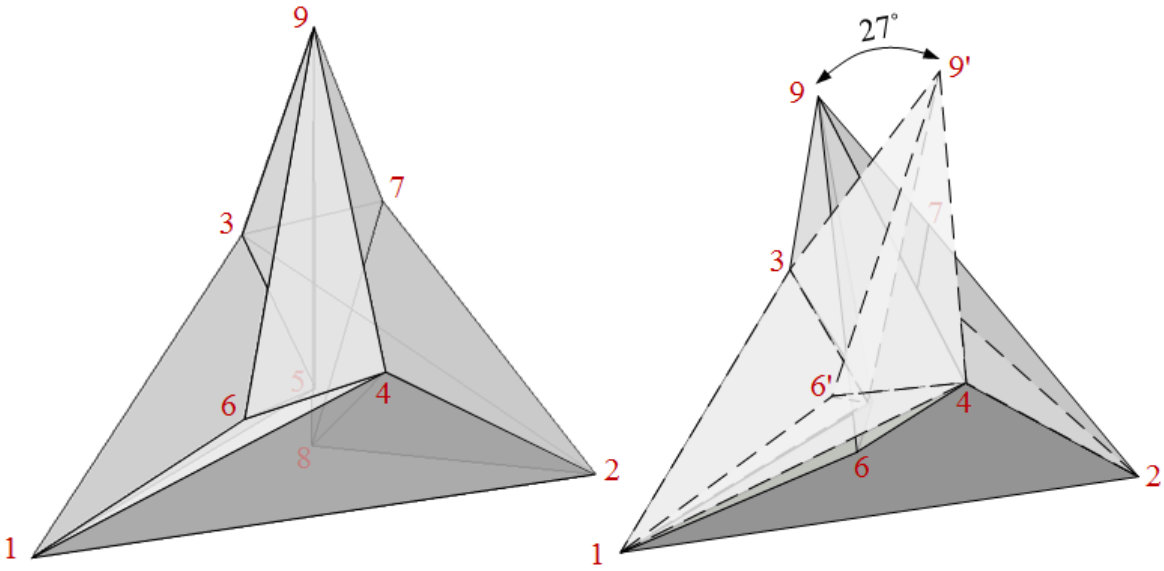

Fig. 2.21 The resultant Steffen flexible polyhedron, after the replacement by crinkles of dihedrals on both sides of the 'near-polyhedron'. With the dimensions specified in Figure 2.16, this polyhedron is able to flex for a range of motion of 27°. The polyhedron in one extreme position is shown in dashed lines and in the other extreme position in solid lines.

the generalisation process and its rationale are discussed in detail in Chapter 4. In this graph the parameter scheme is shown on the *net* of the Steffen flexible polyhedron. A *net* is the folding pattern of a polyhedron on a flat plane so that the pattern can be cut out of the paper to construct a polyhedron. The net of the Steffen flexible polyhedron in Figure 2.21 is shown with the edge lengths given by Steffen (although with generalised parameters), which allow a range of motion of 27°.

During the maximisation of the range of motion, it is also found that as the range of motion grows bigger, the shape of the polyhedron becomes irregular: acute angles in some triangulated faces become severe, i.e. some triangles on the surface become long and thin, as Figure 2.23b shows. In order to achieve considerable range of motion as well as control the shape of the polyhedron, the *regularity* R of a polyhedron is defined: the ratio of the radius of the smallest inscribed circle (the inradius) of all faces to the radius of the largest circumscribed circle (the circumradius) of all faces on the polyhedron. If the faces are numbered 1 to n, and the inradius R_i and circumradius R_c for face j are defined to be $R_i(j)$ and $R_c(j)$ respectively, then

$$R = \frac{\min_{j=1\ldots n} R_i(j)}{\max_{k=1\ldots n} R_c(k)} \tag{2.5}$$

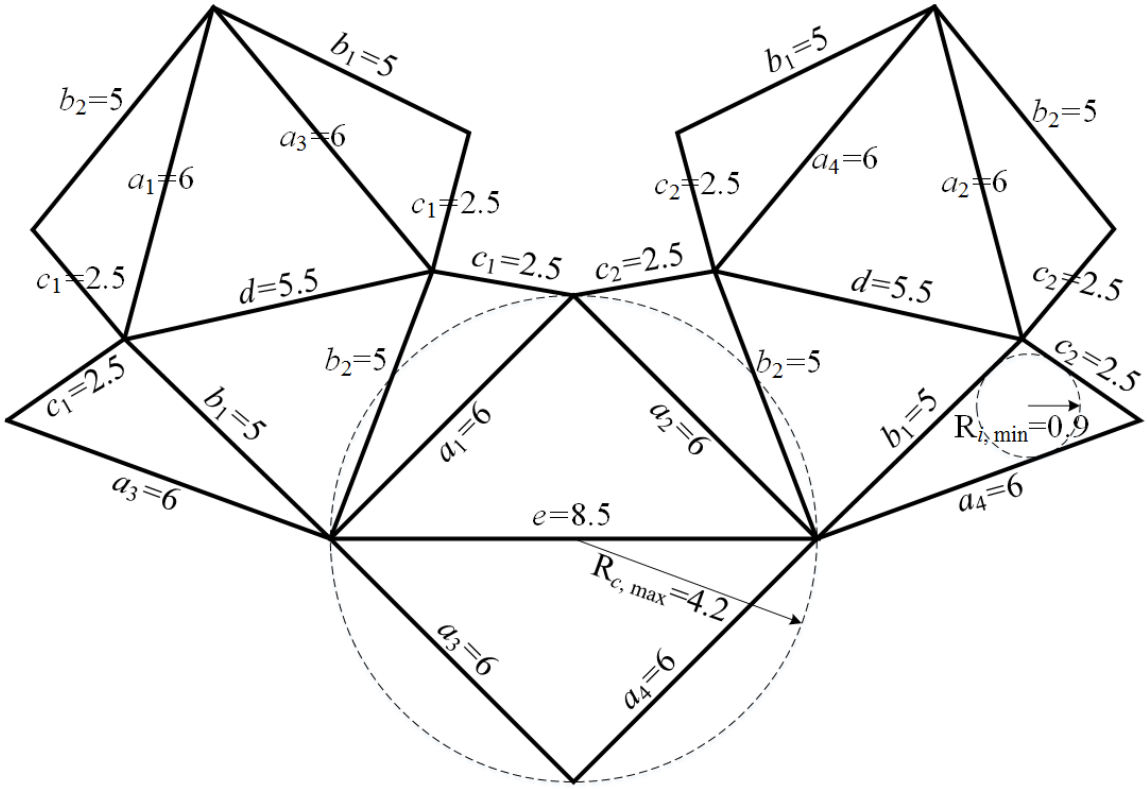

Fig. 2.22 The net of the Steffen flexible polyhedron, with generalised parameters labelled, and with the largest circumscribed circle, the smallest inscribed circle, the minimal inradius $R_{i,\min}$ and the maximal circumradius $R_{c,\max}$ shown. There are 10 length parameters, a_1, a_2, a_3, a_4, b_1, b_2, c_1, c_2, d and e. Their values are those given by Steffen in Figure 2.16. From the values of $R_{i,\min}$ and $R_{c,\max}$ shown, the regularity of this polyhedron is $R = 0.214$.

The net in Figure 2.22 shows the smallest inscribed circle and the largest circumscribed circle of the polyhedron, including the minimal inradius and the maximal circumradius. Note that, the maximum possible value of R for any triangulated polyhedron is 0.5, when all faces are equilateral triangles, for instance, for the regular tetrahedron. This case is shown in Figure 2.23a. The minimum possible value of R is 0. In the numerical calculations of this dissertation, the smallest value selected to is $R = 0.01$, hence here the extreme cases of a very small value of regularity, $R = 0.01$, is demonstrated in Figure 2.23b to provide a sense of shape. This regularity is controlled in the maximisation of the range of motion, hence the range of motion is sacrificed. To find the optimal balance between the regularity of the shape and the range of motion, multi-objective optimisations are conducted. The objectives of this optimisation is the range of motion and the regularity.

This definition of regularity is used to avoid extremities of the relative sizes of the features of the polyhedron. However, there may be other sensible ways in which this could be imposed, for instance, by considering the distribution of the 'angular defect' of 4π for a polyhedron among the vertices. Nevertheless, the impact other schemes might have on the results of this dissertation has not been considered.

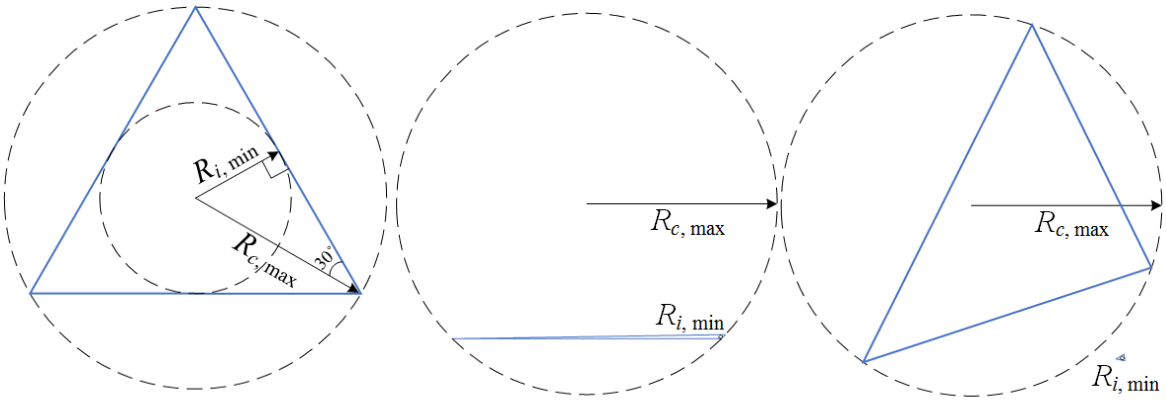

(a) The largest possible value of R. Since the regularity is a global value of a polyhedron, for $R = 0.5$, all triangles are equilateral and congruent.

(b) Two cases of a small value of R. Since the regularity is a global value of the polyhedron, $R_{i,\min}$ and $R_{c,\max}$ can be from different polygons. In this dissertation, since one sort of dimension is much smaller than others, the first case of 'sharp' triangles tend to occur widely.

Fig. 2.23 Two extreme values of the regularity R of a triangulated polyhedron. Polygons are drawn in blues lines; the dashed circles are the in/circum-circles of the triangle.

2.5.2 The two-tetrahedron flexible polyhedron

Instead of being based on a triangle flap and a tetrahedron, this polyhedron has a "near-polyhedron" of two tetrahedra sharing a common edge, shown in Figure 2.24. This foundation is more symmetrical than that of Steffen's and is extendable to repetitive flexible polyhedra. This extendability will be discussed in details in Chapter 6. Further more, this new design makes the polyhedron more able to achieve considerable range of motion. Both advantages of this new flexible polyhedron are discussed in Chapter 5 and 6 respectively.

Since the parameters for this polyhedron were not defined by Tachi, this dissertation defines 13 parameters for the most general variation, the setting of which is shown in Figure 2.25. This is based on the generalisation of the Steffen flexible polyhedron, so the setting of parameters is most general. The details of the rationale of the generalisation will be discussed in Chapter 5. With the given set of parameters, a series of flexible polyhedra are produced with different parameter values during the maximisation of the range of motion. Figure 2.26 shows the net of a result of an optimised two-tetrahedron flexible polyhedron along with its regularity and range of motion given.

The composition of the two-tetrahedron flexible polyhedron in Figure 2.25 shows that its near-polyhedron is triangulated and the crinkles are triangulated from Bricard octahedra, therefore, the established whole polyhedron is triangulated. The near-polyhedron has six vertices, and each crinkle brings two vertices in, so there are 10 vertices in total. The volume of the near-polyhedron is the volume of the two tetrahedra. Knowing that the replacements of dihedrals by crinkles do not alter the volume of the near-polyhedron. The resultant flexible

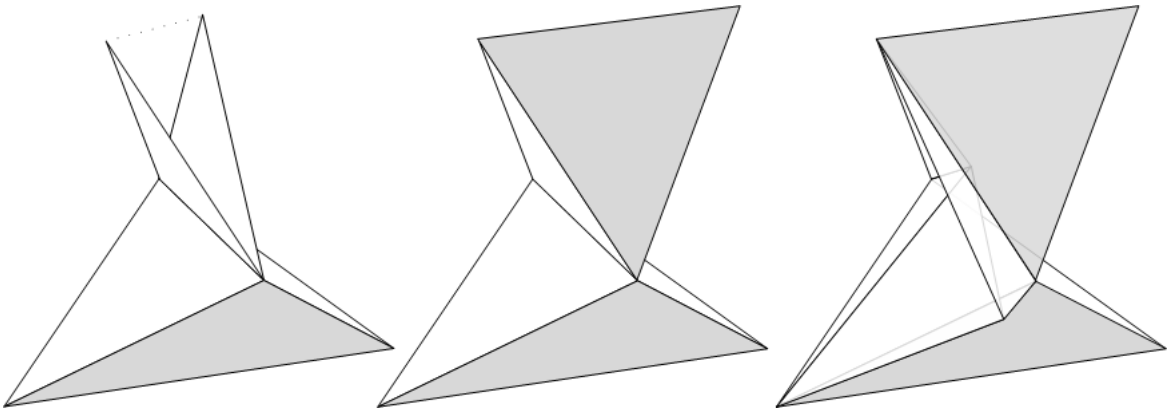

Fig. 2.24 Evolution of the "near-polyhedron" from the Steffen flexible polyhedron to the two-tetrahedron flexible polyhedron. On the left, the double-triangle flap of the Steffen polyhedron is split; in the middle, an edge is added so another tetrahedron forms on the top; on the right, one crinkle replaced one dihedral.

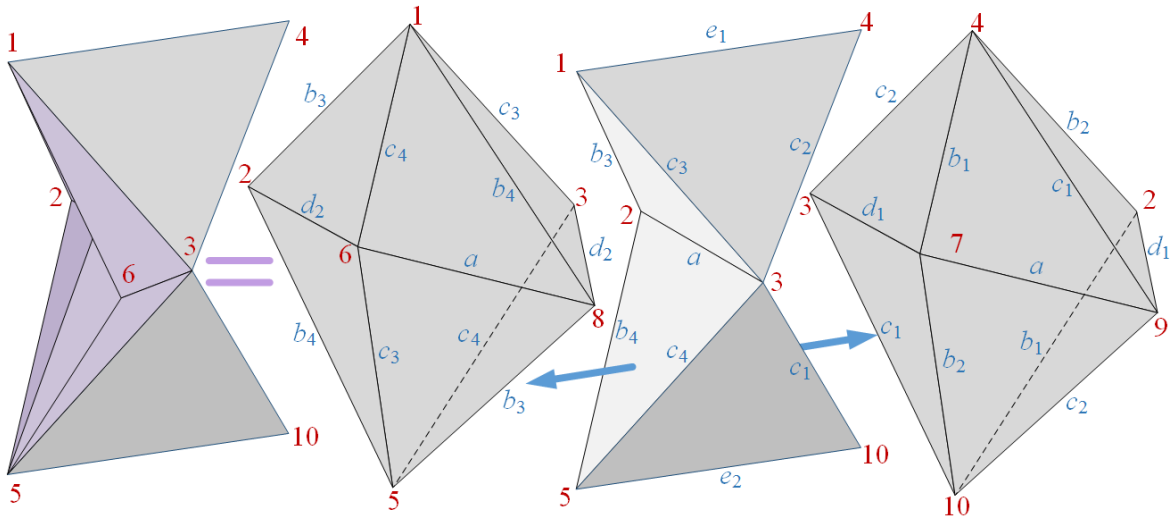

Fig. 2.25 The two-tetrahedron flexible polyhedron dismantled into a "near-polyhedron" and two crinkles, with 13 parameters defined on the edges. The top tetrahedron 1-2-3-4 and the bottom tetrahedron 2-3-5-10 share the edge 2-3, which is a double hinge connected at the ends. One crinkle on the left replaces the dihedral 1-2-5-3, and another crinkle on the right replaces the dihedral 4-2-10-3. The two crinkles have totally different parameters, but they are both chosen to be Type I. Due to the line symmetry, there are $l_{1-2} = l_{5-8}$, $l_{1-6} = l_{3-5}$, $l_{1-3} = l_{5-6}$, $l_{1-8} = l_{2-5}$, $l_{2-6} = l_{3-8}$, $l_{2-3} = l_{6-8}$ in the left crinkle, and the same applies to the right crinkle. Therefore, the hinge 2-3 is, although replaced, guaranteed to be $l_{2-3} = l_{6-8} = l_{7-9} = a$.

polyhedron also has the volume as the two tetrahedra. During the flexing process, the volume of this flexible polyhedron is constant.

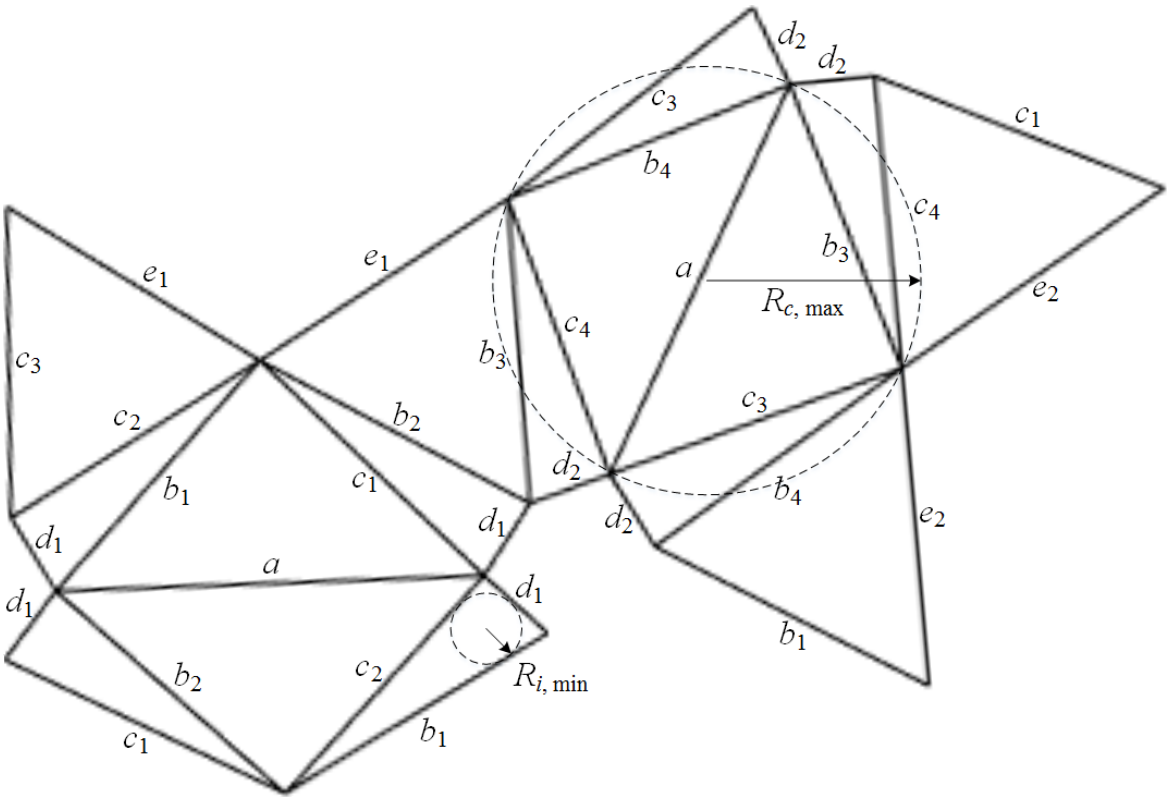

Fig. 2.26 The net of a two-tetrahedron flexible polyhedron, with 13 parameters defined and the largest circumscribed circle, the smallest inscribed circle, the minimal inradius and the maximal circumradius shown. This polyhedron has a regularity of 0.17 and a range of motion of 62°. This is an optimised result, C, shown in Figure 5.3; this net is also shown above C along with its polyhedron.

Chapter 3

Numerical tools

The range of motion of a polyhedron is affected by the lengths of the edges of the polyhedron. According to examination, when one parameter value is, for example, decreased, the range of motion grows; but as this value decreases further, the range of motion actually decreases. When an optimal value is found for this parameter, it does not stay optimal as other parameter values change. Because the length parameters are many, to change all these lengths manually in order to find a bigger range of motion is tedious work. Hence, a computational method is used to find an optimal solution of the parameter values with the maximal range of motion. In order to measure and maximise the range of motion in a flexible polyhedron, the coordinates of vertices are calculated in Matlab.

This chapter describes the numerical tools used in Matlab for optimising flexible polyhedra: it first presents an iterative solution method to establish the computational model of the polyhedron (Section 3.1), then several clash detection methods for calculating the range of motion (Section 3.2), and finally an optimisation tool (Section 3.3). The iterative solution method is used to find the coordinates of triangulated polyhedron vertices; the clash detection methods are used to detect physical touches in order to define two ends of the motion; the optimisation tool is a simulated annealing process that maximises the range of motion of the flexible polyhedra described in following chapters. Note that in Section 3.1, the method is not concerned with the motion of the polyhedron, but finds the position of all nodes for one fixed configuration. In Section 3.2 many possible configurations are considered in order to find when clashes occur that restrict the range of motion. In both Sections 3.1 and 3.2, the behaviour of a polyhedron is considered where all edge lengths are fixed. Only is Section 3.3 do we consider allowing edge lengths to change, to optimise the range of motion.

To demonstrate these tools in detail in this chapter, two examples are chosen: the Steffen flexible polyhedron with generalised parameters and the two-tetrahedron flexible polyhedron. The same methods are also applied to the optimisation of the Steffen flexible polyhedron

with parameters defined by Steffen and n-dof flexible polyhedra that will be introduced in Chapter 6. The application of these computational tools on these flexible polyhedra are not elaborated in detail in this chapter but described in Chapters 4 and 6 respectively.

3.1 Finding coordinates

To detect clashes in order to define the range of motion of a flexible polyhedron, the coordinates of all vertices need to be found. In this section, the flexible polyhedron is neither optimised nor flexing. Only the vertices of the polyhedron flexed at a fixed position are found to establish the computational model at this position. The purpose of the numerical tools described in this section is to define all the vertex coordinates of a flexible polyhedron at a fixed position in a coordinate system.

The polyhedron is fixed in space by given some coordinates of chosen vertices. Based on the coordinates of the constrained vertices and the distances between the vertices, the coordinates of all other vertices are found. The motion of the polyhedron is reduced and the polyhedron is constructed at a particular position, because to find the vertices with given edge lengths, it is easier if the structure is kinematically determinate.

Since the polyhedron system is first rendered kinematically determinate, it is straightforward to calculate coordinates of the vertices from constraints and edge lengths between vertices. Specifically, the method in this calculation process uses given constrained coordinates and initially estimated non-constrained coordinates to produce edge length differences. In a kinematically determinate frame, bar extensions can give nodal displacements. Then, an iterative solution method is used to vary the coordinates until the error of edge lengths is reduced to zero.

This section firstly uses the two examples to demonstrate how specifically a flexible polyhedron is rendered kinematically determinate. Secondly, a modified Maxwell's rule is shown to illustrate the kinematical determinacy and the statical indeterminacy in both examples. Finally, the algorithm used in the iterative process to solve the equation for finding displacements from extensions is presented including the linearisation of the calculation.

3.1.1 Constraints

The Steffen flexible polyhedron and the two-tetrahedron flexible polyhedron each has one single degree of freedom. In the process of establishing the computational model, this degree of freedom is removed by constraining a nodal movement. A coordinate of this node is given a value and is varied as a controlling parameter for different positions of the flex. Thus, at each

position, the polyhedron is kinematically determinate. Likewise, for the flexible polyhedra that have two degrees of freedom described in Chapter 6, two coordinate parameters are used to restrict these two finite mechanisms, so that the system is kinematically determinate. In an n-dof system, one parameter is used to reduce each degree of freedom. This subsection uses two 1-dof examples to show the settings of this parameter along with the use of rigid-body constraints.

In the first example, the Steffen flexible polyhedron is presented to demonstrate its constraint scheme and how the positions of vertices are determined through edge lengths and constraints. This example has the edge lengths suggested by Klaus Steffen in Figure 2.16 but the parameters generalised in Figure 2.22. It is illustrated in Figure 3.1 with its constraints shown in Table 3.1. In the near-polyhedron in Figure 3.1a, nodes 1, 2 and 3 are constrained, the coordinates of which are shown in Table 3.1. The origin is chosen to be at node 1; node 2 is chosen to be on the x-axis. According to bar length $l_{1-2} = e$, the x-coordinate of node 2 is defined, $x_2 = e$. Node 3 is chosen to be in plane XOZ, so the coordinates of node 3 are calculated from the edge lengths of triangle 1-2-3 and the coordinates of nodes 1 and 2. Here, a positive z-coordinate of node 3 is chosen, $z_3 > 0$.

Node 9 is found in a different way: one coordinate is given; two are then found from given edge lengths. The motion of node 9 is rotative about hinge 3-4. This motion is constrained with a value in x axis. This value is given with a parameter Δ. The neutral position of node

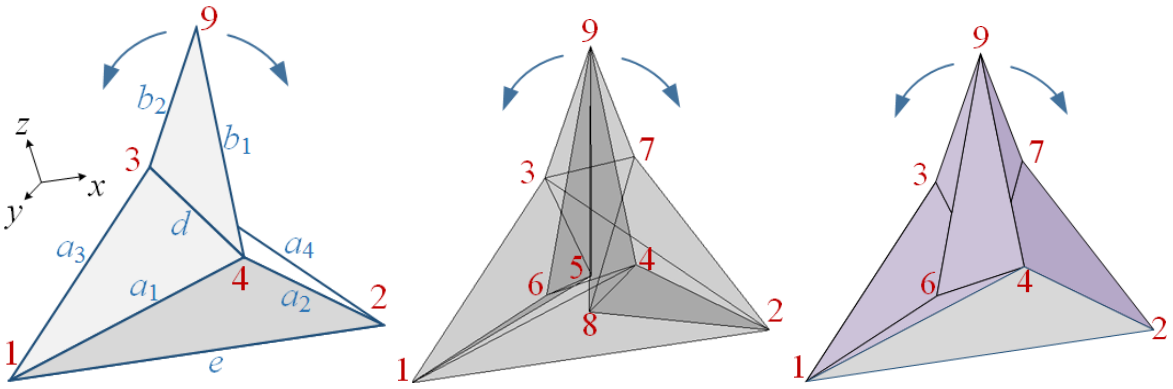

(a) The 'near-polyhedron' of the Steffen flexible polyhedron: a tetrahedron and a triangle linked by a hinge, before the replacements of crinkles on either side.

(b) Transparent Steffen original flexible polyhedron with two crinkles inserted. Hinge line 3-4 disappears; faces △1-3-4, △9-3-4 and △2-3-4 in (a) are replaced.

(c) The opaque Steffen original flexible polyhedron, shown with solid faces, flexing around hinge 3-4.

Fig. 3.1 The Steffen flexible polyhedron with generalised parameters that have values given by Klaus Steffen. All views are from the same point. Note that the y axis is perpendicular to plane 1-2-3 into the page away from vertex 4.

Table 3.1 Given nodal coordinates (constraints) of the Steffen flexible polyhedron with generalised parameter scheme

Node	Given Coordinates
1	(0, 0, 0)
2	$(e, 0, 0)$
3	$(a_3\cos\theta, 0, a_3\sin\theta)$ where $\cos\theta = \frac{a_3^2+e^2-a_4^2}{2a_3e}$
9	$(x_3+\Delta, ?, ?)$

The angle θ used to calculate the coordinates of node 3 is between edge 1-2 and edge 1-3 as shown in Figure 3.2.

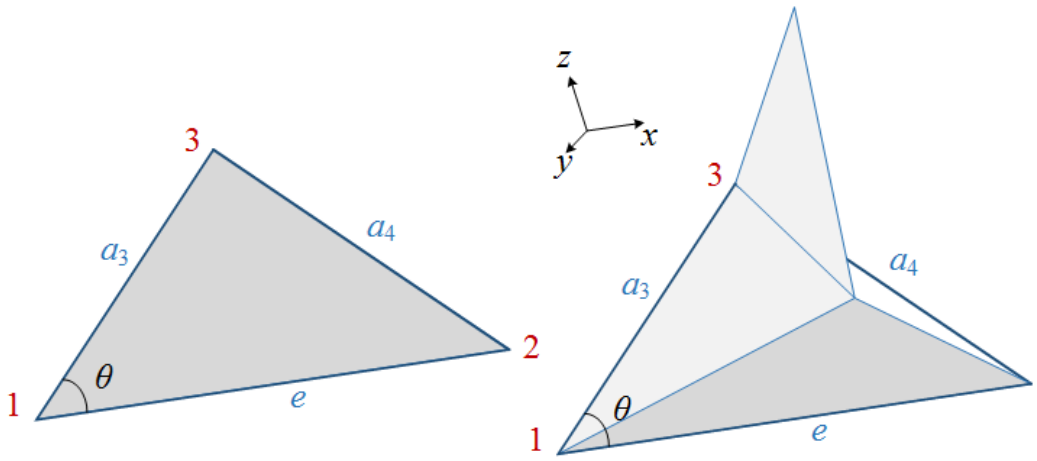

Fig. 3.2 The angle θ involved in the given coordinates of node 3 in Table 3.1, shown separately to demonstrate that θ is between edge 1-2 and edge 1-3.

9 in x direction is chosen to match x_3 when $\Delta = 0$, thus $x_9 = x_3 + \Delta$. Note that this method of specifying x_9 coordinate does not provide a completely general parametrisation of the position of node 9, because as it rotates about the hinge 3-4, x_9 can potentially specify two positions. Nevertheless, since clashes in practice prevent the rotation being greater than 90° and in this range x_9 is unique, this method is sufficient. The other two coordinates of node 9 are then set by the lengths of edges 3-9 and 4-9.

Each of the remaining nodes (4, 5, 6, 7 and 8) can now be found from given edge lengths. Node 4 is in the tetrahedron base. The three unknown coordinates of node 4 are defined by the three known lengths of edges 1-4, 2-4 and 3-4 of the tetrahedron 1-2-3-4; and a negative y-coordinate is chosen. Nodes 5, 6, 7 and 8 are in the crinkles; their situations are similar. Consider, for instance, node 6 on the left crinkle shown in Figure 3.1b and 3.1c. The three unknown coordinates of node 6 are found through the three known lengths 1-6, 4-6 and 9-6. However, edges 1-6, 4-6 and 9-6 can actually determine two positions of node 6, like node 4. Then the choice out of these two solutions determines the crinkled direction. Positions of nodes 5, 6, 7 and 8 are carefully chosen to ensure the crinkles avoid each other as Steffen specified in Figure 2.16. As a result, in Figure 3.1 in the left crinkle, node 6 is chosen to have a smaller x coordinate than node 4 and node 5 to have a greater x coordinate than node 3. Node 5 is defined by edge lengths 1-5, 3-5 and 9-5, so edge 5-6 is not needed in finding the positions of neither node 5 nor node 6. Edge length 5-6 is guaranteed to be the same as edge 3-4 by the line symmetry of the crinkle, therefore, it can be regarded as redundant. The same applies to edge 7-8. Overall, both edges 5-6 and 7-8 are guaranteed to equal the length of the hinge 3-4 due to the symmetry of two crinkles, which is from the line symmetry of Type I Bricard octahedron. Thus, the system has two redundant edges, the consequence of which will be described in Equations (5) in Table 3.3.

Once all the vertex coordinates are found, the shape of the Steffen flexible polyhedron is constructed. Two sets of coordinates have been defined: the coordinates of nodes 1, 2 and 3 and the x coordinate of node 9 are called *given coordinates*, whose values are chosen for constraint reasons; the coordinates of nodes 4, 5, 6, 7 and 8 and the other two coordinates of node 9 are called *unknown coordinates*, which are calculated from edge lengths. This calculation is based on the kinematical determinacy of the system and will be described in Section 3.1.3.

The two-tetrahedron flexible polyhedron has a different configuration, but its vertices are found through edge lengths in the same fashion, as shown in Figure 3.3 and Table 3.2. Again, node 1 is chosen to be at the origin; edge 2-3 is chosen to be parallel to y axis, so that the two vertices have the same x coordinate, $x_2 = x_3$, and their y coordinates have a difference of the edge length 2-3, $y_2 - y_3 = a$. y_2 is chosen to be positive, hence y_3 is negative. Nodes

Table 3.2 Given nodal coordinates (constraints) of the two-tetrahedron polyhedron

Node	Given Coordinates
1	(0, 0, 0)
2	$(c_3\sin\theta_1,\ a-c_3\cos\theta_1,\ 0)$ where $\cos\theta_1=\frac{a^2+c_3^2-b_3^2}{2ac_3}$
3	$(x_2,\ -c_3\cos\theta_1,\ 0)$
10	$(x_3+c_1\sin\theta_2\cos\varphi,\ y_3+c_1\cos\theta_2,\ c_1\sin\theta_2\sin\varphi)$ where $\cos\theta_2=\frac{a^2+c_1^2-b_1^2}{2ac_1}$

The angles θ_1, θ_2 and φ used to calculate the coordinates are demonstrated in Figure 3.4.

1, 2 and 3 are in plane XOY, so the values of x_2 and y_2 are calculated with the three edge lengths 1-2, 2-3 and 1-3 as Figure 3.4a shows. Node 10 is calculated with the three edge lengths 2-3, 2-10 and 3-10 and a control angle φ. φ defines the relative position of the two tetrahedra, and is reflected in x_{10} and z_{10}. It is the angle between plane XOY and plane 2-3-10 as node 10 flexes away from plane XOY as shown in Figure 3.4b. The coordinate values of node 1, 2, 3 and 10 are manually calculated as given constraints. The coordinates of nodes 4 and 5 are calculated from lengths 1-4, 2-4, 3-4 and 2-5, 3-5, 10-5 respectively; node 4 is chosen to have a positive z coordinate and node 5 negative ($z_4 > 0$ and $z_5 < 0$), so the near-polyhedron is established as shown in Figure 3.3a. In Figure 3.3b, nodes 6 and 8 on the left crinkle and nodes 7 and 9 on the right crinkle are found similarly as nodes 5, 6, 7 and 8 in Steffen's crinkles. As in the Steffen flexible polyhedron, edges 6-8 and 7-9 are redundant in determining the positions of these four nodes and are equal to edge 2-3 in length. These two redundancies are demonstrated in the following subsection. Here nodes 4 – 9 are unknown coordinates found through edge lengths.

3.1.2 Counting with Maxwell's rule

The previous subsection showed that a model is established with a constraint scheme that renders the system kinematically determinate. Then, unknown coordinates are found from the known edge lengths. As discussed earlier, in these systems, the number of known edges are greater than the number of unknown coordinates. This means, according to the constraint scheme, each system is overly constrained: they have redundancies and are statically indeterminate. This subsection uses modified Maxwell's rule from the work of Calladine [4] and Pellegrino [21] to explore the kinematical determinacy and these redundancies.

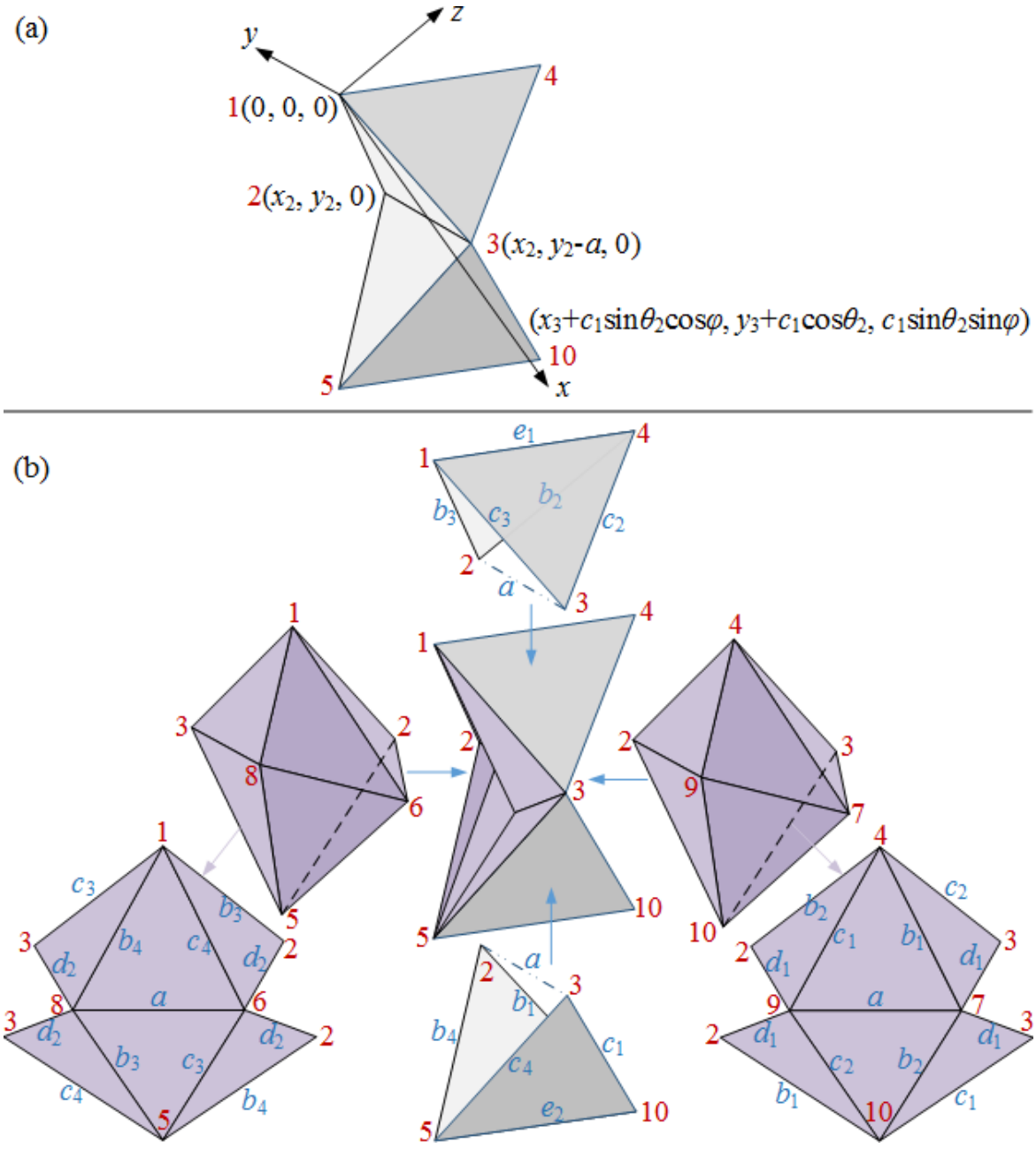

Fig. 3.3 Decomposition of the two-tetrahedron flexible polyhedron (a) The near-polyhedron, composed of two tetrahedra linked by an edge. The origin is chosen to be at node 1, hinge 2-3 is chosen to be parallel with the y-axis ($x_2 = x_3$)and in plane XOY ($z_2 = z_3 = 0$). Thus, the coordinates of nodes 1, 2 and 3 are defined. Node 10 is chosen to be in plane XOY ($z_{10} = 0$) when $\varphi = 0$. Node 4 is chosen to have a positive z coordinate and node 5 a negative z. Node 4 is found through lengths 1-4, 2-4 and 3-4; node 5 through lengths 2-5, 3-5 and 10-5. (b) Decomposition of the two-tetrahedron flexible polyhedron with parameters defined, showing the replacements of dihedrals by crinkles. Nodes 6, 8, 7 and 9 on the crinkles are found from known edge lengths and known nodes. Edges 8-6 and 7-9 are redundant in determining the positions of nodes.

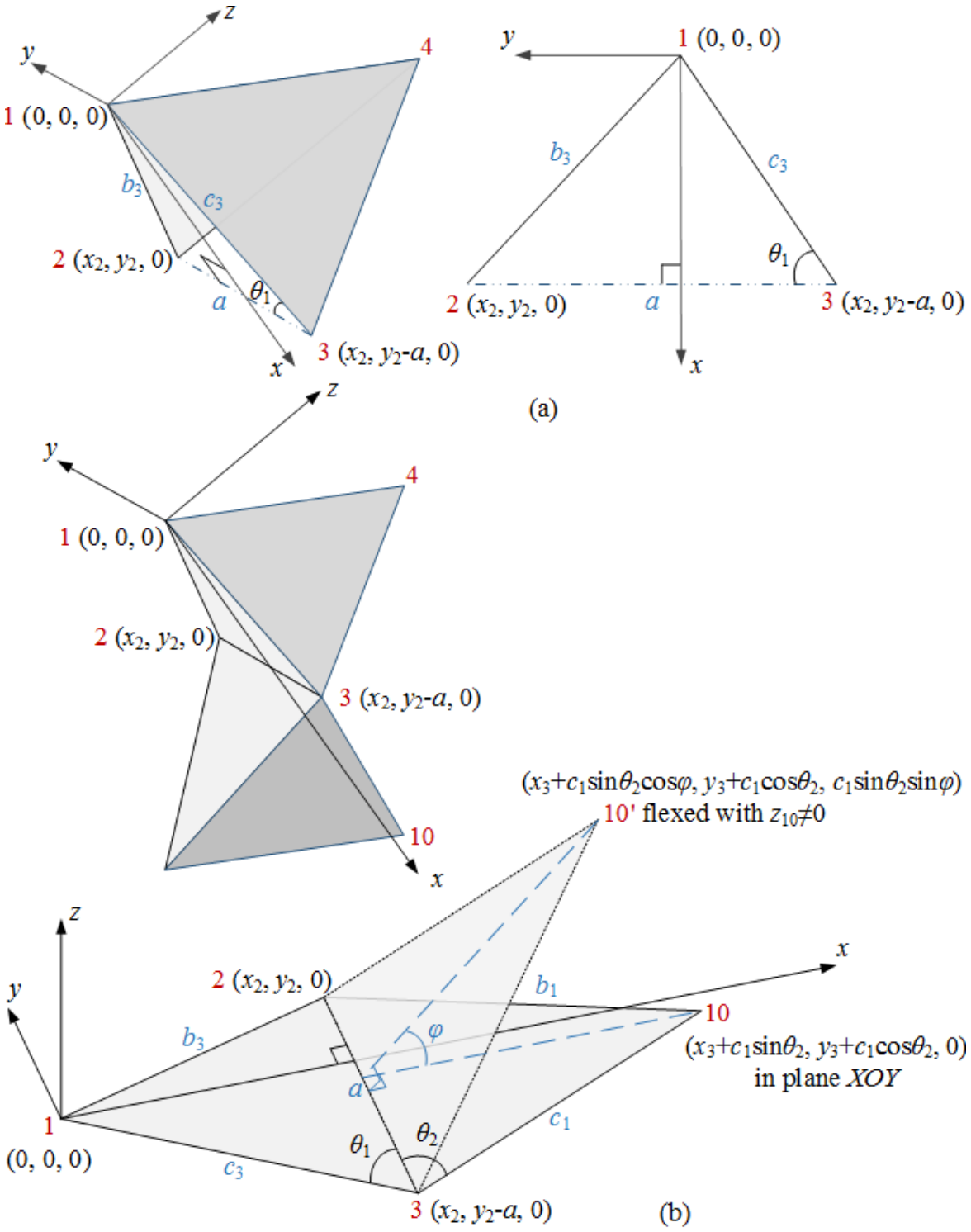

Fig. 3.4 The definition of angle θ_1, θ_2 and φ used in Table 3.2 (a) The angle θ_1 is between edge 1-3 and edge 2-3. x_2 and y_2 are calculated in $\triangle$1-2-3. (b) The angle θ_2 is between edge 2-3 and edge 10-3. φ is between a flexed position of node 10 and the neutral position of node 10 in plane XOY. With θ_2 and φ, three coordinates of node 10 are calculated.

The application of modified Maxwell's equations on the two types of flexible polyhedra are shown in Table 3.3: the Steffen and the two-tetrahedron flexible polyhedra. Since different constraint schemes are considered, various versions of the equations are presented in the table. The final version for each type of polyhedron, Equations (5) and Equations (7), shows what is used in the computational models of this work.

Equations (1) are the modified set of Maxwell's equations. Maxwell's original equation [19] $b-3j+k=0$ suggests the rigidity of a frame, whereas in modified Maxwell's equation this equilibrium means the number of mechanisms and the number of states of self-stress being the same $s-m=b-3j+k=0$. Therefore, Maxwell's original rule for defining the rigidity of frames is insufficient. In the modification, Calladine [4] found that the rank of *equilibrium matrix* [20] can help define the rigidity of frames $m=3j-k-r=0$.

Equations (2) show the counting for the Steffen flexible polyhedron. The polyhedron has 21 edges, $b=21$, nine vertices, $j=9$, and six free-body motion constraints, $k=6$. According to Maxwell, $b-3j+k=21-3\times 9+6=0$, the polyhedron is supposed to be rigid. However, in the modified Maxwell's rule, $s-m=b-3j+k$, the polyhedron has one mechanism, $m=1$, and one state of self-stress, $s=1$. This state of self-stress is caused by a redundant edge, which is from the use of Bricard flexible octahedra. The octahedron guarantees $l_{5-6}=l_{3-4}=l_{7-8}$ in Figure 3.1. Edge 3-4 does not exist, so any one of edges 5-6 and 7-8 is redundant. The rank of the equilibrium matrix is found in computations as 20, $r=20$, under 6 kinematic constraints.

In equations (3), one constraint is added, $k=6+1$, which restricts node 9 and reduces the number of degree of freedom by one, $m=1-1=0$. This constraint is as described before in x direction: a value is given to x_9. The reason for adding this constraint is to render the structure kinematically determinate (having no mechanisms), so that when establishing computational models the unknowns vertex coordinates can be solved from known edge lengths.

Equations (4) consider the virtual bar 3-4, $b=21+1$. Even though there is no physical bar between nodes 3 and 4, the distance between them is invariant and can also be used to find the unknown coordinates. Since the distance between nodes 3 and 4 is guaranteed by crinkles due to the symmetry of Bricard flexible octahedra, this bar is redundant and hence creates one more state of self-stress to the system, $s=1+1=2$.

Table 3.3 Modified Maxwell's equations [4, 21] on Steffen and two-tetrahedron flexible polyhedra

	Modified Maxwell's equations	$s-m=b-3j+k$	$s=b-r$	$m=3j-k-r$	(1)
Steffen flexible polyhedron	With 6 free-body constraints	$1-1=21-3\times 9+6$	$1=21-20$	$1=3\times 9-6-20$	(2)
	With node 9 fixed in x axis	$1-0=21-3\times 9+(6+1)$	$1=21-20$	$0=27-(6+1)-20$	(3)
	Include the virtual bar 34	$2-0=22-3\times 9+(6+1)$	$2=22-20$	$0=27-(6+1)-20$	(4)
	With nodes 1, 2 and 3 fixed Exclude 3 edges with fixed ends	$2-0=19-27+(3\times 3+1)$	$2=19-17$	$0=3\times 9-10-17$	(5)
Two-tetrahedron flexible polyhedron	With 6 free-body constraints	$1-1=24-3\times 10+6$	$1=24-23$	$1=3\times 10-6-23$	(6)
	With nodes 1, 2, 3 and 10 fixed	$6-0=24-3\times 10+(4\times 3)$	$6=24-18$	$0=3\times 10-12-18$	(7)

s represents the number of states of self-stress
m represents the number of mechanisms
b denotes the number of bars of frames or polyhedral edges
j denotes the number of joints or polyhedral vertices
k is the number of kinematic constraints on foundational joints
r is the rank of equilibrium matrix or compatibility matrix

Equations (5) reflect the computational model establishment. In computation, the rigid body motions are restricted by fixing nodes 1, 2 and 3, so there are 9 constraints rather than 6, $k_0 = 3 \times 3$. Again node 9 is constrained in x direction in order to provide a kinematically determinate system, $k = k_0 + 1$. Due to the fact that both ends of edges 12, 23 and 13 are fixed, they need not to be included in the algorithm to find unknown vertices, $b = 22 - 3 = 19$. There are 6 vertices to be found, nodes 4, 5, 6, 7, 8 and 9: the first five each has three unknown coordinates and node 9 has two, which gives $5 \times 3 + 1 \times 2 = 17$ unknowns. The rank of the polyhedron's equilibrium matrix is therefore found as $r = 17$. Since 19 edges are used to find 17 coordinates, there are 2 states of self-stress in the system.

Equations (6) show the counting for the two-tetrahedron flexible polyhedron. This flexible polyhedron has one more vertex, hence three more edges than the Steffen flexible polyhedron: $j = 9 + 1 = 10$ and $b = 21 + 3 = 24$. The difference of these numbers of vertices and edges lies in the composition of their "near-polyhedra": the "near-polyhedron" of the Steffen flexible polyhedron is a triangle attached to a tetrahedron by a common edge; and the "near-polyhedron" of the two-tetrahedron flexible polyhedron is two tetrahedra attached by an edge. Note that a tetrahedron has 1 more vertex and 3 more edges than a triangle. According to the Maxwell's rule, $b - 3j + k = 24 - 30 + 6 = 0$, this polyhedron again is supposed to be rigid; whereas according to the modified Maxwell's rule, the structure has one mechanism, $m = 1$, and one state of self-stress, $s = 1$. The cause of the state of self-stress is the same as in the Steffen flexible polyhedron: one of edges 6-8 and 7-9 is redundant.

Equations (7) show that in Matlab modelling the free-body motions and the one finite mechanism are chosen to be removed by constraining four vertices, nodes 1, 2, 3 and 10, $k = 4 \times 3$. Unlike in Steffen's model, the edges with both ends fixed are not excluded. This is because it is found that the iteration time in the algorithm in the next subsection is not affected, so the calculation efficiency stays the same. Therefore, in this type of flexible polyhedra they are chosen to remain in the system. As a result, the constraints of the ends of edges 1-2, 1-3, 2-3, 10-2 and 10-3 give 5 additional states of self-stress to the system on top of Equations (6), $s = 1 + 5$. The virtual bar 2-3 is not considered for the same reason as in Steffen's model, $b = 24$. There are 10 joints, $j = 10$; six have their coordinates unknown, and the rank of equilibrium matrix is found as $r = 6 \times 3$.

3.1.3 An iterative solution method

In all equations above, the systems are rendered kinematically determinate, $m = 0$, including the computational model establishment, Equations (5) and (7). According to the kinematical determinacy, unknown coordinates can be found through given edge lengths. This subsection

shows an iterative solution method used in solving the equation between the unknown coordinates and given edge lengths.

As stated earlier, a flexible polyhedron is not flexed in this iterative process but stopped at a position. The values of parameters are not varied so the polyhedron is not optimised. The lengths of the edges are corrected in order to find the coordinates of the vertices by a corrector method. In this algorithm, the unknown coordinates are first estimated and then corrected until the errors of edge lengths are small enough. In this method, the initial estimation of coordinate values will give a set of 'incorrect' edge lengths. Compared to the target 'correct' edge lengths, there is a difference, or 'error' in the edge lengths. This difference is further used to adjust the initial prediction of coordinates, so that the error becomes smaller. The corrector method is for minimising this error iteratively until zero so that the correct coordinates of all the vertices are found, hence the model of the polyhedron established.

In this subsection, a set of equations are presented to explain how the correct nodal positions of the unknown vertices are found by adjustments from the initial estimates. Consider an edge of length l_{ij} between two nodes i and j with coordinates (x_i, y_i, z_i) and (x_j, y_j, z_j). At least one of these coordinates is unknown and is, therefore, given an estimated value. Then, the current values at iteration a (x_i^a, y_i^a, z_i^a) and (x_j^a, y_j^a, z_j^a) give a current 'incorrect' edge length:

$$l_{ij}^a = \sqrt{(x_i^a - x_j^a)^2 + (y_i^a - y_j^a)^2 + (z_i^a - z_j^a)^2} \tag{3.1}$$

Hence there is an error, or 'extension' of the edge at the current estimated position.

$$e_k^a = l_k^a - l_k \tag{3.2}$$

A correction needs to be made in order to minimise the error. Then an improved estimate of the coordinates of nodes is found.

$$(x_i^{a+1}, y_i^{a+1}, z_i^{a+1}) = (x_i^a, y_i^a, z_i^a) + (d_{xi}^a, d_{yi}^a, d_{zi}^a) \tag{3.3}$$

The extensions of edges and displacements of nodes has a relationship due to the kinematical determinacy of the system. This relationship can be expressed between two vectors: all nodal

displacements **d** and all bar extensions **e**.

$$\mathbf{d} = \begin{bmatrix} \vdots \\ d_{xi} \\ d_{yi} \\ d_{zi} \\ \vdots \end{bmatrix}, \ \mathbf{e} = \begin{bmatrix} \vdots \\ e_{ij} \\ \vdots \end{bmatrix}$$

The equation of this relationship to be solved in order to remove the extensions is

$$\mathbf{C}^a\mathbf{d}^a = -\mathbf{e}^a \tag{3.4}$$

where $\mathbf{C}^a$, $\mathbf{d}^a$ and $\mathbf{e}^a$ are all found at the current configuration. **C** is the compatibility matrix, as described by [4], and is also called kinematic matrix [21]. It is the transpose of the equilibrium matrix **H**, the detailed description of which can be found in [4, 20, 21].

$$\mathbf{C} = \mathbf{H}^{\mathrm{T}} \tag{3.5}$$

Once a vector of errors $\mathbf{e}^a$ is produced for current configuration, the equilibrium matrix $\mathbf{H}^a$ of the current configuration is used to solve $\mathbf{d}^a$. During this process, Singular Value Decomposition [21] is used, $\mathbf{H}=\mathbf{U}\mathbf{V}\mathbf{W}^{\mathrm{T}}$, to find the minimum-length least-squares solution [24]:

$$-\mathbf{d} = \mathbf{C}^{+}\mathbf{e} = (\mathbf{H}^{\mathrm{T}})^{+}\mathbf{e} = \mathbf{W}\mathbf{V}^{+}\mathbf{U}^{\mathrm{T}}\mathbf{e} \tag{3.6}$$

Note that it is true that $\mathbf{d} = \mathbf{C}^{+}\mathbf{e}$ is the shortest-length least-squares solution to the problem $\mathbf{C}\mathbf{d} = \mathbf{e}$. The diagonal matrix $\mathbf{V}^{+}$ has all its non-zero values reciprocal to the values of **V** so that $\mathbf{V}\mathbf{V}^{+} = \mathbf{I}$.

SVD is chosen because "The Singular Value Decomposition of the equilibrium matrix makes it possible to answer any question of a static, kinematic, or static/kinematic nature for any structural assembly, within a unified computational framework."[20] Due to the fact that the system is kinematically determinate, the least-squares solution is unique, i.e. the 'minimum-length' aspect of the solution is irrelevant. As the original, non-linear equation is consistent, the found least-squares solution is exact. Now the displacements found **d** are used to correct the positions of the estimated vertices $(x_i^a,\ y_i^a,\ z_i^a)$. From the updated positions, an updated extension vector $\mathbf{e}^{a+1}$ is found. This process is repeated until the errors of bars are considered small enough. During the optimisation of flexible polyhedra described in the following chapters, $\max(|\mathbf{e}|) < 10^{-4}$ is used for iteration efficiency; each local optimal is

checked with $\max(|\mathbf{e}|) < 10^{-14}$ when measuring its precise range of motion. Both choices are efficient: the unknown coordinates is usually found in 1 or 2 iterations to the accuracy of 10^{-4}, and in 1 to 7 iterations to the accuracy of 10^{-14}.

3.2 Clash detection methods

The previous section described how vertex coordinates are found in order to establish a configuration for a given flexing position, but did not consider whether the position was physically possible. In practice, the rotation of a flexible polyhedron is restricted by physical contact between rigid polygonal faces, which do not allow intersection. When a solid face not just touches but goes through another, the occurrence of a *clash* is defined.

In this section, three clash detecting methods are proposed, which are described as the Type I clash detecting method, the Type II clash detecting method, and the Volume clash detecting method. The first two methods are simple and time-saving for iteration, thus are used in the optimisations in this work; the third method is a more robust idea but computationally costly, hence is not used in the optimisations performed but is discussed for the sake of interest.

3.2.1 Clash types

Motion of a flexible polyhedron is prevented by the interaction of faces, which is called *clashes*. Specifically, clashes are here defined to be of two basic types, Type I and Type II. A Type I clash occurs between an edge and a face that share a common vertex or between two faces that share a common edge; and a Type II occurs between two faces that do not share any edges. Two types of Type I clash are further distinguished: Type Ia and Type Ib. Type Ia is a clash between a face and an edge that only share a common vertex; Type Ib is a clash between two adjacent faces that share a common edge.

Type Ia and Type Ib clashes are detected in the same way. For example, $\triangle ABC$ and line AD in Figure 3.5a is a Type Ia clash, and $\triangle ABC$ and $\triangle ABD$ in Figure 3.5b is a Type Ib clash. Note that the Type Ib clash between $\triangle ABC$ and $\triangle ABD$ can be represented as a clash between $\triangle ABC$ and line AD as well; therefore, by choosing one face and one line from the other face, the machinery of detecting Type Ia clashes are used to detect Type Ib clashes. Due to the shared parts in both Type Ia and Type Ib, Type I clashes are detected in a much simpler way than Type II clashes.

A Type II clash between two faces is shown in Figure 3.5c. This is the generic case of the position of two triangles: the two faces do not have any particular connections. Even if

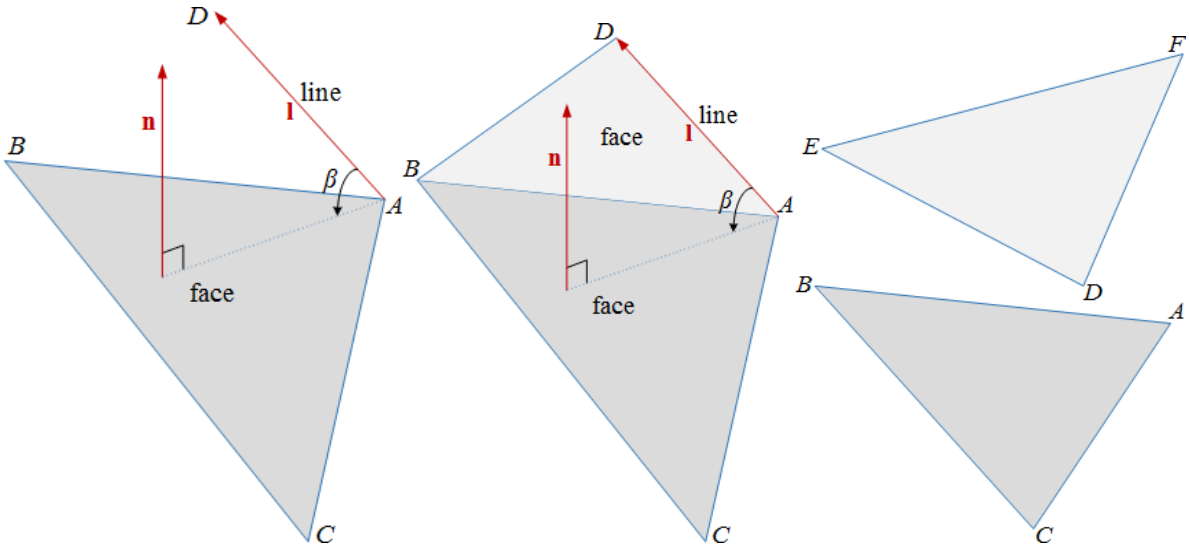

(a) A Type Ia clash between a line AD and a face ABC that share a vertex A. β is the *dihedral angle* between the line and the plane, which is calculated to represent the value of the clash. This is a particular case of Type II.

(b) A Type Ib clash between two faces $\triangle ABC$ and $\triangle ABD$, linked by a common edge AB. This is a particular case of Type Ia. β is used as the *dihedral angle*, which is different from the actual dihedral angle between two planes.

(c) A Type II clash between two triangles $\triangle ABC$ and $\triangle DEF$. A generic example of positions between triangles. This includes the case where two triangles share a vertex or share an edge.

Fig. 3.5 Three types of possible clashes in a flexible polyhedron. Type I is a particular case of Type II. Type Ib is a particular case of Type Ia.

the two faces share a vertex, no line as in Type I can be used. Therefore, no simple detecting mechanisms like the Type I clash detecting method can be used. The simplest known method is proposed in [6] and is used to detect this type of clash. Note that Type I clashes are a particular case of Type II.

In a polyhedron, Type Ia clashes occur between two crinkles; Type Ib clashes occur between a crinkle and a tetrahedron base or within one crinkle itself. Type II clashes do not occur in the Steffen flexible polyhedron but may occur in the two-tetrahedron flexible polyhedron and in a multi-dof flexible polyhedron. This is because that they only occur between crinkles that replace more separate dihedrals. In the Steffen flexible polyhedron, the two crinkles replace a pair of dihedrals that share three vertices, so the clashes between the crinkles are Type Ia. In the two-tetrahedron flexible polyhedron, the replaced dihedrals share two vertices, so the clashes between triangles in the crinkles are more separate and may be Type II.

There are 6 possible clashes in a Steffen flexible polyhedron, shown in Table 3.4, with an example illustrated in Figure 3.6. All potential clashes in a Steffen flexible polyhedron are Type I: two are Type Ia and four are Type Ib. These clashes are in symmetric pairs. For example, as the polyhedron flexes to the left in Figure 3.6b (Vertex 9 comes close to vertex 2), clash between line 8-9 and △5-6-9 may occur; symmetrically when the polyhedron flexes to the right (Vertex 9 comes close to vertex 1), by symmetry line 5-9 may clash with △7-8-9. Like this, in each flexing direction, there are three clashes that are most likely to occur. The table lists them in pairs. Type Ib clashes are not listed as two triangles that share an edge but as Type Ia clashes: one line from a triangle that shares only one vertex with the other triangle is selected.

Table 3.4 Six possible clashes in Steffen flexible polyhedra

Type	Symmetric pair	Line	Face	x_9
Type Ia	{	8-9	5-6-9	+ve
	{	5-9	7-8-9	-ve
Type Ib*	{	5-6	1-4-6	+ve
	{	7-8	2-3-7	-ve
	{	3-5	1-2-3	+ve
	{	4-8	1-2-4	-ve

* Note that Type Ib clashes are described in the form of Type Ia clashes: one line and a triangle are presented, instead of two triangles.

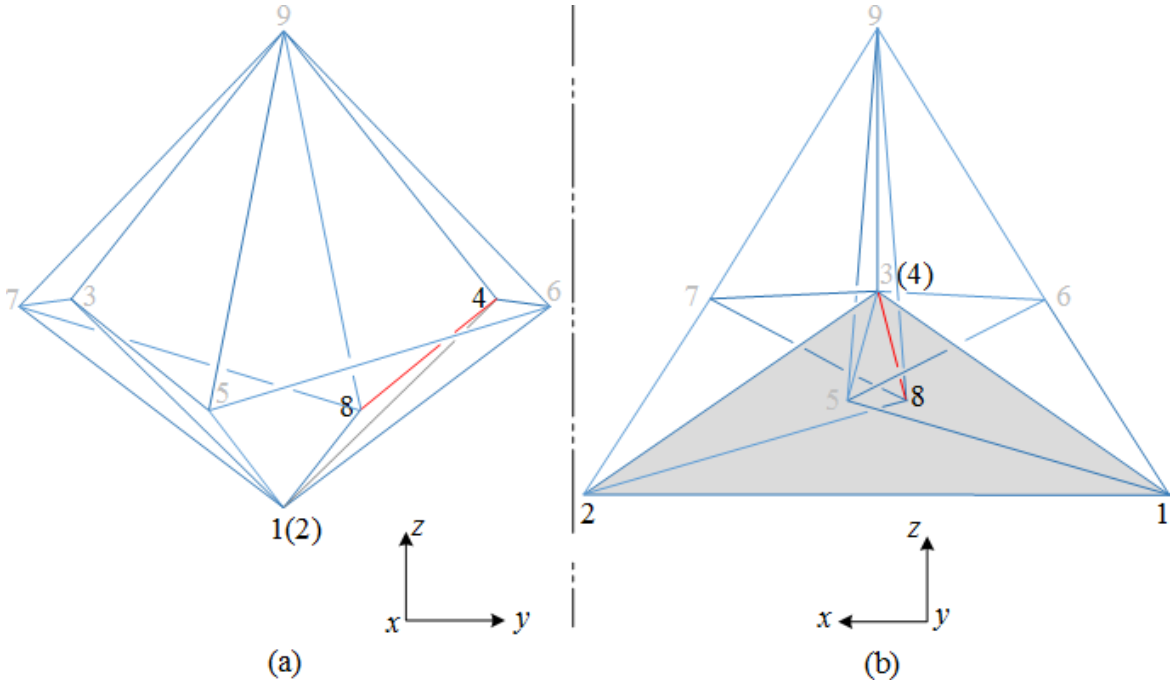

Fig. 3.6 An example of a Type I clash between a line and a face in the Steffen flexible polyhedron. The figure shows the frame of the Steffen flexible polyhedron at neutral position in first angle projection. In view (a), vertex 1 is on top of vertex 2; in view (b), vertex 3 is on top of vertex 4. △1-2-4 is highlighted in grey and line 4-8 in red to demonstrate a potential clash between them. This is innately a Type Ib clash between △1-2-4 and △2-4-8. △2-4-8 is a face on a crinkle; △1-2-4 is a face on the tetrahedron base 1-2-3-4. Line 4-8 is an edge of △2-4-8, which is chosen to be considered as a Type Ia clash against △1-2-4. The coordinates of vertices 1, 2, 4 and 8 are used in the Type I clash detecting method. During the flexing movement of node 9 around hinge 3-4, especially when node 9 rotates towards node 1, line 4-8 can possibly "go across" △1-2-4, which means that the dihedral angle of △1-2-4 and △2-4-8 can turn "negative". A true Type Ia clash is between △5-6-9 and line 8-9.

Table 3.5 Fourteen possible clashes in two-tetrahedron flexible polyhedra

Type	Line	Face
Type Ia	2-6	2-9-10
	3-7	3-1-8
	Face	Face
Type Ib	1-8-6	1-8-3
	7-9-10	2-9-10
	7-3-10	5-3-10
	1-2-6	1-2-4
	1-3-4	7-3-4
	2-5-10	2-5-6
	3-5-8	6-5-8
	7-9-4	2-9-4
Type II	7-9-4	1-8-6
	7-9-4	5-8-6
	7-9-10	1-8-6
	7-9-10	5-8-6

There are 14 possible clashes detected in the two-tetrahedron flexible polyhedron as Table 3.5 shows, with an example illustrated in Figure 3.7. Theoretically, any two faces may clash; but practically, it is time-consuming to calculate all clashes between any two faces in optimisation iterations. During the optimisation of the Steffen flexible polyhedron, it is observed that, no matter how dramatic the polyhedral shape changes, only the listed six clashes occur in all circumstances. However, in the optimisation of the two-tetrahedron flexible polyhedron, the case is more complicated. The chosen 14 potential clashes are sufficient in almost all circumstances but not quite all, as explained below.

The process of optimisation may be gradual; however, on occasions during the process the shape may change suddenly and radically. On such occasions, the shape produced may fail to conform to requirements: clashes that are not specified may occur. Visual checks were made to detect where this occurs. To overcome this problem, two approaches are used: (a) the produced result is discarded, and smaller variations are used to avoid sudden change of shape; (b) the number of possible clashes to be detected needs increase beyond those in Table 3.5. For example, the clash between line 2-6 and face 2-4-9 in Figure 3.7 does not occur except when crinkles change directions. It is due to pure human observation to decide which clashes need be checked. Unacceptable configurations occurs particularly when searching for the greatest regularity and the absolute maximal range of motion, which are extreme cases.

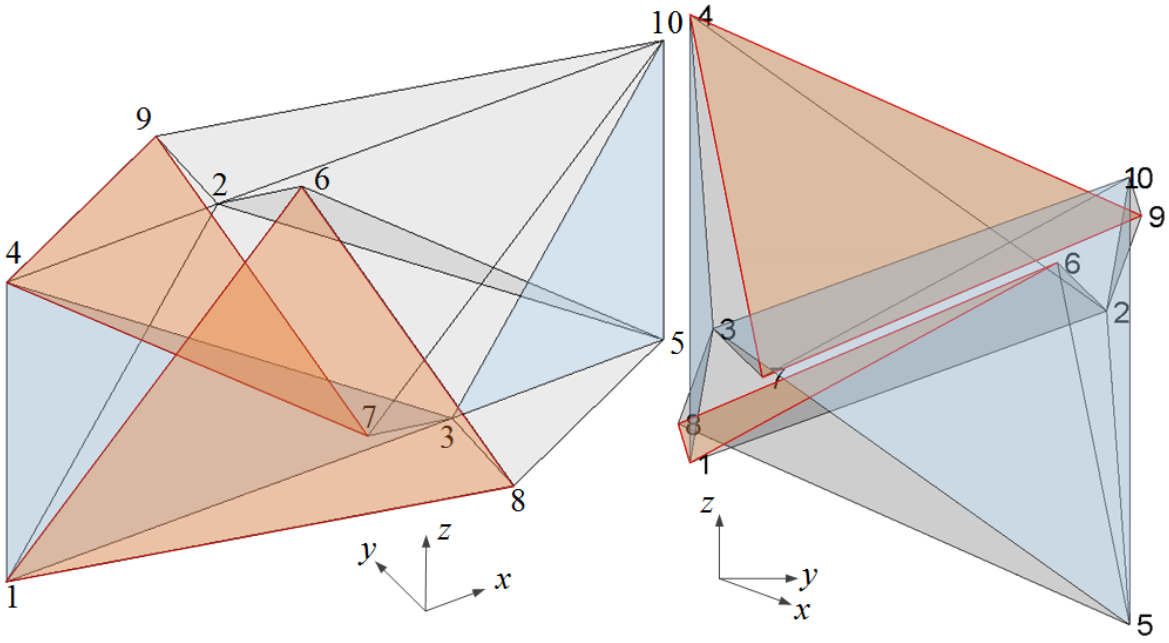

Fig. 3.7 Example of a Type II clash in a two-tetrahedron flexible polyhedron, displayed from two different view points. The near-polyhedron of two tetrahedra linked by the hinge 2-3 is drawn in blue, partially replaced by two crinkles, illustrated in grey; an example of potentially clashing faces, △4-7-9 and △1-8-6, are highlighted in orange. These two triangles are totally separate from each other: they do not share any edges nor vertices. The first view shows the triangles are from two different crinkles; the second view shows the gap between these two crinkles. They can potentially clash as the polyhedron flexes around hinge 2-3.

The chosen 14 potential clashes are sufficient for almost all the change in shape of the two-tetrahedron flexible polyhedron. Two of the 14 clashes are Type Ia, eight are Type Ib, and four are Type II. Four potential clashes in the table do not look very likely in Figure 3.7 but may occur easily in other shapes during the optimisation, so they are included. Clashes other than these 14 pairs are not included because they only occur in extreme cases, for example, clash between face 4-7-9 and face 2-5-6 in Figure 3.7. Due to the configuration, line 1-6 may clash with $\triangle$4-7-9, but this is checked by the clash between $\triangle$4-7-9 and $\triangle$1-6-8 in the list. Only in extreme cases will $\triangle$4-7-9 clash with $\triangle$1-2-6 without clashing with $\triangle$1-6-8. Overall, all other clashes rather than these 14 listed need to be decided on manual observation. Therefore, at the beginning and the end of each run of the optimisation, the shapes of polyhedra are observed manually in order to check the sufficiency and efficiency of current chosen detection of clashes.

The multi-mechanism flexible polyhedra based on this 1-dof two-tetrahedron flexible polyhedron require much more complicated clash consideration. Each model has its own set of many more potential clashes, and is hence not discussed as a general method in this chapter.

3.2.2 Type I clash detection method

Since Type Ib clashes are considered as Type Ia clashes, one simple detecting method is used for both types: examining the dot product of the line vector and the normal vector of the face. The line vector is defined as being positive when acting away from the shared vertex; and the normal vector is defined as being positive when pointing towards the interior of the polyhedron for an internal clash, or towards the exterior for an external clash. For both internal and external clashes, the line and the normal will define a clash when the dot product is negative.

The reason why this method is valid for Type Ia clashes is because in the known flexible polyhedra the projection of the line always lies in the area of the face due to observation. For example, in Figure 3.5a, the projection of line AD onto face ABC never moves beyond line AB nor line AC, as the shape of the polyhedron changes in optimisations. The reason why this detection method is valid for Type Ib clashes is because, in the optimisation of flexible polyhedra, the dihedral angle of the two faces grows no greater than 180°. For example, in Figure 3.5b, the planes of $\triangle ABC$ and $\triangle ABD$ never has a dihedral angle greater than 180° no matter how the shape of polyhedron develops. Otherwise, the clash need to be considered as a more general case: Type II.

The clash value of Type I detecting method can be defined as

$$c = \frac{\mathbf{n} \cdot \mathbf{l}}{|\mathbf{n}||\mathbf{l}|} \tag{3.7}$$

where $\mathbf{n}$ is the vector of the normal of the plane in which the face lies, and points towards the interior of the polyhedron for an internal clash and the exterior for an external clash; and $\mathbf{l}$ is the vector of the line, extending from the common node shared by the face and the line. When c turns from positive to negative, it indicates that a clash occurs; when it stays positive, it suggests no clash.

However, the dihedral angle β between the line and the face has a physical meaning, where $c = \sin\beta$. Therefore, β is more straight forward for human interpretation of the amount of clashes. Hence, it is chosen to be the actual clash value used in the system.

$$\beta = \sin^{-1} c \tag{3.8}$$

An example of a Type I clash is illustrated in the Steffen flexible polyhedron in Figure 3.6. This is a Type Ib clash between $\triangle$1-2-4 and $\triangle$2-4-8, but $\triangle$1-2-4 and line 4-8 are chosen to represent this clash as a Type Ia clash. Genuine Type Ia clashes in this flexible polyhedron are between $\triangle$5-6-9 and line 8-9, and between $\triangle$7-8-9 and line 5-9.

In the case of the example highlighted in Figure 3.6, the vectors which define the plane 1-2-4 are $\overrightarrow{4\text{-}1}$ and $\overrightarrow{4\text{-}2}$. This is an internal clash; external clashes only occur in multi-dof flexible polyhedra. Hence, the normal of this plane that points towards the interior of the polyhedron is $\mathbf{n} = \overrightarrow{4\text{-}2} \times \overrightarrow{4\text{-}1}$. The vector that defines line 4-8 is $\mathbf{l} = \overrightarrow{4\text{-}8}$. The sign of $\mathbf{n} \cdot \mathbf{l}$ determines whether this clash occurs: if $\mathbf{n} \cdot \mathbf{l} > 0$, then no clash occurs; if $\mathbf{n} \cdot \mathbf{l} = 0$, then the line is just in the plane, which is not considered as a clash; only when $\mathbf{n} \cdot \mathbf{l} < 0$, which means the line has moved across the solid face of 1-2-4, can the occurrence of the clash be defined. In the current position in Figure 3.6, $\mathbf{n} \cdot \mathbf{l} = (\overrightarrow{4\text{-}2} \times \overrightarrow{4\text{-}1}) \cdot \overrightarrow{4\text{-}8} > 0$, so there is no clash for the current position of plane 1-2-4 and line 4-8.

3.2.3 Type II clash detection method

In a two-tetrahedron flexible polyhedron, Type I clashes are detected with the method described above; Type II clashes are more complicated, so that a more sophisticated detecting method is used. This subsection describes this second clash detecting method with the example highlighted in Figure 3.7.

An effective detecting method of clash between any two triangles is described in a paper in Chinese [6], which is used here to develop a Matlab function $clash2func$. This function

returns a clash value. The codes of this function is shown in Listing **??** in Appendix A to help explain the detecting mechanism. In the description that follows, references will be made in parentheses to which part of the code implements the material under discussion. Since all the flexible polyhedra calculated in this dissertation are triangulated, a clash in this dissertation is defined by the relationship of two triangular faces. When calculating this relationship, the coordinates of the six vertices of these two triangles are used (code lines 1 – 6). These two triangles are labelled as in Figure 3.5c. One triangle, ABC, is taken as the reference, and the relative positions of vertices D, E and F in the other triangle are then considered (code lines 9 – 12).

In the following cases, no occurrence of clash is immediately considered (code lines 14 – 21): (i) $\triangle ABC$ and $\triangle DEF$ are in the same plane (i.e. D, E and F all lie in the plane defined by $\triangle ABC$), whether they overlap or not; (ii) one edge of $\triangle DEF$ (any two of D, E and F) lies in plane ABC; (iii) one of D, E and F is in plane ABC, and the other two are on the same side of ABC; (iv) D, E and F all lie on the same side of plane ABC. In these cases, the clash value is given as a chosen positive value, as only negative clash values matter in later calculations.

If not in the cases above, then one vertex among D, E and F must lie on one side of plane ABC, while another vertex is on the other side. Therefore, whether a clash occurs or not needs to be identified (code lines 22 – 99): the intersection line between $\triangle DEF$ and plane ABC is first found, and then whether this line segment intersects with $\triangle ABC$ is checked. In order to find the intersecting line segment, D, E and F are relabelled to render D the solo vertex that lies on one side of the plane ABC (code lines 27 – 57). It does not matter whether E and F both lie on the other side of the plane, or one lies on the other side and the other lies in the plane. Line PQ in Figure 3.8a is the intersection line of $\triangle DEF$ and plane ABC, i.e. P and Q are defined as the points at the intersection of lines DE and DF with plane ABC respectively (code lines 61 – 64). Then, planar positions of line PQ and $\triangle ABC$ are investigated in order to check whether there is a clash (code lines 66 – 99). Paper [6] proposed five possible in-plane relationships for them, shown in Figure 3.8a.

A technique described in [6] for defining the five cases in Figure 3.8a is: if three points in a plane are located in an anticlockwise order as A, B and C are in Figure 3.8b, and if, for instance, a point P is inside edge AB (i.e. in zone 1, 2, 3 and 7), then $\overrightarrow{AB} \times \overrightarrow{CB}$ and $\overrightarrow{AB} \times \overrightarrow{PB}$ will be in the same direction (dot product positive); otherwise, if P is outside AB (in zones 4, 5 or 6), then the two cross products will be in opposite directions (dot product negative). Therefore, the positivity of the dot product of these two cross products defines whether a point is inside or outside one edge of $\triangle ABC$ (code lines 68 – 73). This technique can be used to define the position of a point in planar relation to any convex polygon. All three edges of $\triangle ABC$ in Figure 3.8b are checked to locate P and Q into one of the 7 zones.

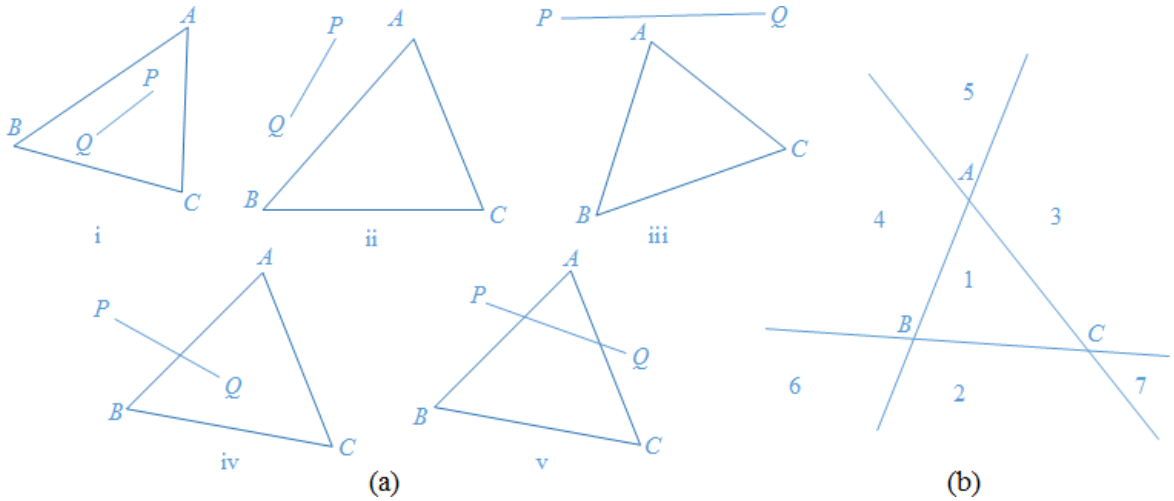

Fig. 3.8 In-plane relationships between a line and a triangle. Both (a) and (b) are redrawn from Figure 5 and Figure 6 respectively in [6] in order to illustrate how a clash can occur between a line segment and a triangle. (a) There are 5 possible in-plane relationships between a line segment and a triangle according to [6]. A, B and C are the vertices of $\triangle ABC$ used in the Matlab function $clash2func$; P and Q are the intersecting points of lines DE and DF respectively with the plane defined by $\triangle ABC$. (b) The three lines of a triangle divides a plane into 7 zones according to [6]. If a point locates in zones 4, 5 or 6, then it is defined as being outside the edge AB, which defines that this point has no clash with $\triangle ABC$. If a point locates in zones 1, 2, 3 or 7, then it is defined as being inside the edge AB. The same applies to a point being outside or inside AC and BC.

Based on this technique, whether P and Q fall into zone 1 in Figure 3.8b is first defined. If any one of P and Q is in zone 1, which is cases (i) and (iv) in Figure 3.8a, then a clash value of the whole length PQ is given as a negative value (code lines 75 – 79). If both P and Q are outside the same edge, case (ii) in Figure 3.8a, including the scenario that PQ touches or lies on the edge (any one or both of P and Q locates in the line), then no clash is considered (code lines 81 – 85). If none of the above cases apply, then both P and Q must be outside $\triangle ABC$ and are on different sides of an edge. Then, whether a section of PQ is in the triangle, situations (iii) or (v) in Figure 3.8a, needs to be identified. This is distinguished by the same technique described above but with an opposite set of vertex relationship: defining whether A, B and C are on the same side of line PQ (code lines 87 – 97).

For all the no clash cases, a positive value of 1 is given. This is because in the penalty function (described in Section 3.3) no matter the clash value is positive or zero, no penalty is given. Only the negative values produces a penalty. However, this approach sacrifices the smoothness of the penalty function. For the clashing cases (i), (iv) and (v) in Figure 3.8a, a negative value of the whole length of line PQ is given rather than only the actual clashing length as [6] suggested. This is for saving time in iterations, however, the smoothness of the clash function is sacrificed.

3.2.4 Volume clash detection method

The previous two methods consume little calculation time, and are thus the only methods used in the optimisations in this dissertation. However, during the optimisation, the shape of a type of flexible polyhedron can change dramatically, hence the clash detection needs to be examined manually to ensure the clashes are still checked correctly. That is to say, inexpensive methods are efficient but not universally robust. This subsection discusses an idea of global clash detection for all types of polyhedra, which should be robust for all cases of clashes. However, this method was not developed sufficiently to be used in practice to generate the results in this dissertation.

A polyhedron is a closed envelope. Any self-intersection creates another closed envelope. This enclosed volume created by clashes is defined as *a negative volume* or *a clash volume*. As shown in Figure 2.2c, the pyramid tip below the bottom of face caused by self-intersection is a negative volume. Multiple self-intersections create multiple negative volumes, which is called as *the negative volume* or *the clash volume* of the polyhedron.

In order to calculate the clash volume of a flexible polyhedron, the original, "unclashed" volume of a polyhedron is first considered. Flexible polyhedra have constant volume. The famous Bellows conjecture about the constant volume of flexible polyhedra has been hotly discussed and finally proved in 1995 [22]. The volume of a flexible polyhedron in this

dissertation is defined by the volume of the tetrahedra in the underlying near-polyhedron. The sum of the volumes of the underlying tetrahedra is the volume of the flexible polyhedron, because the replacement of dihedral surfaces with crinkles does not affect the volume of the tetrahedral chain but simply opens up the hinges make the tetrahedra into a continuous volume.

When clashes occur, there is an envelope enclosing the overall volume that includes both the original positive volume and the clashed negative volume. The decrease of the original volume is of the same amount of the negative volume. Therefore, the subtraction of this *enveloped volume* and the original volume is the clash volume. In order to obtain the clash volume, the envelope of the clashed polyhedron is calculated computationally. Two methods are attempted in Matlab, but both were found to be too time-costly for the optimisation.

The first possible method is through voxelisation. A volume is meshed into numerous voxels. The volume of a unit voxel times the number produces an approximate volume. The fineness of the mesh defines the accuracy and time for calculation. Because this method is either too inaccurate or time-consuming, it is not used in the optimisation.

The second method is a Monte Carlo method. In a sphere or cube which just encloses the polyhedron, numerous points are randomly set inside this sphere or cube, and are checked whether they are inside or outside the polyhedron. No matter they are inside the negative or positive volumes of the polyhedron (As long as they are inside the enveloped volume), they are considered to be inside the polyhedron. The ratio between the number of inside points and the number of set points is approximately the ratio of the enveloped volume of the polyhedron to the volume of the sphere or cube. Because the volume of the sphere or cube is easily known from given dimensions, the enveloped volume of the polyhedron is easily calculated. Like the first method, the accuracy and calculation time depend on the number of set points.

If a more efficient way of calculating the enveloped volume or directly the clash volume is found, this volume clash detecting method will be more general, universally applicable and robust than the Type I and Type II clash detecting methods. The clash value of volume passed on to the penalty function will be smoother than Type II detecting method and more reliable than both Type I and Type II methods. Also, there will be only one clash value rather than a vector of values whose units are not necessarily the same.

Since the clash function is smoother and more robust, the clash volume can be minimised and eliminated quickly in an optimisation. This means a neutral position where no clash or small clash occurs need not to be so carefully found as a starting point of an optimisation: when devising a new polyhedron, a clashed initial configuration can be given.

3.2.5 Finding the range of motion

Each type of flexible polyhedron rotates about a middle hinge. As the polyhedron flexes, the clash values change. Based on these clash detection methods, the feasibility of any position a polyhedron flexes to is defined: if any clash occurs, the current position is not feasible; if no clashes occur, then the current position of the flex is physically possible. A flexible polyhedron has a range of rotational motion where no clash occurs. This range of motion is measured about the virtual hinge that is replaced. That is to say clashes at two ends define a range of motion for a flexible polyhedron. In other words, there is no clash within the range of motion that the polyhedron rotates about its virtual hinge.

For each position a polyhedron flexes to, the clash detection algorithm is run. Clashes are not detected during the continuous movement of the flex but at each discrete step. The steps are made small enough to be able to check all possible clashes within the continuous region of the movement. This simulates clash detection throughout a continuous movement. The discrete steps can theoretically be infinitely small to ensure clashes between big steps do not occur, but for the sake of calculation time, reasonable values are given.

In principle, a big step is first used to detect clashes, then a smaller step is used to detect clashes in the gaps of the big step, then a smaller step is used, etc. However, due to examination of all clash values and clash positions in the polyhedron, it is extremely unlikely that clashes will occur between big steps. Therefore, smaller steps are not used to check clashes between each bigger gap but only at the two ends for more accurate end positions, as the following describes.

The polyhedron is flexed in steps of δ from a chosen neutral position where no clash is known to occur until a clash happens, and is then flexed backwards by a step of δ and forwards again in steps of δ/C until another occurrence of clashes happen. C is a dividing factor, which is dimensionless and is chosen to have any value greater than 1, so that the flexing step in the second round becomes smaller. For more accurate clashing position, the polyhedron is flexed backwards again by a step of δ/C and forwards in steps of δ/C^2 instead, and so on and so forth, until the clashing position is considered accurate enough. In this way, a precise position of one end is found. The other end of the motion is found in the same way. Thus, a full range of motion is measured. The accuracy and efficiency of this method is tuned by the values of δ and C and the number of division by C.

The value of δ is an angle measurement in the model establishment of some polyhedra, and is a linear coordinate value in that of others, as Table 3.2 and Table 3.1 show respectively. This is due to the ease of calculation caused by different parameter settings and constrain schemes. Therefore, two different notations are used from two ways of calculation in measuring the range of motion of different flexible polyhedra.

The first notation of the range of motion is from direct subtraction of the two end position values $\Theta = \varphi' - \varphi''$, so the step sign δ is an angle. φ' is the value of flex φ for one end position, and φ'' is that for the other. This direct calculation is used in the symmetrical Steffen flexible polyhedron with parameters defined by Steffen and the two-tetrahedron flexible polyhedron as Table 3.2 shows. Typical step values are chosen to be $\delta = 1°$ and $C = 100$; the smallest step used is $\delta/C/C$. However, sometimes $\delta = 1°$, $C = 10$ and the smallest step δ/C are used for a quicker check of the range of motion or faster iterations in the optimisation. For final calculation of a Pareto optimal, $\delta = 0.1°$, $C = 10$ and the smallest step $\varphi = \delta/C^3$ are used for prudence. The range of step values recommended are $\delta \in [0.1°, 10°]$ and $C \in [2, 100]$.

The second notation of the range of motion Φ is calculated from two extreme positions of a rotating vertex. The rotation of this vertex is not given by φ directly but a position parameter Δ in one of its coordinate, as Table 3.1 shows. This is used in the Steffen flexible polyhedron with generalised parameters and multi-hinge flexible polyhedra, which will be introduced later. During the optimisation, Φ is used instead of $\Delta' - \Delta''$.

Φ is an angle, but the step value δ of Δ is a dimensionless coordinate value as Table 3.1 shows. Typical values chosen here are $\delta = 1$ and $C = 100$; the smallest step used is $\delta/C/C$. For quick check of range of motion and faster iterations, $\delta = 1$, $C = 10$ and the smallest step $\delta/C/C$ are used; for measurement of a Pareto optimal, $\delta = 0.1$, $C = 10$ and the smallest step δ/C^3 are used. The range of values recommended are $\delta \in [0.1, 10]$ and $C \in [2, 100]$.

3.3 Simulated Annealing optimisation

In order to increase the range of motion for each type of polyhedron, an optimisation method is used. The optimisation maximises the angle of rotation by varying the edge lengths of the polyhedron. Here a Simulated Annealing (SA) method is chosen, which is a global optimisation method that searches over the global area in order to try to find the globally lowest point. SA uses a heuristic technique, which finds an approximate rather than an exact solution but is speedy and sufficient. Each optimum is achieved from an annealing process where a simulated cooling scheme is given. The cooling speed controls the time given for the global search. The time does not necessarily allow the global search to find the actual minimum solution but close. Therefore, amount of time given in the annealing process is critical. Because standard SA functions look for a minimum, the range of motion is calculated as a negative value in this process to be minimised. The simulated annealing function used here is a Matlab implementation [25], the theory of which is based on document [16]. The

boundary condition of this SA search is implemented by a penalty function, where feedback is given to the result.

3.3.1 SA function

Optimisation input: The function has two inputs: a parameter vector and a coordinate calculation function. The parameter vector includes the values of defined dimensional parameters and the values of the two end positions. For example, there are 10 dimensional parameters generalised for a Steffen flexible polyhedron, a_1, a_2, a_3, a_4, b_1, b_2, c_1, c_2, d and e. They define edge lengths as shown in Figure 2.22. With the value of $e = 8.5$ fixed for reference, the values of the other 9 parameters are given to the parameter vector in order to be varied for a better range of motion. For a two-tetrahedron flexible polyhedron, there are 13 dimensional parameters defined, a, b_1, b_2, b_3, b_4, c_1, c_2, c_3, c_4, d_1, d_2, e and e_2. These define the edge lengths as shown in Figure 2.25 and Figure 2.26. With the value of $e = 7.5$ fixed, the values of the other 12 parameters are passed on to the parameter vector in its optimisation. The two end position values are the values of φ' and φ'', or of Δ' and Δ'' defined in the previous section.

Parameter perturbations: All values in the parameter vector, including the end position values, are perturbed slightly and randomly. (All the edge length parameter values and the end position values input into the parameter vector are perturbed slightly and randomly.) These input variables are perturbed by a generator function, which generates a new vector slightly different from the original input. The default generator in the downloaded function is used, in which only one element in the vector is chosen randomly and differed slightly at once. The choice of the element is through random permutation by using the Matlab function *randperm*. Then the chosen element is given a value drawn from the standard normal distribution by the Matlab function *randn*, chosen by the downloaded SA function. The chosen *randn* gives pseudorandom values. Pseudorandomness is sufficiently almost random for current perturbations and is simple and quick for calculations. In order to perturb slightly, this value is divided by a magnification factor of P. A default value of $P = 100$ is used initially, but is adjusted to $P \in [1, 10^5]$ for the efficiency of different optimisations. Common values used in this dissertation are $P = 50$, $P = 80$, $P = 20$, $P = 10$, $P = 1000$ and $P = 10000$ in a descending order of frequency.

Regularity control: The perturbed vector is then passed onto a selection of regularity of the polyhedral shape. This is because as described in Section 2.5.1 that, during the optimisation, it is observed that as the range of motion grows, the regularity of the polyhedral shape decreases. Therefore, a concept of regularity is defined to control the shape of the polyhedron. Then, a multi-objective optimisation is conducted: increasing the regularity of

the shape while increasing the range of motion. In the SA function, the regularity of the polyhedron is pushed towards a certain direction before the range of motion is optimised. Specifically, the regularity is calculated after each selection/perturbation of new parameters. Only when the regularity is greater or smaller than a certain value R can the new parameters be passed on to the coordinate calculation function for detecting clashes. Otherwise, the parameter vector is re-perturbed and the regularity is checked until qualified. The threshold value R is varied from zero until the range of motion sacrifices to zero; optimised results for each chosen R are produced.

The input function: A coordinate calculation function is for finding the coordinates of all vertices in order to calculate possible clashes. It uses all perturbed values, including one of the two perturbed end position values, and the fixed e value to find the coordinates of all vertices, using the method described in Section 3.1. From the vertex coordinates, clashes are detected according to description in Section 3.2. From the two perturbed end position values, all coordinates of two positions are found, then two vectors of clashes are produced. They are both passed onto a Penalty Function.

Cooling Scheme: The speed of the cooling down process affects the success of finding a better result: if the cooling process is slow enough, enough time is allowed to search for a much better optimal; if the system is cooled down fast, the number of iterations are fewer, so the optimal may be much better but not the best. The virtual temperature value T used in the cooling system is decreased in each iteration. The initial temperature is chosen to be 1, and the cooling function is $T_{new} = \mu \cdot T_{old}$. The choice of μ affects the efficiency of finding a better result: if the cooling process is too slow, it costs too much time to find a solution which is not necessarily much better. Initially a default value of $\mu = 0.8$ is used, but occasionally for quick tests $\mu = 0.2$ is used. In order to achieve "very fine" optimal results, in most cases $\mu = 0.99$ is used, sometimes even $\mu = 0.998$ is used. A slow annealing process is very helpful in obtaining better optimals, but $\mu = 0.999$ is found to be too slow. The stop value is used as the default $T = 10^{-8}$.

Optimisation output: The SA function returns a parameter vector that has produced the best penalised range of motion. Note that the target value is negative in SA. This range of motion is the smallest value of all throughout an entire cooling process. However, because the end position values produced in this vector are randomly perturbed, they do not happen to be the values calculated from the dimensional parameter values in the same vector. Moreover, the penalised range of motion is not necessarily the precise range of motion calculated from the dimensional parameter values in the vector. Therefore, outside the SA function, the output dimensional parameter values are used to calculate the range of motion starting from a mid, neutral position specified by the mean value of the two perturbed end position values. This

process is as described in Subsection 3.2.5. This accurate range of motion is compared with the range of motion produced by the initially input dimensional parameter values. Whichever vector that produces a larger range of motion is given to the next run of SA.

3.3.2 Penalty function

A penalty function is for penalising a range of motion. The range of motion in this SA process needs to be penalised because it is directly added in the case of φ or calculated in the case of Δ from the two perturbed end position values, $\varphi' - \varphi''$ or Φ. That is to say, in the SA optimisation process, the range of motion is not measured by flexing the polyhedron from a "no-clash" neutral position to a "clashed" end position as described in Subsection 3.2.5, but is directly added or calculated from the two end position values whether or not clashes actually occur at these two positions. Therefore, this range of motion is not necessarily correct. If no clash occurs at any of the two positions, this range of motion may be underestimated, and this underestimated value is used to compete against other results; if any clash occurs at any of the positions, the range of motion is over-ambitious and needs to be penalised. The amount of the biggest clash defines the amount of penalty. The penalty function in Equation 3.9 calculates this amount. The range of motion is penalised by clashes at both ends, so this function is applied twice on the range of motion. This way, it serves as a boundary condition to the SA function. At each end, a couple of clashes may occur simultaneously; the smallest clash value is used by the penalty function, $\beta = \min(clash)$.

$$p(\beta) = \begin{cases} T(e^{-\frac{\beta}{T}} + \frac{\beta}{T} - 1) & \beta < 0 \\ 0 & \beta \geq 0 \end{cases} \tag{3.9}$$

If the smallest value is positive or zero, it means no clash or just some touches occur, then no penalty is given; if the smallest value is negative, the penalty is an exponential function of the clash value β over temperature T, as shown in Figure 3.9. Parameter T is a simulated temperature in the SA system, used by a simulated cooling scheme. In the SA function, the cooler the system is the stricter the penalty becomes. The curves of the penalty function are plotted in Figure 3.9 with two different temperature values $T = 0.1$ and $T = 1$. This demonstrates the penalty becomes more severe when the system cools down. Also, for each value of T, the bigger the smallest clash β is, the stricter the penalty is.

As previously stated that since the SA function searches for the minimum, the range of motion measured needs to be output as a negative in order to find the maximum. Therefore, the penalty function produces a positive penalty from the exponential function to be added onto the negative range of motion.

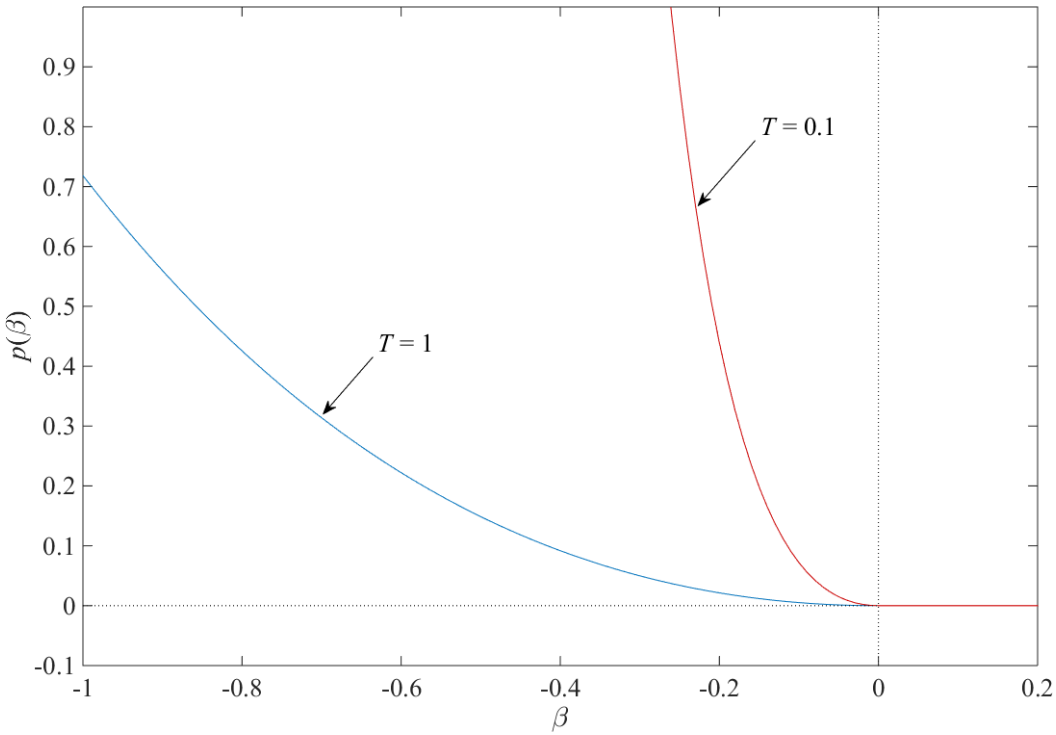

Fig. 3.9 The Penalty function $p(\beta)$ as a function of the smallest clash value β. The penalty is designed to penalise $\beta < 0$ in the optimisation. Curves for two values of annealing temperature T . As temperature T decreases, the penalty becomes severe. With the default stop value of T in the cooling scheme, $T = 10^{-8}$, the penalty values $p(\beta)$ are considered to be infinite by Matlab when $\beta < 10^{-6}$.

3.4 Overview of the optimisation process

Here a complete overview of the optimisation of the range of motion of flexible polyhedron is given. Figure 3.9 gives a flowchart, in which differently coloured blocks represents different Matlab functions: the optimisation process includes the SA optimisation function, labelled in a dashed frame, and the calculation function of the range of motion, coloured in blue. The SA optimisation function has two inputs: a vector of parameter values and the coordinate calculation function coloured in pink. This coordinate calculation function is used again in the blue block after each run of the SA function for checking the validity of the SA result. In the pink block, an iterative solution method used to correct edge lengths in order to find vertex coordinates is coloured in yellow. In the blue block, the range of motion is not calculated from two given end positions. Instead, the two end positions are found from a 'no clash' neutral position until clashes occur. This check is a manual control outside each SA run. As the green blocks indicate, inside the SA function, perturbations and cooling scheme are used as designed in the downloaded Matlab package.

The flowchart is explained specifically here. The optimisation starts with the downloaded Matlab SA function (in the dashed frame). This Matlab function requires two inputs: one input is a vector of values; the other is a coordinate calculation function coloured in a pink block. The flowchart starts with the value input. This vector contains two kinds of values: a set of initial values of variable parameters of edge lengths, and two values of the two end positions. These two end position values can be accurate or random, because they will be used to compete against other results later. Then, the whole vector of values is perturbed with a default perturbation scheme, described in Subsection 3.3.1 and labelled here in green. From the perturbed values of length parameters, the regularity of the polyhedron is calculated. Then, this regularity is selected in a loop: only when the value is greater or smaller than a set value is this perturbed vector passed on to the next stage; otherwise, all values of the vector are re-perturbed until R is satisfactory.

In the next stage, all values are passed into the coordinate calculation function, labelled in the pink block. This function is the input function of the SA function. It establishes the computational model by finding all the coordinates of vertices of the polyhedron, described in Section 3.1, and detects clashes as described in Section 3.2. This function in pink is used twice in SA, each time with one end position value to establish the model of one configuration. The two values of end positions are perturbed from the previous stage.

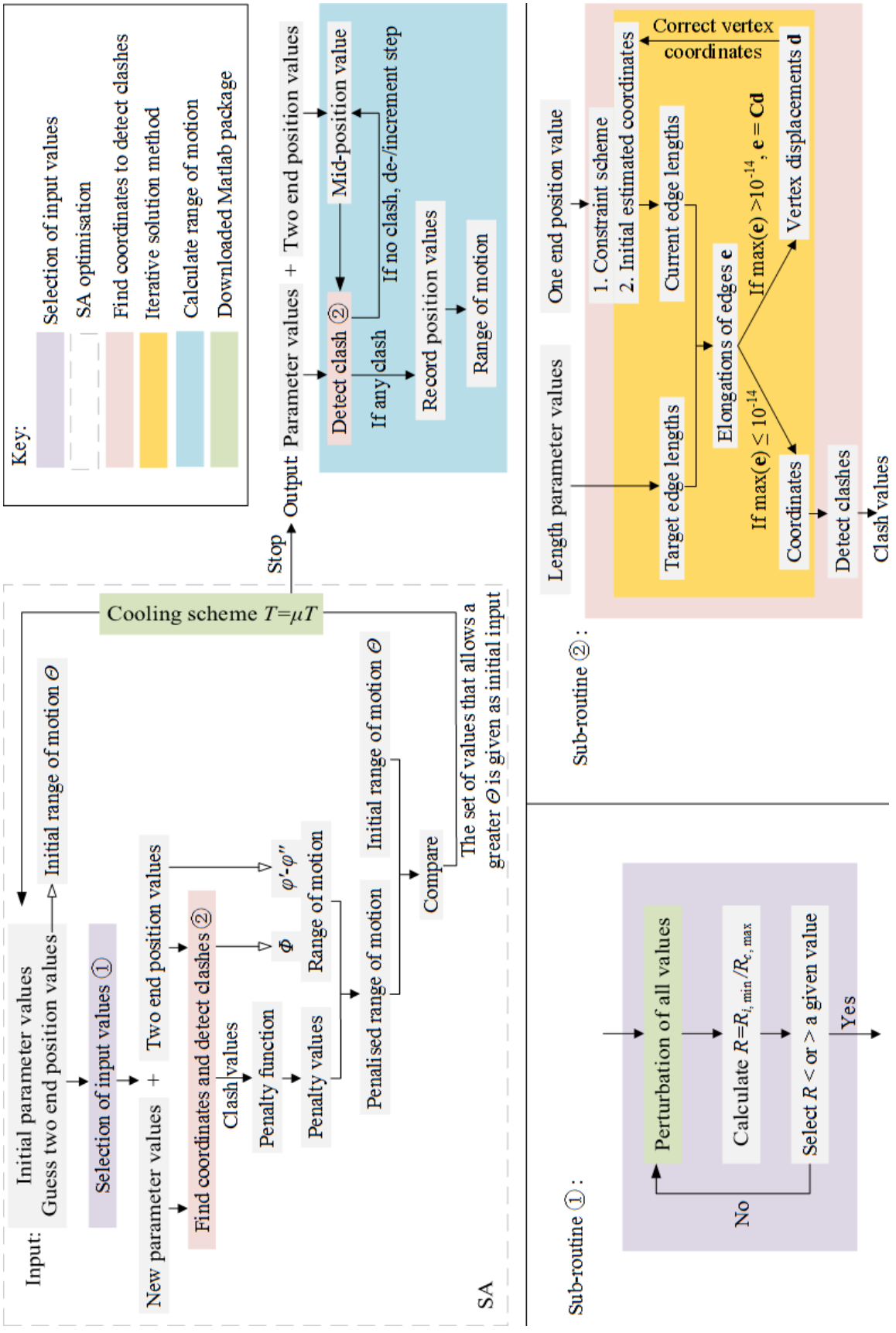

Fig. 3.10 Algorithm of the optimisation process in this dissertation

This function first gives constraints, considering the coordinates that specify an end position, φ', φ'', Δ' or Δ''. Secondly, the function gives estimated coordinates to unconstrained vertices. It then calculates initial edge lengths from the constrained and estimated coordinates. These calculated lengths are compared to the correct edge lengths given by the selected parameters passed on from previously perturbed and result. As a result of this comparison, elongations of the lengths **e** are produced. Then, an iterative solution method is used to correct the estimated coordinates until the elongations of edge lengths **e** are small enough. This iterative solution method is described in Subsection 3.1.3 and labelled here in the yellow block. If the elongations are significant, they will be used to calculate displacements **d** of unconstrained coordinates. This **d** is used to correct the initial estimated coordinates, as Equation 3.3 shows. This process is iterated until **e** is small enough. Then, the corrected coordinates along with the constrained coordinates are output.

The found coordinates of all vertices are then used to calculate clashes for current position, as described in Subsection 3.3.1. Whether clashes occur or not, the clash values are passed onto a penalty function, as shown in Equation 3.9. The penalty function, based on whether the clash values are positive or negative, decides how much penalty to give, as illustrated in Figure 3.9, to the range of motion. The range of motion to be penalised is added up directly from the values of the perturbed two end position values $\varphi' - \varphi''$, or calculated from the coordinates found Φ from both perturbed end positions Δ' and Δ'', hence is not accurate. The penalised range of motion is not necessarily accurate either, but competes against the initial range of motion from the input that is also not necessarily accurate. After numerous iterations, the SA system is cooled down according to a cooling scheme, described in Section 3.3. When the cooled down function is stopped, an optimised result is regarded as found. The vector of values now contains an optimised set of values.

The range of motion produced by the optimised end position values in the output vector is not necessarily accurate, and is therefore manually checked in the blue block. This is a range-of-motion calculation function, described in Subsection 3.2.5. In this function, the coordinate calculation function (in pink) is used many times again. The two end position values produced from the SA function is first used to find their mean value. This is assumed to be a position where no clash should occur. This value is then used to give constraint to the moving vertex in the coordinate calculation function (in pink). The coordinate calculation function uses the length parameter values from the SA result to find unconstrained coordinates. After the iterative corrector method, coordinates of all vertices are found. With all coordinates known, the clashes are detected. Then, clash values are output from the pink block. If no clash occurs, the mean value is incremented as described in Subsection 3.2.5, the coordinates and then clashes are calculated again in the pink block. This loop continues until any clash

value becomes negative, then this incremented value φ' or Δ' is recorded. Afterwards, the mean value is decremented until any clash occurs, and φ'' or Δ'' is recorded. The accurate range of motion of the parameter values produced by SA is now produced. For more accurate range of motion, smaller steps of the increments and decrements are used as described in Subsection 3.2.5. Note that, in the optimisation process, the calculated Φ, as defined in Subsection 3.2.5, from the two end position values specified by Δ' and Δ'' is used for the comparison of range of motion instead of the dimensionless value $\Delta' - \Delta''$, because their relationship is not perfectly linear.

Chapter 4

Optimisation of the Steffen flexible polyhedron

When Steffen described his flexible polyhedron, he gave a set of parameters of the edge lengths $a - e$ that give a symmetric polyhedron. As the edge lengths vary, a series of flexible polyhedra are produced. With the parameter values varied, these polyhedra here are called *symmetrical* Steffen flexible polyhedra. Steffen also suggested "a good choice of" values for the parameter he defined. With these specific values the polyhedron is called here the Steffen *original* flexible polyhedron. In fact, the symmetry of the Steffen polyhedron is not a necessary part of its flexibility — the two crinkles do not have to be identical. To make use of this freedom, later in the chapter the parameters defined by Steffen are generalised by breaking the symmetry to allow more room for the lengths to vary. The Steffen flexible polyhedra with newly defined parameter scheme are here referred as *generalised/general* Steffen flexible polyhedra. All these flexible polyhedra are called *Steffen flexible polyhedra*.

This chapter first presents the composition of the Steffen flexible polyhedron with the Steffen original flexible polyhedron as an example (Section 4.1). Then, with the parameters defined by Steffen, the range of motion of the Steffen flexible polyhedron is optimised, so that a series of symmetrical Steffen flexible polyhedra are produced (Section 4.2). Lastly, to improve the range of motion even further, the generalised Steffen flexible polyhedron is introduced and optimised (Section 4.3).

4.1 The original Steffen flexible polyhedron

One year after Connelly described crinkles and proved the existence of a flexible polyhedron [9], Steffen described a simple example in his letter to I.H.E.S [23]. The polyhedron

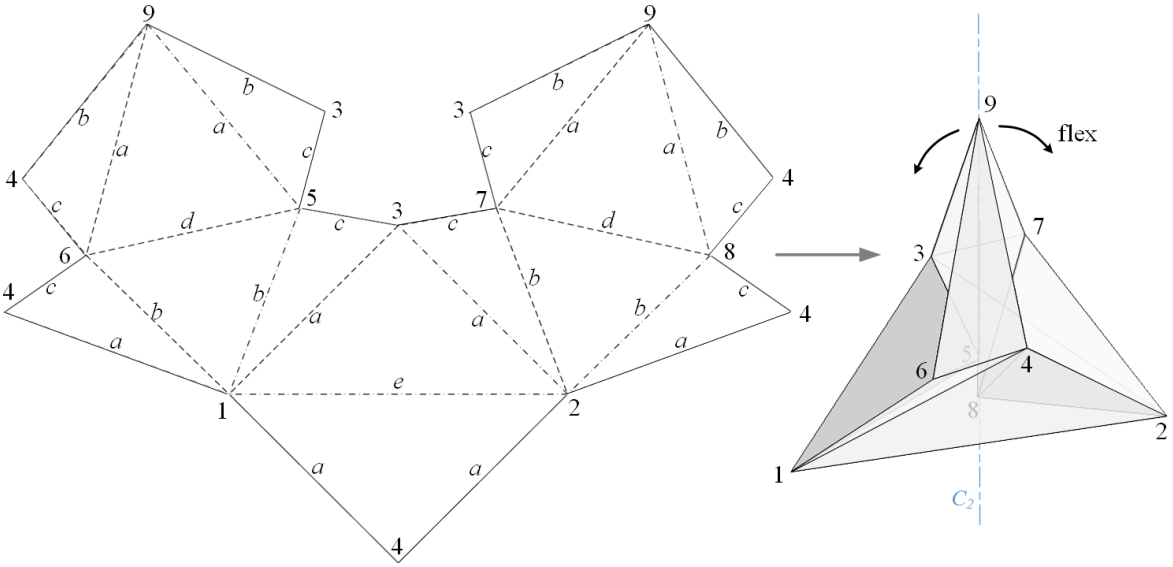

Fig. 4.1 The net of the original Steffen flexible polyhedron and the folded up polyhedron, the edge lengths of which are suggested by Steffen. The parameters defined by Steffen are shown in the net. Due to this parameter setting, the Steffen flexible polyhedron is line-symmetrical. The line of symmetry goes through vertex 9 and the midpoint of line 1-2. Rotating about this C_2 axis, vertices 1, 3, 5 and 6 become 2, 4, 8 and 7. The crinkle on the left has vertex 5 pushing into the polyhedron, and vertex 6 sticking out. Symmetrically, in the right crinkle, vertex 8 is pushed in, and vertex 7 pops out.

he discovered is shown in Figure 4.1 and Figure 4.2 with the parameters he defined in the letter shown on the edges. He specified that a good choice of parameter values are $a = 6$, $b = 5$, $c = 2.5$, $d = 5.5$ and $e = 8.5$. With these dimensions, this polyhedron is here called the Steffen original flexible polyhedron.

This polyhedron is the simplest known flexible polyhedron: it has only 9 vertices, just one more than a cube. It is a triangulated polyhedron: all the polygons composed of the polyhedron are triangles. Hence, if all the rigid faces are removed to leave a pin-jointed frame defined by the original edges, the remained frame will not have any extra mechanisms and will share the kinematics of the original polyhedron with stiff faces. Due to Steffen's parameter setting, the Steffen flexible polyhedron is a line-symmetrical polyhedron. The line of symmetry goes through vertex 9 and the midpoints of line 1-2 and line 3-4 in Figure 4.1. Rotating about this C_2 axis, vertices 1, 3, 5 and 6 become 2, 4, 8 and 7.

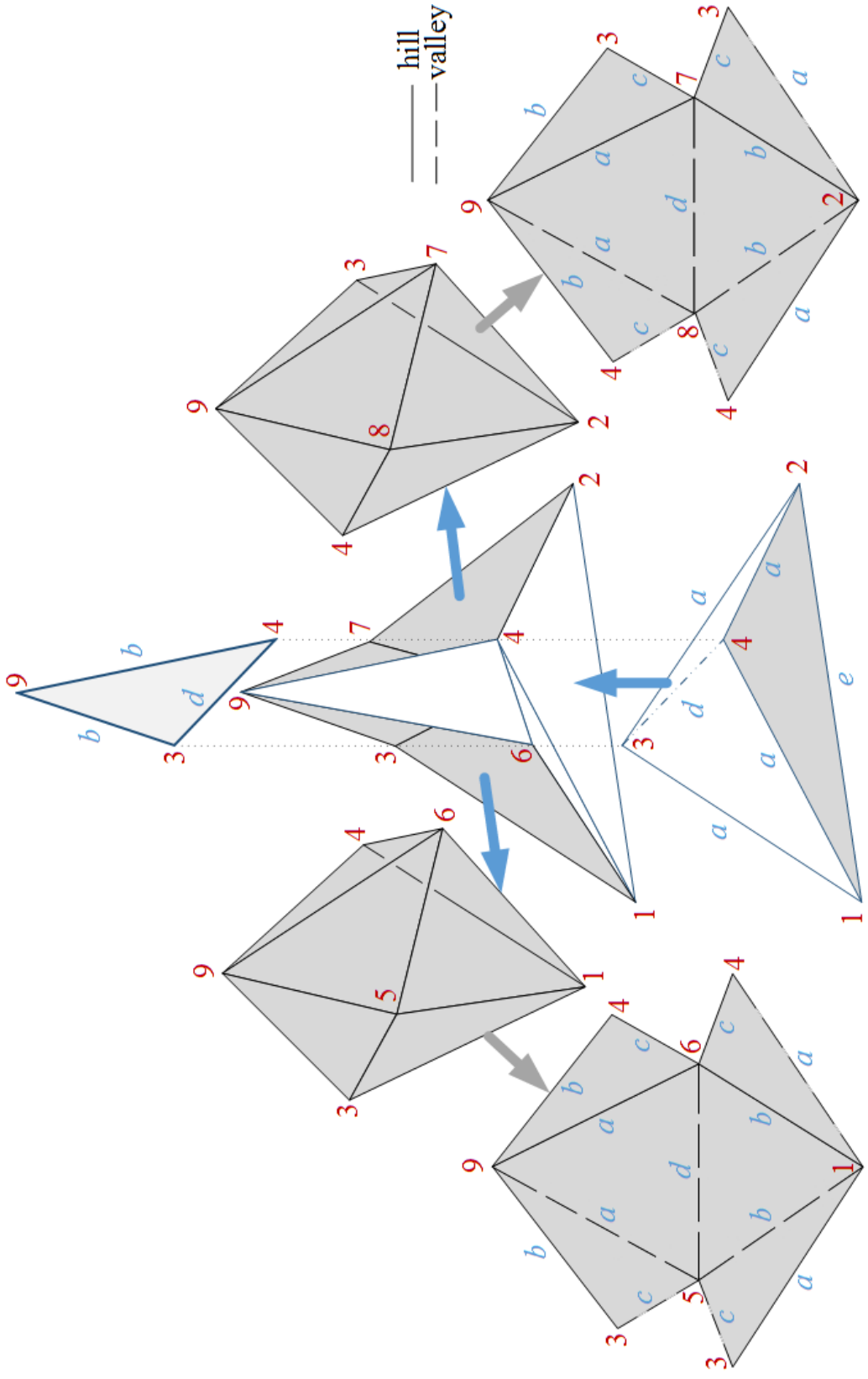

Fig. 4.2 Decomposition of the original Steffen flexible polyhedron. The replaced double-flap triangle is shown at the top, lined up with the tetrahedron at the bottom. The hinge linking the flap 3-9-4 and the tetrahedron 1-2-3-4 is line 3-4. The crinkles that replaced dihedrals 1-3-9-4 and 2-3-9-4 are shown in grey by the sides. Vertices 5 and 8 tuck into the page on the crinkles and points into the polyhedron; vertices 6 and 7 pop out of the page on the crinkles as they stick out on the polyhedron. The nets of the crinkles are shown with hills and valleys indicated. The parameters labelled are Steffen's design.

How the net folds up to form the Steffen flexible polyhedron is shown in Figure 4.1. On the net, vertices 6 and 8 fold into the page, as vertices 5 and 7 fold out of the page, so that on the polyhedron, vertices 6 and 8 stick out and vertices 5 and 7 tuck inwards. For the symmetrical Steffen flexible polyhedron, the crinkles can be in the other direction as shown in Figure 1.6 and Figure 2.16, i.e. vertices 6 and 8 tuck inwards and vertices 5 and 7 stick out.

The decomposition of this polyhedron is shown in Figure 4.2 in order to demonstrate the composition. The double-flap that is replaced by the crinkles is shown above the polyhedron, $\triangle$3-4-9. The crinkle on the left replaces $\triangle$1-3-4 and $\triangle$3-4-9 along with one of the double edge 3-4; the crinkle on the right replaces $\triangle$2-3-4 and the other $\triangle$3-4-9 in the flap along with the other edge 3-4. Thus, hinge 3-4 does not physically exist. However, both crinkles still flex about line 3-4, so the whole polyhedron bends around the virtual hinge 3-4.

Note that there is one redundancy in a Bricard flexible octahedron, so the crinkle maintains the length of the removed edge. Therefore, when two crinkles connect at vertices 3 and 4, each crinkle guarantees a length 3-4, hence, there is one redundancy. As the polyhedron flexes, the original length 3-4 is maintained.

The directions of crinkles are shown as hills and valleys in the nets of the crinkles in Figure 4.2. The parameter setting by Steffen makes both these two crinkles identical and also the net of each crinkle has a plane of symmetry. Further, the tetrahedron 1-2-3-4 beneath the hinge (which is the base of the polyhedron) also has two planes of symmetry and a line of symmetry due to the crinkle directions. Overall, the whole resultant polyhedron is line-symmetrical.

Figure 4.3 shows how a crinkle in the Steffen flexible polyhedron is derived from a Type I Bricard flexible octahedron. It takes one crinkle off the polyhedron and shows the C_2 axis of the crinkle. Through the view point along this C_2, a Type I octahedron drawn by Bricard is compared with this crinkle.

The volume of the Steffen polyhedron is equal to the volume of the tetrahedron base 1-2-3-4 and does not change during the flex. This is because (i) a Bricard flexible octahedron has zero volume, composed of a positive and negative volume, and (ii) the double flap 3-4-9 also has zero volume. The replacement with a crinkle adds a volume and subtracts an equal volume, hence does not change the volume of the original surface. The constant volume of the Steffen flexible polyhedron is proven by Alexandrov [2].

The directions of crinkles are crucial. If both vertices 5 and 7 point in and both vertices 6 and 8 stick out in Figure 4.2, for example, then the polyhedron will be plane-symmetric. The plane of symmetry will contain bar 3-4 and be perpendicular to line 1-2. However, this arrangement of the directions of crinkles in Steffen's model does not allow the crinkles to

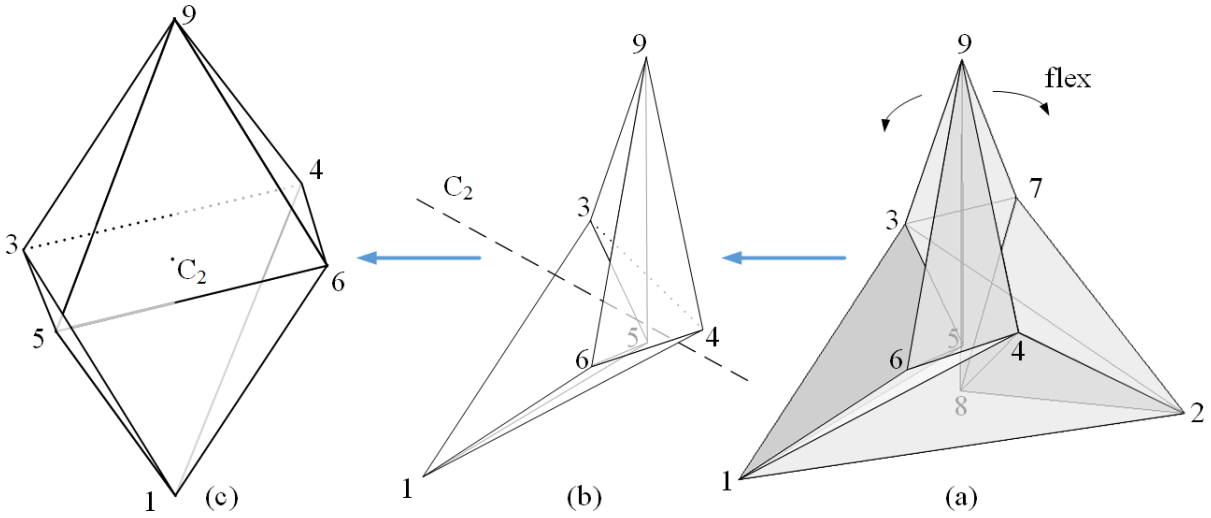

Fig. 4.3 Type I Bricard flexible octahedron used in the Steffen flexible polyhedron. (a) The original Steffen flexible polyhedron. Vertex 9 is able to rotate about the virtual hinge 3-4. (b) The left crinkle in the Steffen flexible polyhedron is taken out. The C_2 axis of the Type I crinkle is shown. The virtual hinge is drawn in a dotted line. The view point in (b) is the same as the view point in (a); the view point in (c) is along the marked C_2 axis. If faces △1-3-4 and △1-4-9 were added back on, the crinkle would become a complete octahedron. Vertex 5 goes behind the resumed dihedral 1-3-9-4, and vertex 6 in front.

avoid each other but constantly clash into each other. In this Steffen polyhedron configuration, only line-symmetrical arrangement of crinkle directions allow the avoidance of clashes. From Figure 4.4, it can be seen that if the crinkle directions allow the polyhedron to be plane-symmetrical, then vertices 5 and 7 will constantly clash into each other. Only when two crinkles crinkle towards the same direction about each of vertices 3 and 4 can the crinkles possibly avoid each other.

However, as the polyhedron flexes, a clash will occur at some point. This clash will stop the flex from going any further. As the polyhedron is symmetrical, the end of the flex on both sides are the same, caused by symmetrical clashes, as shown in Figure 4.5. As the tetrahedron base 1-2-3-4 is invariant during the flex, i.e. vertices 1, 2, 3 and 4 do not change position, the two extreme flexing ends are shown in the same view point, with vertex 9 goes the furthest. As discussed before, there are six potential clashes in a Steffen flexible polyhedron. Their clash values in the Steffen original flexible polyhedron at both ends are given in Table 4.1. When the polyhedron flexes to the left, node 9 is going in the negative direction on x axis, x_9 is -ve. As the polyhedron flexes to the right, node 9 is moving towards the positive direction on x axis, x_9 is +ve.

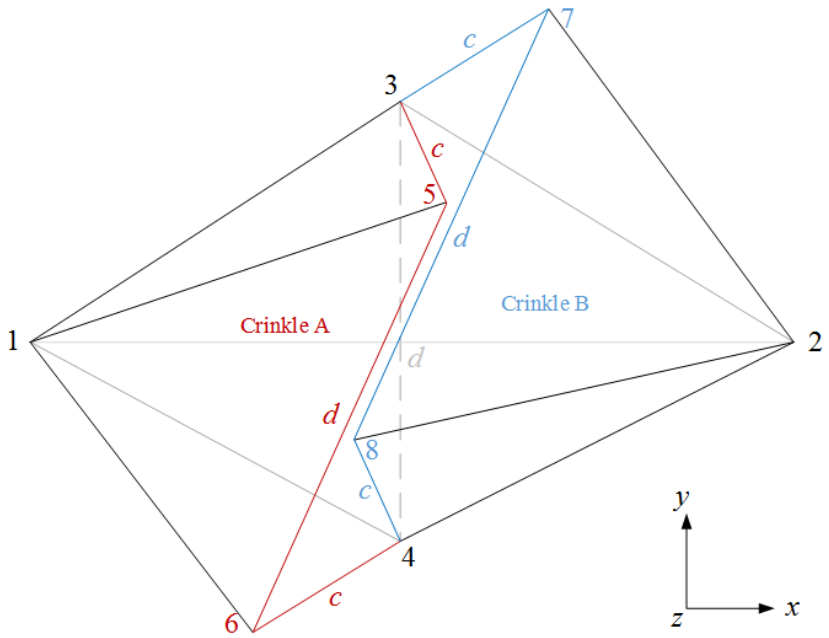

Fig. 4.4 A top view of the Steffen original flexible polyhedron. Any faces containing vertex 9 (the upper part of the crinkles) are removed. The cut edges through the middle of the crinkles are shown in red and blue. This view shows how the crinkles replace hinge 3-4 to avoid clashes from each other and leave a gap between edges 5-6 and 7-8. Note that only edges 1-2 and 3-4 are in true view, hence edges 3-5, 3-7, 4-6 and 4-8 are not in true view.

Table 4.1 Clash values at two end positions of the Steffen original flexible polyhedron

Type	Symmetric pair	Line	Face	$\beta(x_9\text{-ve})$	$\beta(x_9\text{+ve})$
Type Ia	clash A^+	8-9	5-6-9	2.0°	5.8°
	clash A^-	5-9	7-8-9	5.8°	2.0°
Type Ib	clash B^+	5-6	1-4-6	−0.2°	16.7°
	clash B^-	7-8	2-3-7	16.7°	−0.2°
	clash C^+	4-8	1-2-4	2.0°	5.9°
	clash C^-	3-5	1-2-3	5.9°	2.0°

* Note that Type Ib clashes are shown as Type Ia clashes: one line from a triangle is chosen, as shown in Figure 3.5b. Clashes are named in pairs.

** Note that β is the angle between the chosen line and its projection onto the other triangle, defined as Eqn 3.8 shows. A positive β is when the clash does not occur.

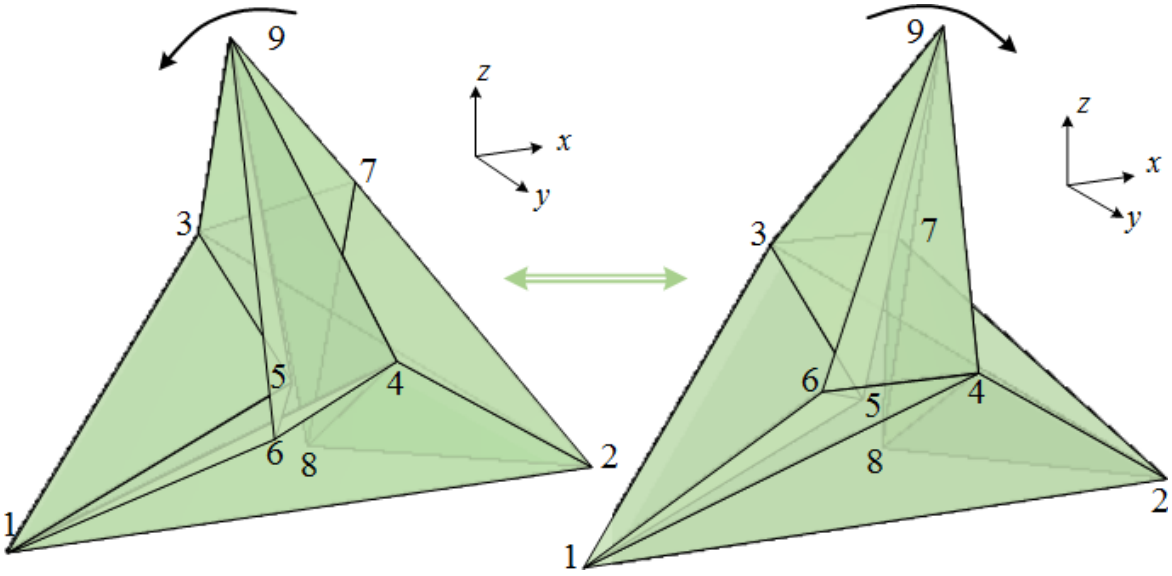

Fig. 4.5 Two end positions of the Steffen original flexible polyhedron. A semi-opaque model shows the two extreme positions that the polyhedron can flex to. The view points are the same; node 9 is flexed to different extreme positions. The flexing movement to each side is stopped by a clash. Due to the line symmetry, the limit of motion on each side is the same, caused by a clash of a symmetrical pair. Although a couple of clashes can occur simultaneously, the movement of the Steffen original flexible polyhedron is stopped by only one clash on each side. On the left, the flex is stopped by clash between △1-5-6 and △1-4-6, which has an angle of 17° between them in the stop on the right. Symmetrically, on the right, it is the clash between △2-3-7 and △2-8-7 that stops the rotation.

The end on the left in Figure 4.5 is caused by clash between △1-5-6 and △1-4-6. Note that the points shown have actually gone slightly beyond the clash at $\beta = 0$ to $\beta = -0.2$. Although clash between △1-2-4 and △8-2-4 and clash between △5-6-9 and line 9-8 are also about to occur, the dihedral angles β for these two clashes are both 2°, as Table 4.1 shows. Note that β is the angle between the chosen line and its projection onto the other triangle, defined as Equation 3.8 shows. In this position, the clashes that are not very likely to occur are between △1-2-3 and △1-5-3 and between △7-8-9 and line 9-5, as the dihedral angles β between them are both 6°. The clash between △2-3-7 and △2-8-7 is far from occurrence, the dihedral angle of which is β =17°. Note that the dihedral angle β is defined to be the angle between the line and the plane of the face for Type Ia clashes, and for Type Ib clashes it is between the selected line from one face and the plane of the other face. For both Type Ia and Type Ib, β is shown in Figure 3.5.

Symmetrically, when flexing to the right, the stop is caused by the clash between △2-3-7 and △2-8-7. Clashes between △1-2-3 and △1-5-3 and between △7-8-9 and line 9-5 are also about to occur, as the dihedral angles β between them are also both 2°. The clash values β for the other three clashes are 6°, 6° and 17° similarly.

In each direction the polyhedron is able to flex by 13.7° before a clash, allowing a full range of motion of 27.4°. This range of motion is shown in three different view angles in Figure 4.6. A cardboard model of this range of motion is shown in Figure 4.7. A side view of the mid-position and top side views of two end positions are shown.

The degree to which the clashes are about to occur at each flexing step, and the full range of motion, are shown in Figure 4.8. Each circle represents a clash value in degrees in

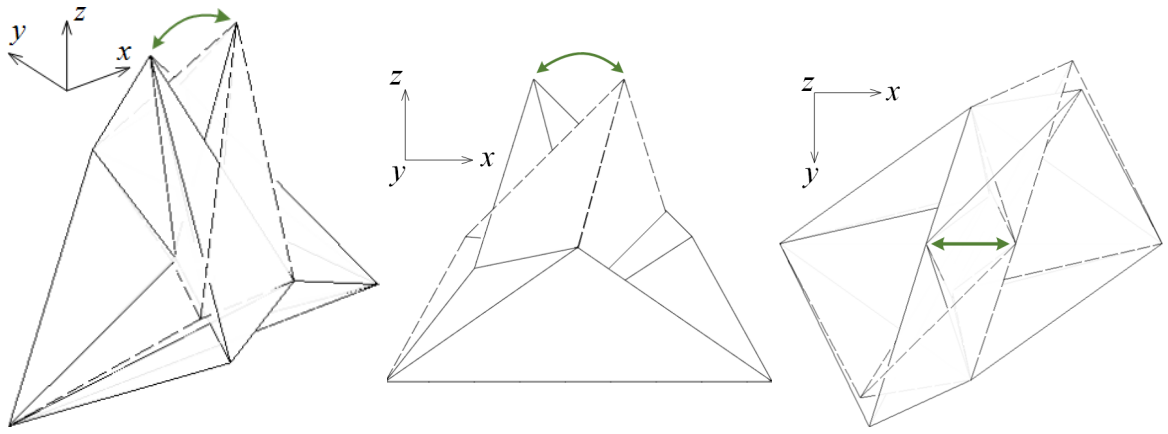

(a) Isometric view (b) Side view (c) Top view

Fig. 4.6 Different views of the Steffen original flexible polyhedron in both end positions. The solid line draws the polyhedron flexing to the left end; the dotted line draws the polyhedron when flexing to the right end.

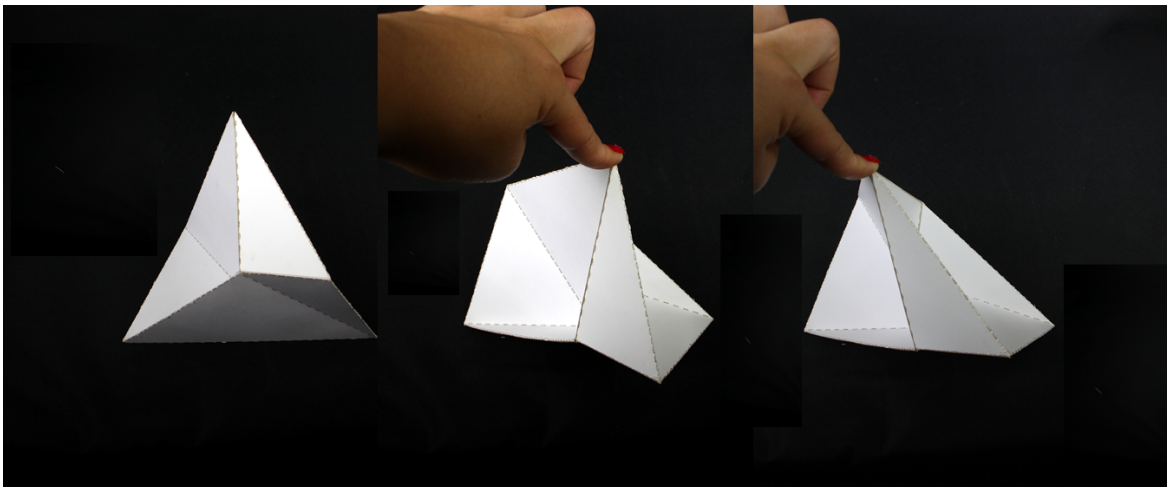

Fig. 4.7 A physical model of the Steffen original flexible polyhedron in the neutral mid-position in side view and two extreme positions in top side view.

the y-axis for a flexing position given in the x-axis. There are six clashes, so there are six coloured lines presenting them in the graph. The red clash line on the left and the green clash line on the right respectively restrict the polyhedron's motion to 13.7° on each side.

4.2 Optimising the symmetric Steffen flexible polyhedron

Although the range of motion of the Steffen original flexible polyhedron is much larger than Connelly's first examples, 27° is still not considerable for potential engineering applications. Therefore, to explore the full potential of Steffen's design, the flexible polyhedron with parameters defined by Steffen is optimised in this section for the maximal range of motion.

Both Table 4.1 and Figure 4.8 show that only one clash occurs to stop the rotation of the Steffen original flexible polyhedron. If this clash can be delayed until another clash occurs, the range of motion may be greater. If all clashes are postponed until there is no room to go any further, then all the clashes or at least some of the clashes may occur at the same time. At this time, the range of motion of the polyhedron is likely to be improved.

To explore the design of Steffen's, the first round of optimisation uses the parameters given by Steffen, shown in Figure 4.2. These parameters make the polyhedron line-symmetrical, so the results produced here are called symmetrical Steffen flexible polyhedra. Numeric tools described in Chapter 2 are used in this optimisation. However, due to the symmetry of the parameter scheme designed by Steffen, the computational model is set up in a simpler way than shown in Figure 3.1 and only half of the range of motion is calculated. Vertices 1 and 2 have the same choice but $y_3 \neq 0$, rather $y_9 = 0$. That is to say, hinge 3-4 is perpendicular to

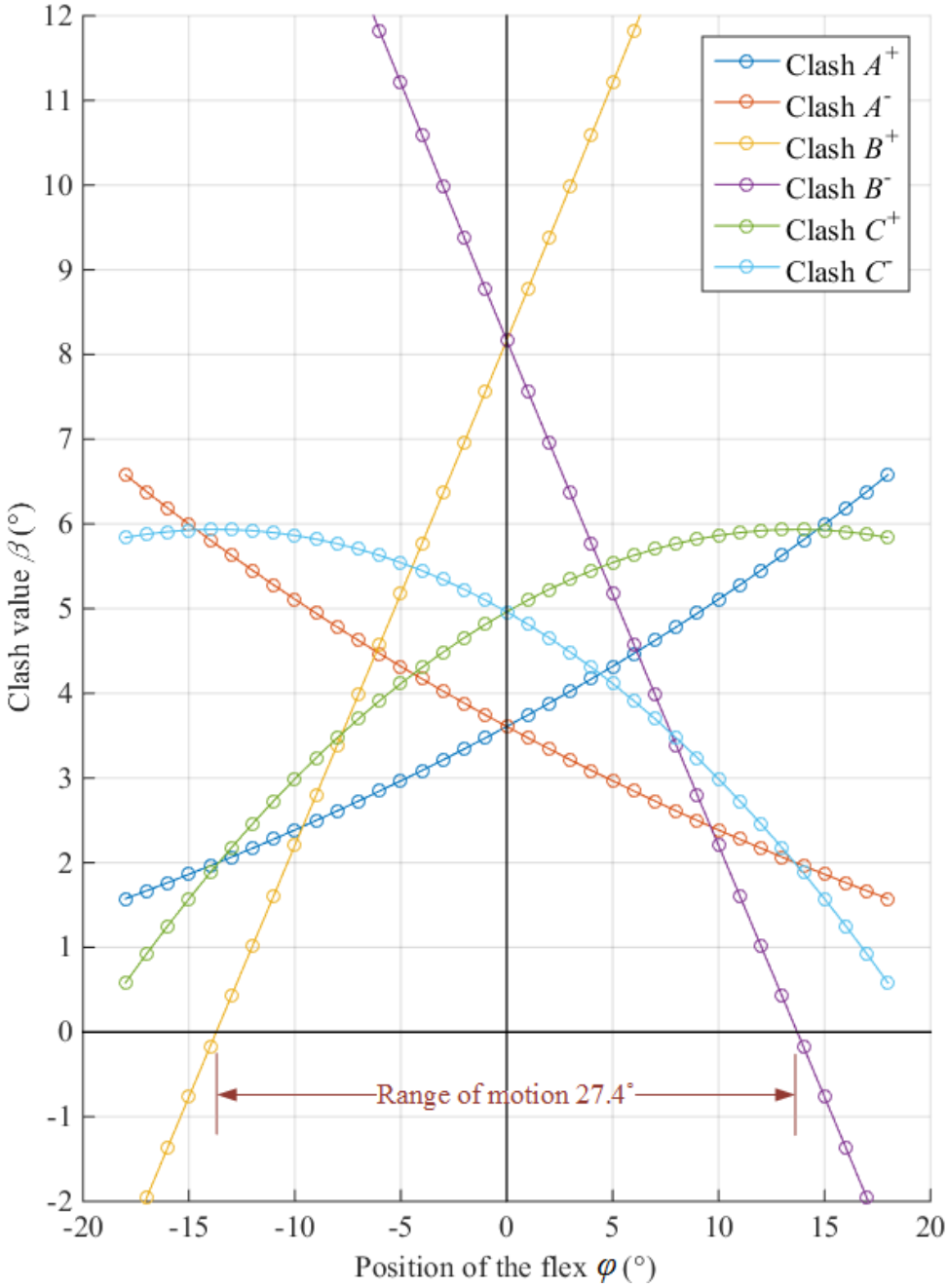

Fig. 4.8 Clashing values of the Steffen original flexible polyhedron against the rotation of polyhedron. On the x-axis are the angles of rotation away from the middle neutral position (unit in degrees); on the y-axis are the angles of six clashes inside the polyhedron (unit in degrees). Six clashes are labelled as in Table 4.1.

plane XOZ; the midpoint of 3-4 and vertex 9 is in plane XOZ. The coordinates of vertices 3 and 4 are calculated and given as constraints. All coordinates of vertex 9 are also calculated with an angle variable φ defining the rotational angle away from the mid-neutral position. If $\varphi = \varphi'$ when a clash first occurs, $2\varphi'$ is the range of motion.

The optimisation starts with initial values given by Steffen, $a = 6$, $b = 5$, $c = 2.5$, $d = 5.5$ and $e = 8.5$. With e stays invariant as reference, a, b, c and d are varied according to the perturbation scheme described in the simulated annealing algorithm. The optimised results are presented in Figure 4.9.

As described before, the optimisation is a multi-objective optimisation, also called Pareto optimisation. The two objectives are the range of motion and the regularity. The results in Figure 4.9 are shown on a plot of range of motion against regularity. Each orange cross is the result of an optimisation run. The optimisation started from the original Steffen flexible polyhedron, which is shown as a green triangle on the graph, A. A blue line drew as part of the convex hull of the Pareto optimals and coordinate axes is the Pareto Front of the multi-objective optimisation.

It is observed that, as the regularity decreases and the range of motion grows, the "depth" of the crinkles shrinks, which means the value of parameter c in Figure 4.4 becomes very small. When the range of motion reached the maximum angle, 52.5° at B, the long and sharp triangles are most severe. This irregularity of triangles can also be observed in the net of result C, which is slightly more regular than B. From the green polyhedron above C, it is noticeable that the Steffen polyhedron now looks almost like its "near-polyhedron".

As described in Section 2.5.1 and Section 3.3.1, the regularity is given a threshold value. This threshold value pushes the regularity to be greater or smaller. While achieving the largest Pareto Front, ten values of the regularity are selected, $R^C = 0.05$, $R^D = 0.1$, $R^E = 0.17$, $R^F = 0.2$, $R^G = 0.25$, $R^H = 0.3$, $R^I = 0.33$, associated with points C, D, E, F, G, H, I in Figure 4.9. When the regularity is restricted to these values, the SA process does not necessarily just produce polyhedra with these regularity values precisely all the time. The actual R values and range of motion are plotted on the graph in Figure 4.9. For the absolute maximum range of motion, the regularity is allowed to change freely. When the regularity reaches the value of 0.013, the range of motion of on each side becomes 26.25°. Due to the symmetry, the full range of motion for the absolute maximum is 52.5°. As the regularity goes below 0.013, the numerical methods used become difficult to find a solution. To save time, optimisation further than this point is not conducted.

On the other side of the Pareto front, the regularity is enlarged until the range of motion is sacrificed to ideally zero. When the regularity is pushed to as large as 0.34, it becomes

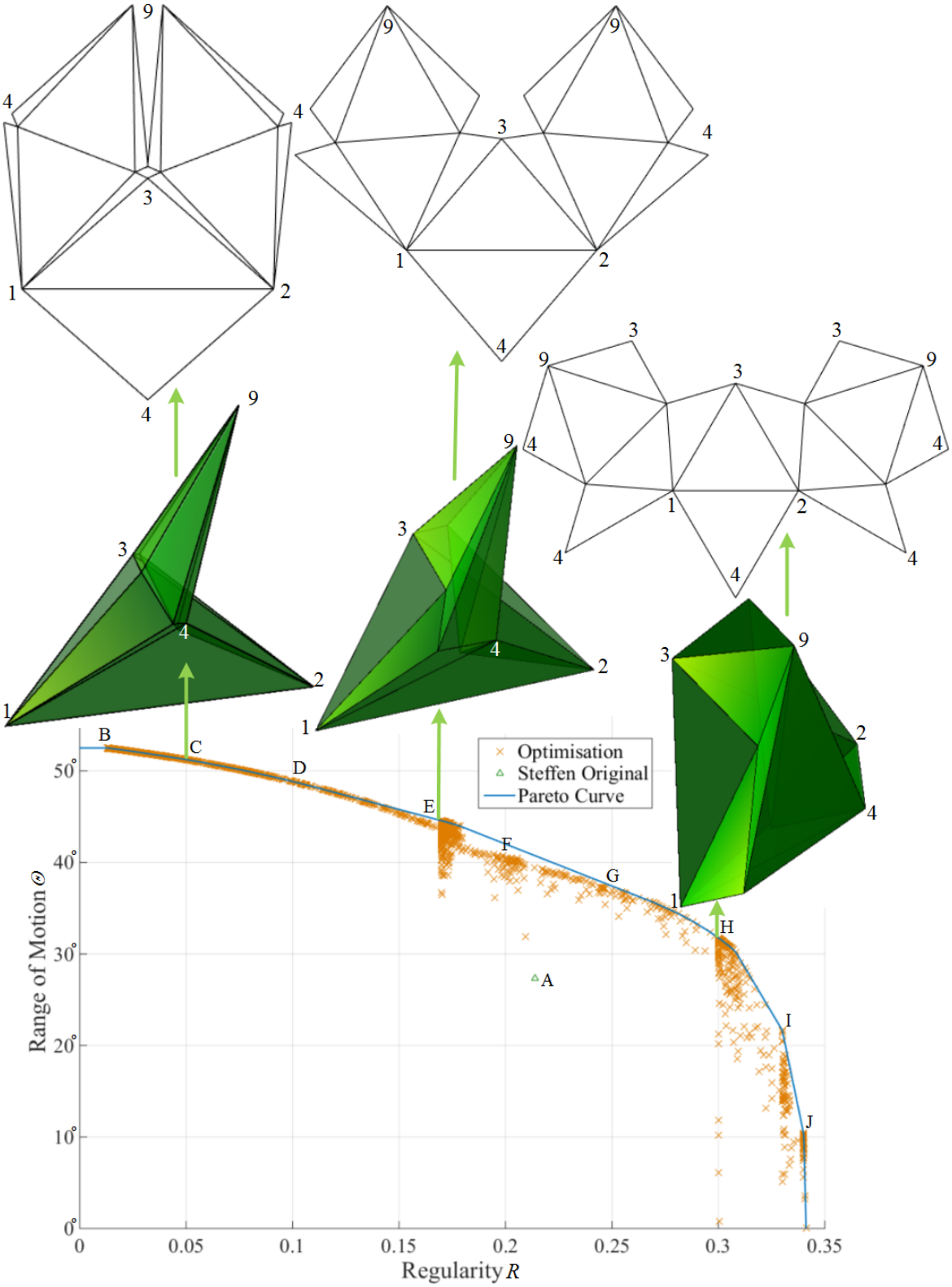

Fig. 4.9 Multi-objective optimisation results of the symmetrical Steffen flexible polyhedron. The varied parameters are defined by Steffen, hence the resultant polyhedra are line-symmetrical. The graph shows their range of motion against their regularity. Each orange cross in the graph represents a local optimal. The range of motion and regularity of the original Steffen flexible polyhedron are shown as a green triangle, A. The blue line on the convex hull of these optimised results is the Pareto Front. Three polyhedra, C, E and H are shown in 3D, and their nets are above. The parameter values for ten polyhedra A – J are given in Table 4.2.

numerically difficult to push it even greater. To save optimisation effort, the optimisation is stopped here. The range of motion is reduced to 10.4°.

The original Steffen flexible polyhedron with dimensions suggested by Steffen, A, shown as a green triangle on the graph, has a large distance away from the Pareto front above it (between F and G), this polyhedron can have a further range of motion of 15° without sacrificing any regularity. With the same range of motion (between H and I), the polyhedron can be much more regular, $R = 0.2139 \rightarrow 0.32$. Between point E $(R, \Theta) = (0.17, 44.5°)$ and point H $(R, \Theta) = (0.3, 31.8°)$, the optimised polyhedra are reasonably regular and have a larger range of motion than the Steffen original flexible polyhedron.

There are nine optimals, B – J, labelled on the Pareto front. Three of them, C, E and H, are chosen to be illustrated above the Pareto Front in Figure 4.9 in order to demonstrate their shapes and nets. The difference of their shapes, hence regularity, can be observed in both the polyhedra (coloured in green) and the nets. The degree to which the polyhedron is able to flex can also be observed, as the polyhedra (in green) are all flexed to the right end of their motion. All nine results along with the original Steffen flexible polyhedron, A, are presented in Table 4.2 with their data to provide a more specific idea of the optimised results. The range of motion Θ is shown in a descending order, as the regularity R ascends. Length parameters a and d change dramatically, and the crinkle depths c varies most, whereas b stays more or less the same around 6. Note that e is fixed as reference for the comparison of values. All four variables grows closer to e as the regularity increases. The table demonstrates that the original Steffen flexible polyhedron, A, does not reach its maximum potential. Data of more Pareto optimals are listed in Table B.1 in Appendix B.

Table 4.2 Data of chosen Pareto optimals of symmetrical Steffen flexible polyhedra

Polyhedra labelled in Figure 4.9	Result Index	Objectives Θ	Objectives R	Parameters a	Parameters b	Parameters c	Parameters d	Parameters e
	B	52.5°	0.013	5.5897	5.5464	0.1215	3.9486	8.5
	C	51.2°	0.05	5.6666	5.4959	0.4807	4.2500	8.5
	D	48.8°	0.1	5.7925	5.4370	0.9988	4.6816	8.5
	E	44.6°	0.17	6.5480	5.7564	1.8818	5.5754	8.5
	F	40.5°	0.2	8.0459	6.5934	2.7175	6.3879	8.5
	A	27.4°	0.2139	6	5	2.5	5.5	8.5
	G	37.0°	0.25	8.5291	6.4675	3.7932	7.1545	8.5
	H	31.8°	0.3	8.4308	5.9183	4.8679	7.7451	8.5
	I	21.7°	0.33	8.8174	5.7959	5.9376	8.4761	8.5
	J	10.4°	0.34	8.1383	5.7008	5.5161	8.5020	8.5

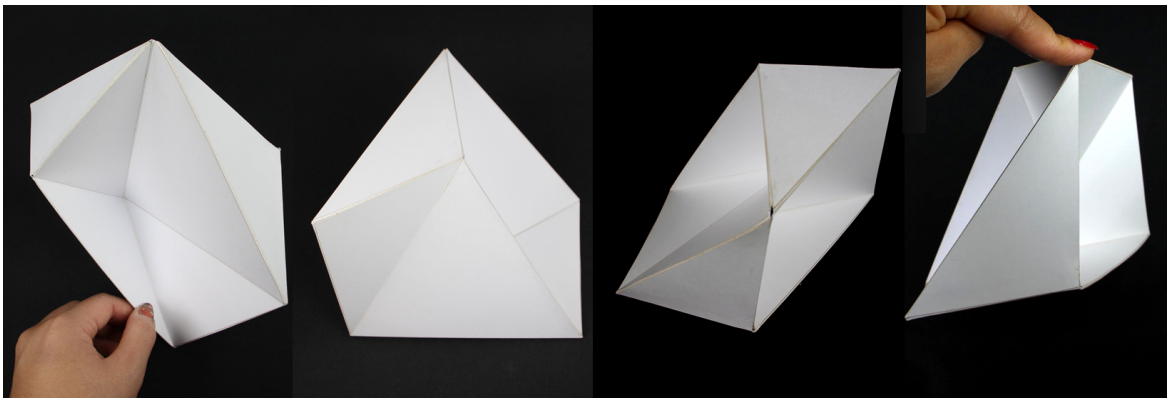

Fig. 4.10 Physical model of an optimised symmetrical Steffen flexible polyhedron on the Pareto front, H in Figure 4.9 and Table 4.2. This polyhedron has a regularity of 0.3 and a range of motion of 32°. It is at the mid-neutral position. The front view, side view, top view and top side view are shown.

The most regular example of the three illustrated Pareto optimals in Figure 4.9, C, E and H, is H. This example is much more regular than the Steffen original polyhedron and still has a larger range of motion. This is observable in Figure 4.9 between point A and H. The regularity of H is 0.3 and the range of motion is 31.8°. Here H is chosen to be demonstrated in more detail in Figure 4.10 and Figure 4.11. A physical model of H is shown in Figure 4.10. The same view points are shown in the first two images as the first two view points in Figure 4.11. A top view is given in the third image; a top side view is given in the last image. All four images are of the polyhedron H in the mid-neutral position. The Matlab images in Figure 4.11 are shown with the polyhedron flexed to one end position; this end position is the same in all three images, as the two flexing end positions are identical due to symmetry. In Figure 4.11 clashes can be observed in different views. In this position, node 9 is flexed towards node 1, so x_9 coordinate has the smallest value. As Table 4.3 shows, three clashes occur almost simultaneously: the valley 8-9 clashes onto face 5-6-9; the dihedral 5-1-4-6 almost touches: the dihedral angle between $\triangle$1-4-6 and $\triangle$1-5-6 is close to zero; and the dihedral 1-2-4-8 almost clashes as well: the dihedral angle between $\triangle$1-2-4 and $\triangle$2-4-8 is even closer to zero. All these three clashes can be observed in each of the semi-opaque models in Figure 4.11.

The six clashes in the symmetrical Steffen flexible polyhedron, H, are shown in pairs in Table 4.3. There are one pair of Type Ia clashes and two pairs of Type Ib clashes. Within each pair, one of them occurs as the polyhedron flexes to one direction, and the other clash occurs as the polyhedron flexes to the other direction. At both extreme ends, the degree to which they are likely to occur is the same due to the symmetry. Again the Type Ib clashes are shown in the form of Type Ia clashes. The dihedral of Type Ib clashes — two triangles

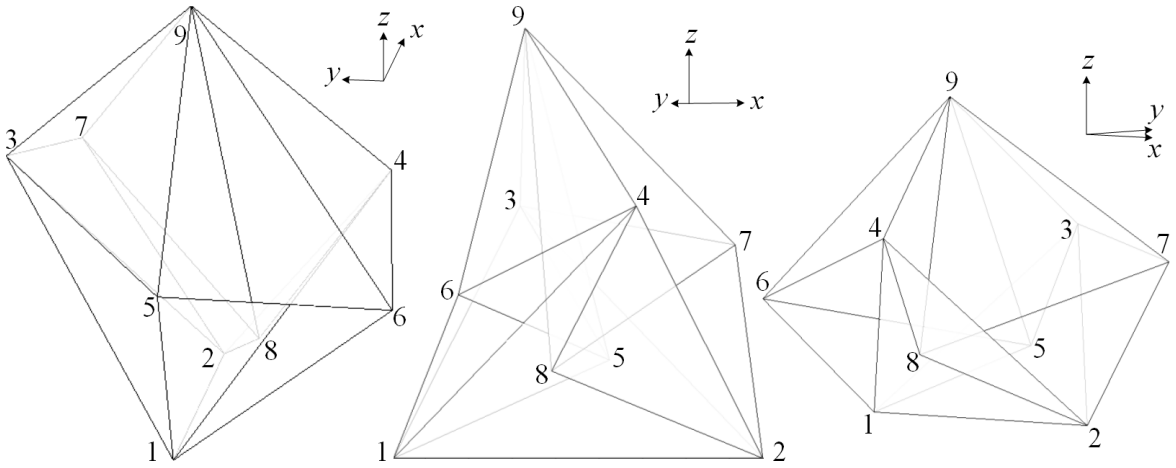

Fig. 4.11 One extreme position of an optimised symmetrical Steffen flexible polyhedron on the Pareto front, H in Figure 4.9 and Table 4.2, $R = 0.3$, $\Theta = 32°$. This semi-opaque model shows the end position where node 9 flexes towards node 1. The flexing movement is stopped by three clashes all together. In the left view (front view), the line 8-9 and △5-6-9 clearly clash; in the middle view (side view), △1-4-6 and △1-5-6 clearly clash; in the right view, △1-2-4 and △2-4-8 clearly clash. The clash values for both ends are shown in Table 4.3.

Table 4.3 Six clash values at both ends of the optimised symmetrical Steffen flexible polyhedron H $R = 0.3$, $\Theta = 32°$

Type	Symmetric pair	Line	Face	$\beta(x_9\text{-ve})$	$\beta(x_9\text{+ve})$
Type Ia	clash A^+	8-9	5-6-9	$-0.0°$	$4.9°$
	clash A^-	5-9	7-8-9	$4.9°$	$-0.0°$
Type Ib	clash B^+	5-6	1-4-6	$0.002°$	$20.0°$
	clash B^-	7-8	2-3-7	$20.0°$	$0.002°$
	clash C^+	4-8	1-2-4	$0.0007°$	$5.6°$
	clash C^-	3-5	1-2-3	$5.6°$	$0.0007°$

* Note that Type Ib clashes are shown as Type Ia clashes and that β is the angle between the line and its projection onto the triangle, defined as Eqn 3.8.

that share an edge — has one line chosen from one triangle, and the dihedral angle β is the angle between the chosen line and its projection onto the other triangle.

In this optimised example, H, all three clashes on one side occurs simultaneously. Table 4.3 shows clash values at both ends but does not show how the clash values change between the two ends. Figure 4.12 shows clash values at each flexing step, backward and forward, even after a clash occurs. The graph shows that three coloured clash lines go across the x-axis at more or less the same point. This point is 16° away from the origin on each side, giving a full range of motion of 32°. Comparing to Figure 4.8, the clash point is pushed from within 15° to beyond 15° on each side of x-axis.

A physical model of a Pareto result that is fairly regular and has a large range of motion is shown in Figure 4.13. This model is E in Figure 4.9 and Table 4.2, having a regularity of 0.17 and a range of motion of 45°. Side view of this polyhedron in two end positions and the mid-position is shown in the first row; the second row shows the top side view of the same positions.

A sensitivity study is conducted on two examples to show how sensitive the range of motion of an optimised polyhedron is to its parameter values. The first example chosen is the polyhedron that has the largest range of motion, result B in Figure 4.9 and Table 4.2. The second example chosen is the polyhedron that has a fairly large regularity, result H. Figure 4.14 shows that, in general, parameters d (the curve in purple) and e (in green) have least influence. They are the dimensions of the tetrahedron base. The crinkle depth parameter c (in yellow) has a much greater influence, but no greater than parameters a and b (in blue and orange respectively). The range of motion of B is extremely sensitive to these two parameters. In the second graph, when the polyhedron is more regular, the influences of parameters are more evenly distributed. Parameters a and b have much less influence, more or less than parameters c and d, although b still has the most influence. However, the range of motion becomes more sensitive to d and e.

4.3 Generalisation of the Steffen flexible polyhedron

The flexible polyhedron designed by Steffen is simple and symmetrical. It has the potential to achieve a range of motion greater than 50°. However, it is discovered that this configuration has the potential to achieve further larger range of motion, and the simplicity of parameter setting and symmetry need not to be kept. Only the local symmetry required by the crinkles (described in Section 2.3 and Section 2.4) need to be kept in order to guarantee the length of the replaced hinge, and hence guarantee flexibility. To fully explore the maximum range of

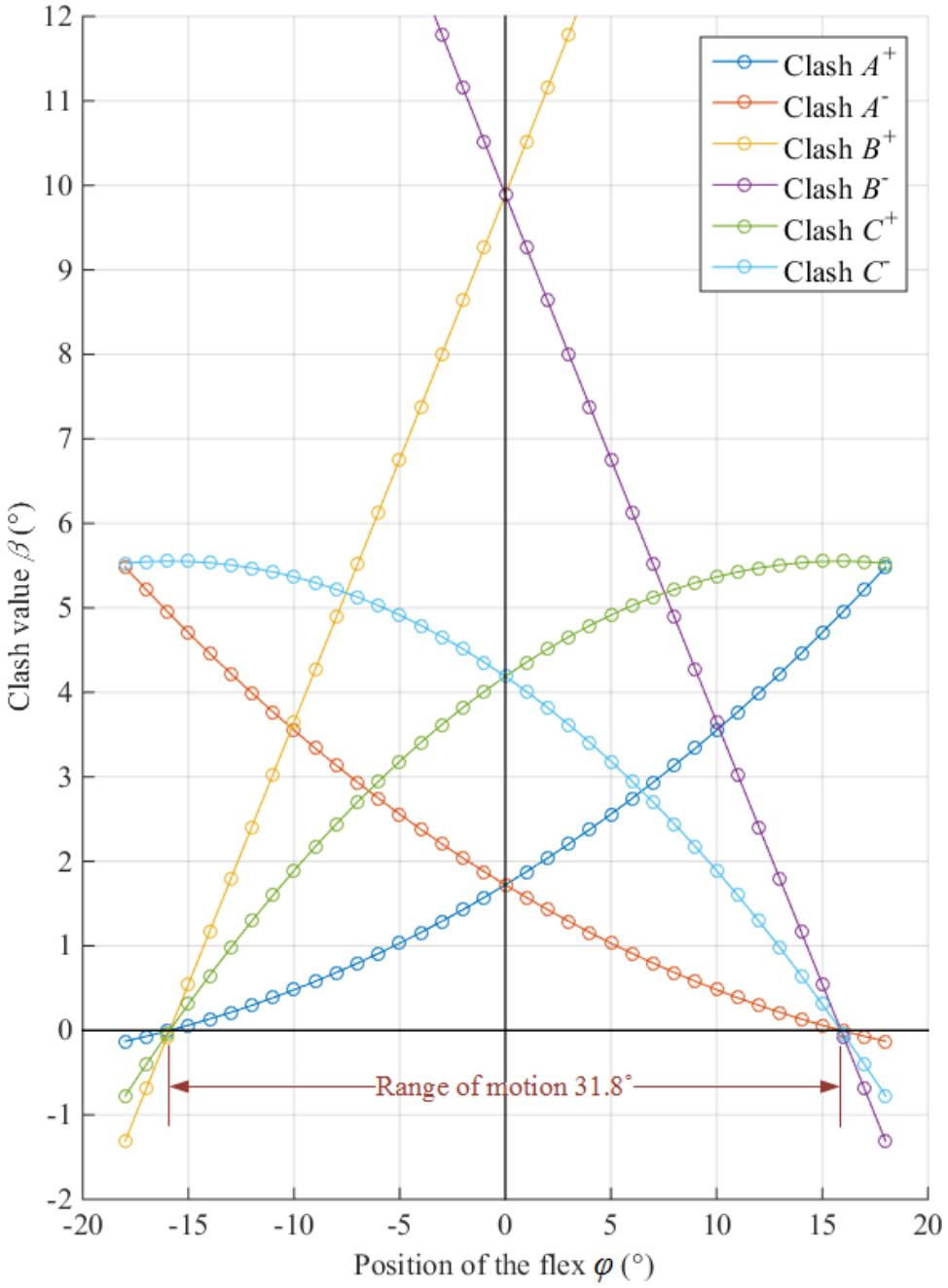

Fig. 4.12 Clashing values of an optimised symmetrical Steffen flexible polyhedron, H, against the flexing position. This polyhedron is on the Perato Front of optimised symmetrical Steffen flexible polyhedron with the parameters defined by Steffen, labelled H in Figure 4.9, $R = 0.3$, $\Theta = 32°$. On the x-axis are the angles of rotation away from the middle neutral position; on the y-axis are the angles of six clash values at each flexed position. Clash names are labelled as in Table 4.3.

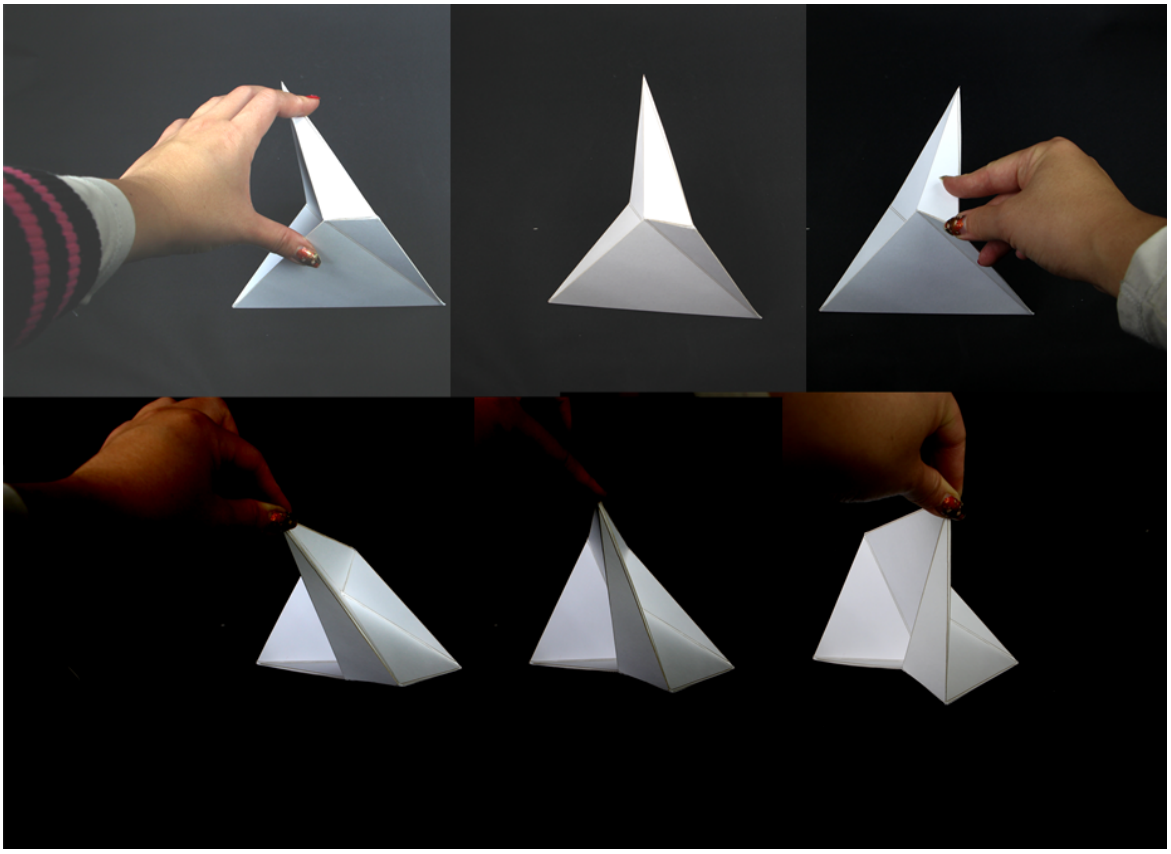

Fig. 4.13 Physical model of an optimised symmetrical Steffen flexible polyhedron on the Pareto front. This is E in Figure 4.9 and Table 4.2, $R = 0.17$, Θ =45°. Two extreme positions and the mid neutral position are shown. Two view points are shown for these three positions: side view and top side view.

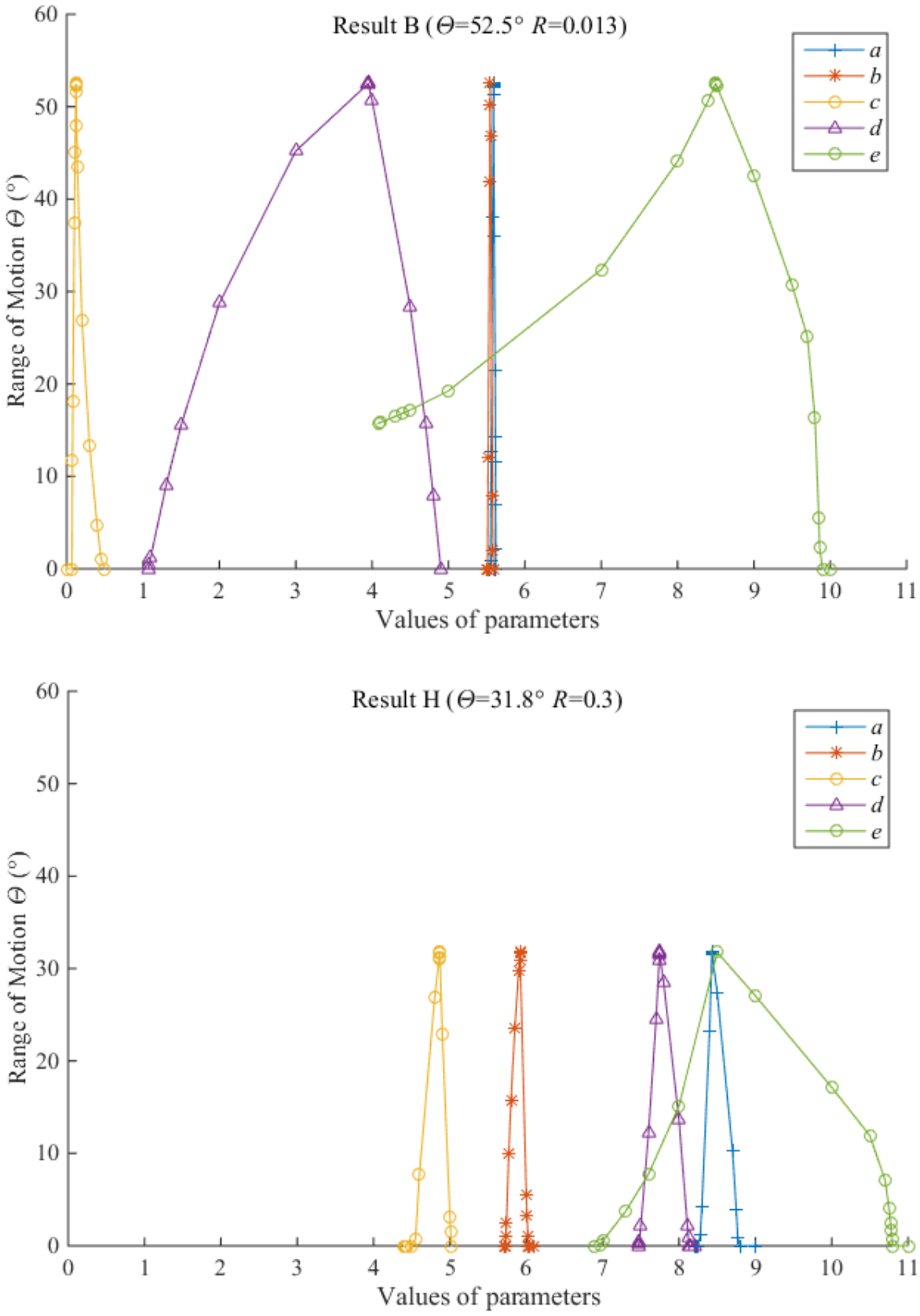

Fig. 4.14 Sensitivity of the range of motion to the variations of length parameter values. Two optimised results on the Pareto Front are used, B and H. For each coloured plot, one parameter varies as all other parameters retain the values shown in Table 4.2.

motion of this 9-vertex flexible polyhedron with such a simple design, many more parameters are introduced to allow more freedom to vary the bar lengths.

From Figure 4.2 it can be seen that the crinkle on the left does not need to be the same as the crinkle on the right, as long as they maintain the same length of hinge 3-4. Therefore, these two crinkles can have completely different sets of parameters as Figure 4.15 shows. The only edges that are shared are 3-9 and 4-9; and the only lengths that needs to be the same are $l_{3-4} = l_{5-6} = l_{7-8}$. Because Steffen chose to use Type I crinkles, there are six equal edges by symmetry in the crinkle on the left, $l_{3-4} = l_{5-6}$, $l_{3-5} = l_{4-6}$, $l_{3-9} = l_{1-6}$, $l_{5-9} = l_{1-4}$, $l_{4-9} = l_{1-5}$ and $l_{6-9} = l_{1-3}$; and in the crinkle on the right, there are $l_{3-4} = l_{7-8}$, $l_{3-7} = l_{4-8}$, $l_{4-9} = l_{2-7}$, $l_{8-9} = l_{2-3}$, $l_{3-9} = l_{2-8}$ and $l_{7-9} = l_{2-4}$. The nearly-polyhedron does not need to be symmetrical either. The replaced flap can have three different lengths, hence edge lengths 3-9 and 4-9 can be different $l_{3-9} \neq l_{4-9}$. The tetrahedron at the bottom can have six different lengths $l_{1-4} \neq l_{2-4} \neq l_{1-3} \neq l_{2-3} \neq l_{1-2} \neq l_{3-4}$, giving four extra parameters.

Note that in any replacement, either Type I crinkle, Type II crinkle or Type III crinkle can be chosen. Because Steffen chose two Type I crinkles and they seem to be able to give considerable range of motion, in the generalisation these two Type I crinkles continue to be used. Theoretically, Type II and Type III crinkles can also be used in any combination and might be able to produce even better results; however these possibilities are not yet explored. Instead, the capability of the two Type I crinkles are fully searched in this dissertation.

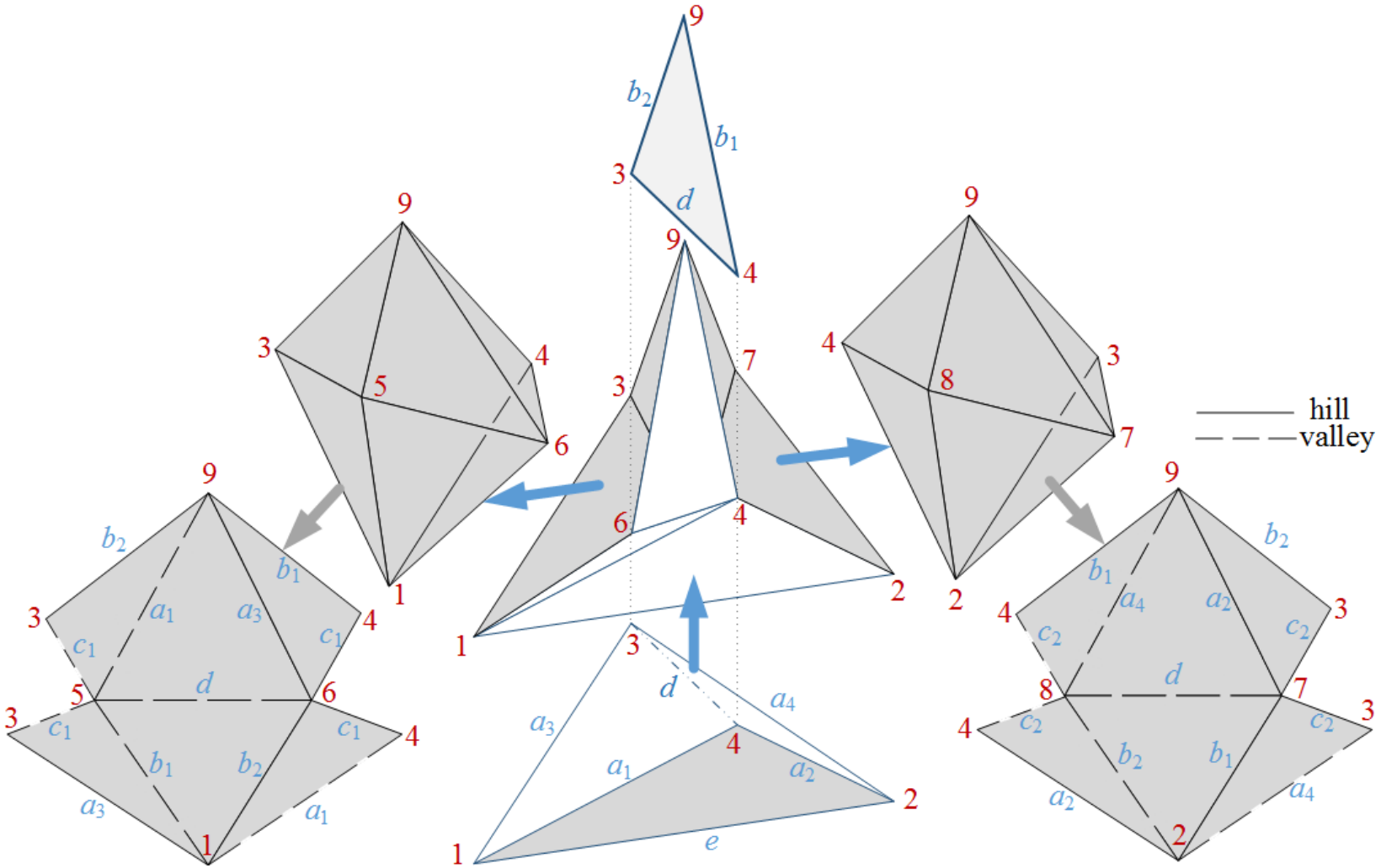

Fig. 4.15 Decomposition of the generalised Steffen flexible polyhedron with parameters newly-defined, but drawn with the edge lengths suggested by Steffen. Both the triangle flap and the tetrahedron have more freedom to vary the lengths. The crinkles are still Type I, so they are still line-symmetric. However, each has its own set of parameters, so that they have more room to change shape in order to avoid clashes. The hinge length l_{3-4} is the same in the tetrahedron and in the two crinkles, $l_{3-4} = l_{5-6} = l_{7-8}$.

As shown above, a general crinkle has six parameters as shown in Section 2.3. Two general Type I crinkles need 12 parameters. However, because the hinge length 3-4 needs to be the same, the same parameter d is used in both crinkles. This reduces the use of one parameter. Also, since these two crinkles share the edges 3-9 and 4-9, in both crinkles the same parameters need to be used, b_1 and b_2. This reduces two more parameters. Including the bottom edge of the tetrahedron e, the new parameter scheme gives 10 parameters for a general Steffen flexible polyhedron. Steffen's design could have 5 more parameters to allow more variation for a better range of motion.

These 10 parameters are optimised to maximise the range of motion with the numerical tools described in Chapter 2. e is again chosen to be invariant during the optimisation $e = 8.5$ for reference reasons. The computation model is set exactly as described in Section 3.1, different from the model in Section 4.2 for symmetrical Steffen flexible polyhedra. The start point of the optimisation of this generalised Steffen flexible polyhedron is also the Steffen original flexible polyhedron, the dimensions of which for the new parameters are shown at the top as polyhedron A in Table 4.4.

Optimised results are presented in Figure 4.16. Each orange cross represents a local optimal, which is the global optimal from an SA run. The regularity of the shape is restricted at more than 10 different values. The regularity is pushed to the maximum value of 0.35, where the range of motion sacrifices to zero. In search of the absolute maximum range of motion, the regularity is not restricted. The maximal range of motion is increased to almost 60° as a result of the generalisation of parameters. The regularity of the polyhedron that has

Table 4.4 Data of Pareto optimals of generalised Steffen flexible polyhedra (labelled in Figure 4.16)

Result Index	Objectives		Parameters									
	Θ	R	a_1	a_2	a_3	a_4	b_1	b_2	c_1	c_2	d	e
A	27.2°	0.219	6	6	6	6	5	5	2.5	2.5	5.5	8.5
B	58.9°	0.019	5.92	5.49	10.00	9.50	9.28	5.34	0.97	0.36	6.25	8.5
C	56.2°	0.05	6.02	4.91	10.36	9.36	8.67	4.42	2.46	0.98	6.55	8.5
D	51.1°	0.1	6.33	7.65	7.73	6.41	6.79	6.62	1.45	1.51	9.64	8.5
E	48.9°	0.15	6.58	7.64	7.69	6.61	6.51	6.49	1.96	1.93	8.68	8.5
F	46.8°	0.18	6.67	7.78	7.67	6.63	6.35	6.36	2.32	2.38	8.50	8.5
G	43.6°	0.213	7.07	8.08	8.08	7.07	6.38	6.38	2.95	2.95	8.56	8.5
H	36.7°	0.27	7.62	8.39	8.39	7.62	6.11	6.12	4.11	4.11	8.49	8.5
I	26.9°	0.32	8.96	9.08	9.08	8.97	5.85	5.85	5.94	5.95	8.44	8.5
J	10.2°	0.34	8.22	8.17	8.17	8.22	5.72	5.72	5.57	5.57	8.50	8.5
K	0.6°	0.348	8.79	8.06	8.04	8.78	5.88	5.89	6.01	6.01	8.53	8.5

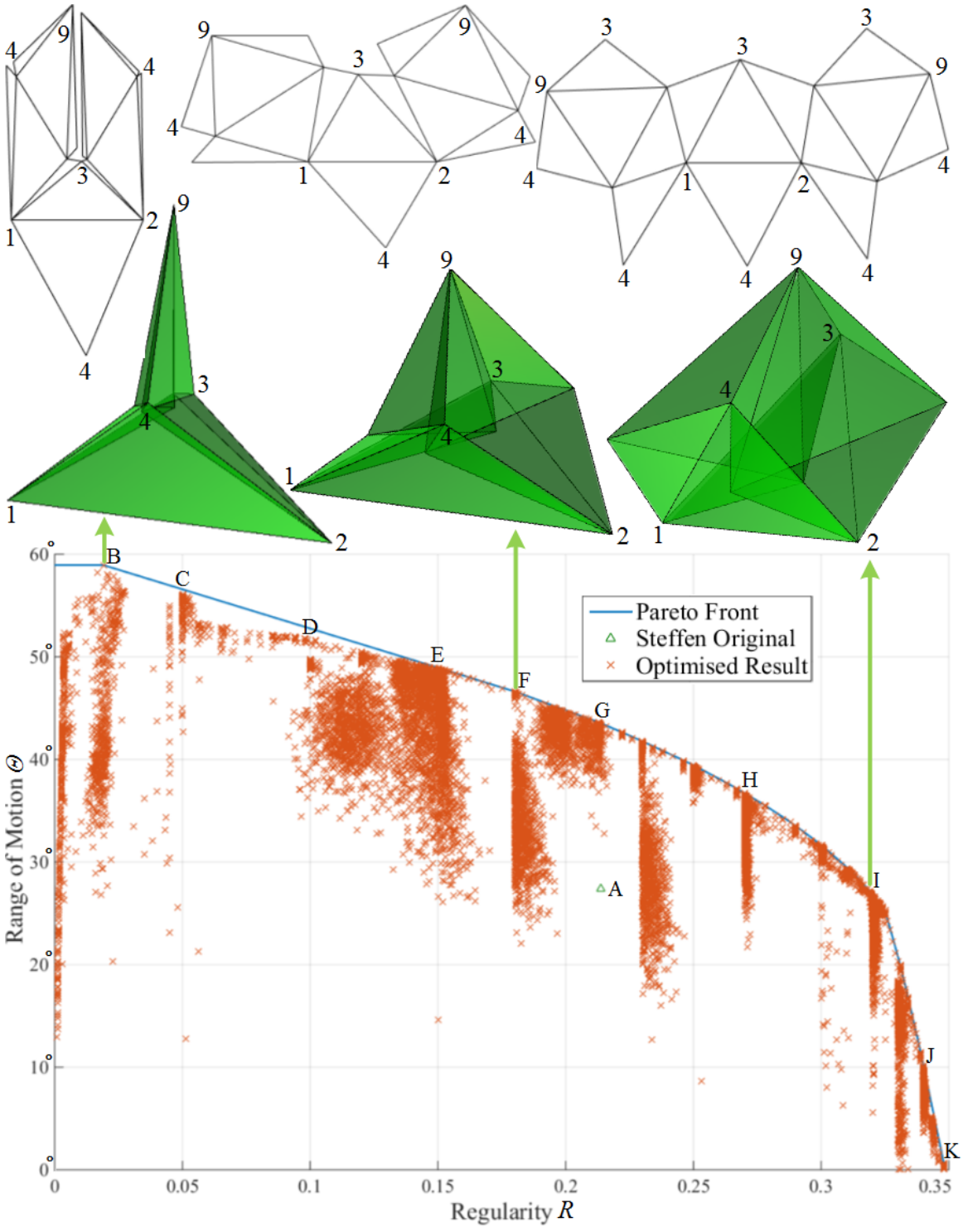

Fig. 4.16 Pareto optimisation results of the generalised Steffen flexible polyhedron. The polyhedron has newly-defined parameters shown in Figure 4.2, generalised from those given by Steffen: each crinkle is still line-symmetric, but the whole polyhedron is not symmetric anymore. Each orange cross in the graph is the result of one optimisation run. The Steffen original flexible polyhedron is shown as a green triangle, A. The blue part of the convex hull of these optimised results is the Pareto Front, on which three results with different regularities (B, F and I) are shown with their models and nets above. The data of labelled results A – K are shown in Table 4.4.

the absolute maximum range of motion is reduced to less than 0.02. When the regularity is pushed to be even smaller values than 0.02, the maximum range of motion actually decreases.

Ten results on the Pareto Front B – K are chosen to present their data in Table 4.4. Table 4.4 only provides approximate values of parameters to two decimal places. They are not accurate enough to produce the corresponding range of motion shown, but considering page space and the convenience of reading, these data are only here to provide an idea of the dimensions and the tendency of dimension changes as the targets Θ and R differ. More accurate values and more Pareto optimals are presented in Table B.2 in Appendix B.

Out of the ten chosen Pareto optimals, three of them with very different regularities are chosen to show the difference of their shapes and nets above the Pareto Front in Figure 4.16. At the top on the right, the result that has the largest range of motion, B, has its polyhedron shape and net shown on the top of the results, whose data are shown in the second row of Table 4.4. From its net, it can be seen that the polyhedron is highly asymmetrical. It has two different crinkles. The "irregular" triangles are long and thin. A more regular example on the Pareto front is result F, which has a regularity of 0.18. Its polyhedron shape and net are also shown above the Front and its data are in Table 4.4. Its regularity is close to that of the Steffen original flexible polyhedron but its range of motion is almost 20° more. Another result chosen to demonstrate its shape and net is result I. It is a polyhedron that shares the range of motion of the Steffen original flexible polyhedron but is much more regular. The net shows that this polyhedron is more or less symmetrical, whereas polyhedra, F and B, grow more and more asymmetrical. This is explained by the comparison graphs of the two optimisations in Figure 4.17 and Figure 4.18.

Both optimised results of the symmetrical Steffen flexible polyhedron and of the generalised Steffen flexible polyhedron are shown in Figure 4.17; their Pareto Fronts are shown independently in Figure 4.18. The data are the same as those shown in Figure 4.9 and Figure 4.16. The results of optimisation with originally defined symmetrical parameters are shown in purple as plus signs; and those with generalised parameters are shown as crosses in orange. It can be observed that the generalised parameters allow more room to achieve a higher range of motion without losing any regularity. This is most evident when the regularity is small: irregular polyhedra benefit more from the generalisation of parameters. The maximal difference is 6.4°. This difference narrows as the regularity grows. When the regularity approaches 0.3, there is no difference made by the generalisation of the parameters. The slight differences are believed to be the result of computation limitations. It is concluded that symmetry does most advantage on highly regular flexible polyhedra. This explains why result I in Figure 4.16 has a more or less symmetrical shape.

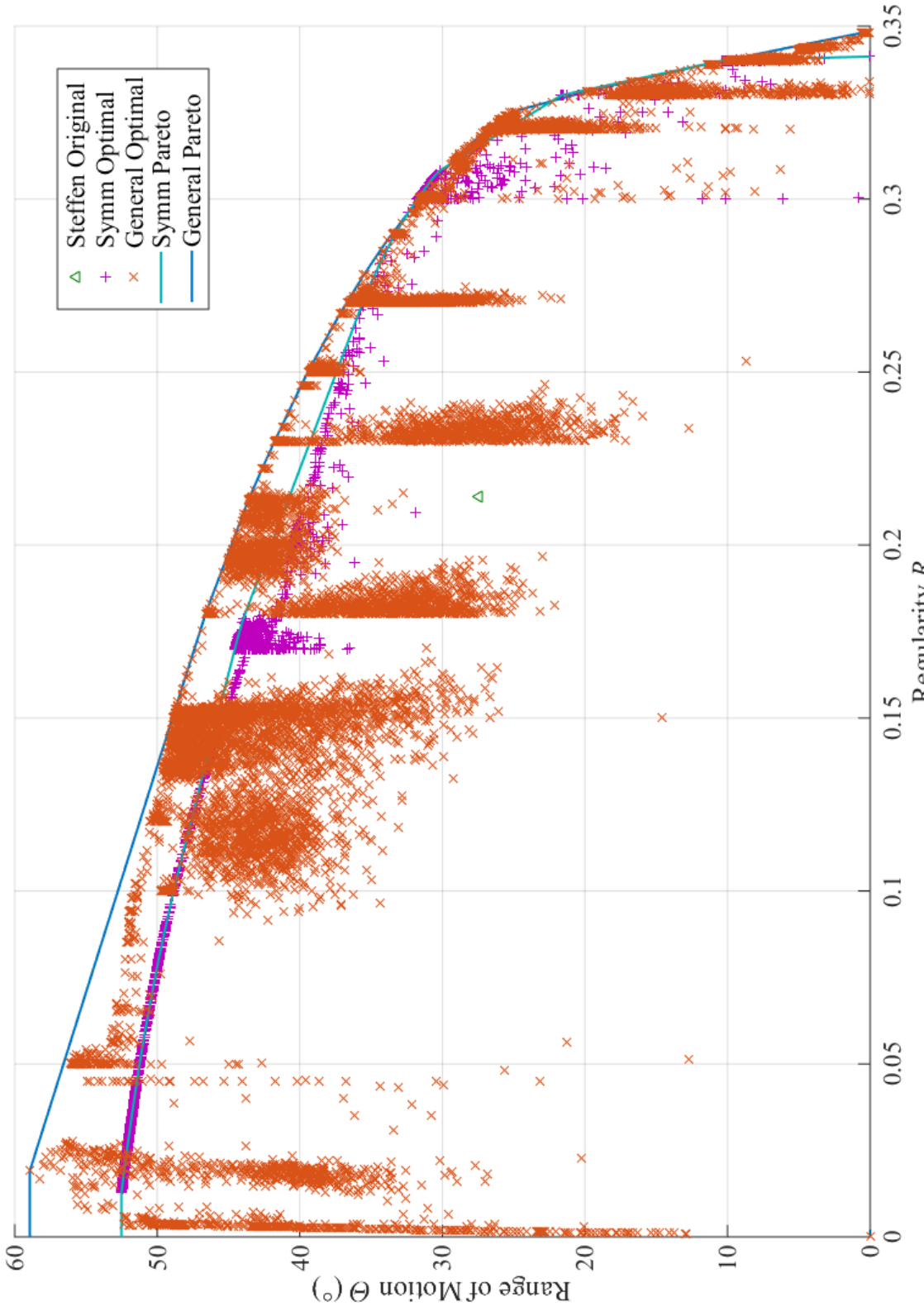

Fig. 4.17 Comparison of Pareto results of symmetric and generalised Steffen flexible polyhedra. The plus sign in purple shows the results of symmetric Steffen flexible polyhedra; the green curve is its Pareto front. Each orange cross represents a result of the generalised Steffen polyhedron; the blue curve shows its Front. Both sets of data are the same as shown in Figure 4.9 and Figure 4.16 respectively.

The tendency of optimised generalised results being symmetrical can be observed in Table 4.4. Results D – K have $a_1 \approx a_4$, $a_2 \approx a_3$, $b_1 \approx b_2$, $c_1 \approx c_2$ and $d \approx e$. It can be seen in Figure 4.18 that this means the two crinkles are getting identical. Moreover, from polyhedron I onwards, results I – K have $(a_1 \approx a_4) \approx (a_2 \approx a_3)$. From Figure 4.18 this along with $b_1 \approx b_2$ means that the net of each crinkle is getting more plane symmetrical (as discussed in Section 4.1). This is close to the parameter setting originally defined by Steffen. This tells that the gap between the two Pareto Fronts in Figure 4.18 for $R = 0.1 \sim 0.3$ is mainly due to the difference of $a_1 \approx a_4$ and $a_2 \approx a_3$. The gap for $R < 0.1$ is principally because of the difference between a_1 and a_4 and between a_2 and a_3.

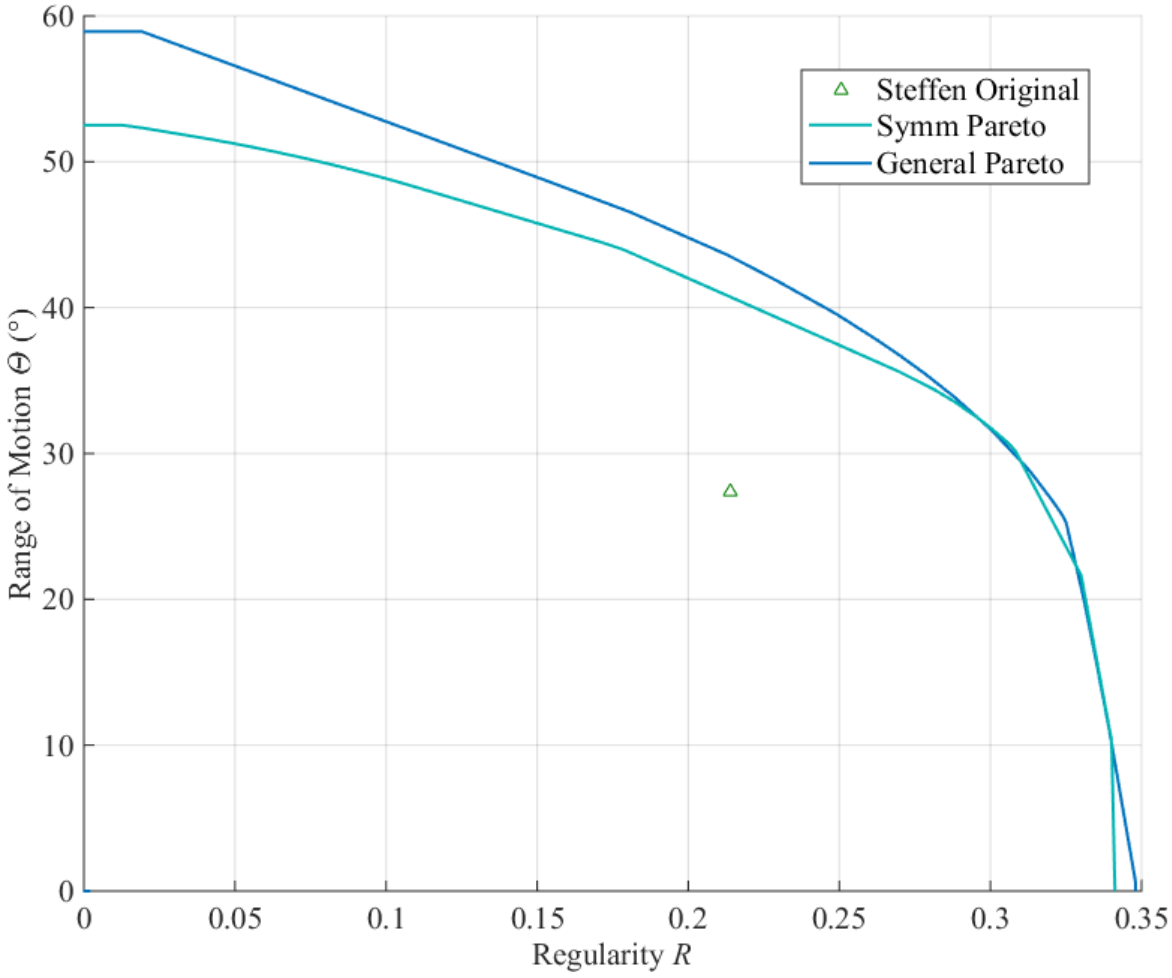

Fig. 4.18 Comparison of Pareto Fronts of the symmetric and the generalised Steffen flexible polyhedra. The green curve shows the Pareto Front symmetric Steffen flexible polyhedra; the blue curve shows that of generalised Steffen flexible polyhedra. The fronts are extracted from Figure 4.17 for a clearer comparison.

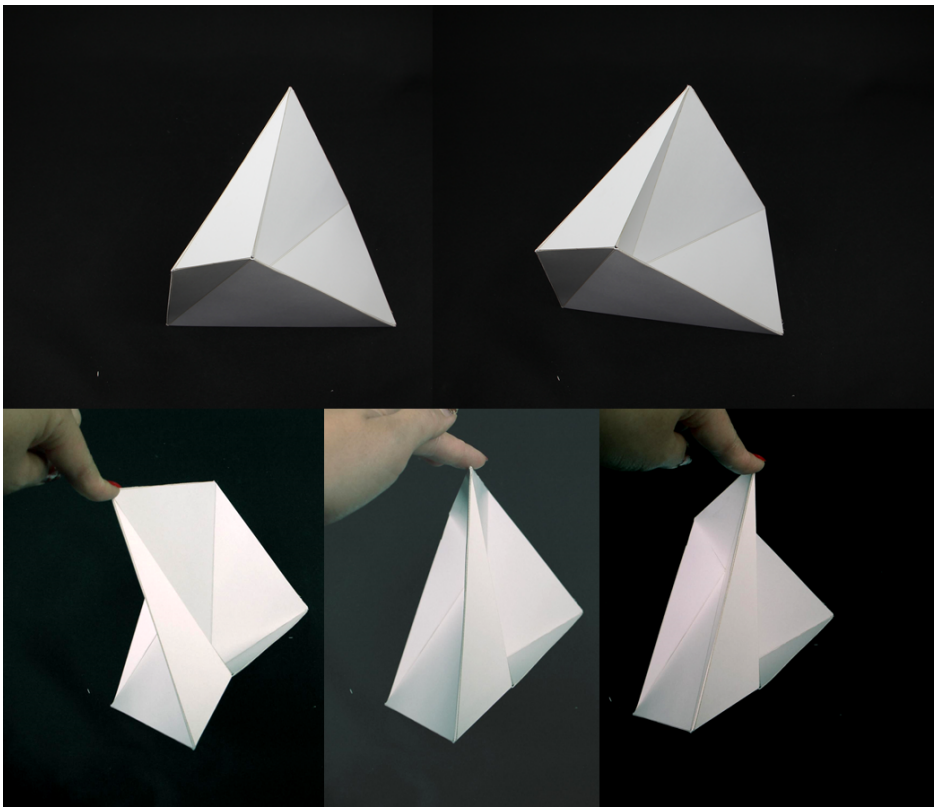

Fig. 4.19 Physical model of an optimised result, F, of the general Steffen flexible polyhedron on the Pareto front in Figure 4.9 and Table 4.2. Regularity 0.18; range of motion 47°. Two side views of a neutral position are shown on top; two end positions and a neutral position are shown below.

On the Pareto Front, an optimised result, F, is chosen to examine the clashes. This polyhedron is reasonably regular, $R = 0.18$, and has a reasonably large range of motion, $\Theta = 47°$. A physical model of F is shown in Figure 4.19. The first row shows the mid-position in two different side views; the second row shows the flex to the left end, at a neutral position, and to the right end.

A semi-opaque model of the polyhedron F is shown in Figure 4.20. The range of motion of this polyhedron is shown in Figure 4.20a with two end positions. The polyhedron flexing to the left end is drawn in solid lines; the polyhedron flexing to the right end is drawn in dashed lines. Clashes at the end to the left are shown in Figure 4.20b–d. In this position, vertex 9 flex towards vertex 1, x_9-ve. The clash between edge 9-8 and triangle 9-5-6 stops the flex of the polyhedron, which can be observed most evidently in Figure 4.20b. There are two other clashes that almost occur, whose values are not negative but small enough, shown in Table 4.5. One of them is between the dihedral 8-1-2-4, which can be seen in all three views of Figure 4.20b–d: the angle between $\triangle$8-2-4 and $\triangle$1-2-4 is almost zero. Another clash is

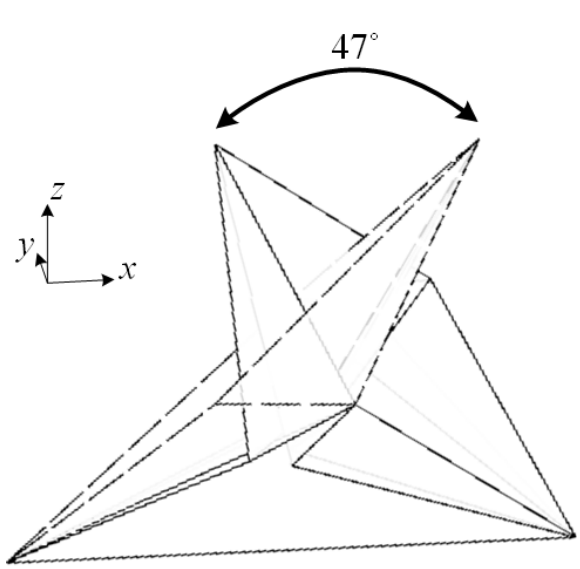

(a) Two ends of the polyhedron. The left end is drawn in solid lines, and the right end is in dashed lines.

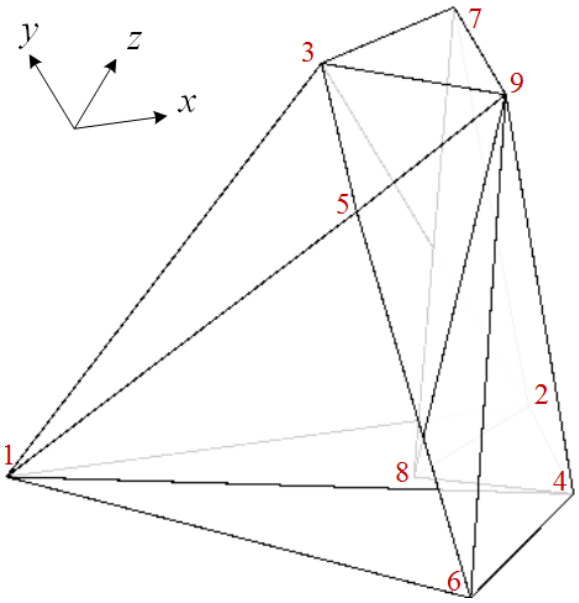

(b) Top left side view. Clash between edge 8-9 and triangle 5-6-9 occurs. Clash between edge 5-9 and △7-8-9 is far from occurrence.

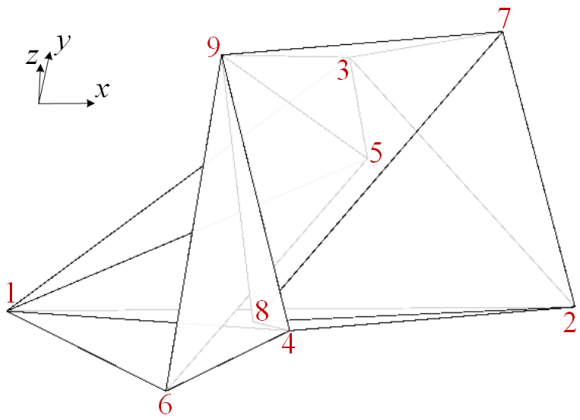

(c) Top right side view. Clash between △5-1-6 and △4-1-6 occurs. Clash between △8-2-4 and △1-2-4 is about to occur.

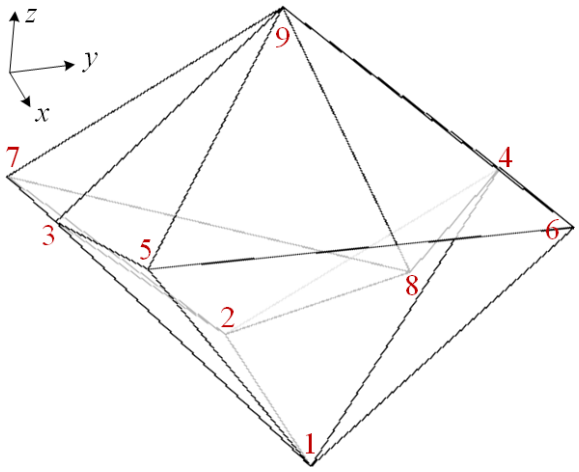

(d) Left view. There is an angle between the dihedral 1-2-3-5. △2-7-8 and △2-3-7 are far from clash.

Fig. 4.20 Semi-opaque model of an optimised result, F, of the generalised Steffen flexible polyhedron, $R = 0.18$, $\Theta = 47°$. The left end position in (a) is also shown alone in (b – d) without the dashed right end, in order to show the clashes at one end. Different view points are chosen. Clash values are given in Table 4.5.

Table 4.5 Clash values at both end positions of the generalised Steffen Pareto optimal F $R = 0.18$, $\Theta = 47°$

Type	Symmetric pair	Line	Face	$\beta(x_9\text{-ve})$	$\beta(x_9\text{+ve})$
Type Ia	clash A^+	8-9	5-6-9	$-0.0°$	$7.3°$
	clash A^-	5-9	7-8-9	$7.3°$	$-0.0°$
Type Ib	clash B^+	5-6	1-4-6	$0.01°$	$21.7°$
	clash B^-	7-8	2-3-7	$21.4°$	$0.01°$
	clash C^+	4-8	1-2-4	$0.05°$	$8.6°$
	clash C^-	3-5	1-2-3	$8.7°$	$0.01°$

between dihedral 1-4-6-5, which is observed most clearly in Figure 4.20c. The other three clashes are far from occurrence. Table 4.5 shows that the angle between line 5-3 and $\triangle$3-2-1 is 9 degrees. It is shown in Figure 4.20d that there is a clear angle between the two triangles in dihedral 1-2-3-5. Figure 4.20d also shows that $\triangle$2-7-8 and $\triangle$2-3-7 are far from clash. Another clash can be clearly seen in Figure 4.20b that the edge 5-9 is far away from $\triangle$9-7-8.

Clash values at both ends in Table 4.5 can be seen at two ends of the graph in Figure 4.21. The graph shows the six clash values at each position of the flex. The step value is $\delta = 2.5°$. The flex starts from $\Delta = 0$ in Table 3.1. The polyhedron is flexed forward after a clash occurs, and is flexed backward after another clash occurs. The forward range of motion is 11°; the backward range of motion is 36°. The clashes look symmetric. This is because the parameter values render the polyhedron close to symmetrical.

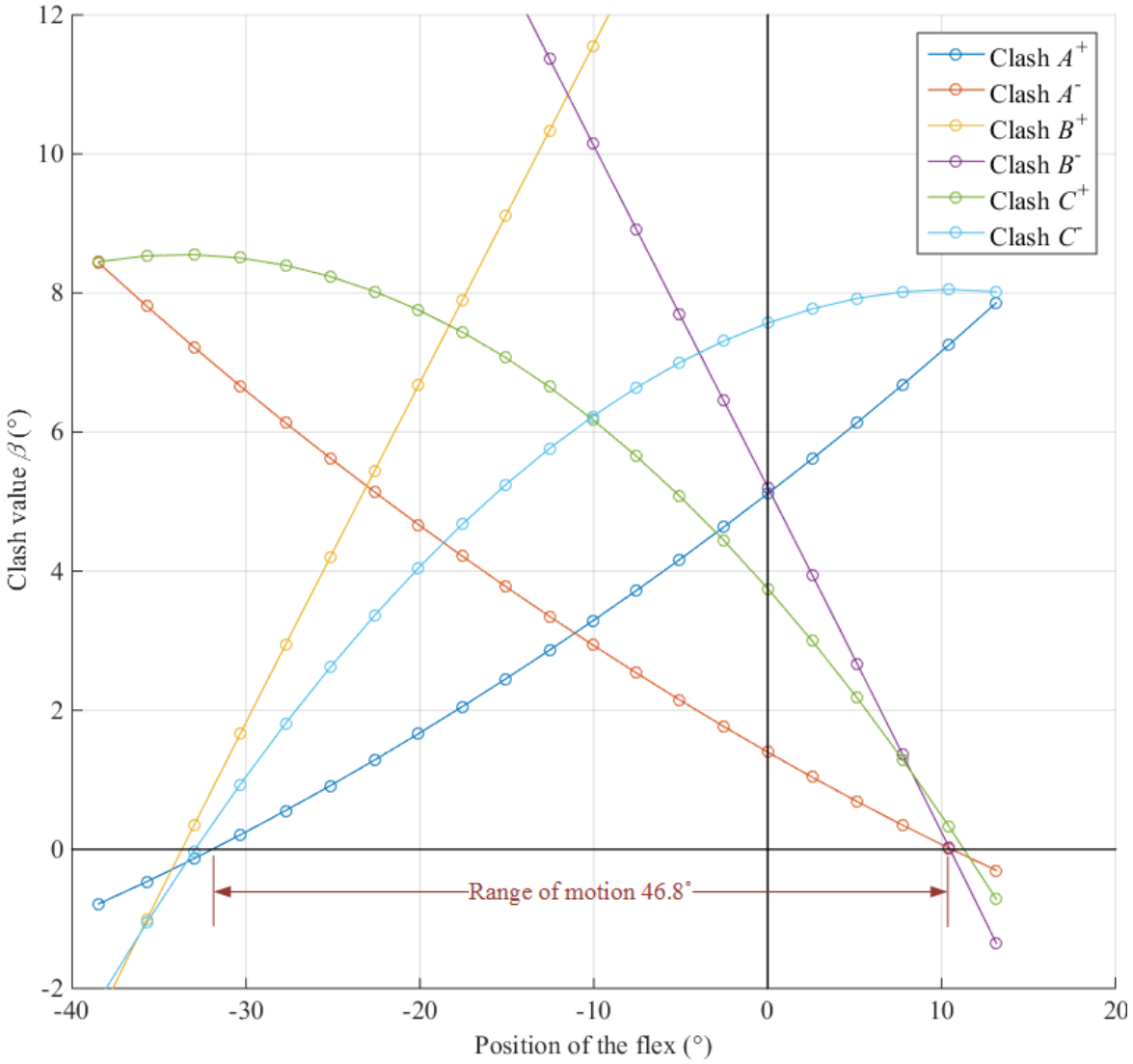

Fig. 4.21 Clashing values of the Perato optimal of the general Steffen flexible polyhedron, labelled F in Figure 4.16, with a range of motion of 47° and a regularity of 0.18. On the x-axis are the angles of rotation away from a chosen neutral position; on the y-axis are the angles of six clash values at each flexed position. Clashes are named as in Table 4.5.

Chapter 5

Optimisation of the two-tetrahedron flexible polyhedron

This chapter presents the two-tetrahedron flexible polyhedron, and describes how its range of motion can be improved. As Section 2.5 described, this new flexible polyhedron is a triangulated polyhedron, originally suggested by Tomohiro Tachi[1]. This chapter describes the composition of this flexible polyhedron and its difference from the Steffen flexible polyhedron. The most general set of parameters are given in order to optimise its range of motion. It is found that this new type of flexible polyhedron is able to achieve a better range of motion than Steffen's while having a greater regularity.

5.1 Initial configuration

The shape and the net of the flexible polyhedron Tachi discovered was shown in Figure 2.17. Tachi found this polyhedron in 2011. This dissertation started in 2012 to work on Tachi's discovery. From the net in Figure 2.17, it can be seen that all polygons of this polyhedron are triangles. The configuration of this polyhedron has only one more vertex than Steffen's 9-vertex, triangulated polyhedron. This 10-vertex polyhedron has the same rationale of composition but a slightly different near-polyhedron.

From the net provided by Tachi in Figure 2.17, the polyhedron seems highly symmetrical. As is shown in the generalisation of the Steffen flexible polyhedron, as long as the crinkles have equal lengths as their underlying Bricard flexible octahedra require, other edges need not be the same length. However, if each edge is given an individual parameter to vary, a valid shape is highly unlikely to be found in computation. This is because the formulation of

[1] Personal communication

flexible polyhedra relies on the use of crinkles. The redundancy of Bricard flexible octahedra means some edge lengths define the lengths of others. Therefore, some edges need to be given the same parameters in order to establish numerical models correctly. Based on this knowledge, the parameters of this new polyhedron are defined. The next section will describe the decomposition of the Tachi flexible polyhedron and show the use of crinkles and give the most general setting of parameters. With these parameters, optimisation on the range of motion is conducted to see whether this polyhedron can achieve more than the Steffen flexible polyhedron.

5.2 Defining Parameters

This section examines the composition of the new flexible polyhedron in comparison with that of the Steffen flexible polyhedron in order to define parameters for its optimisation.

Both the Steffen and the two-tetrahedron flexible polyhedra are configured based on the replacement of crinkles: the crinkles replace dihedrals in a 'nearly' flexible polyhedron in order to separate the clashing part to make a polyhedron. Previously, it was shown that the Steffen flexible polyhedron is composed of crinkles and a base part. This base is a near-polyhedron with two dihedrals removed. Here in the two-tetrahedron flexible polyhedron, the same crinkles are used to replace two dihedrals of a slightly different near-polyhedron, as shown in Figure 5.1. It was shown in Chapter 1 that the near-polyhedron of Steffen is a tetrahedron linked to a triangle flap by a sharing edge. Here the near-polyhedron is also triangulated, but instead of using a triangle flap, another tetrahedron is used to link the first tetrahedron. Therefore, this flexible polyhedron is based on two tetrahedra sharing an edge, as shown in the middle of Figure 5.1, hence it is given the name *two-tetrahedron* flexible polyhedron. This near-polyhedron is shown previously in Figure 2.24 and Figure 2.25. Here a more detailed decomposition is shown in Figure 5.1.

The near-polyhedron of the two-tetrahedron flexible polyhedron is shown in Figure 5.1; tetrahedron 1-2-3-4 and tetrahedron 2-3-5-10 are linked by edge 2-3. This near-polyhedron is able to flex about the hinge 2-3. The dihedrals to be replaced are shown on the sides, dihedral 1-2-5-3 and dihedral 4-2-10-3. When they are replaced, the near-polyhedron only has dihedral 1-2-4-3 on the top and dihedral 2-5-3-10 at the bottom left, shown above and below the near-polyhedron. These two dihedrals are linked at vertex 2 and vertex 3, as shown in Figure 5.2.

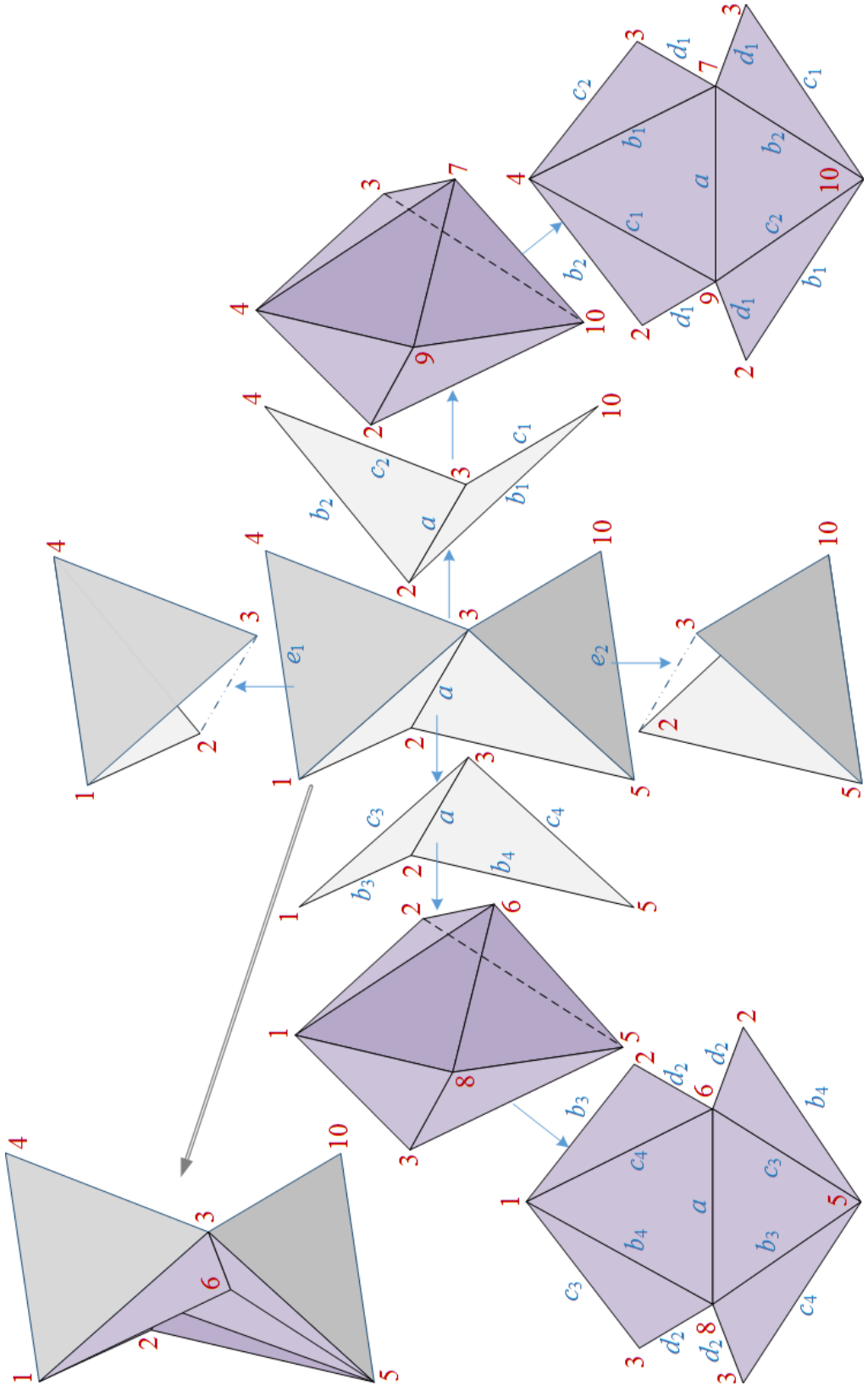

Fig. 5.1 Decomposition of the two-tetrahedron flexible polyhedron with parameters defined. These parameters are the most general set; the edge lengths are provided by Tachi. The crinkles are Type I as in the Steffen flexible polyhedron, hence line-symmetric: a set of 6 parameters are given to each crinkle, with one shared, $l_{6-8} = l_{2-3} = l_{7-9} = a$. Another two parameters, e_1 and e_2, are given to the edges of the near-polyhedron. Therefore, there are 13 parameters.

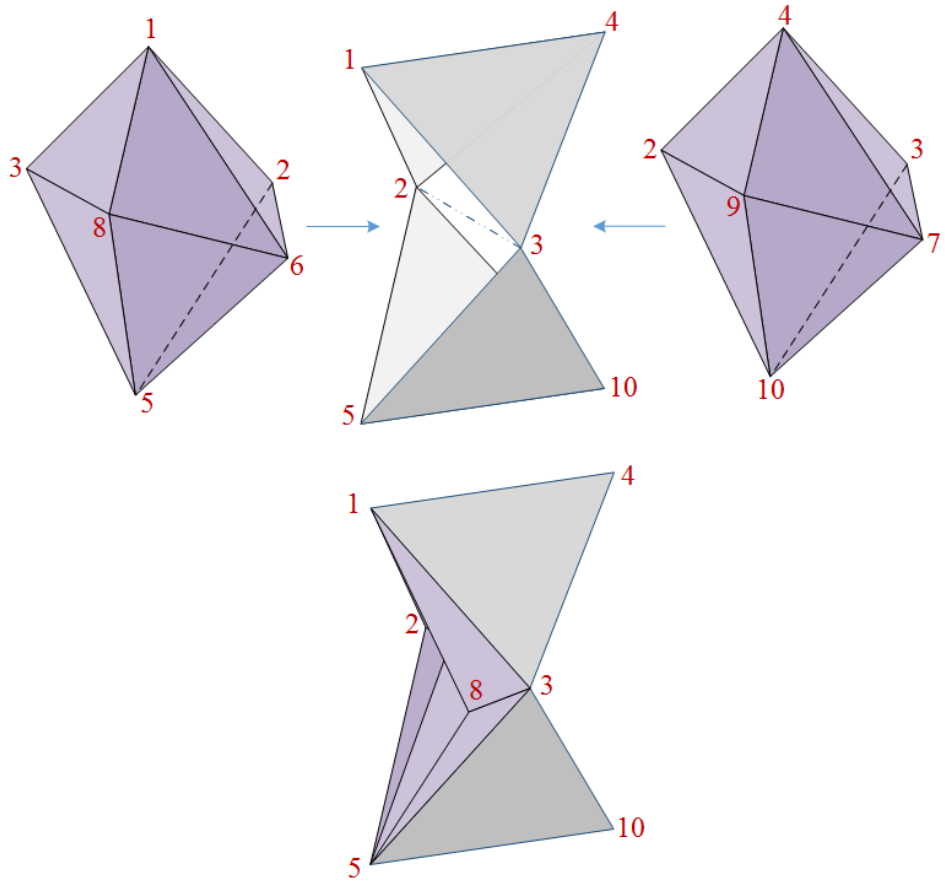

Fig. 5.2 Components of the two-tetrahedron flexible polyhedron. The base and two crinkles assemble to make the two-tetrahedron flexible polyhedron.

Each replaced dihedral plus the replacing crinkle is a Bricard octahedron. The dimensions Tachi first used make the crinkles Type I and as symmetrical as Steffen's choice. As a result, this chapter chooses to explore the use of Type I crinkles only. In future work, the other two types of crinkles may be used and explored for their advantages. In the two-tetrahedron flexible polyhedron, the two Type I Bricard octahedra both flex about hinge 2-3. After the replacement, if the crinkles do not clash against each other, then the whole polyhedron is able to flex about the same hinge 2-3 as its near-polyhedron does. Due to the line symmetry of Type I Bricard flexible octahedron, there are six pairs of equal edges. Therefore, this dissertation gives six parameters for each crinkle to vary its lengths in order to find larger range of motion of this polyhedron. In the crinkle on the right, as Figure 5.2 shows, parameters given are

$$l_{2-3} = l_{7-9} = a, \quad l_{2-10} = l_{4-7} = b_1, \quad l_{4-2} = l_{7-10} = b_2,$$
$$l_{3-10} = l_{4-9} = c_1, \quad l_{4-3} = l_{9-10} = c_2, \quad l_{2-9} = l_{3-7} = d_1.$$

In the crinkle on the left, there are

$$l_{2-3} = l_{6-8} = a, \quad l_{1-2} = l_{8-5} = b_3, \quad l_{2-5} = l_{1-8} = b_4,$$
$$l_{1-3} = l_{6-5} = c_3, \quad l_{3-5} = l_{1-6} = c_4, \quad l_{2-6} = l_{3-8} = d_2.$$

Note that the two crinkles replace the same hinge 2-3, so there is

$$l_{2-3} = l_{6-8} = l_{7-9} = a.$$

Therefore, there are 11 parameters used for the edges of the two crinkles. Note that the two crinkles in this flexible polyhedron need not share any edges, as in the Steffen flexible polyhedron. This is because their near-polyhedra are different. The near-polyhedron in Figure 5.2 has the top and the bottom edges that are not shared with crinkles, edge 1-4 and edge 5-10. To give more freedom for the basic part to vary in shape in order to achieve a wider range of motion, parameters e_1 and e_2 are given to these two edges, $l_{1-4} = e_1$ and $l_{5-10} = e_2$. Overall, there are 13 parameters defined for this polyhedron.

This flexible polyhedron has three more parameters than the Steffen generalised flexible polyhedron. This is because its near-polyhedron has one extra vertex and hence three edges, as Figure 2.24 shows. Three more parameters allow this polyhedron to have more room to change shape, hence it is likely to achieve a better range of motion than Steffen's.

As in the Steffen flexible polyhedron, the value of one parameter is chosen to be fixed for comparison purposes. In the two-tetrahedron flexible polyhedron, the top edge e_1 is chosen, $e_1 = 7.5$. The other 12 parameters are changed in value in the optimisation.

5.3 Optimising the range of motion

This section uses the numerical tools described in Chapter 3 to optimise the range of motion of the newly discovered two-tetrahedron flexible polyhedron. The Simulated Annealing method described in Section 3.3 is used to randomly perturb parameter values, cool down the selection process, and find an optimal for each run. A penalty function is used as the boundary condition of the optimisation. The penalty values are from the calculation of clashes, which is based on the clash detection methods described in Section 3.2. In order to detect clashes for the two extreme positions suggested by perturbed end values, all the vertices need to be found for each position. Then the iterative solution method described in Section 3.1 is used to find the coordinates of vertices for any position that the polyhedron flexes to. The

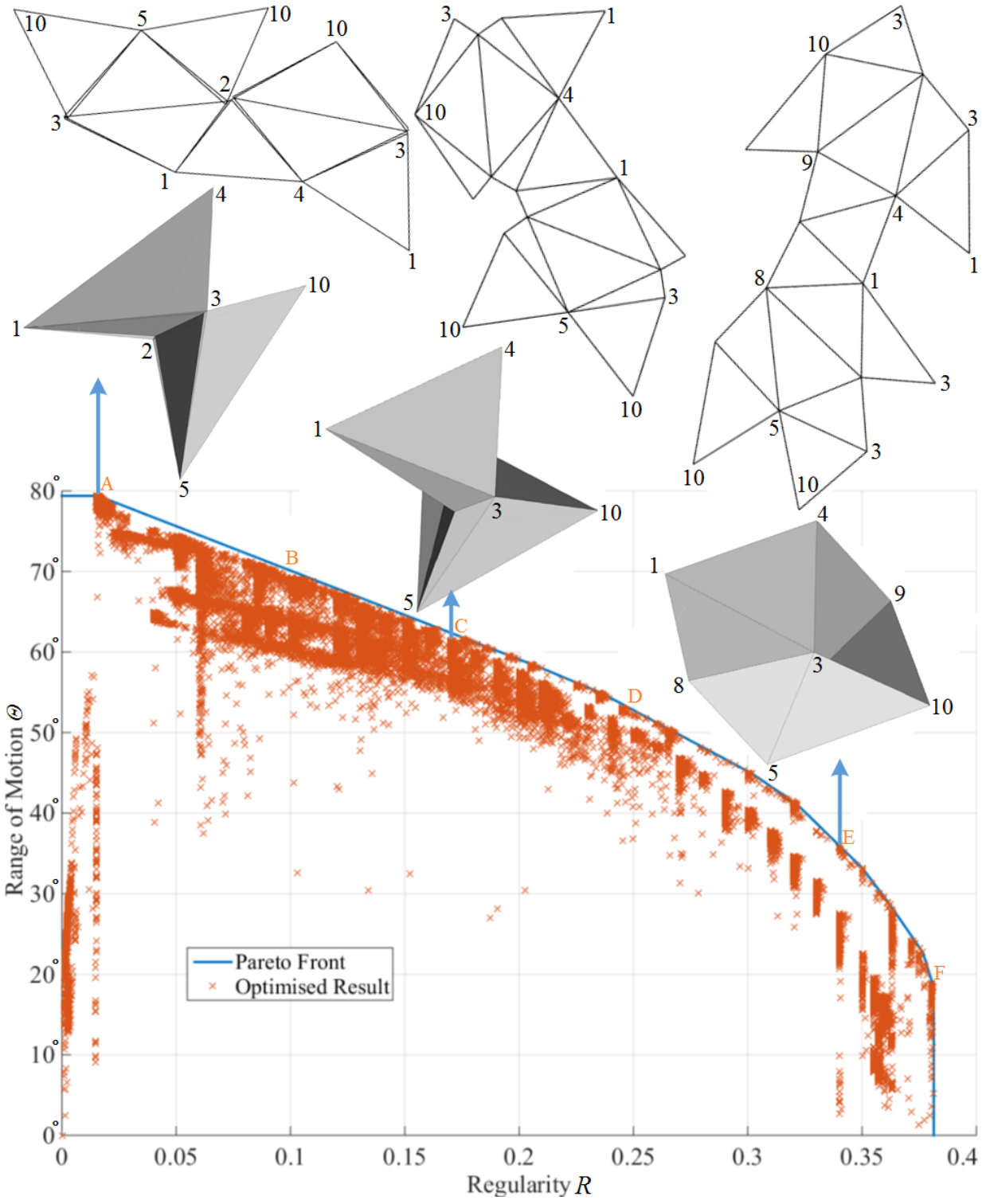

Fig. 5.3 Optimisation results of the two-tetrahedron flexible polyhedron. Each red cross is the result of an SA optimisation run. The blue curve is the Pareto Front of these optimals. Three Pareto optimals are chosen as examples: their polyhedra and nets are shown above the graph to demonstrate the variation of shapes.

computational model of this polyhedron is as Table 3.2 describes. The optimised results are shown in Figure 5.3.

Each red cross on the graph in Figure 5.3 is a result from an SA optimisation run. The blue line is the Pareto Front of this optimisation, on which neither the range of motion Θ nor the regularity R can improve without the other suffering.

The largest range of motion is nearly 80°, as result A shows. When the range of motion approaches 80°, the regularity decreases to 0.016. When the regularity is pushed to be even smaller, the range of motion does not increase anymore but actually decreases. The shapes of these polyhedra ($R < 0.016$) are examined: the clashes are the same as those $R > 0.016$. As the regularity is pushed to 0.38, the range of motion is decreased to 19°, as result F shows.

There are three results, A, C and F, on the Pareto Front whose polyhedral shapes and nets are chosen to be shown above the graph. From the nets, the change of regularity can be seen. The parameter values of these three polyhedra are shown in Table 5.1, where six optimals on the Pareto Front are chosen to have their data shown. Their parameter values, the range of motion allowed by these values, and the regularity given by these dimensions are shown in the table. This table only shows one decimal to provide an approximate idea of the change of dimensions. Since the optimised range of motion is highly sensitive to edge lengths, more detailed dimensions accurate to four decimal places of more Pareto optimals are shown in Appendix B, Table B.3.

The six Pareto optimals in the table shows that the crinkle depths, d_1 and d_2, are extremely small when the range of motion is large; and both grow towards the fixed value $e_1 = 7.5$, when the range of motion is sacrificed towards zero. These "crinkle depths" are the key factors that influence the regularity of the polyhedral shape.

Pareto Fronts of the Steffen generalised flexible polyhedron and the two-tetrahedron flexible polyhedron are compared in Figure 5.4. The solid blue curve is the Pareto Front of the multi-objective optimisation of the two-tetrahedron flexible polyhedron. The dashed blue

Table 5.1 Data of six Pareto optimals of the two-tetrahedron flexible polyhedron

	Θ	R	a	b_1	b_2	b_3	b_4	c_1	c_2	c_3	c_4	d_1	d_2	e_1	e_2
A	79.4°	0.02	10.6	6.9	7.3	6.9	7.3	7.3	6.9	7.2	6.8	0.2	0.3	7.5	7.6
B	69.2°	0.1	9.9	7.0	7.2	7.0	7.2	7.2	6.8	7.2	6.8	1.1	1.2	7.5	7.9
C	61.4°	0.17	10.9	7.8	7.7	7.7	7.7	7.9	7.5	7.9	7.4	2.2	2.2	7.5	8.1
D	52.1°	0.25	10.1	8.7	7.5	7.0	7.9	7.1	7.8	8.8	7.3	3.3	3.3	7.5	8.1
E	36.0°	0.34	10.2	10.0	7.9	6.8	7.7	7.0	7.9	9.9	7.7	5.4	5.6	7.5	8.2
F	18.9°	0.38	9.8	9.3	7.6	6.0	6.2	6.1	6.4	9.4	7.6	6.8	7.0	7.5	7.6

* Models A – F are labelled in orange letters on the Pareto Front in Figure 5.3.

curve is that of the Steffen generalised flexible polyhedron. The initial starting point of both optimisations — the Steffen original flexible polyhedron — is shown as a green triangle on the graph.

The improvement in the range of motion of the two-tetrahedron flexible polyhedron is considerable. Figure 5.4 shows that the Steffen general flexible polyhedron pushes the biggest range of motion from Steffen's 27° to almost 60°, and the optimisation of the two-tetrahedron flexible polyhedron increases it further to 80°. Connelly's initial polyhedron has a limited range of motion of possibly around 10°. Now the greatest range of motion of flexible polyhedron is 80°. However, in future work it may be that another polyhedron is able to provide a larger range of motion with a greater regularity, in short, a better Pareto Front.

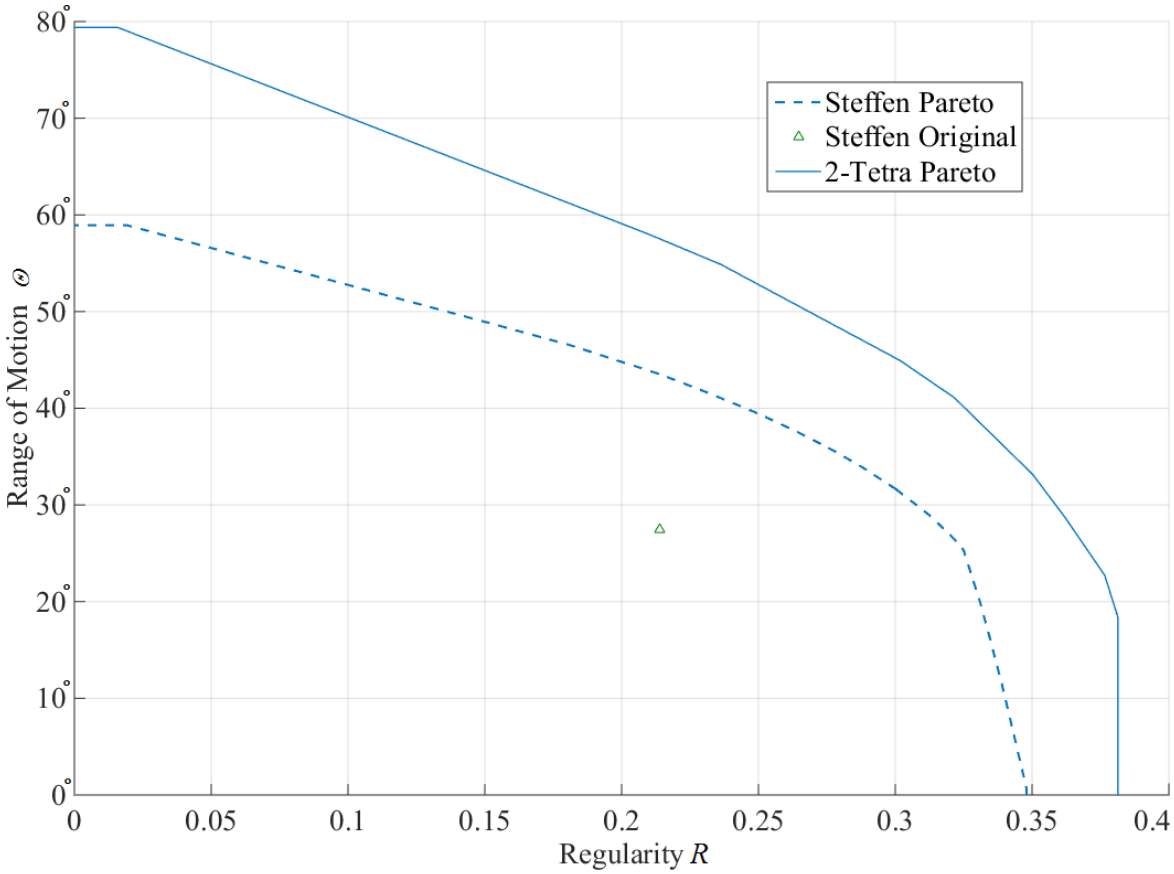

Fig. 5.4 Comparison of Pareto Fronts of the Steffen generalised flexible polyhedron and the two-tetrahedron flexible polyhedron. The dashed blue line is the Pareto Front of the bi-objective optimisation of the Steffen generalised flexible polyhedron; and the solid blue line is that of the two-tetrahedron flexible polyhedron. Data extracted from Figure 4.17 and Figure 5.3 respectively.

Meanwhile, the two-tetrahedron flexible polyhedron also achieved a greater largest possible regularity value: from $R_{\max} = 0.35$ of Steffen's to 0.38. Further improvement may be achievable with more numerical efforts.

The optimised results of the Steffen symmetric flexible polyhedron, the Steffen generalised flexible polyhedron and the two-tetrahedron flexible polyhedron are plotted in the same graph in Figure 5.5 for comparison.

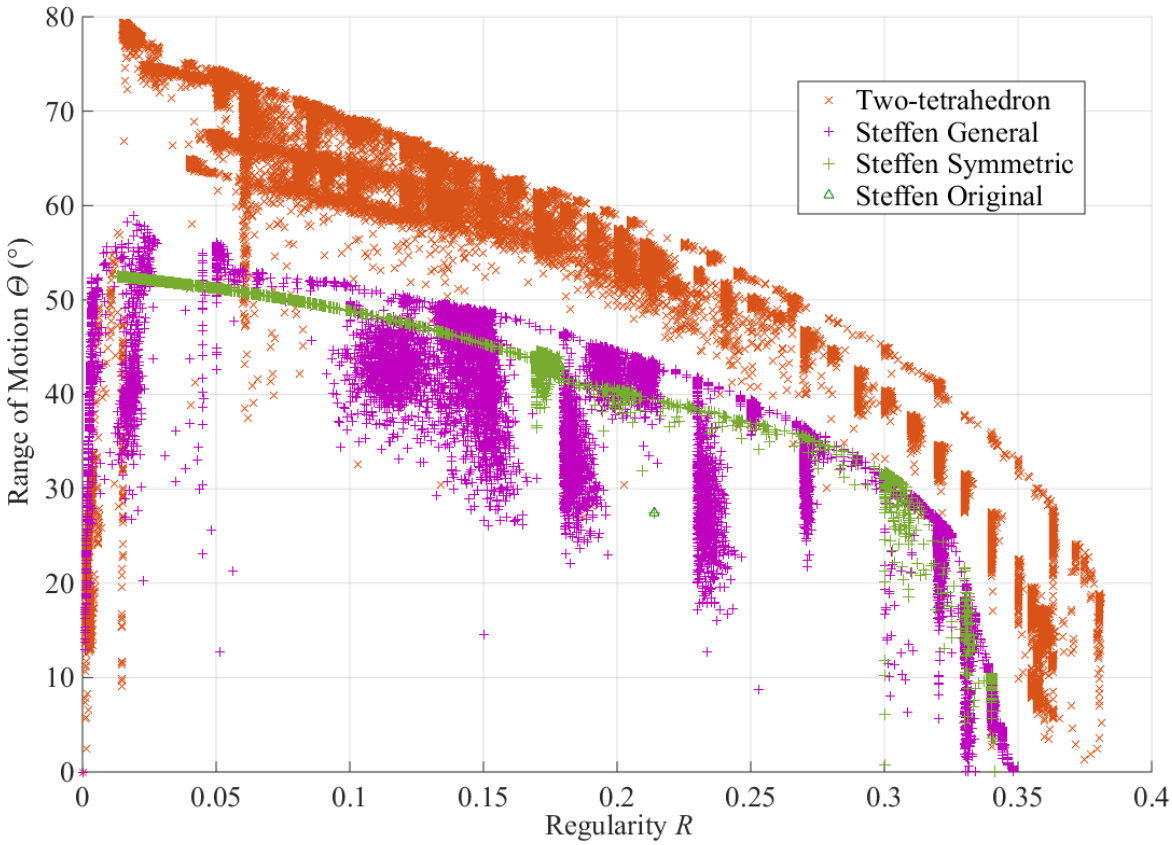

Fig. 5.5 Comparison of optimised results of the Steffen flexible polyhedron and the two-tetrahedron flexible polyhedra. Each orange cross represents an optimised result of the two-tetrahedron flexible polyhedron; each purple "+" represents a result of the Steffen generalised flexible polyhedron; each green "+" represents a result of the Steffen symmetric flexible polyhedron; and the green triangle represents the Steffen original flexible polyhedron. Data extracted from Figure 4.17 and Figure 5.3.

5.4 An example of a Pareto optimal

As an example, one of the optimised results on the Pareto Front in Figure 5.3, labelled as B, is examined closely in this section. This chosen polyhedron has a regularity of 0.1 and a range of motion of 69.2°.

The net of the polyhedron B is shown in Figure 5.6, along with its parameter setting, parameter values and how its regularity value of 0.1 is obtained from $R_{i,\min}$ and $R_{c,\max}$. The shapes of the polygons of this polyhedron are shown: the smallest inscribed circle of all triangles is next to one of the crinkle depth, d_2; the largest circumcircle is of one of the replaced triangles, $\triangle$1-2-3, which is congruent with $\triangle$7-9-10. The smallest inradius, $R_{i,\min} = 0.4963$, and the greatest circumradius, $R_{c,\max} = 4.9595$, give the regularity of this shape, $R = R_{i,\min}/R_{c,\max} = 0.1001$.

A folded model from the net is shown in Figure 5.7. This is a cardboard model of the Pareto optimal B, showing the front and back the polyhedron of a neutral position in the first row, and the two extreme end positions in the second row.

The range of motion of this polyhedron is shown with this polyhedron drawn in two extreme end positions in Figure 5.8a. In these figures, the tetrahedron 1-2-3-4 is fixed, and the tetrahedron 2-3-5-10 flexes about hinge 2-3. When node 10 flexes towards node 4 ($z_{10} = +ve$), tetrahedron 2-3-5-10 is drawn in dashed lines; when node 10 flexes away from

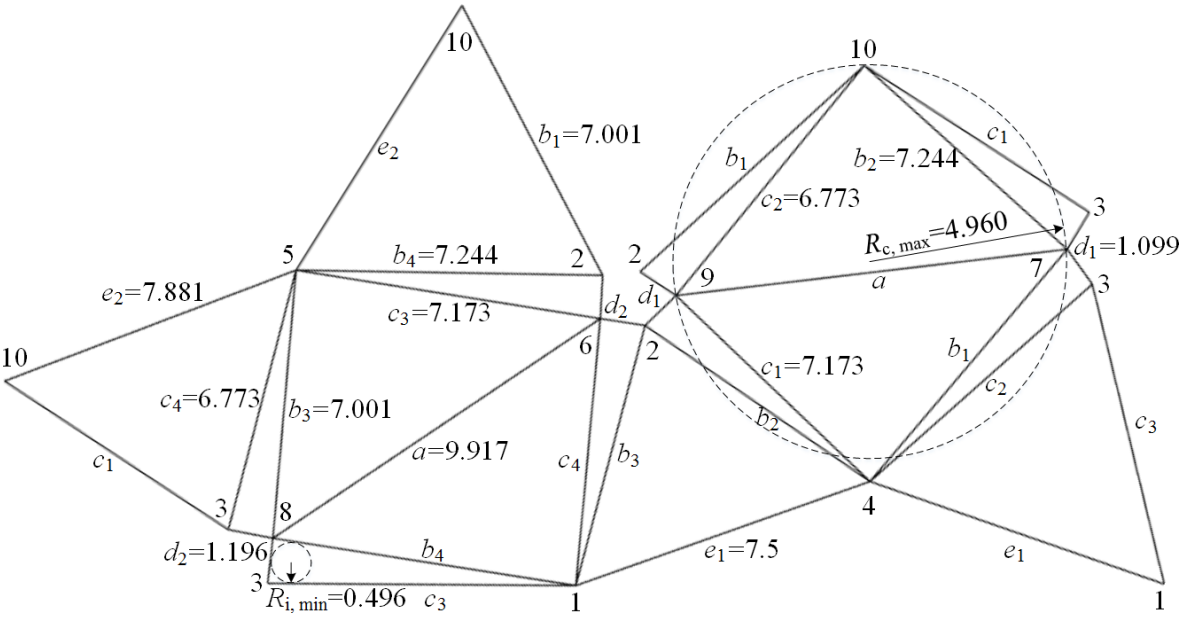

Fig. 5.6 The net of the Pareto optimal B of the two-tetrahedron polyhedron. This polyhedron has a range of motion of 69.2°. Optimisation parameters and their optimised values are shown, along with its regularity.

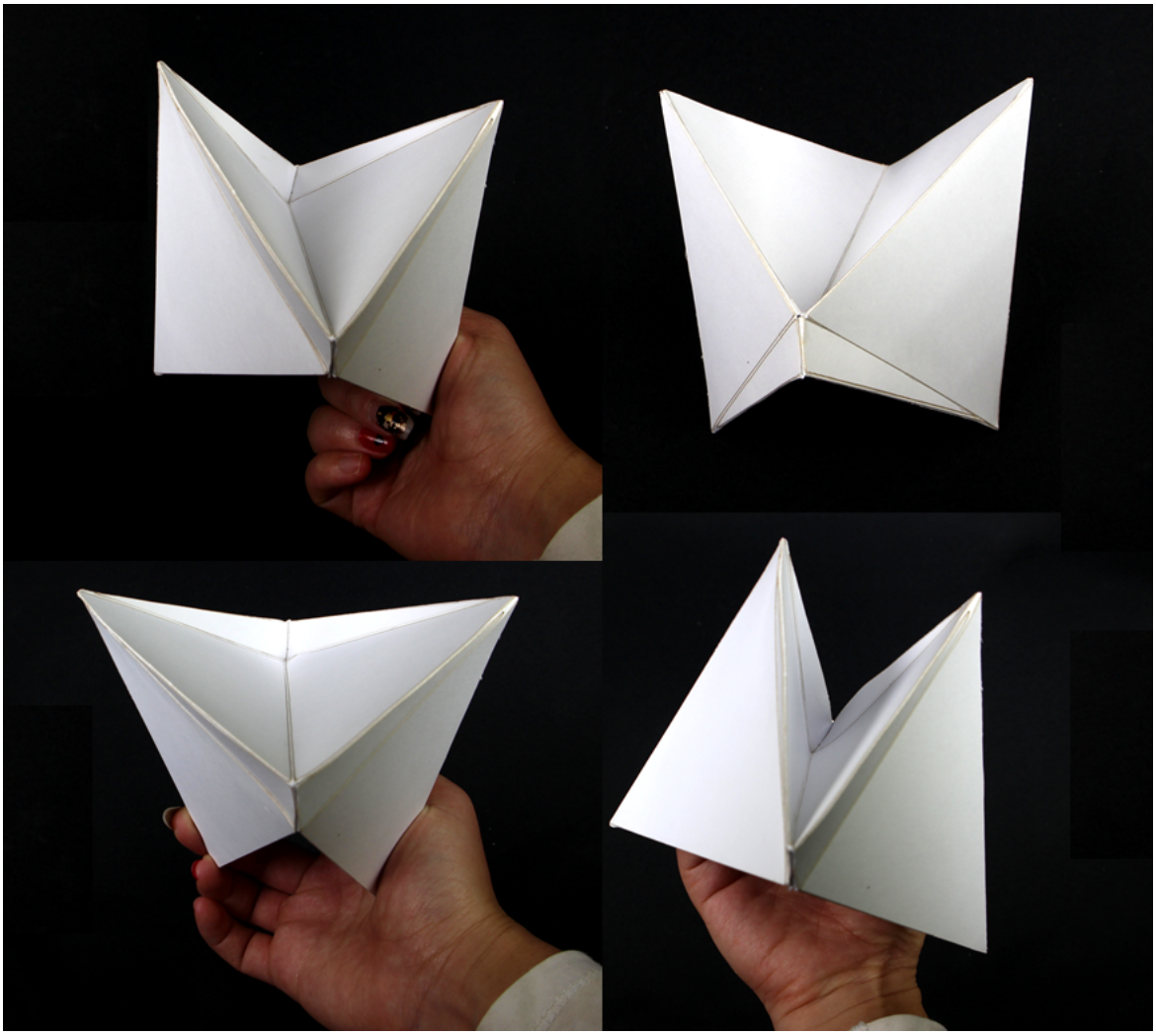

Fig. 5.7 Physical model of an optimised result of the two-tetrahedron flexible polyhedron on the Pareto front, B in Figure 4.9 and in Table 4.2. This polyhedron has a regularity of 0.1 and a range of motion of 69°. A neutral position of the front and back of the polyhedron is shown in the second row; two extreme positions of the flex are shown in the first row.

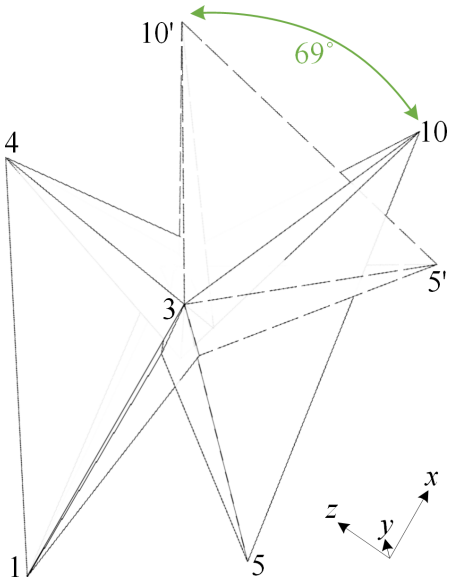

(a) Two extreme positions of the flex.

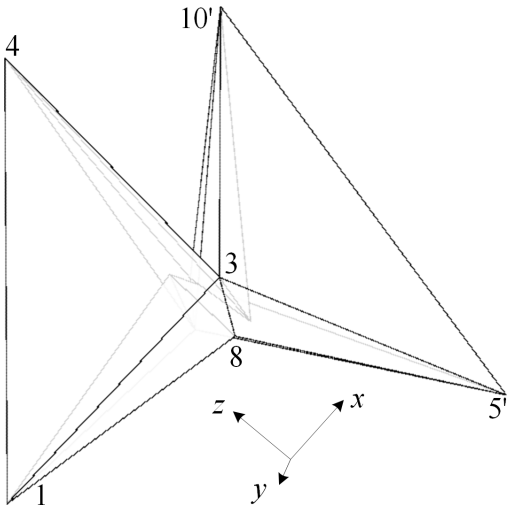

(b) One extreme position, when node 10 flexes towards node 4 ($z_{10} = +ve$).

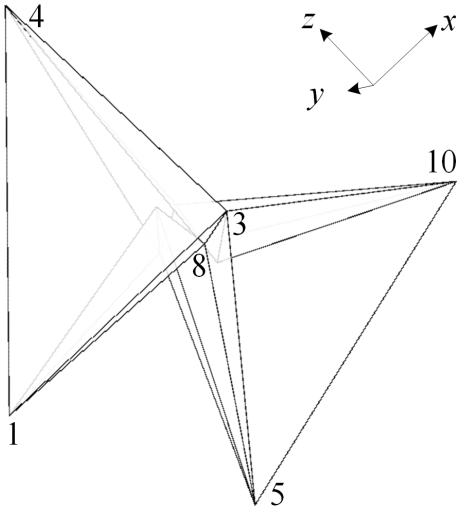

(c) The other extreme position, when node 10 flexes away from node 4 ($z_{10} = -$ve).

Fig. 5.8 Two end positions of the optimised two-tetrahedron flexible polyhedron on the Pareto Front, B, $R = 0.1$, $\Theta = 69.2°$.

node 4 ($z_{10} = -ve$), tetrahedron 2-3-5-10 is drawn in solid lines. The coordinate system of this polyhedron is defined as in Table 3.2. A semi-opaque model in two extreme positions are shown respectively in Figure 5.8b and Figure 5.8c to demonstrate their clashes. During the flex between these two positions, there is no clash occurrence.

One of the two extreme positions is chosen in order to show clearly which clashes stop the flex at one end, and different views of a transparent model at this position are displayed in Figure 5.9. The position in Figure 5.8c is chosen. In this position, tetrahedron 2-3-5-10

Table 5.2 Clash values at two end positions of a two-tetrahedron flexible polyhedron (Result B in Figure 5.3 and Table 5.1, $R = 0.1$, $\Theta = 69.2°$)

Type	Pair	Label	Line	Face	$\beta(z_{10}$+ve)	$\beta(z_{10}$-ve)
Type Ib	{	A^+	6-8	3-1-8	24.3°	−0.0°
	{	A^-	7-9	2-9-10	−0.0°	28.0°
	{	B^+	3-7	3-5-10	22.4°	0.1°
	{	B^-	2-6	2-1-4	0.01°	16.8°
	{	C^+	7-4	4-1-3	6.9°	1.6°
	{	C^-	6-2	2-5-10	12.4°	49.0°
	{	D^+	7-9	9-2-4	18.8°	32.5°
	{	D^-	6-8	8-3-5	33.2°	22.4°
	{	E^+	7-3	3-5-8	19.3°	5.3°
	{	E^-	6-2	2-4-9	4.6°	16.3°
Type	Pair	Label	Face	Face	$\beta(z_{10}$+ve)	$\beta(z_{10}$-ve)
Type II	{	F^+	7-9-10	5-6-8	1	1
	{	F^-	7-9-10	1-6-8	1	1
	{	G^+	4-7-9	5-6-8	1	1
	{	G^-	4-7-9	1-6-8	1	1

* Note that Type Ib clashes are presented as Type Ia clashes: a line from one of the two triangles is chosen; β is the angle between this line and its projection onto the other triangle.
* β for Type II clashes is between two separate triangles and is defined in Section 3.2.3.

flexes downwards, i.e. node 10 rotates away from node 4 ($z_{10} = -ve$). The values of clashes at this end is shown in the last column of Table 5.2. As Figure 5.9a shows, the clash between △1-6-8 and △1-3-8 occurs. Figure 5.9b and Figure 5.9c show the clash between △3-7-10 and △3-5-10. Figure 5.9c also shows that the clash between △7-3-4 and △1-3-4 does not occur. Figure 5.9d shows a Type II clash between △1-6-8 and △4-7-9 is close to occurrence.

The values of these all clashes at both ends are listed in Table 5.2. Figure 5.9b and Figure 5.9c also show that the angle between dihedral 6-2-10-5 is very large — the table indicates 49°. Figure 5.9b also shows that there is a gap between 6-2 and △2-4-9. All four figures show that the clash between 3-7 and △3-5-8 does not yet occur, as the angle between them is 5° in the table. All four figures also show that △7-9-10 does not clash with △1-6-8 at all in this configuration.

Table 5.2 shows Type Ib clashes as Type Ia clashes: the chosen lines of Type Ib clashes are shown. For example, line 6-8 is chosen from △1-6-8; the dihedral angle β is between line 6-8 and its projection onto △1-3-8.

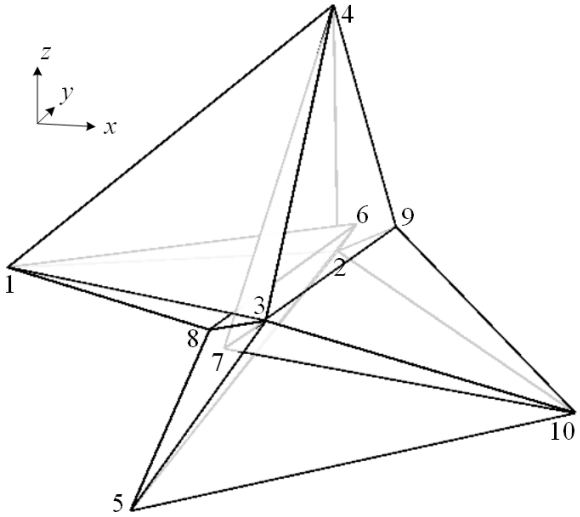

(a) The clash between △1-6-8 and △1-3-8 is shown most evidently in this view. The clash between △5-6-8 and △3-5-8 is far from occurrence. The angle between edge 7-9 and △2-4-9 is 32°.

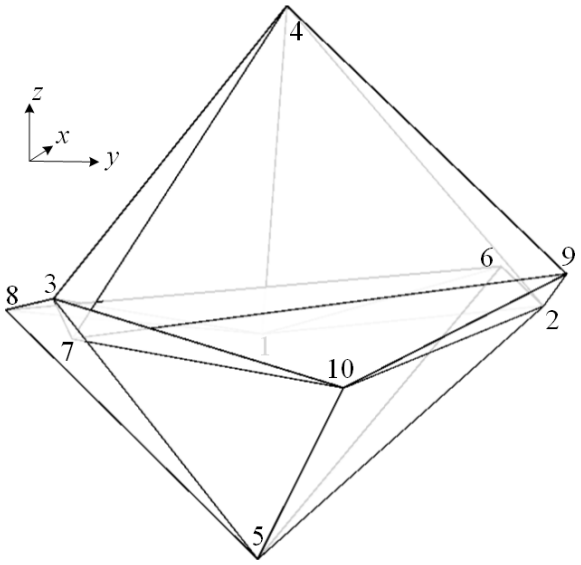

(b) The clash between △3-7-10 and △3-5-10 occurs. The clash between △7-9-10 and △2-9-10 is not likely to occur at all but, in the opposite end position, it occurs as the clash between △1-6-8 and △1-3-8 does.

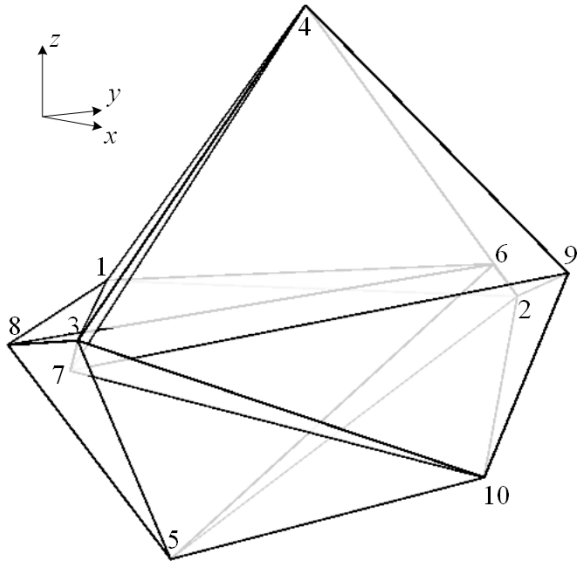

(c) The clash between △3-7-10 and △3-5-10 almost occurs. The clash of dihedral 1-3-7-4 does not yet occur, as the angle between 7-4 and △1-3-4 in Table 5.2 is 2°.

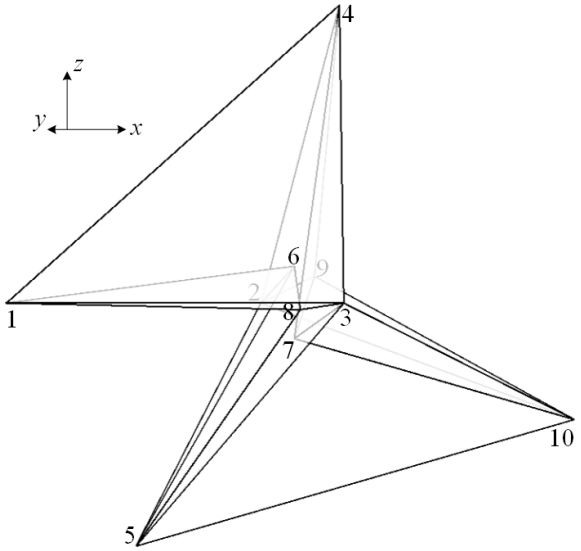

(d) △7-9-10 does not clash with △5-6-8. △4-7-9 almost clashes against edge 6-8. Table 5.2 shows that there is not yet a clash between △4-7-9 and dihedral 1-6-5-8.

Fig. 5.9 Four different views that show different clashes in the Pareto optimal B of the two-tetrahedron flexible polyhedron at an end position when node 10 flexes away from node 4, $z_{10} = -ve$.

The clash values in Table 5.2 only shows the clash values at two ends, but does not show the development of these clash values between the two ends. The graph in Figure 5.10 shows the values of the clashes at each flexing step. The step value is 4°. The polyhedron is flexed forward to 48° when a couple of clashes occur, and is flexed backward to −24° when a different couple of clashes occur, giving a range of motion of about 70°.

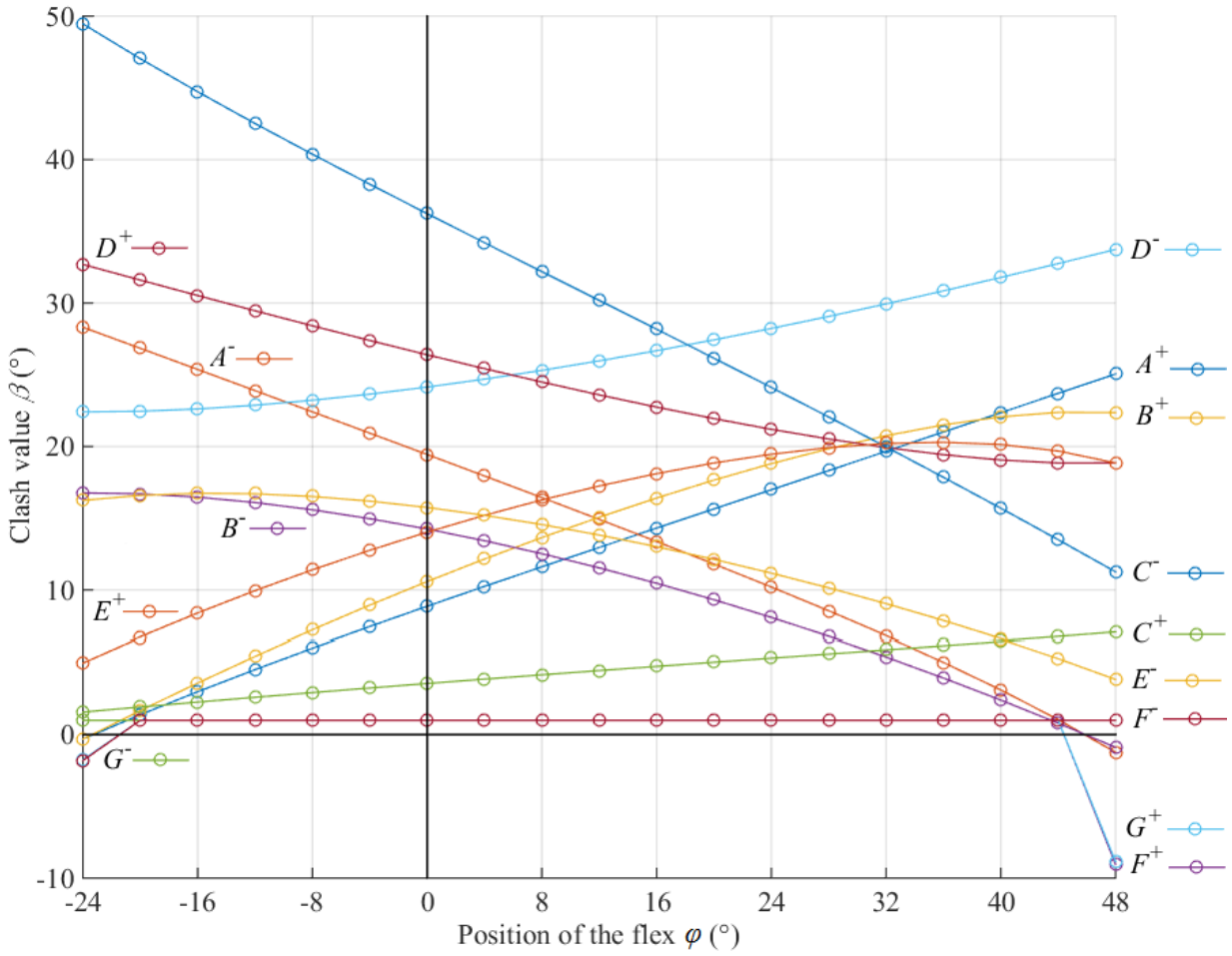

Fig. 5.10 Clash values of the Perato optimal B of the two-tetrahedron flexible polyhedron. It is labelled B in Figure 5.3; it has a range of motion of 70° and a regularity of 0.1. On the x-axis are the angles of rotation away from the chosen neutral position in Table 3.2; on the y-axis are the angles of ten Type I clashes in the polyhedron (unit in degrees) and the values of four Type II clashes. As the values of Type II clashes are given as a positive value or a negative value, here these values are given in degrees.

Chapter 6

Discovery of multiple degrees of freedom

6.1 Potential of the two-tetrahedron polyhedron

Comparing to the Steffen flexible polyhedron, the new two-tetrahedron flexible polyhedron is more able to achieve a wider range of motion while having a fairly regular shape. In other words, it is easier for the two-tetrahedron flexible polyhedron to avoid clashes. Because of this discovery, it is wondered if this type of flexible polyhedron is used to configure a single polyhedron with more than one degree of freedom, it might be as well easier to avoid clashes.

This chapter continues to work on triangulated flexible polyhedra, and uses the idea of triangulated near-polyhedron with dihedrals replaced by crinkles to create multi-dof flexible polyhedra. It first describes the composition of a two-dof flexible polyhedron [18] (Section 6.2), then presents an n-dof flexible polyhedron composed of repetitive unit cells (Section 6.3), and finally prospects for the chances of building a flexing polyhedral torus where the range of motion might not be limited by clashes (Section 6.5). This section describes the possible combination of near-polyhedra (Subsection 6.1.1) and the possible insertion of crinkles (Subsection 6.1.2).

6.1.1 The near-polyhedra

It was previously shown that the base of the two-tetrahedron flexible polyhedron is a near-polyhedron of two tetrahedra, with two of the four faces in each tetrahedron replaced by crinkles. Potentially the remaining two faces of each tetrahedron could also be replaced. In order to achieve this, this chapter first considers adding another tetrahedron to one end of the two-tetrahedron flexible polyhedron, as shown in Figure 6.1a. The end edge of the previous polyhedron becomes another hinge; and the two dihedrals around the new hinge can then be replaced as previously done in the Steffen flexible polyhedron and in the two-tetrahedron

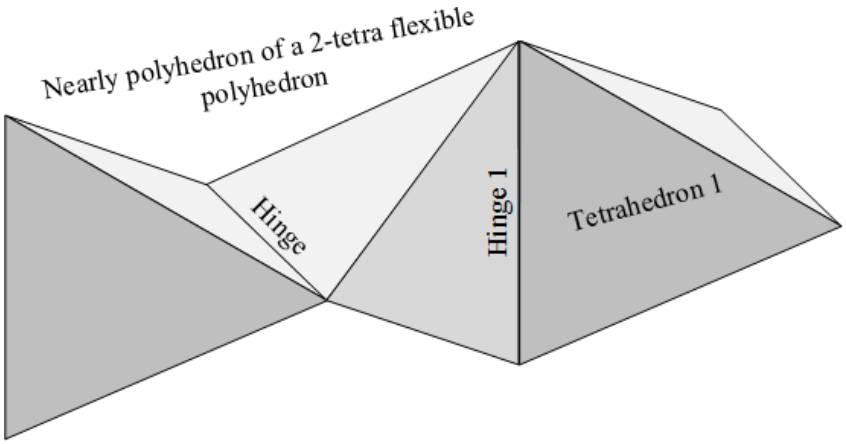

(a) The near-polyhedron of the 2-dof flexible polyhedron, composed of three tetrahedra, inspired by the near-polyhedron of the two-tetrahedron flexible polyhedron. Another tetrahedron is added to the end of the original two-tetrahedron, indicated as Tetrahedron 1. One more hinge is produced, indicated as Hinge 1.

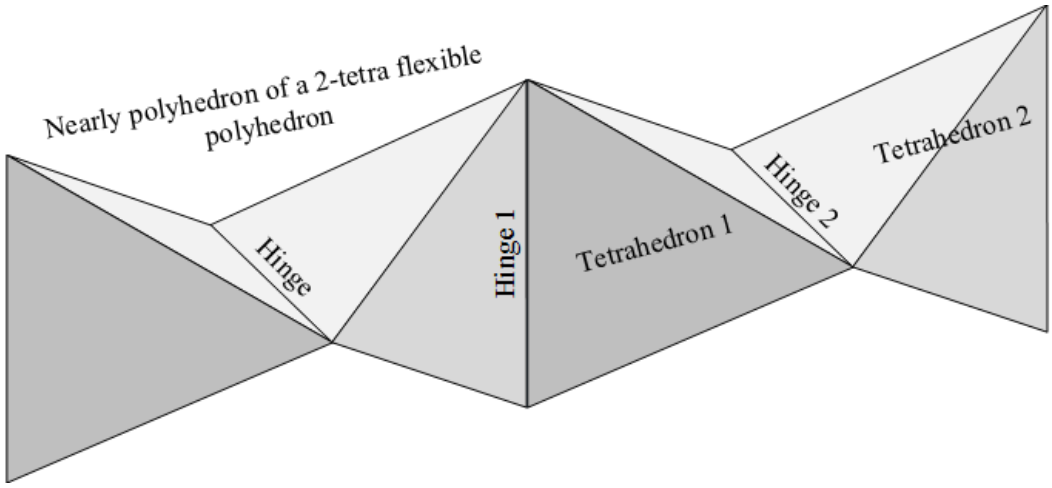

(b) The near-polyhedron of the 3-dof flexible polyhedron, composed of four tetrahedra. Another tetrahedron is added to the end of the three-tetrahedron chain, indicated as Tetrahedron 2. One more hinge is produced, Hinge 2.

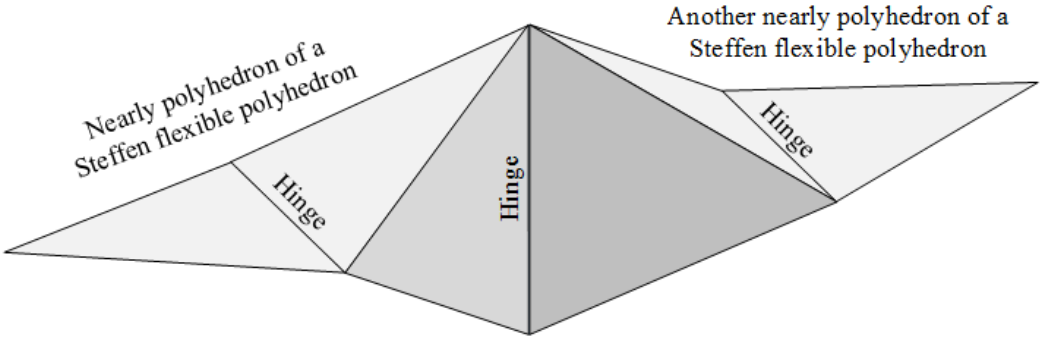

(c) Two near-polyhedra of the Steffen flexible polyhedron linked by the bottom edges. There are three hinges in this new near-polyhedron, two of which are the hinge in each of the Steffen polyhedra. Previously dihedrals around the hinge in a Steffen polyhedron are replaced (coloured in light grey); now the remaining dihedrals around the new middle hinge can be replaced by crinkles similarly (coloured in dark grey).

Fig. 6.1 Near-polyhedra of possible multi-dof flexible polyhedra

flexible polyhedron. If the new pair of replacing crinkles do not clash against any parts of the polyhedron, then a polyhedron with two degrees of freedom is achieved.

Similarly, if another tetrahedron is attached to the end of this new two-dof flexible polyhedron, as Figure 6.1b shows, then by replacing the dihedrals around the third hinge, a three-dof flexible polyhedron is possibly made. Likewise, any number of degrees of freedom in one single polyhedron can potentially be achieved.

Alternatively, the near-polyhedron of the Steffen flexible polyhedron can also be used to create multi-dof polyhedron, but as Figure 6.1c shows that the maximum number of hinges that can be produced is three. This is not as extendable to n degrees of freedom as the two-tetrahedron flexible polyhedron. In Figure 6.1b, it can be seen that unlimited number of extra tetrahedra can be added, and that any two adjacent tetrahedra is a near-polyhedron of a two-tetrahedron flexible polyhedron. Therefore, the feasibility of the original two-tetrahedron flexible polyhedron can be duplicated. However, in Figure 6.1c, no further hinges can be added. As a result, this dissertation leaves the discussion of two-dof and three-dof polyhedra based on the Steffen flexible polyhedron to future explorations, and focuses on the extensions of the two-tetrahedron flexible polyhedron.

6.1.2 The crinkles

Crinkles cannot immediately be added to the multi-dof near-polyhedron. When the new pairs of crinkles are in place, there are likely to be clashes. When all clashes are avoided, a feasible solution of a flexible polyhedron is found. To achieve this, all clashes are calculated according to the methods described in Section 3.2, and are minimised with tools described in Section 3.3. However, random perturbations with a highly unfeasible start is unlikely to bring feasible answers. This is especially true when some of the clash calculation functions for clash values are not smooth. Therefore, manual methods are described in this chapter based on the experience of the avoidance of crinkles in a one-dof system to help avoid clashes around the second and third hinges etc. This search for an initial feasible start point is not necessary in one-dof systems, because Steffen and Tachi already provided an initial feasible solution that could then be further optimised.

Consider the one-dof two-tetrahedron flexible polyhedron system, as shown in Figure 6.2. It is known from previous experience that if edge 1-2 and edge 1-3 in Figure 6.2a are longer than edges 5-2 and 5-3, $c > b$, and edges 4-2 and 4-3 are shorter than edges 10-2 and 10-3, then after replacement of dihedrals the resultant two crinkles can avoid each other as shown in Figure 6.2c. This is due to the symmetry of crinkles: as Figure 6.2b shows, Type I line-symmetric crinkles are chosen, A and B, which imposes the condition that $l_{4-3} = l_{10-6} = b$, $l_{4-8} = l_{10-2} = c$, $l_{4-6} = l_{10-3} = c$, $l_{4-2} = l_{10-8} = b$, $l_{3-8} = l_{2-6} = h$, $l_{6-8} = l_{2-3} = a$. Thus,

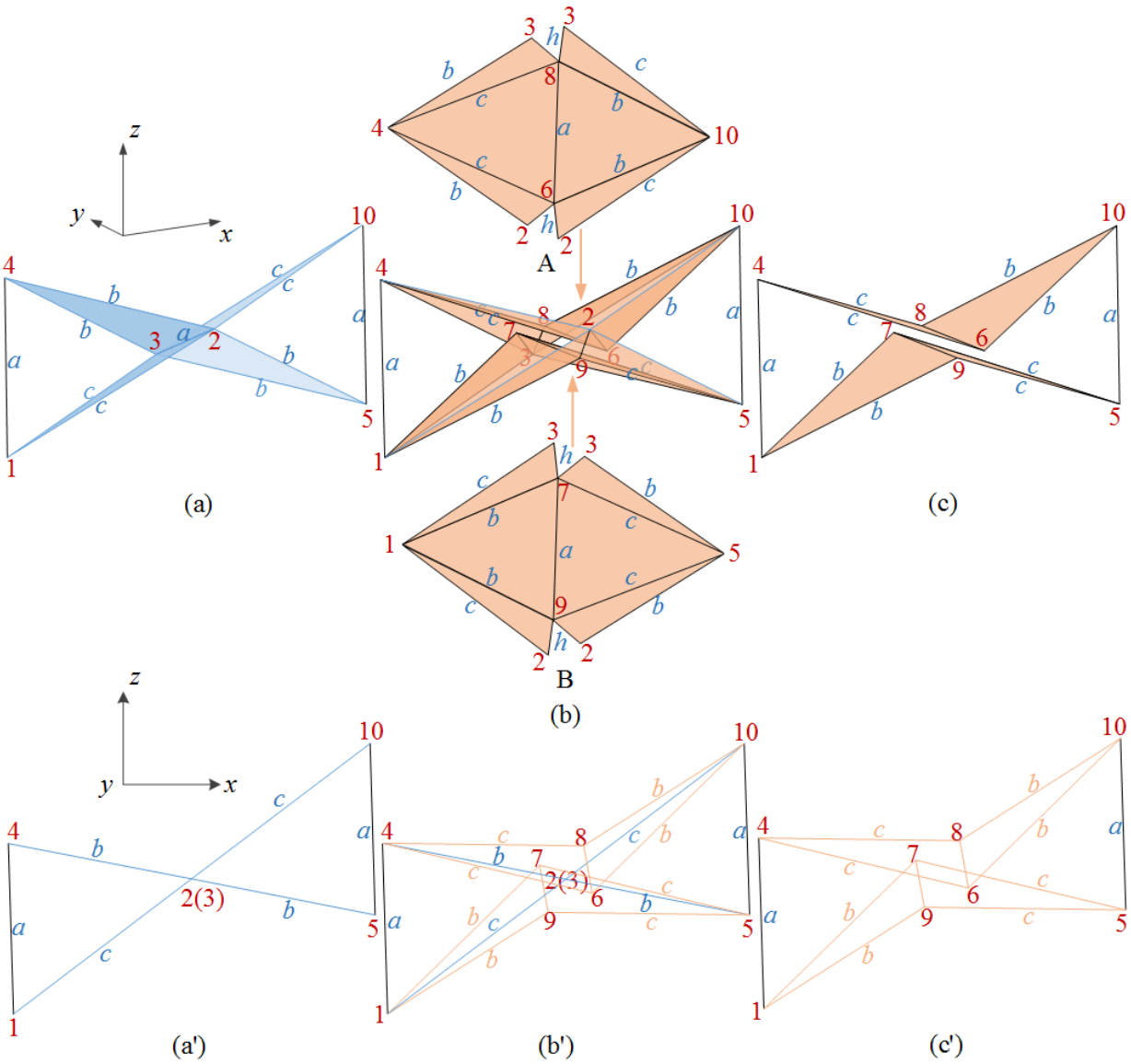

Fig. 6.2 Crinkle avoidance of the two-tetrahedron flexible polyhedron, showing the pair of crinkles avoiding each other. The viewpoint in (a) – (c) is chosen to show the gap between the two crinkles, while the viewpoint in (a′) – (c′) is along hinge 2-3. (a, a′) Framework of the near-polyhedron, with two replaced dihedrals drawn in blue. (b) Framework of the polyhedron with the pair of crinkles highlighted in orange. The net of each crinkle is shown in A and B. Parameter b is set to be smaller than c, so that the two crinkles can avoid clashes. A gap in between is noticeable. (b′) The side view of (b), showing both the dihedrals in blue and the dihedrals in orange. (c, c′) Only the two dihedrals in the middle of the crinkles (in orange) are shown, which are identical to the replaced dihedrals in blue but rotated.

in Crinkle A edges 4-6 and 4-8 are longer than edges 10-6 and 10-8, $c > b$; in Crinkle B edges 1-7 and 1-9 are shorter than edges 5-7 and 5-9. Therefore, edge 6-8 shifts to the left of the original hinge 2-3, and edge 7-9 shift to the right of hinge 2-3. Thus, clashes are avoided. As a result, in Figure 6.2 parameter b is set to be smaller than c.

To demonstrate this idea of avoidance due to Type I symmetry more clearly, the avoidance of crinkles can be seen in another way. When the dihedral 4-2-10-3 in Figure 6.2a is rotated about a C_2 axis going through the midpoint of line 4-10, it becomes the dihedral 4-6-10-8 in Figure 6.2c. Similarly, when dihedral 1-2-5-3 in Figure 6.2a rotates around a C_2 axis through the midpoint of line 1-5, it becomes dihedral 1-9-5-7 in Figure 6.2c. Therefore, if parameter b is smaller than c, then a gap in Figure 6.2c occurs between these two rotated dihedrals. These two dihedrals are part of crinkle A and crinkle B respectively. In these six images (a) – (c′), the original dihedrals before rotation are shown in blue faces and blue lines, and after rotation in orange.

The same avoiding idea is used for the second pair of crinkles about the second hinge, and the third pair of crinkles about the third hinge, so on and so forth. The next section shows that this manual configuration is successful in finding an initial feasible solution of a new flexible polyhedron.

6.2 Two finite mechanisms in one polyhedron

This section presents a two-dof flexible polyhedron, and shows how its initial feasible solution is found by choosing parameter values and crinkle directions.

The near-polyhedron of the two-dof flexible polyhedron is presented in Figure 6.3a. It is constructed as described in Figure 6.1b. It has two degrees of freedom: this is a chain of three tetrahedra linked one after another by two sharing edges. Each linking edge performs as a hinge where a finite mechanism is allowed. In the one-dof two-tetrahedron flexible polyhedra, the dihedral 4-2-10-3 is replaced by crinkle A in Figure 6.3b, and the dihedral 1-2-5-3 by crinkle B. Thus, one pair of crinkles around one hinge is inserted. Now in the two-dof near-polyhedron, the same pair of crinkles replace the same pair of dihedrals about the same hinge. Moreover, another pair of dihedrals need to be replaced by another pair of crinkles. The remaining faces on tetrahedron 2-3-5-10 are $\triangle$2-5-10 and $\triangle$3-5-10. Along with $\triangle$5-10-16 and $\triangle$5-10-15 of tetrahedron 5-10-15-16, the dihedral 2-5-16-10 and dihedral 3-5-15-10 are replaced by another pair of crinkles. The dihedral 2-5-16-10 is replaced by crinkle C in Figure 6.3b and dihedral 3-5-15-10 by crinkle D. Thus, the second pair of crinkles around the second hinge is inserted.

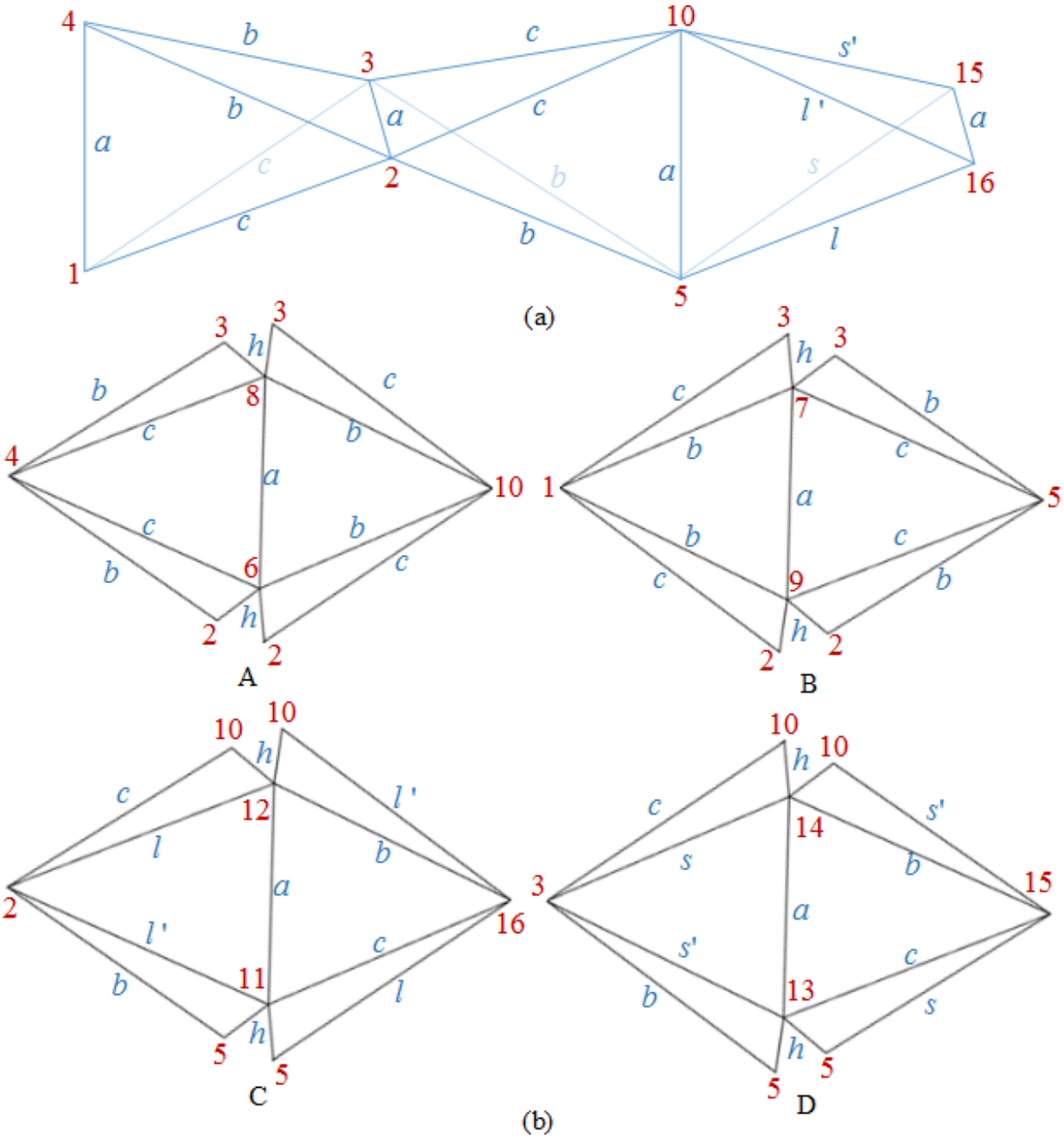

Fig. 6.3 Composition of a flexible polyhedron that has two degrees of freedom, with newly introduced parameters. (a) A near-polyhedron that has two hinges. (b) Nets of two pairs of crinkles A, B, C and D that replace two pairs of dihedrals around hinges 2-3 and 5-10. ('Mountains' and 'valleys' of the crinkles are specified later in finding a feasible solution.) A – D are all Type I crinkles, derived from Type I Bricard flexible octahedra.

The second pair of crinkles needs to avoid clashes against each other as the first pair does in order to "open up" the second hinge to allow the volume of the whole polyhedron to be continuous. Therefore, in Figure 6.3a, parameters l and l' are introduced to render $l_{5-16} > l_{2-5}$ ($l > b$) and $l_{10-16} < l_{2-10}$ ($l' > c$); and parameters s and s' are introduced to allow $l_{5-15} < l_{3-5}$ ($s < b$) and $l_{10-15} < l_{3-10}$ ($s' < c$). Thus, in crinkle C as shown in Figure 6.3b), due to $l_{5-16} = l_{2-12} = l$ and $l_{10-16} = l_{2-11} = l'$, line 11-12 "shifts" to the right; and in crinkle D, line 13-14 "shifts" to the left. As a result, when hinge 5-10 is "opened up", a gap is created between the two new crinkles, so that the volume enclosed by the second two tetrahedron becomes continuous. In this 2-dof system, four more parameters l, l', s and s' are introduced to allow the crinkles to avoid each other in order to find a feasible position where no clash occurs.

Although the techniques described above allow a start to be made, the design needs to avoid any clashes. The possible clashes are both between different crinkles and within a crinkle itself. Clashes between crinkles are around the six edges of tetrahedron 2-3-5-10. Around hinge 2-3, crinkle A may clash against crinkle B; and around hinge 5-10, crinkle C against crinkle D. About edges 2-5, 3-5, 2-10 and 3-10, the possible clashes are between different pairs of crinkles, B and C, B and D, A and C, and A and D respectively. Possible clashes within a crinkle itself were discussed in the last paragraph of Section 2.4.2.

6.2.1 A feasible solution

In order to find a solution where no clashes occur, the optimisation method designed to maximise the range of motion described in Section 3.3 is used here to eliminate clashes. Clash calculation methods described in Section 3.2 are used to find clash values here. The smallest clash value of all β is set as the objective of the SA optimisation. Thus, by reducing the clash values, a feasible solution where all clash values are positive was found, i.e. no clash occurs. Based on this feasible solution, the range of motion about both hinges are optimised. Now the smallest range of motion is used as the objective of the optimisation, during which it is maximised. A result of an SA run is presented in Figure 6.4 with two end positions about the hinge 5-10, showing the maximum and minimum rotation before clashes occur. This is not necessarily the best solution but it does allow a considerable range of motion about each hinge, 37° and 38°. One end position rotated about the second hinge is drawn in dashed lines, and the other is drawn in solid lines. The parameter values of this polyhedron are shown in Table 6.1. A comprehensive optimisation of the two-dof polyhedron has not been attempted.

The directions of hills and valleys of the crinkles in Figure 6.4 are: vertices 8 and 7 in Crinkles A and B go into the page in Figure 6.3b, and vertices 6 and 9 go out; in Crinkles C

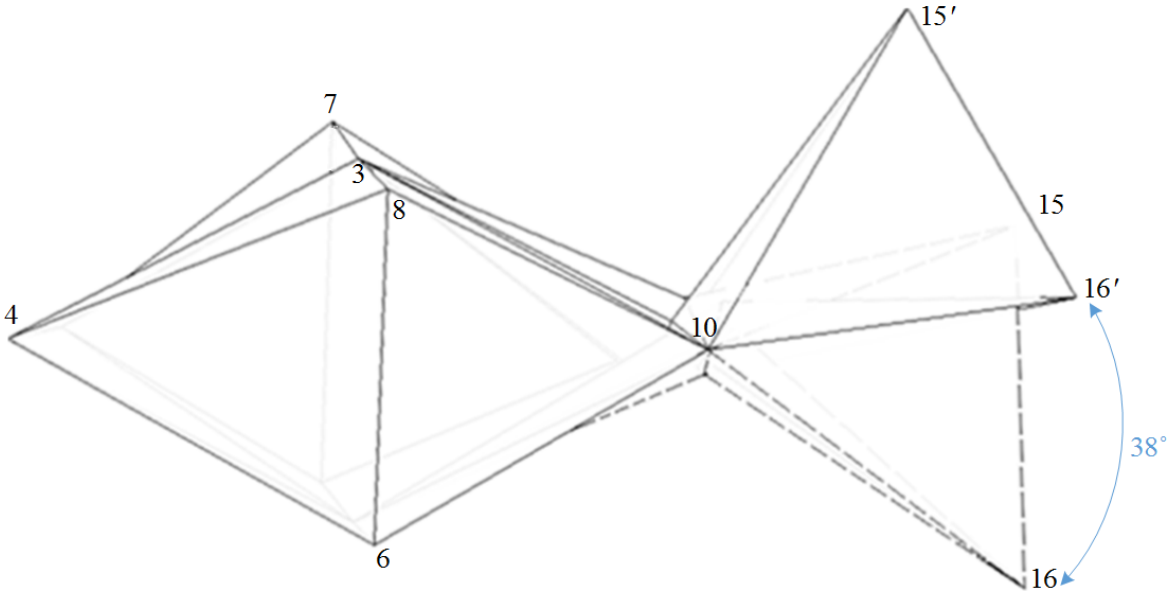

Fig. 6.4 A three-tetrahedron flexible polyhedron showing two positions of the flexing motion about the second hinge. The range of motion around the first hinge is 36.5°, around the second hinge is 38.2°. Vertices 7 and 8 point into the page, and vertex 6 sticks out of the page. This crinkle direction is chosen as it is found to allow large ranges of motion.

Table 6.1 Parameter values of the 2-dof flexible polyhedron shown in Figure 6.4

Parameters and result	a	b	c	h	s	s'	l	l'	Θ_1	Θ_2
Values	6	8	8.5	1	7.8	7.7	8.9	8.52	36.5°	38.2°

and D vertices 12 and 14 go inwards in Figure 6.3b, and vertices 11 and 13 go out of the page. This setting of directions is found to produce a good range of motion about both hinges.

6.2.2 Mutual influence of the range of motion

This section considers whether the rotation of one hinge affects the rotation of the other in a 2-dof polyhedron. The particular example in Figure 6.4 is investigated. The range of motion about both hinges are measured in the following way: the position of one hinge is first fixed, while the position of the other is tracked; then the position about the first hinge is changed and fixed, and the full range of motion of the other is tracked again; so on and so forth. Then, the system is considered the other way around: the range of motion of the first hinge is measured while the second is fixed at different positions. It is found that their range of motion is not limited by the position of each other, as shown in Figure 6.5, so that both hinges can rotate independently.

In the graph, θ_1 is the rotational angle about hinge 2-3, and θ_2 is the rotational angle about hinge 5-10. Both rotational angles measure the current rotational position away from a chosen neutral position. According to the range of θ_1 in the graph, the range of motion Θ_1 about hinge 2-3 is constantly 36.5°, irrespective of the position of hinge 5-10 within its no clash range; the value range of θ_2 shows that the range of motion Θ_2 about hinge 5-10 is

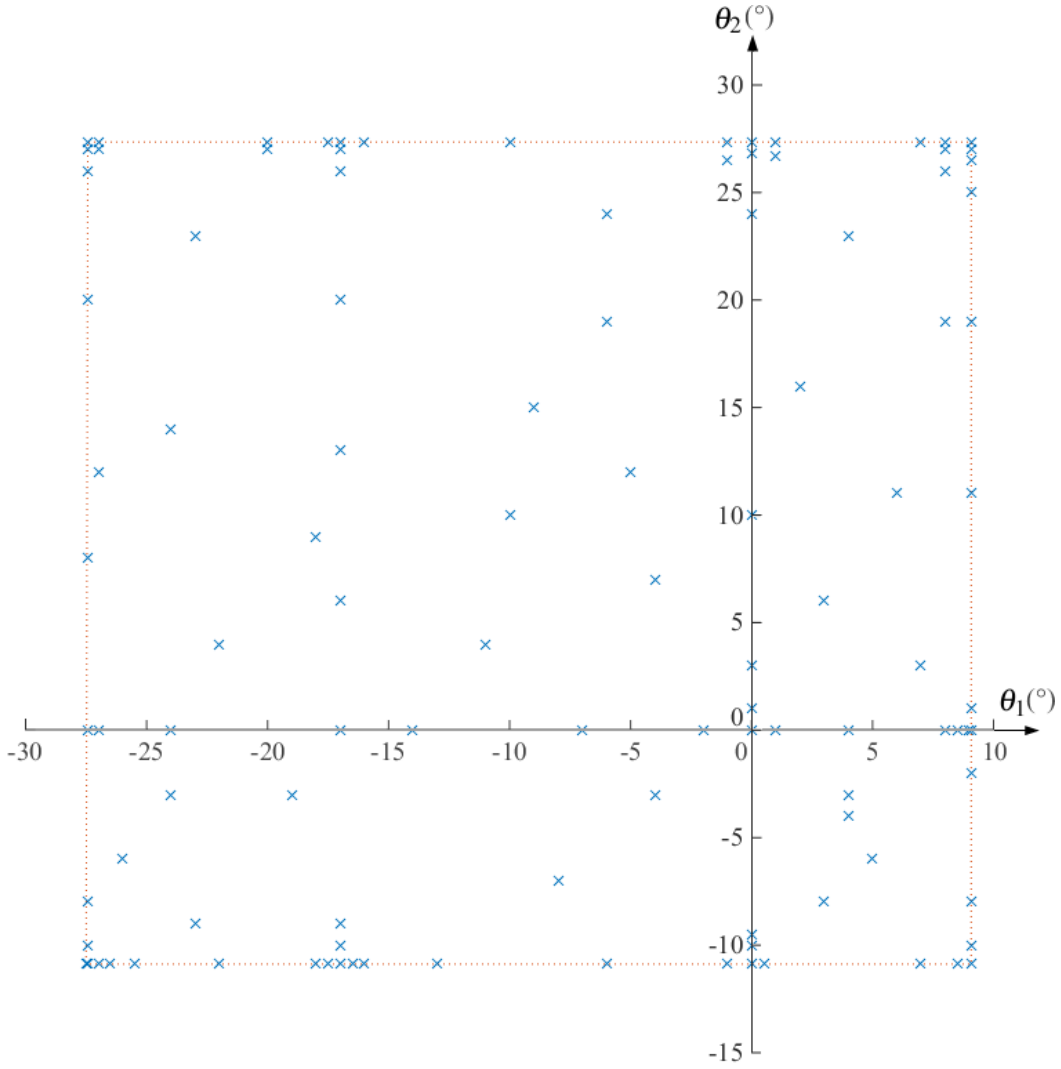

Fig. 6.5 Independence study of the rotations of the two hinges. Rotation θ_1 about hinge 2-3 against the rotation θ_2 about hinge 5-10 in the 2-dof polyhedron shown in Figure 6.4. The rotational angle θ_1 is perpendicular to line 2-3; the rotational angle θ_2 is perpendicular to line 5-10. Each blue cross represents a feasible solution where no clash occurs in the polyhedron. There are 109 results on this graph. They show that the full range of motion Θ_1 about hinge 2-3 is 36.5°, and is independent of the rotation of hinge 5-10; the full range of motion Θ_2 about hinge 5-10 is 38.2°, not limited by the rotation of hinge 2-3.

38.2°, irrespective of the position of hinge 2-3 with in the 36.5° range. This indicates that the rotation of each hinge in this polyhedron is not coupled to the other.

It is observed that the only chance for the position of one hinge to limit the rotation of the other is by the clashes between different pairs of crinkles. However, the clashes around edges 2-5, 3-5, 2-10 and 3-10 seem not easy to occur. Thus, when feasible solutions are sought, or when the system is optimised to find a better range of motion, clashes on these edges are easy to avoid. Therefore, it seems that the principle clashes are still between each pair of crinkles, in this case between A and B, and between C and D.

This observation is only true for this particular example, clashes between different pairs of crinkles may in other cases couple the rotations of different hinges.

6.3 Unit cell of a repetitive polyhedron

Based on the knowledge of the 2-dof system, this section considers whether any number of degrees of freedom can be created in a single polyhedron, and whether an n-dof polyhedron can be a repetitive system. This section extends the 2-dof polyhedron to a 2-dof polyhedron composed of unit cells as a repetitive system.

In order to make a polyhedron repeatable, the three tetrahedra in Figure 6.6 are made identical. With the replacement of crinkles in the right directions (shown in Figure 6.7b), this setting of parameters (the height of crinkles, h, is not showing) gives global and local symmetry to the polyhedron. The global symmetry is line symmetry: the C_2 axis goes through the midpoints of edges 2-10 and 3-5. The local symmetry is of two adjacent tetrahedra, and is inversion in a point. The point of reflection of the first two tetrahedron is the midpoint of edge 2-3. Through this point, vertex 1 becomes vertex 10, vertex 4 becomes vertex 5, and vertex 2 becomes vertex 3. This global and local symmetry gives the polyhedron the simplest form and is extendable to more degrees of freedom as a repetitive system. Specifically, the global and local symmetry ensure that the first pair of tetrahedra is identical to the second pair of tetrahedra, and that the last tetrahedron is in the same position as the first tetrahedron. Therefore, each pair of tetrahedra is a unit cell of a repetitive system. Although for a repetitive system, there need not be overall symmetry, here optimisation with parameters shown in Figure 6.6 is conducted.

The start point of this optimisation has the initial parameter values chosen as $a = 1$, $b = 1$, $c = \sqrt{2}$, $d = \sqrt{3}$ and $h = 0.5$. All parameter values are varied apart from a. However, there are clashes in the polyhedron with these dimensions, so the clashes are minimised first. Then after the clashes are eliminated, the range of motion is maximised. A result of 13.7° is achieved and presented in Figure 6.7b, Figure 6.8 and Figure 6.9, whose parameter

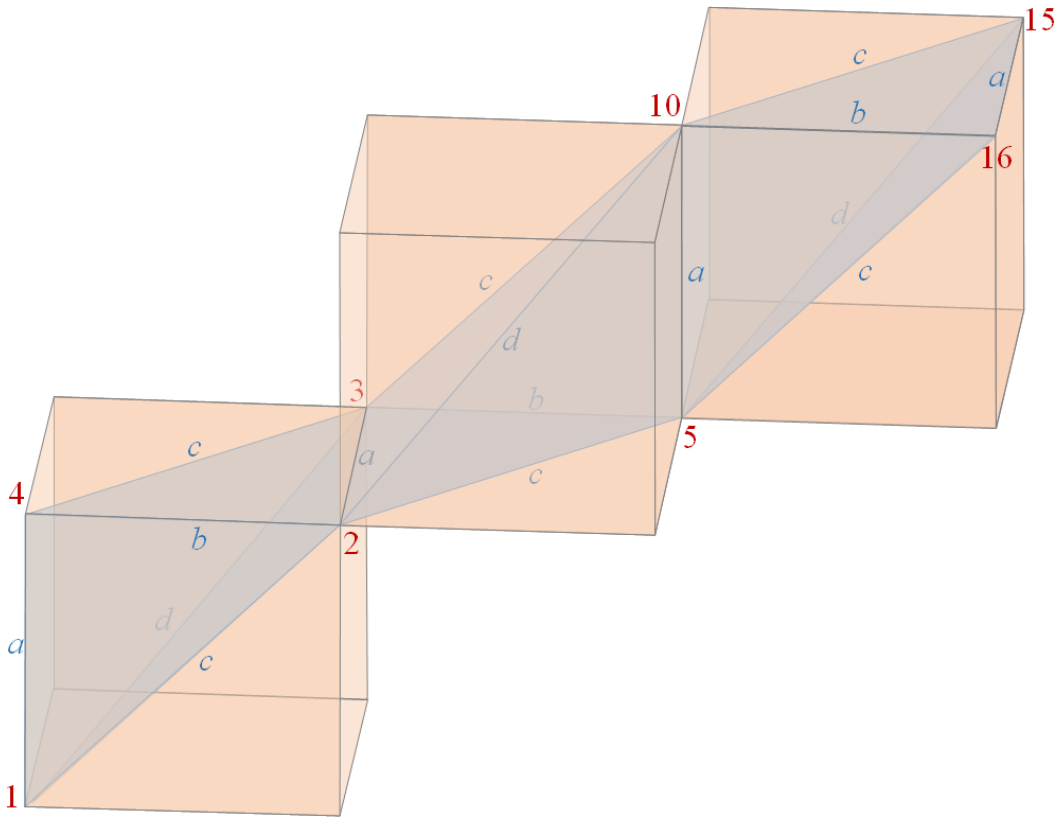

Fig. 6.6 A 2-dof near-polyhedron that is repeatable. The three tetrahedra are identical, each is part of a cube. The chain has a global symmetry: a line of symmetry goes through the midpoints of edge 3-5 and edge 2-10. Every two adjacent tetrahedra have a local symmetry: it is an inversion through the midpoint of hinge 2-3 and hinge 5-10 respectively.

values are $a = 1$, $b = 1.091$, $c = 1.377$, $d = 1.750$ and $h = 0.534$. Again, no comprehensive optimisation has been attempted.

The near-polyhedron and of the flexible polyhedron of the feasible solution are shown in Figure 6.7. The shape of the near-polyhedron in Figure 6.7a is not much different from that in Figure 6.6. The crinkle depth $h = 0.534$ and crinkle directions are shown in Figure 6.7b, Figure 6.8 and Figure 6.9. Vertices 7 and 8 go out of the page and vertices 6 and 9 into the page in Figure 6.8 (and in Crinkles A and B in Figure 6.3). In Crinkles C and D in Figure 6.3, vertices 12 and 14 stick into the page while vertices 11 and 13 stick out.

The range of motion of one hinge is presented in Figure 6.8. The polyhedron has a global line of symmetry, so the two hinges are identical. Note that in this parameter setting, due to unit cells, the configuration about each hinge in a n-dof polyhedron is identical. The cardboard model in Figure 6.9 shows the two motions in one perspective. On the left the polyhedron is rotated about hinge 2-3; on the right the polyhedron is rotated about hinge 5-10.

The net of this polyhedron is shown in Figure 6.10, on which the parameters of all edges are shown. The hills and valleys of this polyhedron are shown in dashed and solid lines respectively as indicated.

If more parameters are given to a polyhedron to vary the shape, it is likely that a better range of motion will be achieved. Here, possible sets of parameters are given for future exploration. In this generalisation of parameter settings, the global and local symmetry need not be retained. The global symmetry is broken by one new parameter, c', shown in Figure 6.11a. This setting still guarantees that the first tetrahedron is identical to the last, so the polyhedron is still extendable. However, the interaction of each pair of crinkles is different, so that the two pairs of tetrahedra are not identical anymore. If the two hinges do not affect the rotation of one another, then the the connection about hinge 2-3 can be repeated about hinge 15-16. This can also gives an n-dof repetitive system.

The local symmetry is broken by giving four more parameters to the middle tetrahedron, a_2, b_2, c_2 and d_2, as shown in Figure 6.11b. However, the global symmetry remains by the parameter setting of c', so that the connection between the first two tetrahedra is the same as the connection between the last two tetrahedra. The polyhedron now is not necessarily extendable. To give most freedom for the polyhedron to vary in shape, Figure 6.11c gives an independent set of parameters to each tetrahedron. Now there are 16 parameters besides the crinkle height h, which can be generalised in the same way: each crinkle need not maintain the same height as others, not even the crinkles of the same pair. There are four crinkles, so there are h_1, h_2, h_3, h_4. Overall, there is a maximum number of 20 parameters for the most generalised 2-dof flexible polyhedron.

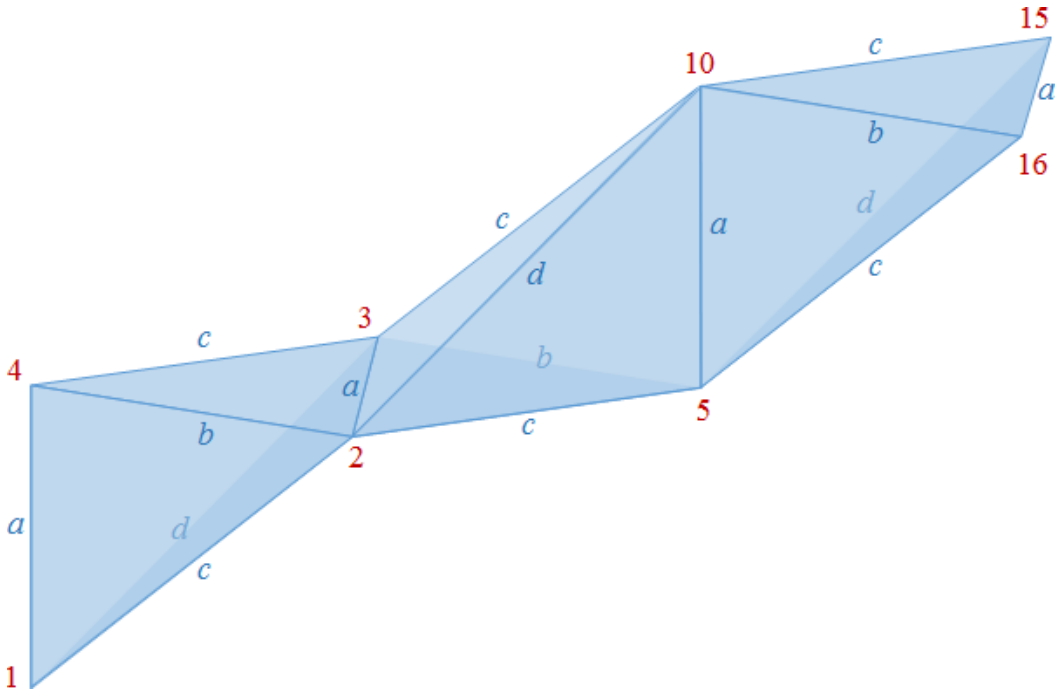

(a) Near-polyhedron of a repeatable 2-dof flexible polyhedron. Its parameter setting follows Figure 6.6 but with different values $a = 1$, $b = 1.091$, $c = 1.377$ and $d = 1.750$.

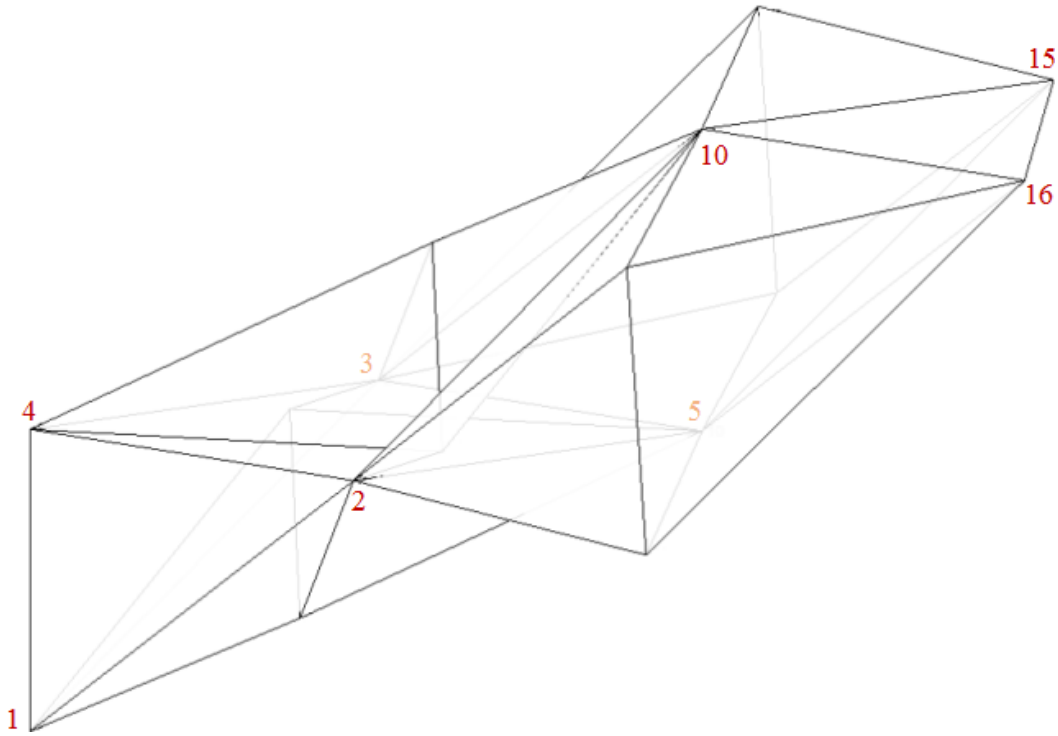

(b) A repeatable 2-dof flexible polyhedron of unit cells. Due the symmetry, this polyhedron is extendable to a polyhedron with unlimited number of hinges. Each hinge in this polyhedron has a range of motion of 14°. Only hinge ends are numbered in red.

Fig. 6.7 A feasible solution of a repetitive flexible polyhedron with two degrees of freedom. Its parameter values are $a = 1$, $b = 1.091$, $c = 1.377$, $d = 1.750$ and $h = 0.534$. Both images show true view of hinge 5-10.

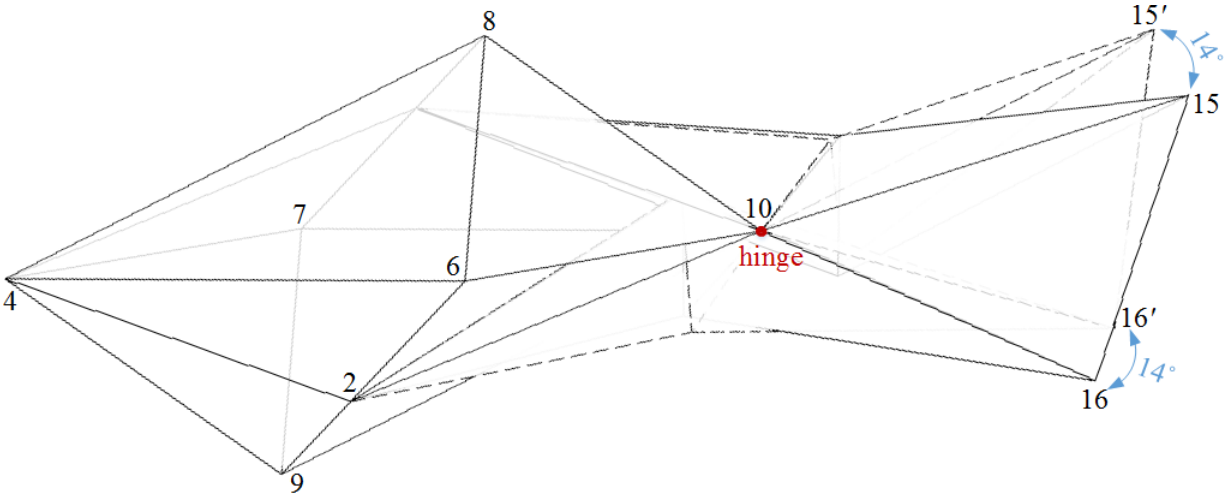

Fig. 6.8 Two end positions around the second hinge in a 2-dof polyhedron of unit cells. The first two tetrahedra are fixed; the third tetrahedron is rotated around hinge 5-10. The full range of motion of each hinge is 13.7°. The image shows two extreme positions of the rotational range for one hinge. The view point is through hinge 5-10. However, due to unit cells, the configuration about each hinge in this 2-dof polyhedron is identical.

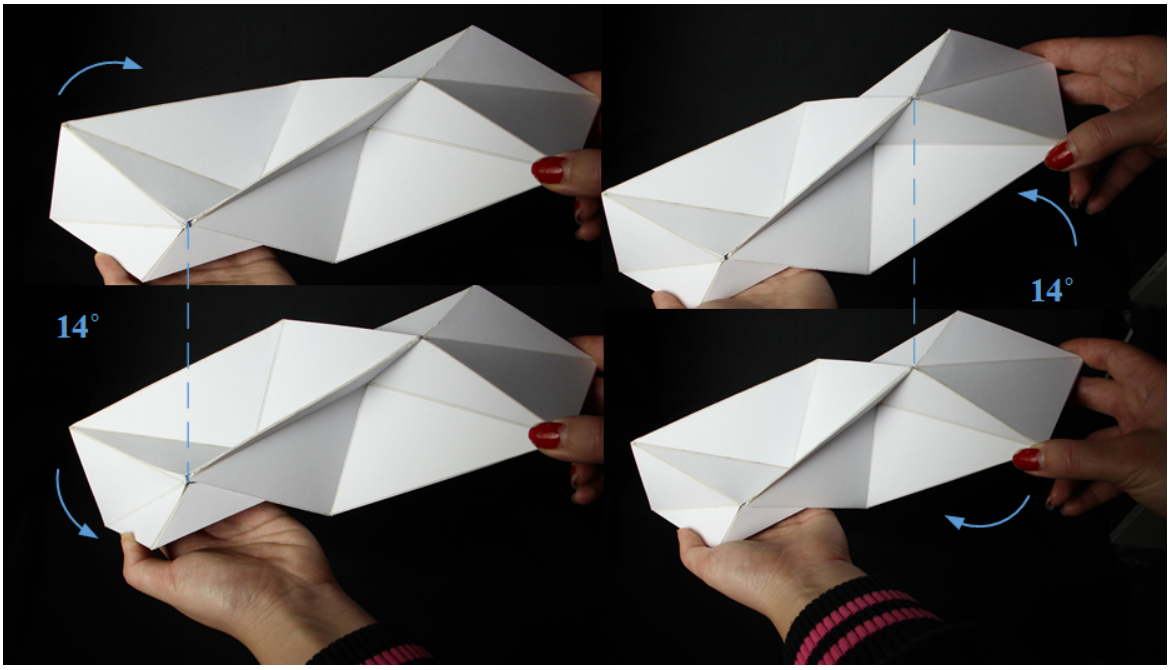

Fig. 6.9 Physical model of the 2-dof flexible polyhedron of unit cells, showing the rotation about each hinge (14°) through the same view point. The perspective is a view point above the perspective in Figure 6.7b.

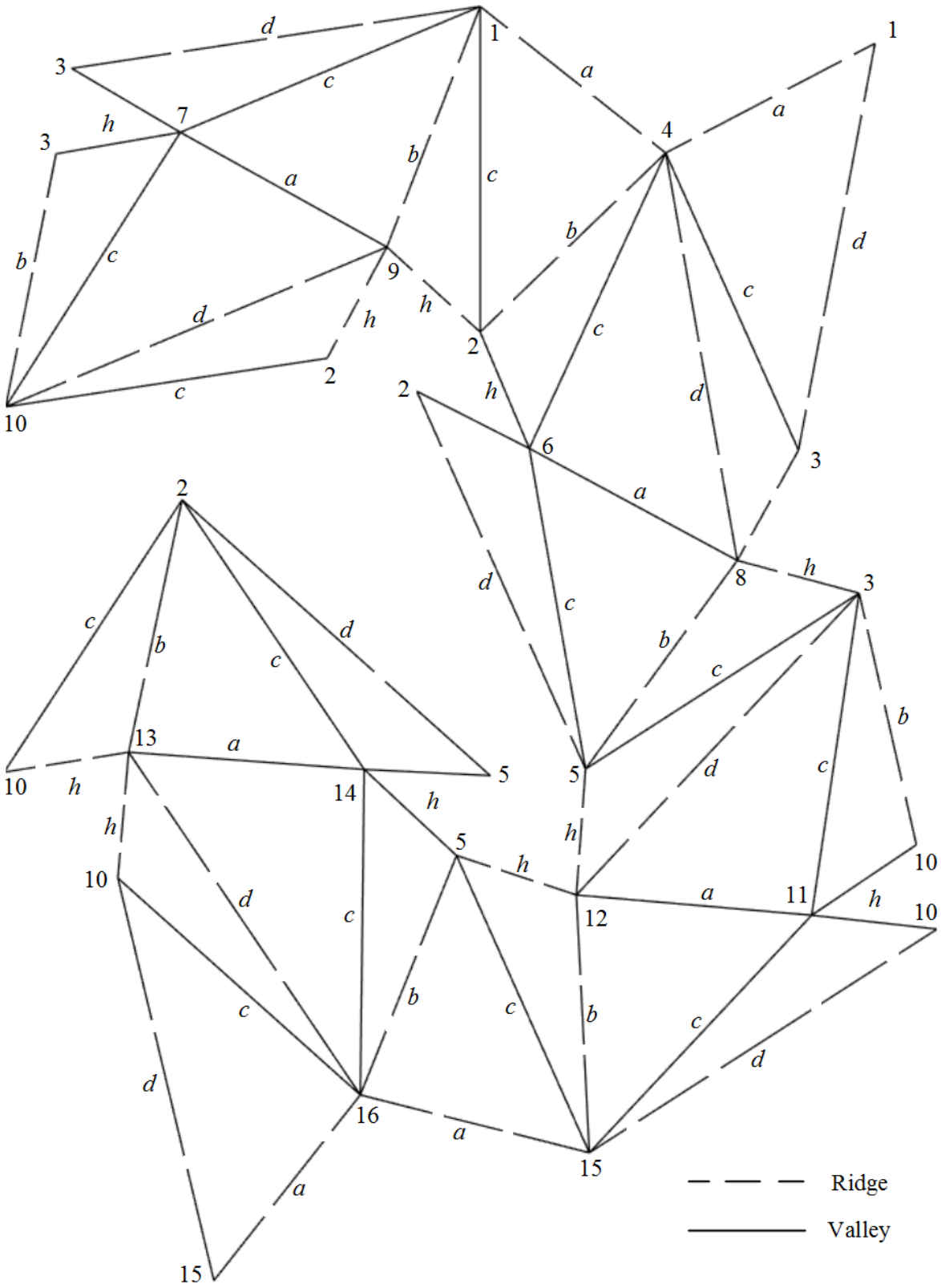

Fig. 6.10 Net of the 2-dof flexible polyhedron of unit cells, with parameter values $a = 1$, $b = 1.091$, $c = 1.377$, $d = 1.750$ and $h = 0.534$ and the range of motion about each hinge of 13.7°. Due the global and local symmetry, the nets of all four crinkles are identical, with the ridge and valley directions in each pair different.

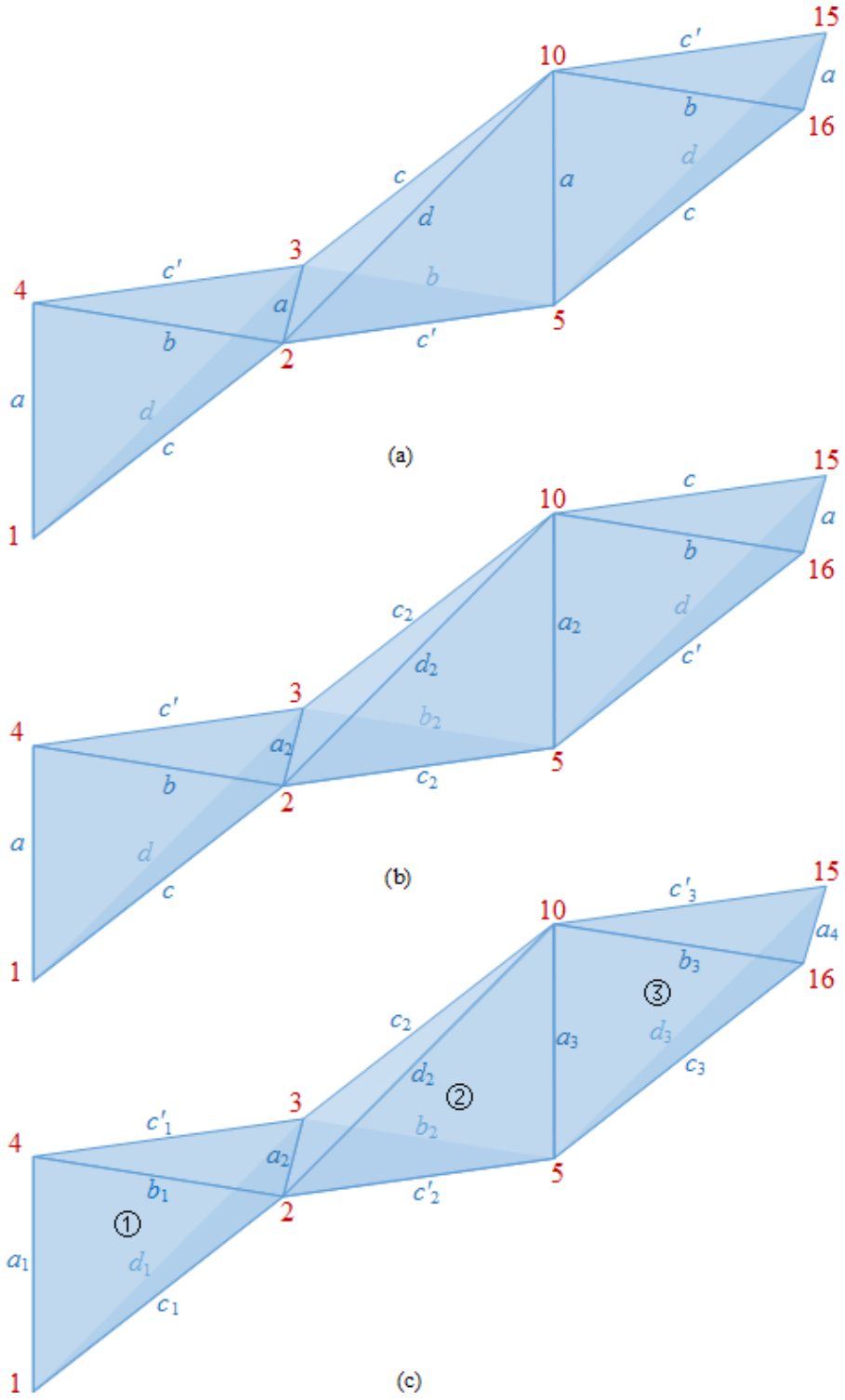

Fig. 6.11 Various parameter schemes for a 2-dof flexible polyhedron. (a) The global symmetry is broken by adding one more parameter c', but all tetrahedra are still identical so that the polyhedron is extendable to repetitive n-dof systems. (b) The global symmetry is retained, but the local symmetry about each hinge is broken by introducing four more parameters to the central tetrahedron. (c) A completely general set of parameters which preserves neither local nor global symmetry; there are now 16 parameters, plus the unshown heights of four crinkles.

6.4 A polyhedron of three mechanisms

Based on the most general setting of parameters of the 2-dof flexible polyhedron, a feasible solution here is given to the most general 3-dof flexible polyhedron as an example of n-dof general polyhedron. This feasible solution is a good starting point of potential future optimisation of the most general 3-dof flexible polyhedron. This feasible solution allows a range of motion of 14° about each hinge, and is the solution found for the 2-dof flexible polyhedron of unit cells shown in Figure 6.7. Because the repetitive system of unit cells allows any number of degrees of freedom to be in one single polyhedron, here a 3-dof example is shown. There are 27 parameters in the most general 3-dof flexible polyhedron. Its near-polyhedron shown in Figure 6.7 has 21 parameters, five more than that of 2-dof.

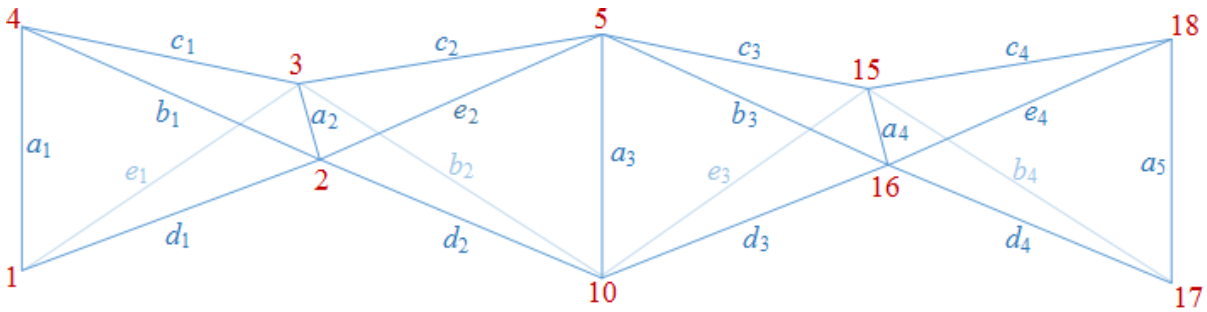

Fig. 6.12 near-polyhedron of a three-dof flexible polyhedron. The most general set of parameters are given. There are 21 parameters in this near-polyhedron.

Table 6.2 Parameter values of Figure 6.12, allowing a range of 14° about each hinge

Parameters	$a_1 = a_2 = a_3 = a_4 = a_5$	$b_1 = b_2 = b_3 = b_4$	$c_1 = c_2 = c_3 = c_4$ $d_1 = d_2 = d_3 = d_4$	$e_1 = e_2$ $e_3 = e_4$	$h_1 = h_2 = h_3$ $h_4 = h_5 = h_6$
Value	1	1.091	1.377	1.75	0.534

6.5 Non-stop flexible polyhedral tori

An n-dof polyhedron can allow a total range of motion in one direction of 360°, when n is great enough. Then, the "tail" of this polyhedron can possibly be configured to link the "head" to form a polyhedral torus. A flexible polyhedral torus is defined here as a torus composed of polygons, connected by edges, where every edge is rotated about during the flex. In other words, there are no adjacent polygons that stay the same angle to each other during the flex as previous polyhedra do. Specifically, the two end edges of each n-dof polyhedron (one

'end edge' of the Steffen flexible polyhedron) are not rotated about during any motion. For example, edge 1-4 and edge 15-16 in Figure 6.7.

A flexible polyhedral torus has the potential to be configured to flex in one direction in a loop repetitively without clashes. The challenge of configuring such a polyhedral torus is the compatibility of the underlining near-polyhedron and the inserted crinkles. Two potential *near-polydedral tori* are shown in Figure 6.13, which shows two rings of 6 and 12 regular tetrahedra respectively. They are able to rotate repetitively without any clashes [14]. If all the dihedrals about each hinge in these rings are replaced by crinkles, and a feasible solution where no clash occurs is found, a flexible polyhedral torus is created. If the motion is large enough and is repetitive without a clash, then a non-stop flexible polyhedral torus would be achieved. To make progress, it is likely that the ring would have to be formed from many polyhedra. However, no further exploration has been carried out.

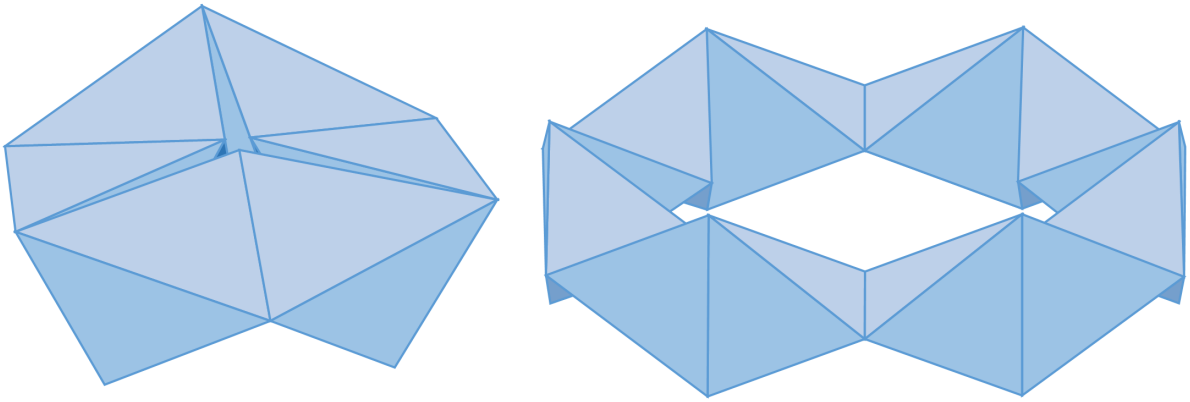

Fig. 6.13 A ring of 6 regular tetrahedra and a ring of 12 regular tetrahedra. Both are able to rotate in one direction in a loop repetitively without the need to stop. The mechanisms of these tetrahedral rings are discussed in [14]. Images re-drawn from figures in [14].

Chapter 7

Conclusions and Future work

7.1 Conclusions

This dissertation first synthesised the story of the rigidity and flexibility of polyhedra. Then, based on an understanding of Bricard flexible polyhedra, three types of crinkles were described in detail. With the replacement of crinkles, two simple triangulated one-dof flexible polyhedra were presented. Based on the understanding of these two examples, the range of motion about the hinge was maximised. The Steffen original flexible polyhedron was maximised first with the parameters suggested by Steffen. The result doubled the maximum possible range of motion of flexible polyhedra. According to the understanding of crinkles, Steffen's setting of parameters was generalised. A second round of optimisation was conducted to further improve the range of motion of flexible polyhedra. Based on the techniques acquired in optimising the Steffen flexible polyhedron, the second simplest flexible polyhedron provided by Tachi was optimised with the most general parameter setting. The optimisation result tripled the absolute maximal range of motion of a flexible polyhedron, from Steffen's 27° to 80°.

Multiple finite mechanisms in one single polyhedron were achieved based on the extension of the two-tetrahedron flexible polyhedron. Any number of degrees of freedom is possible in a polyhedron. A feasible solution for a 2-dof flexible polyhedron was first presented. Then a feasible solution of a repeatable polyhedron of unit cells was found with the simplest parameter setting. Its unit cell allows n-dof flexible polyhedron. Based on observations, the rotation of different hinges were found to be independent of each other. From previous experience that an extended set of parameters were likely to provide an extended range of motion, the most general 3-dof polyhedra was presented as an example of an n-dof flexible polyhedron. Lastly, the ways to configure a flexible polyhedral torus

was suggested. This flexible polyhedral torus may even flex for an infinite range of motion without clashes.

7.2 Future work

This dissertation has not explored all the combinations and the maximal possible range of motion of all types of flexible polyhedra. The optimisation on the range of motion of the two types of one-dof polyhedra were conducted within a limited amount of time. During the optimisations, it was found that the range of motion is sometimes highly sensitive to the parameter values and computational efforts. Therefore, if more time is allowed, more efforts may produce better results. In all flexible polyhedra, only Type I crinkles were considered. The possible advantages of Type II and Type III crinkles were not explored. In this dissertation, only simple examples — triangulated polyhedra — were discussed. Polyhedra composed of polygons other than triangles may also be interesting to explore.

There is much potential work proposed in the chapter of multi-hinge flexible polyhedron. The maximal range of motion of n-dof flexible polyhedra is not optimised at all. In future work, the range of motion of the unit cell would first be maximised. The absolute maximal range of motion of the most general 2-dof and 3-dof flexible polyhedra can then be explored. The most interesting result of all would be a feasible solution of a flexible polyhedral torus, especially a flexible polyhedral torus that is able to rotate without clashes.

References

[1] Aleksandrov, V. A. (1995). A new example of a flexible polyhedron. *Siberian Mathematical Journal*, 36(6):1049–1057.

[2] Alexandrov, V. (2011). The Dehn invariants of the Bricard octahedra. *Journal of Geometry*, 99(1-2):1–13.

[3] Bricard, R. (2010). Memoir on the Theory of the Articulated Octahedron. Translated from Mémoire sur la théorie de l'octaèdre articulé, *J.Math.Pures Appl.* 1897, 3, 113-150. by E. A. Coutsias, University of New Mexico.

[4] Calladine, C. R. (1978). Buckminster Fuller's "Tensegrity" structures and Clerk Maxwell's rules for the construction of stiff frames. *International Journal of Solids and Structures*, 14(2):161–172.

[5] Cauchy, A. L. (1813). Sur les polygones et les polyèdres, Second Mémoire. *Journal de l'Ecole Polytechnique*, XVIe Cahier(Tome IX):87.

[6] Chen, X., Liu, J., Chou, W., and Wang, T. (2005). Algorithm of fast calculate exact contacted position among virtual objects. *Journal of Beijing University of Aeronautics and Astronautics*, 31(7):799–804.

[7] Connelly, R. (1975). An attack on rigidity. I, II. *Bulletin of the American Mathematical Society*, 81(3):566–569.

[8] Connelly, R. (1976). An immersed polyhedral surface which flexes. *Indiana Univ. Math. J.*

[9] Connelly, R. (1977). A counterexample to the rigidity conjecture for polyhedra. *Publications Mathématiques de L'Institut des Hautes Études Scientifiques. https://www.youtube.com/watch?v=reO7Qx3HiIg*, 47(1):333–338.

[10] Connelly, R. (1978). A flexible sphere. *The Mathematical Intelligencer*, 1(3):130–131.

[11] Connelly, R. (1979). The rigidity of polyhedral surfaces. *Mathematics Magazine*, 52(5):275–283.

[12] Connelly, R., Sabitov, I., and Walz, A. (1997). The bellows conjecture. *Contrib. Algebra Geom*, 38:1–10.

[13] Euler, L. (1862). Leonhardi euleri opera postuma mathematica et physica anno mdccclxliv detecta. *Leipzig:Voss(Petropoli)*, Tomus 1:494–496.

[14] Fowler, P. and Guest, S. D. (2005). A symmetry analysis of mechanisms in rotating rings of tetrahedra. *Proceedings of the Royal Society A: Mathematical, Physical and Engineering Sciences*, 461(2058):1829–1846.

[15] Gluck, H. (1974). Almost all simply connected closed surfaces are rigid. *Proceedings of the Geometric Topology Conference*, 438:225–239.

[16] Kirkpatrick, S., Gelatt, C. D., and Vecchi, M. P. (1983). Optimization by Simulated Annealing. *Science*, 220(4598):pp. 671–680.

[17] Lijingjiao, I., Tachi, T., and Guest, S. (2015). Optimizing the Steffen flexible polyhedron. In *Proceedings of the International Association for Shell and Spatial Structures*, August, Amsterdam.

[18] Lijingjiao, I., Tachi, T., and Guest, S. (2016). Flexible polyhedra with two degrees of freedom. In *Proceedings of the International Association for Shell and Spatial Structures*, September, Tokyo.

[19] Maxwell, J. C. (1864). On the calculation of the equilibrium and stiffness of frames. *Philosophical Magazine Series 4*, 27:294–299.

[20] Pellegrino, S. (1993). Structural computations with the singular value decomposition of the equilibrium matrix. *International Journal of Solids and Structures*, 30(21):3025–3035.

[21] Pellegrino, S. and Calladine, C. R. (1986). Matrix analysis of statically and kinematically indeterminate frameworks. *International Journal of Solids and Structures*, 22(4):409–428.

[22] Sabitov, I. K. (1998). The Volume as a Metric Invariant of Polyhedra. *Discrete & Computational Geometry*, 20(4):405–425.

[23] Steffen, K. (1978). A symmetric flexible Connelly sphere with only nine vertices. *Letter to L'Institut des Hautes Études Scientifiques*.

[24] Strang, G. (2006). *Linear algebra and its applications*. Thomson Brooks/Cole, Belmont, Calif, 4th edition.

[25] Vandekerckhove, J. (2006). General simulated annealing algorithm. *MathWorks*, http://uk.mathworks.com/matlabcentral/fileexchange/10548-general-simulated-annealing-algorithm?s_tid=srchtitle.

[26] Walz, A. B. (2000). *On the Bellows conjecture*. Dissertation, Cornell University.

Appendix A

Matlab function codes

Listing A.1 Matlab function of Type II clash calculation

```
function [clash] = clash2func(A,B,C,D,E,F)
%CLASH2FUNC returns a scalar value of the clash between two triangles.
%CLASH2FUNC takes 6 input parameters: A, B, C, D, E and F.
%A, B & C store the vertex coordinates of one triangle ABC; D, E & F of the other triangle DEF.
%A, B, C, D, E and F are 3*1 vectors, each containing three coordinates of a vertex in a triangle.
%The method of defining clashes between two triangles used in this function is from document [6].
%(Iila Lijingjiao, 13th January, 2016)

%Define the locations of D, E and F in relation to plane ABC:
%The positivity of p, q and r tells D, E and F are on which side of or in plane ABC.
N=cross(A-B,C-B);   % find a normal of ABC
p=dot(N,D-A);q=dot(N,E-A);r=dot(N,F-A);

if p>=0&&q>=0&&r>=0||p<=0&&q<=0&&r<=0
   %If at least two of D, E and F are in plane ABC:
   %two triangles are in-plane; one edge of DEF lies on ABC,
   %then there is just a touch, which is considered as no clash.
   %Alternatively, if all D, E and F are on one side of plane ABC,
   %or only 1 vertex is in plane ABC with the other 2 on the same side,
   %then also no clash occurs.
   clash=1;  %A positive value is given.
else
   %Otherwise, one of D, E and F are on one side,
```

```
24    %the other two are on the other side;
25    %or one is in plane ABC, two are on opposite sides.
26
27    %In order to obtain the clash line of triangle DEF and plane ABC,
28    %D, E, F and N are swapped to put D on one side of plane ABC alone,
          and E and F on the other side or one in plane ABC.
29    %see [6] for principles: Sections 3.1 and 3.2.1 and Figure 3.
30
31    %If p is positive,
32    %then D is on the side of plane ABC where N points towards;
33    %if p is negative, D is on the other side;
34    %if p is zero, D is in plane ABC.
35    %The same applies to q for E and r for F.
36    if p*q*r>=0 %If two are negative; or one negative, one zero,
37       if p*q>=0 %If both p & q are negative, or either is 0,
38          d=D; D=F; F=d; %then D and F are swapped.
39       end
40       if p*r>=0 %If p and r both are negative, or one is zero,
41          d=D; D=E; E=d; %D and E are swapped.
42       end
43    else        %Otherwise, two are positive and one is negative,
44                %so N needs to change sign.
45       if p*q>0  %If the two positives are p and q,
46          N=-N; d=F; F=D; D=d; %then swap D and F, change N.
47       end
48       if q*r>0  %If the two positives are q and r,
49          N=-N;  %only the normal changes direction.
50       end
51       if p*r>0  %If the two positives are p and r,
52          N=-N; d=E; E=D; D=d; %then swap D and E, change N.
53       end
54    end
55    %Rearranged result: D is alone on the side N is pointing towards.
56    %DF and DE are rearranged above in order to intersect plane ABC,
57    %see [6]: Section 3.2.1 and Figure 3.
58
59    %Define in-plane positions of line PQ and triangle ABC:
60
61    %Find intersecting point P between line DF and plane ABC
62    DG=dot(N,D-A); DH=DG+dot(N,A-F); P=D+DG/DH*(F-D);
63    %Find intersecting point Q between line DE and plane ABC
64                   Dh=DG+dot(N,A-E); Q=D+DG/Dh*(E-D);
65
66    %Check P and Q are on which side of lines AB, BC and CA.
```

```
67    %See principle in [6] (section 3.1, section 3.2.2 and figure 4)
68    a=cross(A-B,C-B)'*cross(A-B,P-B);
69    b=cross(B-C,A-C)'*cross(B-C,P-C);
70    c=cross(C-A,B-A)'*cross(C-A,P-A);
71    d=cross(A-B,C-B)'*cross(A-B,Q-B);
72    e=cross(B-C,A-C)'*cross(B-C,Q-C);
73    f=cross(C-A,B-A)'*cross(C-A,Q-A);
74
75    if a>0&&b>0&&c>0||d>0&&e>0&&f>0
76       %If either points P or Q is inside triangle ABC,
77       %cases (i) or (iv) in Figure 2.6(a) in Jingjiao Li's dissertation,
78       clash=-norm(P-Q); %then clash value equals negative PQ length.
79    end
80
81    if a<=0&&d<=0||b<=0&&e<=0||c<=0&&f<=0
82       %If P & Q are both outside or touches same edge of triangle ABC,
83       %case (ii) in Figure 2.6(a) in the dissertation of Jingjiao Li's,
84       clash=1; %then no clash. A positive value is given.
85    else
86
87       %Check A, B and C are on which side of line PQ,
88       %see principle in Section 3.2.2 of [6].
89       g=cross(A-P,Q-P)'*cross(B-P,Q-P);
90       h=cross(C-P,Q-P)'*cross(A-P,Q-P);
91       if g>0&&h>0
92          %If B and C are on the same side of line PQ as A,
93          %case (iii) in Figure 2.6(a) in Jingjiao Li's dissertation,
94          clash=1; %then no clash.
95       else %Otherwise, at least one of B and C is not on the same side
              of line PQ as A, case (iv),
96          clash=-norm(P-Q); %the clash is considered to be equal to PQ.
97       end%of checking if A, B and C are on different sides of line PQ.
98
99    end %of checking cases (ii), (iii) & (v) in Figure 2.6(a) of Jingjiao
          Li's dissertation
100 end %of if more than one of D, E and F are in plane ABC.
101
102 end %of function CLASH2FUNC.
```

Appendix B

Data of Pareto optimised flexible polyhedra

Table B.1 Data of Pareto optimals of symmetrical Steffen flexible polyhedra

Result	Objectives		Parameters				
Index	Θ	R	a	b	c	d	e
B	**52.5°**	**0.013**	**5.5899**	**5.5464**	**0.1218**	**3.9489**	**8.5**
2	52.3°	0.02	5.6033	5.5366	0.1871	4.0039	8.5
3	52.0°	0.03	5.6318	5.5308	0.2829	4.0878	8.5
4	51.6°	0.04	5.6517	5.5165	0.3793	4.1685	8.5
C	**51.2°**	**0.05**	**5.6666**	**5.4959**	**0.480**	**4.2500**	**8.5**
5	50.8°	0.06	5.6880	5.4828	0.5785	4.3314	8.5
6	50.4°	0.07	5.7097	5.4689	0.6792	4.4146	8.5
7	49.9°	0.08	5.7336	5.4554	0.7850	4.5020	8.5
8	49.4°	0.09	5.7647	5.4486	0.8893	4.5911	8.5
D	**48.8°**	**0.1**	**5.7925**	**5.4370**	**0.9988**	**4.6816**	**8.5**
9	48.2°	0.11	5.7951	5.4053	1.1033	4.7562	8.5
10	47.6°	0.12	5.8162	5.3872	1.2155	4.8439	8.5
11	47.0°	0.1293	5.8446	5.3757	1.3257	4.9330	8.5
12	46.2°	0.14	5.8486	5.3410	1.4451	5.0152	8.5
13	45.4°	0.15	5.8851	5.3316	1.5686	5.1149	8.5
14	44.5°	0.16	5.9069	5.3096	1.6929	5.2067	8.5
E	**44.6°**	**0.17**	**6.5480**	**5.7564**	**1.8818**	**5.5754**	**8.5**
15	44.0°	0.1785	6.5513	5.7178	1.9933	5.6545	8.5
16	41.4°	0.18	7.9110	6.6602	2.3461	6.1127	8.5
17	40.9°	0.1904	7.9907	6.6373	2.5317	6.2523	8.5
F	**40.5°**	**0.2**	**8.0459**	**6.5934**	**2.7175**	**6.3879**	**8.5**
18	39.7°	0.2091	8.2124	6.6339	2.9133	6.5404	8.5
A	**27.4°**	**0.2139**	**6**	**5**	**2.5**	**5.5**	**8.5**
19	39.0°	0.2205	8.3712	6.6339	3.1730	6.7259	8.5
20	38.2°	0.2308	8.3415	6.5354	3.3421	6.8473	8.5
21	37.8°	0.24	8.3858	6.4834	3.5275	6.9742	8.5
G	**37.0°**	**0.25**	**8.5291**	**6.4675**	**3.7932**	**7.1545**	**8.5**
22	36.1°	0.2627	8.4623	6.3160	4.0191	7.2875	8.5
23	35.6°	0.27	8.3734	6.2074	4.1202	7.3392	8.5
24	34.6°	0.2789	8.4971	6.1757	4.3896	7.5070	8.5
25	34.0°	0.284	8.3534	6.0600	4.4253	7.5107	8.5
26	33.1°	0.29	8.3444	6.0028	4.5518	7.5882	8.5
H	**31.8°**	**0.3**	**8.4308**	**5.9183**	**4.8679**	**7.7451**	**8.5**
I	**21.7°**	**0.33**	**8.8174**	**5.7959**	**5.9376**	**8.4761**	**8.5**
J	**10.4°**	**0.34**	**8.1383**	**5.7008**	**5.5161**	**8.5020**	**8.5**

All results chosen here are on the Pareto Front in Figure 4.9.
Results labelled in letters A – J are from Table 4.2 and are presented in bold font.

Table B.2 Data of Pareto optimals of generalised Steffen flexible polyhedra

Index	Θ	R	a_1	a_2	a_3	a_4	b_1	b_2	c_1	c_2	d	e
1	12.9°	0.001	5.8917	5.4722	10.1370	9.3713	9.2850	5.4178	1.0036	0.0913	5.8856	8.5
2	53.1°	0.009	5.9480	5.4139	10.1791	9.4598	9.3032	5.3384	1.0637	0.2212	5.9105	8.5
B	**58.9°**	**0.0192**	**5.9227**	**5.4879**	**10.0019**	**9.5044**	**9.2819**	**5.3377**	**0.9650**	**0.3593**	**6.2461**	**8.5**
C	**56.2°**	**0.05**	**6.02**	**4.91**	**10.36**	**9.36**	**8.67**	**4.42**	**2.46**	**0.98**	**6.55**	**8.5**
3	51.7°	0.098	6.4884	7.6698	7.4790	6.3414	6.6011	6.7556	1.3540	1.3959	9.4283	8.5
4	50.5°	0.12	6.4685	7.6568	7.7282	6.5150	6.6675	6.6311	1.6560	1.6267	9.2408	8.5
5	0°	0.13	8.7900	8.0600	8.0400	8.7800	5.8800	5.8900	6.0100	6.0100	8.5300	8.5
6	49.6°	0.136	6	6	6	6	5	5	2.5	2.5	5.5	8.5
E	**48.9°**	**0.15**	**6.5758**	**7.6357**	**7.6935**	**6.6053**	**6.5079**	**6.4881**	**1.9570**	**1.9313**	**8.6839**	**8.5**
F	**46.8°**	**0.18**	**6.6682**	**7.7787**	**7.6742**	**6.6295**	**6.3525**	**6.3576**	**2.3232**	**2.3817**	**8.4972**	**8.5**
7	45.4°	0.19	7.0737	8.0746	8.0935	7.0823	6.5396	6.5335	2.6379	2.6289	8.6351	8.5
8	0°	0.2	6.58	7.64	7.69	6.61	6.51	6.49	1.96	1.93	8.68	8.5
9	0°	0.21	8.98	9.10	9.11	8.98	5.85	5.85	5.96	5.96	8.46	8.5
G	**43.6°**	**0.213**	**7.0674**	**8.0777**	**8.0787**	**7.0675**	**6.3761**	**6.3777**	**2.9517**	**2.9505**	**8.5583**	**8.5**
10	0°	0.22	7.07	8.08	8.08	7.07	6.38	6.38	2.95	2.95	8.56	8.5
11	41.8°	0.23	6.9942	8.0400	8.0241	6.9892	6.2078	6.2085	3.2099	3.2185	8.5134	8.5
12	39.1°	0.25	7.0497	8.0988	8.0872	7.0442	6.0672	6.0748	3.6012	3.6055	8.5370	8.5
13	0°	0.26	6.58	7.64	7.69	6.61	6.51	6.49	1.96	1.93	8.68	8.5
H	**36.7°**	**0.27**	**7.62**	**8.39**	**8.39**	**7.62**	**6.11**	**6.12**	**4.11**	**4.11**	**8.49**	**8.5**
14	0°	0.28	5.92	5.49	10.00	9.50	9.28	5.34	0.97	0.36	6.25	8.5
15	0°	0.29	6	6	6	6	5	5	2.5	2.5	5.5	8.5
16	31.5°	0.3	8.8476	9.1462	9.1398	8.8477	6.1690	6.1683	5.3087	5.3122	8.4926	8.5
17	28.4°	0.31	6.02	4.91	10.36	9.36	8.67	4.42	2.46	0.98	6.55	8.5
I	**26.9°**	**0.32**	**8.9643**	**9.0803**	**9.0768**	**8.9654**	**5.8469**	**5.8462**	**5.9439**	**5.9467**	**8.4391**	**8.5**
18	20.3°	0.33	6.33	7.65	7.73	6.41	6.79	6.62	1.45	1.51	9.64	8.5
J	**10.2°**	**0.34**	**8.2205**	**8.1707**	**8.1688**	**8.2168**	**5.7152**	**5.7163**	**5.5713**	**5.5706**	**8.5019**	**8.5**
19	1.9°	0.346	8.79	8.06	8.04	8.78	5.88	5.89	6.01	6.01	8.53	8.5
K	**0.6°**	**0.348**	**6.67**	**7.78**	**7.67**	**6.63**	**6.35**	**6.36**	**2.32**	**2.38**	**8.50**	**8.5**

All results chosen are on the Pareto Front in Figure 4.16. Results labelled in letters B – K are from Table 4.4 and are presented in bold font.

Table B.3 Data of Pareto optimals of two-tetrahedron flexible polyhedra

	Θ	R	a	b_1	b_2	b_3	b_4	c_1	c_2	c_3	c_4	d_1	d_2	e_1	e_2
A	**79.4°**	**0.016**	**10.5575**	**6.8962**	**7.2996**	**6.9266**	**7.2709**	**7.2757**	**6.8598**	**7.1846**	**6.8196**	**0.1728**	**0.2493**	**7.5**	**7.5535**
1	73.9°	0.04	10.1	8.7	7.5	7.0	7.9	7.1	7.8	8.8	7.3	3.3	3.3	7.5	8.1
2	74.6°	0.05	10.9	7.8	7.7	7.7	7.7	7.9	7.5	7.9	7.4	2.2	2.2	7.5	8.1
3	70.2°	0.07	10.2	10.0	7.9	6.8	7.7	7.0	7.9	9.9	7.7	5.4	5.6	7.5	8.2
4	60.8°	0.09	10.6	6.9	7.3	6.9	7.3	7.3	6.9	7.2	6.8	0.2	0.3	7.5	7.6
B	**69.2°**	**0.1**	**9.9**	**7.0**	**7.2**	**7.0**	**7.2**	**7.2**	**6.8**	**7.2**	**6.8**	**1.1**	**1.2**	**7.5**	**7.9**
5	61.4°	0.12	10.9	7.8	7.7	7.7	7.7	7.9	7.5	7.9	7.4	2.2	2.2	7.5	8.1
6	65.3°	0.14	10.2	10.0	7.9	6.8	7.7	7.0	7.9	9.9	7.7	5.4	5.6	7.5	8.2
7	64.3°	0.15	9.8	9.3	7.6	6.0	6.2	6.1	6.4	9.4	7.6	6.8	7.0	7.5	7.6
C	**61.5°**	**0.17**	**10.7611**	**7.8164**	**7.7626**	**7.6931**	**7.7447**	**7.8923**	**7.4600**	**7.9165**	**7.4135**	**2.1408**	**2.1326**	**7.5**	**8.0839**
8	61.7°	0.18	10.9	7.8	7.7	7.7	7.7	7.9	7.5	7.9	7.4	2.2	2.2	7.5	8.1
9	60.6°	0.19	10.1	8.7	7.5	7.0	7.9	7.1	7.8	8.8	7.3	3.3	3.3	7.5	8.1
10	59.6°	0.2	10.2	10.0	7.9	6.8	7.7	7.0	7.9	9.9	7.7	5.4	5.6	7.5	8.2
11	58.5°	0.21	9.8	9.3	7.6	6.0	6.2	6.1	6.4	9.4	7.6	6.8	7.0	7.5	7.6
12	56.6°	0.22	9.9	7.0	7.2	7.0	7.2	7.2	6.8	7.2	6.8	1.1	1.2	7.5	7.9
13	56.1°	0.23	10.9	7.8	7.7	7.7	7.7	7.9	7.5	7.9	7.4	2.2	2.2	7.5	8.1
14	54.9°	0.24	10.1	8.7	7.5	7.0	7.9	7.1	7.8	8.8	7.3	3.3	3.3	7.5	8.1
D	**53.1°**	**0.25**	**10.2**	**10.0**	**7.9**	**6.8**	**7.7**	**7.0**	**7.9**	**9.9**	**7.7**	**5.4**	**5.6**	**7.5**	**8.2**
15	51.7°	0.26	9.8	9.3	7.6	6.0	6.2	6.1	6.4	9.4	7.6	6.8	7.0	7.5	7.6
16	50.4°	0.27	10.6	6.9	7.3	6.9	7.3	7.3	6.9	7.2	6.8	0.2	0.3	7.5	7.6
17	48.1°	0.28	9.9	7.0	7.2	7.0	7.2	7.2	6.8	7.2	6.8	1.1	1.2	7.5	7.9
18	45.3°	0.3	10.0765	9.1387	7.5620	6.9263	7.7037	6.9299	7.7408	9.0451	7.3500	4.2529	4.2287	7.5	8.0301
19	41.9°	0.32	9.8	9.3	7.6	6.0	6.2	6.1	6.4	9.4	7.6	6.8	7.0	7.5	7.6
E	**36.0°**	**0.34**	**10.2**	**10.0**	**7.9**	**6.8**	**7.7**	**7.0**	**7.9**	**9.9**	**7.7**	**5.4**	**5.6**	**7.5**	**8.2**
20	33.7°	0.35	9.8	9.3	7.6	6.0	6.2	6.1	6.4	9.4	7.6	6.8	7.0	7.5	7.6
21	30.1°	0.36	9.8	9.3	7.6	6.0	6.2	6.1	6.4	9.4	7.6	6.8	7.0	7.5	7.6
22	24.1°	0.37	9.8	9.3	7.6	6.0	6.2	6.1	6.4	9.4	7.6	6.8	7.0	7.5	7.6
F	**18.9°**	**0.38**	**9.8248**	**9.3041**	**7.6191**	**6.0042**	**6.2360**	**6.1191**	**6.3792**	**9.3612**	**7.5745**	**6.7780**	**6.9647**	**7.5**	**7.5570**

All results chosen here are on the Pareto Front in Figure 5.3. Results labelled in letters A – F are from Table 5.1 and are presented in bold font.